TECHNISCHE UNIVERSITÄT DRESDEN

Faculty for Environmental Sciences / Department of Forest Sciences

Institute of Wood and Plant Chemistry

Physico-Chemical Processes during Reactive Paper Sizing with Alkenyl Succinic Anhydride (ASA)

Dissertation to reach the academic degree
"Doktor-Ingenieur" (Dr.-Ing.)

handed in by

M.-Eng., Dipl.-Ing. (FH) Sebastian Porkert

born November 14th 1984 in Gräfelfing, Germany

Reviewer:

Mr. Prof. Dr. habil. Steffen Fischer

Technische Universität Dresden / Faculty for Environmental Sciences, Department of Forest Sciences, Institute of Wood and Plant Chemistry

Mr. Prof. Dr. Stephan Kleemann

University of Applied Sciences Munich, Faculty 05, Process Engineering for Paper and Packaging, Paper Technology

Mr. Prof. Dr. Frank Miletzky

Technische Universität Dresden / Faculty for Mechanical Sciences and Engineering, Institute for Wood and Fiber Materials Technology

Place and Date of Defense: Tharandt, December 9th 2016

Declaration of Compliance / Übereinstimmungserklärung

Die Übereinstimmung dieses Exemplars mit dem Original der Dissertation zum Thema:

“Physico-Chemical Processes during Reactive Paper Sizing with Alkenyl Succinic Anhydride (ASA)”

wird hiermit bestätigt.

Breitbrunn am Ammersee, 16. Februar 2017

…….

Sebastian Porkert

TECHNISCHE UNIVERSITÄT DRESDEN

Faculty for Environmental Sciences / Department of Forest Sciences

Institute of Wood and Plant Chemistry

Physico-Chemical Processes during Reactive Paper Sizing with Alkenyl Succinic Anhydride (ASA)

Dissertation to reach the academic degree
"Doktor-Ingenieur" (Dr.-Ing.)

handed in by

M.-Eng., Dipl.-Ing. (FH) Sebastian Porkert

born November 14th 1984 in Gräfelfing, Germany

Reviewer:

Mr. Prof. Dr. habil. Steffen Fischer

Technische Universität Dresden / Faculty for Environmental Sciences, Department of Forest Sciences, Institute of Wood and Plant Chemistry

Mr. Prof. Dr. Stephan Kleemann

University of Applied Sciences Munich, Faculty 05, Process Engineering for Paper and Packaging, Paper Technology

Mr. Prof. Dr. Frank Miletzky

Technische Universität Dresden / Faculty for Mechanical Sciences and Engineering, Institute for Wood and Fiber Materials Technology

Munich, June 8th 2016

Munich 2016

© Copyright by Sebastian Porkert

For Lilli

“*What was scattered gathers. What was gathered blows away.”*
Heraclitus

Acknowledgment

At this point, I would like to announce my special gratitude to my doctoral advisors Prof. Dr. habil. Steffen Fischer of Technische Universität Dresden and Prof. Dr. Stephan Kleemann of Munich University of Applied Sciences, for their excellent supervision from 2011 to 2016 and especially for their trust in my abilities as well as for granting the freedom of including my individual approaches and implementations during this work. As this dissertation derives from the cooperation between Munich University of Applied Sciences and Technische Universität Dresden, I would like to especially thank my supervisors for having given me the chance to unfold my potentials within this academic program.

I would also like to thank the work group under the supervision of Mr. Fischer for their kind help and advice, and especially for their friendly, cooperative and integrating ways of interaction. This always made me feel welcome whenever I visited the Institute for Wood and Plant Chemistry at the Tharandt campus.

I thank the members of the “Arbeitskreis Wet End Prozesse” of the IVP e.V. for their constructive input and their excellent support.

My special thanks go toward my colleagues of Munich University of Applied Sciences and the Institut für Verfahrenstechnik Papier e.V. (IVP), as they always were of great constructive help throughout the ups and downs of the time working on my doctoral thesis. With special emphasis I would like to thank Mr. Jürgen Belle, who, with his superb critical, but constructive reflections and considerations, is not only a colleague of excellent kind, but meanwhile a person I would not like to miss as a friend.

I have to express my special gratitude to my whole family and friends, for their unconditional support throughout the last years, for their good advice, their back up as well as for just being there, whenever needed.

Above all, I especially thank my loving wife Janina and my daughter Lilli. Without you Janina, I would not be where I am now, nor would I be as happy as I am. Thank you Lilli for just being my wonderful daughter. With every smile shared, you make me feel more complete.

.

The financial support for the presented work was given from 01.01. - 31.12.2012 by the „Kuratorium für Forschung und Technik der Zellstoff und Papierindustrie im Verband Deutscher Papierfabriken e.V. (VDP)“, Bonn, within the research project Infor 159 “Optimierung der ASA Leimung”, and from 01.04.2013 - 31.12.2015 by the IGF research project 17757-N “ReLeiPa”

The IGF-Research Project 17757-N „Ressourcenschonung durch Leimungsmittel-einsparung bei der Herstellung von Papier und Karton“ ReLeiPa of the research coordination insitution Verband der Deutschen Papierfabriken e.V. (VDP) was supported over the AiF within the support program of the Industrielle Gemeinschaftsforschung (IGF) by the federal ministry for economic affairs and energy on behalf of a decision by the German Bundestag.

Supported by:

on the basis of a decision
by the German Bundestag

Abstract

Sizing (hydrophobization) is one of the most important process steps within the added-value chain of about 1/3rd of the worldwide produced paper & board products. Even though sizing with so-called reactive sizing agents, such as alkenyl succinic anhydride (ASA) was implemented in the paper industry decades ago, there is no total clarity yet about the detailed chemical and physical mechanisms that lead to their performance. Previous research was carried out on the role of different factors influencing the sizing performance, such as bonding between ASA and cellulose, ASA hydrolysis, size revision as well as the most important interactions with stock components, process parameters and additives during the paper making process. However, it was not yet possible to develop a holistic model for the explanation of the sizing performance given in real life application. This thesis describes a novel physico-chemical approach to this problem by including results from previous research and combining these with a wide field of own basic research and a newly developed method that allows tracing back the actual localization of ASA within the sheet structure.

The carried out measurements and trial sets for the basic field of research served to evaluate the stock and process parameters that most dominantly influence the sizing performance of ASA. Interactions with additives other than retention aids were not taken into account. The results show that parameters, such as the content of secondary fibers, the degree of refining, the water hardness as well as the suspension conductivity, are of highest significance. The sample sets of the trials with the major impacting parameters were additionally analyzed by a newly developed localization method in order to better understand the main influencing factors.

This method is based on optical localization of ASA within the sheet structure by confocal white light microscopy. In order to fulfill the requirements at magnification rates of factor 100 optical zoom, it was necessary to improve the contrast between ASA and cellulose. Therefore, ASA was pretreated with an inert red diazo dye, which does not have any impact on neither the sizing nor the handling properties of ASA. Laboratory hand sheets that were sized with dyed ASA, were analyzed by means of their sizing performance in correlation to measurable ASA agglomerations in the sheet structure. The sizing performance was measured by ultrasonic penetration analysis. The agglomeration behavior of ASA was analyzed automatically by multiple random imaging of a sample area of approx. 8650 µm² with a minimum resolution for particles

of 500 nm in size. The gained results were interpreted by full factorial design of experiments (DOE). The trials were carried out with ASA dosages between 0% and 0.8% on laboratory hand sheets, made of 80% bleached eucalyptus short fiber kraft pulp and 20% northern bleached softwood kraft pulp, beaten to SR° 30, produced with a RDA sheet former at a base weight of 100 g/m² oven dry.

The results show that there is a defined correlation between the ASA dosage, the sizing performance and the number and area of ASA agglomerates to be found in the sheet structure. It was also possible to show that the agglomeration behavior is highly influenced by external factors like furnish composition and process parameters. This enables a new approach to the explanation of sizing performance, by making it possible to not only examine the performance of the sizing agent, but to closely look at the predominant position where it is located in the sheet structure. These results lead to the explanation that the phenomenon of sizing is by far not a pure chemical process but rather a more physical one. Based on the gained findings it was possible so far to optimize the ASA sizing process in industrial-scale by means of ~ 50% less ASA consumption at a steady degree of sizing and improved physical sheet properties.

Table of Content

List of Illustrations

List of Tables

List of Formulas

List of Abbreviations

AA	-	accelerated aging
abbr.	-	abbreviation
Aggl_A	-	total agglomeration area
Aggl_AV	-	average agglomerate size
Aggl_N	-	number of agglomerates
AI	-	Adobe Illustrator
AKD	-	alkylketen dimere
approx.	-	approximately
ASA	-	alkenyl succinic anhydride
ATR	-	attenuated total reflection
BM	-	board machine
CA_{max}	-	maximum contact angle
CEL	-	cutting edge length
CELL	-	cellulose
CMYK	-	cyan-magenta-yellow-black (color space)
CTMP	-	chemical thermo mechanical pulp
DART-MS	-	direct analysis in real time – mass spectroscopy
D-ASA	-	ASA, dyed with 5% Sudan Red 7B
DIP	-	deinked pulp
DNA	-	deoxyribonucleic acid
DOE	-	design of experiments
e.g.	-	exempli gratia, for example
etc.	-	et cetera, and other things, and so forth
EUKA	-	eucalyptus kraft pulp
FAA	-	fatty acid anhydride
F-ASA	-	ASA, dyed with 0.1% Nile Red
f.l.r.t	-	from left to right
FTIR	-	Fourier transformed infrared spectroscopy
GC	-	gas chromatography
GCC	-	ground calcium carbonate
HPLC	-	high performance liquid chromatography
hyd. phil.	-	hydrophilic
hyd. phob.	-	hydrophobic
IF	-	infinite focus
IFM	-	infinite focus measure suit
IGC	-	inverse gas chromatography
IR	-	infrared
IUPAC	-	International Union of Pure and Applied Chemistry
IVP e.V.	-	Institut für Verfahrenstechnik Papier e.V.
KBr	-	potassium bromide
LED	-	light emitting diode
Mid-IR	-	mid-range infrared
MLR	-	multi linear regression

MPixel	-	mega pixel / million pixels
MS	-	mass spectroscopy
MSOHO		maleated high oleic sunflower oil
MUAS	-	Munich University of Applied Sciences
NBSK	-	northern bleached softwood kraft pulp
NIR	-	near infrared
NR	-	Nile Red
n.V.	-	no value
OBA	-	optical brightening agent
OCC	-	old corrugated container board
OD	-	oven dry
PAAE	-	poly amidoamine epichlorhydrin resin
PAC	-	poly aluminum chloride
PAM	-	polyacrylamide
PANS	-	poly aluminum nitrate sulfate
PC	-	paper chromatography
PCC	-	precipitated calcium carbonate
PDA	-	dynamic penetration analyzer
PEI	-	polyethylenimine
PLS	-	partial least square regression
PM	-	paper machine
PPH	-	pigment polymer hybrid
PS	-	Adobe Photo Shop
PSA	-	polymeric sizing agent
PUD	-	poly urethane micro dispersions
Py-GC	-	pyrolysis – gas chromatography
Py-GC-MS	-	pyrolysis – gas chromatography – mass spectroscopy
R_1, R_X	-	aliphatic rests
RDA	-	retention drainage analyzer
rel. hum.	-	relative humidity
RGB	-	red-green-blue (color space)
RNA	-	ribonucleic acid
RSA	-	reactive sizing agent
SAA	-	styrene acrylic acid solution polymers
SAE	-	styrene acrylate emulsion polymer
SEC	-	selective energy consumption
SEL	-	specific edge load
SGW	-	stone ground wood
SMA	-	styrene maleic acid anhydride solution polymers
SR7B	-	Sudan Red 7B
t_{60}	-	time elapsed after 40% intensity loss (PDA)
TiO_2	-	titanium dioxide
TLC	-	thin layer chromatography
t_{max}	-	time elapsed till intensity peak (PDA)
TMP	-	thermo mechanical pulp

ToF-SIMS	-	time of flight - secondary ion - mass spectroscopy
TPM	-	trial paper machine
US	-	ultra sonic
UV	-	ultra violet
vs.	-	versus
w	-	with
w/o	-	without
XPS	-	x-ray photoelectron spectroscopy

1 Introduction and Problem Description

Sizing / hydrophobization is one of the most important steps in the added value chain for about 1/3rd of the globally produced board and paper grades. It is the only way to define the behavior of a substrate towards the ad- and absorption of aqueous substances such as water, inks or glues without changing the sheet morphology or composition. Within these processes, the sizing agents are either applied internally during the wet-end processes or on the surface within the paper machine. The main sizing agent classes by mass shares are: rosin sizes, alkylketene dimers (AKD), alkenyl succinic anhydrides (ASA) and polymeric sizing agents (PSA). Being one of the most costly grafting steps for the affected grades, the sizing procedure has always been in the focus of optimization. Since the days of steadily rising raw material and energy prices and narrowing ecological tolerances, paper & board production had to become a highly scientific and fully automatized industrial branch. Dominant and high customer requirements to the product, on either the converting, printing or the end-user side do not allow any unpredictable variations as such. To guarantee a lucrative, efficient, ecologically friendly, sustainable and optimal process, the production steps have to be very fast, free of losses and within a narrow range of tolerances. Even though sizing with the so-called reactive sizing agents ASA and AKD was implemented in the paper industry decades ago, there is no total clarity yet about the detailed chemical and physical mechanisms that lead to their performance.

1.1 Initial Situation

ASA is the number one representative of the group of reactive sizing agents. It is, from the point of traditional knowledge, supposed to generate its sizing action by the formation of covalent bonds with the stock’s cellulose during the papermaking process.

Driven by the high anhydride-based reactivity it is also prone to rapid hydrolysis with the process water. This undesired concurrence reaction is supposed to minimize the sizing performance and to interfere with the paper or board machines process stability. Within the water loops, hydrolyzed ASA is able to form salts with metal ions, especially calcium. These salts, if not carried out of the system with the

stock, form sticky deposits within the approach flow system and the paper machines wet end section, potentially causing severe interferences during the production process.

On the opposite side of this traditional understanding of reactive sizing with ASA are some recent findings of several research groups, showing that the amount of bound ASA in a ready-made sized paper sheet is close to zero. Hence, the sizing performance is still given; these findings are contrary to the traditional understanding of the physical and chemical mechanisms that lead to the hydrophobizing performance of ASA.

These findings question the validity of published mechanism models that were commonly used for the explanation of ASA sizing performance generation.

At the moment, there is no valid holistic chemical and physical performance model available, which describes the aspects of reactive sizing with ASA.

1.2 Objective

It is the objective of the presented work to create a path to holistic understanding of the occurring physico-chemical mechanisms which lead to ASA's hydrophobizing performance. This goal should be reached by closing the gap between the two commonly used performance explanation attempts, which are based either on the generation of ester bonds between ASA and the cellulose or on a physical distribution of ASA on the fiber surface. This attempt includes an approach to performance explanation via on the one hand a comprehensive analysis of sizing performance interfering factors, and the development of a novel measurement method which allows to trace ASA's distribution behavior on a microscopic scale within the structures of ready-made sheets on the other hand. The combination of the results of both attempts should finally be the foundation for the explanation of the so far not yet clarified puzzle pieces to ASA's holistic sizing performance explanation. It is the final goal of this work to utilize the gained knowledge for the development and implementation of novel sizing mechanism based approaches to ASA performance improvement, in order to optimize the industrial sizing processes by significant means.

2 Theoretical Approach

The following section will describe the theoretical background of this thesis. The first Chapter will deal with the modern paper industry as such, including production rates, produced grades as well as past and future trends. This will be followed by a Chapter on the raw materials for the production of paper & board with a special focus on the required chemical additives, the key ingredients to modern high-performance papermaking. The third Chapter is on the topic of paper & board sizing. First, the theory of sizing will be described, followed by some information on the main sized paper & board grades, the nowadays mostly used sizing agents, and the explanation of the used methods for sizing agent amount and sizing degree determination. The special focus of this Chapter will be on the sizing agent “alkenyl succinic anhydride” (ASA), its production, processing, application, mechanistic reaction models and causes for interactions. This Chapter will be followed by a description of the limitations of state of the art sizing analysis, directly leading into the last Chapter, which will describe the theoretical background of the invented optical analysis method.

2.1 The Modern Paper & Board Industry on the Example of Germany

The process of modern paper & board production is by far not comparable to the handicraft it used to be until Henry Fourdrinier filed the patent for the first machine [1] for continuous production of paper in 1807. Since this time, the whole production process has evolved from a rather mechanical one to a highly automated high-tech process. In order to fulfill the customer demands, regarding quality and quantity, the processes had to become more productive and accurate over all. This is why modern paper machines are hardly operated by men, but by fully integrated, intelligent computer systems [2], which are just surveilled and adjusted by the personnel. Driven by this change in automation and by the recent developments in machine technology, it is today possible to produce for example newsprint at 2010 m/min [3] or tissue at 2210 m/min [4], at machine widths over 11 m. The yearly production rates of the largest machines exceed 1.2 billion tons [5]. Only the invention and the ability of producing such machines made it possible to fulfill the demand of the steadily growing world paper & board market. As it can be seen in

Figure 2.1-1 [6], the German and world production as well as the consumption followed an almost linear growth until the year 2009, the year the last world financial and economic crisis hit the markets. Even though the German economy is one of the strongest and most solid in the world, it had to suffer as well. Only governmental economic stimulus packages were able to stabilize the markets [7]. Since that point in time, the German paper industry is recovering slowly, while the world paper industry is still, after a short recession, on the rising branch. By now, the German production has reached almost the rates of 2008. With a yearly production in 2014 of 22.535 million tons, Germany is the biggest paper & board producing economy in Europe and the fourth strongest in the world (403 mio. t./2013), behind Japan (26.2 mio. t./2013), the USA (73.8 mio. t./2013) and the world leader China (104.7 mio. t./2013).

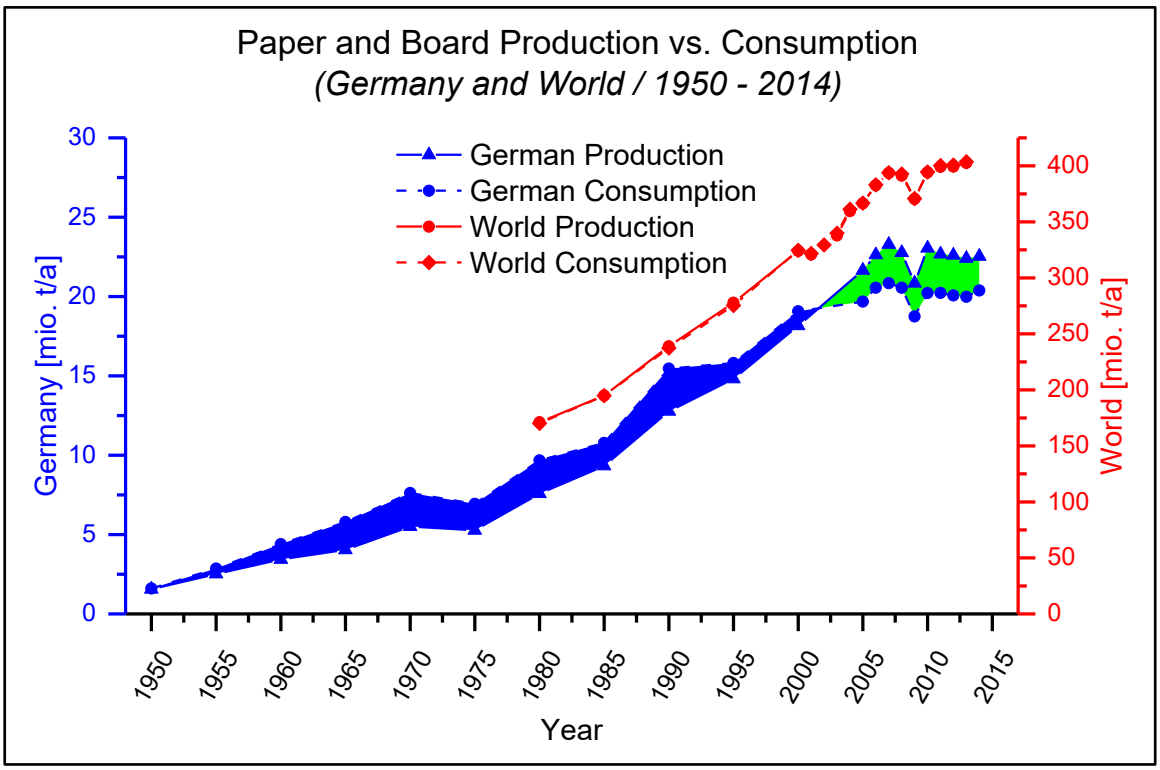

Figure 2.1-1: Paper & Board Production vs. Consumption (Germany & World / 1959 - 2014) [6]

The crisis was the trigger for the last significant structural changes in the paper industry. Figure 2.1-2 [6, 7] shows, that even though the gross production is almost equal, the shares of the produced grades differ quite a lot between 2008 and 2014. While the graphical grades, once the German paper industry's backbone, lost almost 8% of their share (1.85 mio. t./a), the packaging grades extended theirs by 8% (1.67 mio. t./a), making it the most important branch.

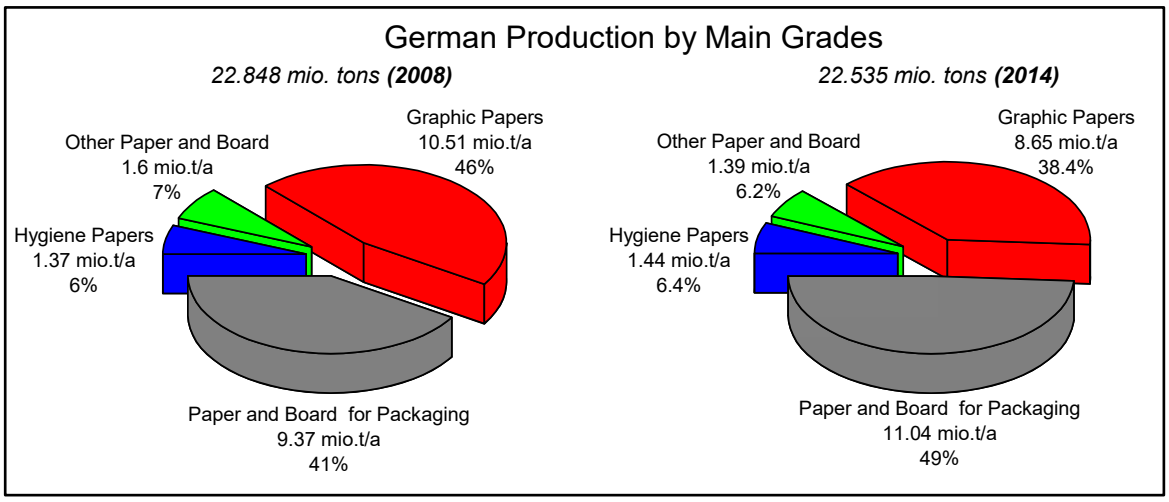

Figure 2.1-2: German Production by Main Grades (2008 & 2014) [6, 7]

This change is mainly triggered by a steady demand decrease of printed media such as books, magazines and newspapers, driven by ongoing digitalization, and at the same time by a demand increase in required packaging media for the rising branches of logistics and online based mail-order business. This trend is supposed to continue for the following years, forcing further reorganizations within the German paper industry [6]. Another important trend of the recent years is an achieved optimized production towards higher energy and raw material efficiency, as well as towards a maximum of sustainability [8, 9]. For the export based German market (Figure 2.1-1 / green shading) this trend arose out of the necessity to remain competitive amongst other producing countries, especially to countries from the Asian market.

2.1.1 **Raw Materials for the Production of Paper & Board**

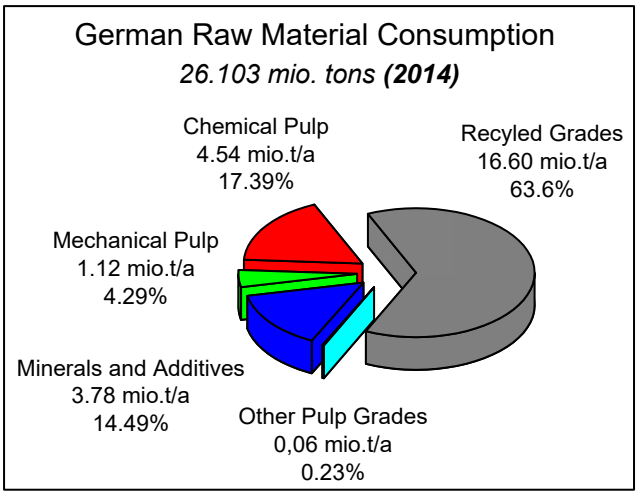

Figure 2.1-3: Raw Material Consumption (Germany / 2014) [6]

The raw material composition for produced paper & board grades in Germany is based on the utilization of ~ 85% fiber compounds and ~ 15% non-fibrous materials. As can be seen in Figure 2.1-3 [6] the recycled grades, also known as secondary fibers, form the foundation for Germany's production with a share of 63.6%.

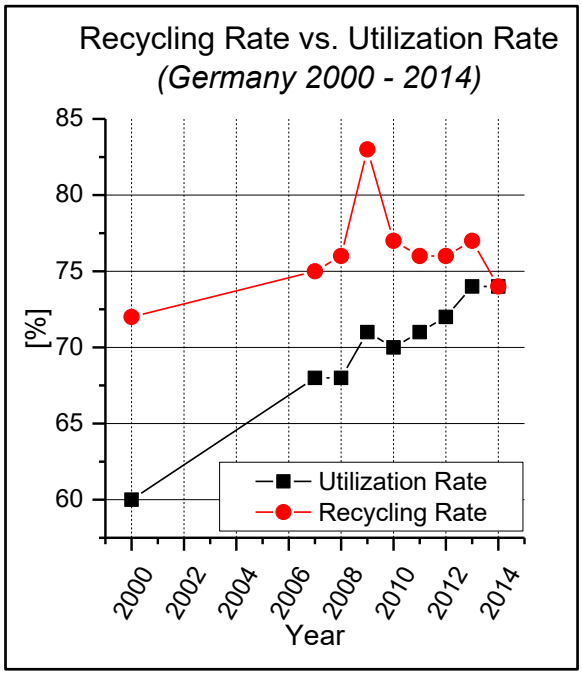

Figure 2.1-4: Recycling Rate vs. Utilization Rate (Germany / 2000 - 2014) [6]

Primary fibers account for the second largest share with 21.68%. This share is made up of 4.29% mechanical pulp (e.g., SGW, TMP, CTMP) and 17.39% chemical pulp (e.g., long/short fiber kraft or sulfite pulp). Minerals and additives make up an overall share of 14.49%. The detailed composition of this fraction will be discussed in the following section. The smallest share of 0.23% consists of other pulp grades (e.g., dissolving or medical pulp). The previously mentioned trend of sustainability is visualized in Figure 2.1-4 [6]. This figure displays the progress of the recycling and utilization rate of the last 14 years. It shows impressively that Germany has reached its own zenith of secondary fiber usage. A further increase in secondary fiber utilization will only be possible by importing an excess of waste paper from abroad. Driven by the market forces and the international competition, this will only be possible by accepting higher raw material prices.

The following figure (Figure 2.1-5 / 1 [6, 10]) displays in detail the composition of the “minerals and additives” share. As minerals and additives make up only a small share of the raw material composition for early papermaking, they are key ingredients of today’s papermaking. Minerals have an overall share of 76.3%. This share is made up of 48.5% coating pigments and 27.8% fillers. Typical minerals used for this purpose are clay, GCC, PCC, titanium dioxide and many more. The second largest share with 9.5% is the product group of starches. This group consists of all different kinds of starch types starting from native starches, over thermally and enzymatically degraded starches to specialty starches, such as anionic, cationic or amphoteric starches. The major part of the starches is used as internally applied dry strength agent, while some special modified starches can serve as retention aids, emulsification agents, and many other.

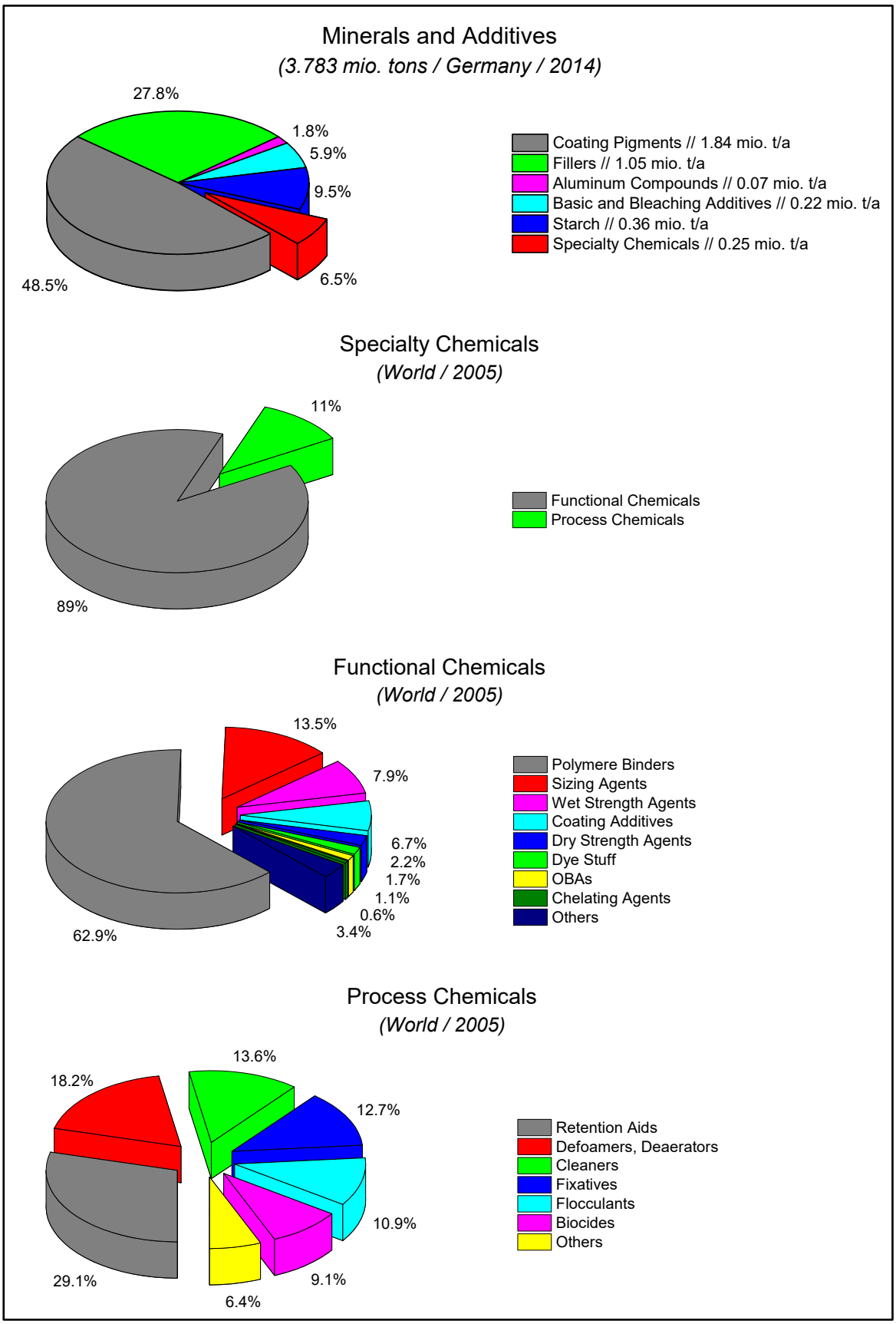

Figure 2.1-5 Minerals & Additives, Specialty Chemicals, Functional Chemicals, and Process Chemicals (Germany / 2014 & World / 2005) [6, 10]

The third largest share is made up by specialty chemicals, which will be described in detail in the next section. Basic and bleaching agents mostly used during the production of virgin fibers account for 5.9%. The smallest group with 1.8% is the product class of aluminum compounds such as alum, PAC or PANS. These products are mainly used as flocculation agents or as fixatives in combination with rosin size.

The share of specialty chemicals is the key ingredient to today's high-performance papermaking. The group of special chemicals is split into two sub-groups, functional chemicals and process chemicals (Figure 2.1-5 / 2 [6, 10]). Functional chemicals have the ability to change, improve or define the final product's properties. These properties can be of morphological, physical, optical or chemical nature. The three main groups of functional chemicals are polymeric binders (62.9%), sizing agents (13.5%) and wet strength agents (7.9%). The group of sizing agents will be described in Chapter 2.2.6. The residual additives contributing to functional chemicals are by shares: coating additives, dry strength agents, dyestuff, OBAs, chelating agents and others chemicals (Figure 2.1-5 / 3 [6, 10]).

The overall smallest group of raw materials is represented by the process chemicals. These chemicals have the ability to influence and improve the production process. Nevertheless some of these products, especially retention aids and fixatives have the capability of improving paper parameters or contributing to the performance of functional chemicals. The three main product classes of chemicals are retention aids (29.1%), defoamers/deaerators (18.2%), and cleaners (13.6%). The residual additives contributing to this group are by shares: fixatives, flocculants, biocides and others chemicals (Figure 2.1-5 / 4 [6, 10]).

2.2 The Sizing of Paper & Board

2.2.1 **Introduction to Paper & Board Sizing**

Sizing is one of the most important process steps within the added-value chain of about 1/3rd of the worldwide produced paper & board products [10]. This process is well known since the early days of papermaking. Not comparable to today's sizing processes, in former time's single paper sheets were rendered for a certain degree resistant to water absorption by dipping them into a tub of animal or

vegetable glue with subsequent drying [11]. The process changed during the years of industrialization into the first applications where natural sizing agents where applied to the stock prior to sheet forming on a continuous working paper machine [11, 12]. The focus of modern paper sizing is the improvement or the adjustment of printability, convertibility and the durability against water or humidity by the application of highly specific, mostly synthetic sizing agents.

Even though this process step is that important and well known, the phrase “sizing” can have different meanings and can therefore be confused. This is why the next section of this Chapter will deal with the origin of the word sizing, its historical and present meaning, and how it is defined for the content of this thesis.

The origin of the words “sizing” or “size” can be explained via three approaches. The first is the derivation from the Swedish and French word “size” [11], which stands for glue and can be explained by early hand papermaking, where the sheets were treated by dipping into a tub of animal glue.

The second approach is that the word sizing derives from the actual size/dimension change of a paper stack after being dipped into water [11].

The third explanation is said to originate from the Latin word “assidere", which is supposed to have changed over years in Italian papermaking into the word “sisa” and then “size”, meaning, “set in place” [12]. This theory could not be reconstructed, because intense research did not confirm the stated meaning of “assidere" [13].

The present meaning of the word “sizing” is somehow still confused in two ways. On the one hand, there is the process of “surface sizing” [14-17] with starch in so-called size presses to improve the paper’s strength or surface properties. On the other hand, there is the treatment with sizing agents, either internally [16, 18] or on the surface [19, 20] to improve and control the papers absorbency behavior towards aqueous fluids [11].

For the content of this thesis, the word “sizing” is defined as the treatment of paper & board with chemical additives in order to control or improve the absorbency behavior towards aqueous fluids.

2.2.2 The Definition of Paper & Board Sizing

The gross of the sheet structure (substrate) is made up of cellulosic fibers. These, in combination with other sheet ingredient, form a very fine and extremely porous structure, which is capable of absorbing water many times over its own weight within only an instant of time. If the fibers were not made hydrophobic in an artificial way, water contact would lead to immediate structural and strength losses [11, 21, 22]. To avoid this phenomenon, the substrate has to be sized. The process of sizing, in accordance to earlier publications [10, 11, 21, 23], can be defined as following:

"Sizing is:
hydrophobization of paper / board
by internal or surface application
of predominantly hydrophobic,
surface active additives." [24]

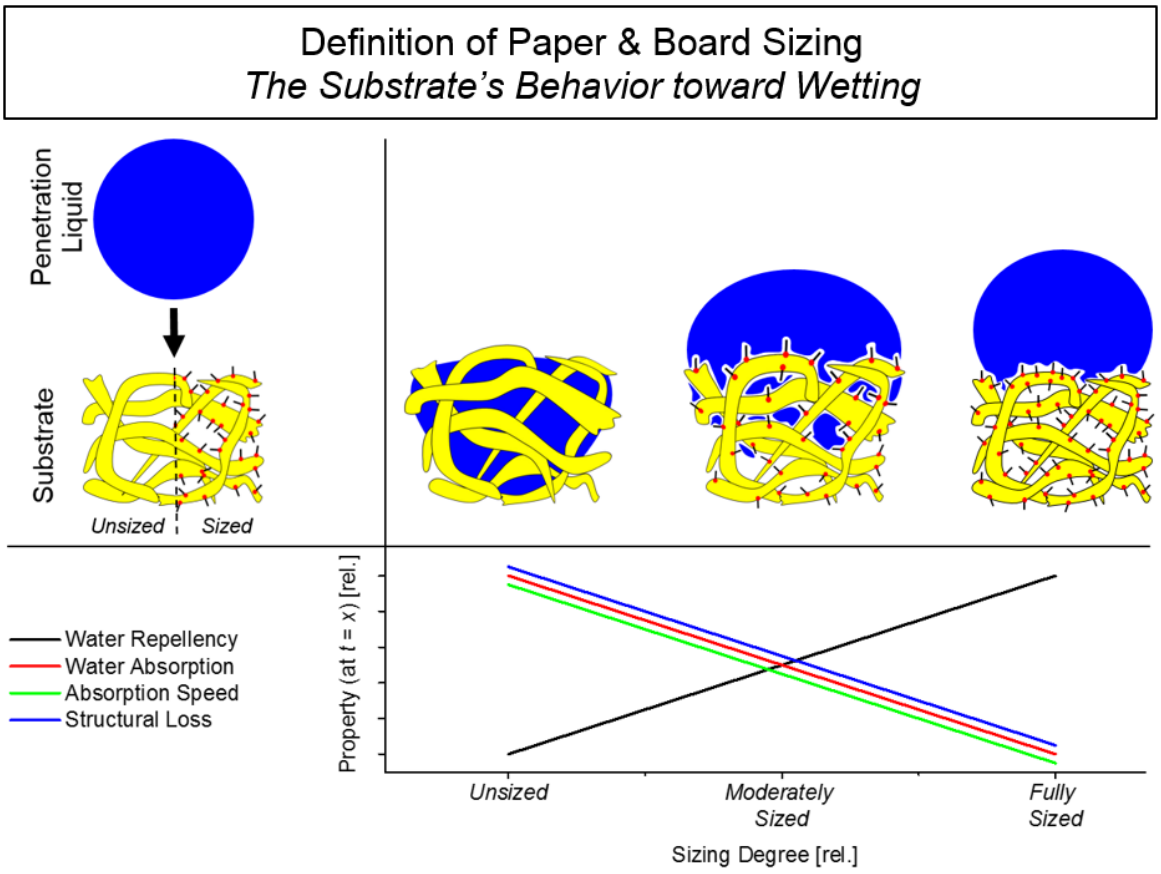

Figure 2.2-1: Definition of Paper & Board Sizing. The Substrate's Behavior toward Wetting.

This artificially generated hydrophobicity stands in direct correlation to the absorption behavior of the substrate. By adjusting the degree of hydrophobicity, or in other words, the sizing degree, it is possible to control the relative amount of fluid that is absorbed per unit of time. Meaning, the higher the degree of sizing, the higher the degree of water repellency and the lower the degrees of water absorption, absorption speed and structural loss (Figure 2.2-1) [11, 21, 22]. Along with the above-mentioned facts, sizing agents also affect other existential substrate properties. These are physical properties such as tensile strength, dimensional stability, stiffness, friction coefficient, smoothness or porosity. In addition to these, they can also interact with others, such as brightness, ink holdout, linting or feathering [10].

2.2.3 The Global Markets for Sized Paper & Board Products and Sizing Agents

Figure 2.2-2/1 [10] displays the results of the last published inquiry from 2005, contributed to the globally produced sized and unsized paper & board grades. This inquiry stated that 32.7% of the globally produced grades are sized to some extent. These grades were further broken down into the shares which were produced by a specific group of sizing agent. The four main sizing agent groups that were taken into consideration are ASA, AKD, rosin sizes and PSA's, which are the most common systems today. As can be seen in Figure 2.2-2/2 [10], 34.9% were sized by ASA, 28% by rosin size, 27.1% by AKD and 10% by PSAs. Switching the few from the production of sized grades to the required amount of sizing agents, Figure 2.2-2/3 [10] shows quite a different share distribution. The overall sizing agent consumption of 438,000 tons contributed 0.11% to the whole produced grades and 0.34% to the sized grades. The total amount of sizing agents was made up of 67.5% rosin sizes, 15.8% AKD, 10.8% ASA and 5.8% PSA's. The combination of the data from the globally produced sized grades and their respective sizing agent demand gives the information on the average sizing agent consumption, as shown in Figure 2.2-3 [10]. The calculated worldwide average dosage values are 0.1% for ASA, 0.19%, for AKD, 0.8% for rosin sizes and 0.19 % for PSA's.

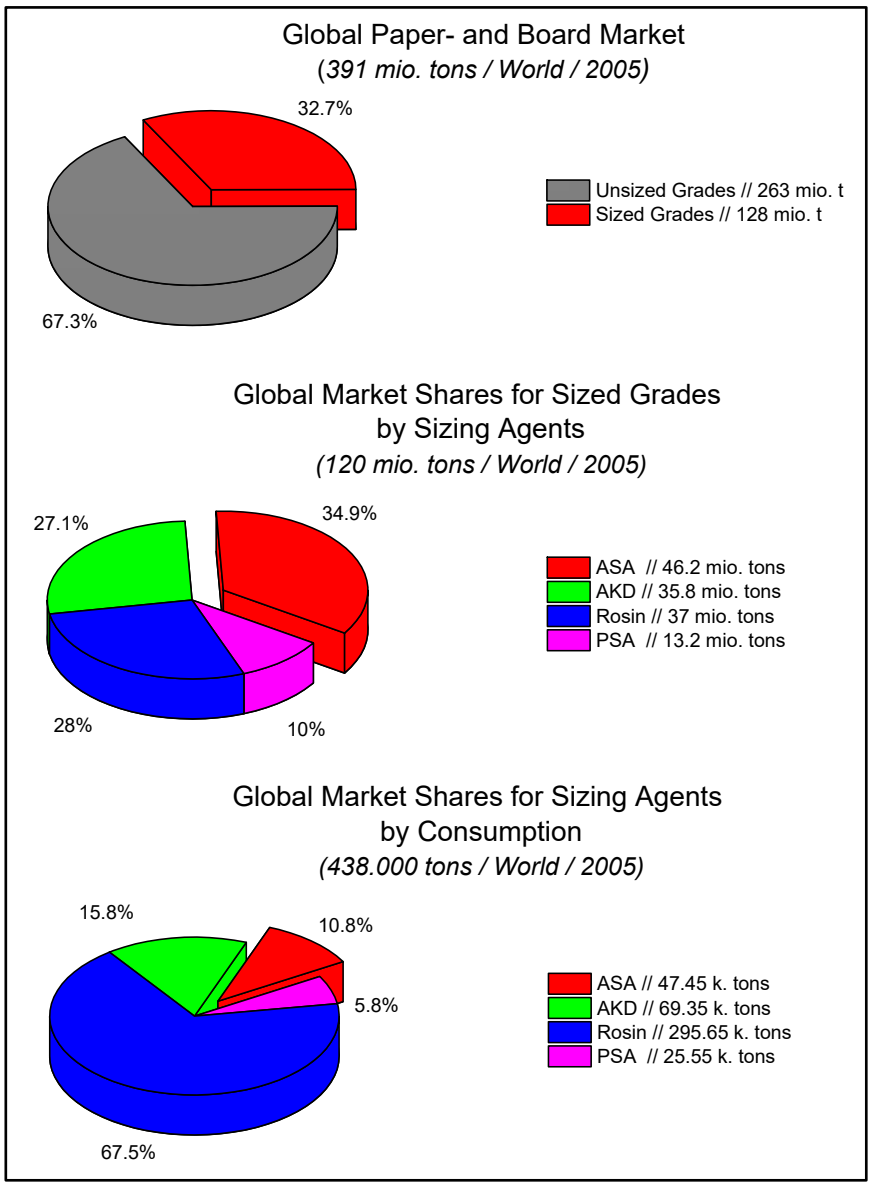

Figure 2.2-2: Global Sized / Unsized Paper- and Board Market, Global Market Shares for Sized Grades by Sizing Agent, and Global Market Shares for Sizing Agents (2005) [10]

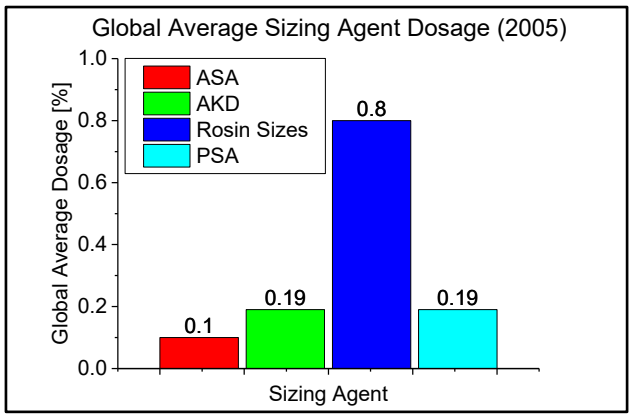

Figure 2.2-3: Global Average Sizing Agent Dosage [10]

2.2.4 Physical and Chemical Background to the Mechanisms of Surface-Wetting and Penetration

Water ad- and absorption, or in other words the sizing degree, is defined by the physical and chemical mechanisms of wetting and penetration. The theories to these mechanisms are very complex in nature and only approximations to the real occurring phenomena with paper as substrate [22, 25]. Simplified, water pickup happens via two phases. The first phase is the initial contact with the liquid, the so-called surface wetting. The second phase, during which the liquid enters into the structure of the substrate, is called penetration phase. In the following chapter both phases will be described by the most used approaches, surface wetting and penetration. The key factors to wetting and penetration are the chemical nature of cellulose (Figure 2.2-5) and the porous structure of the substrate (Figure 2.2-4 [26]).

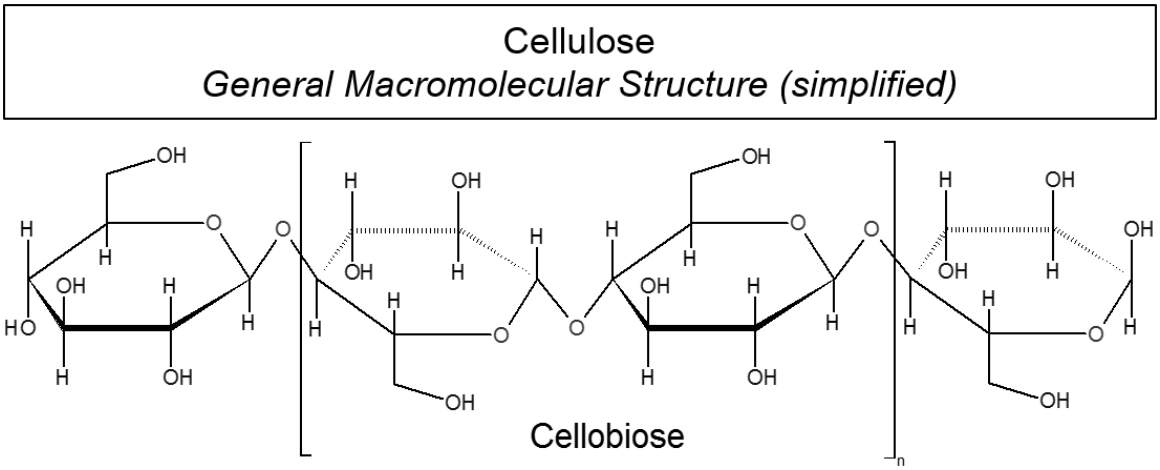

Figure 2.2-5: Cellulose Macromolecule (simplified), with Cellobiose Repetition Unit

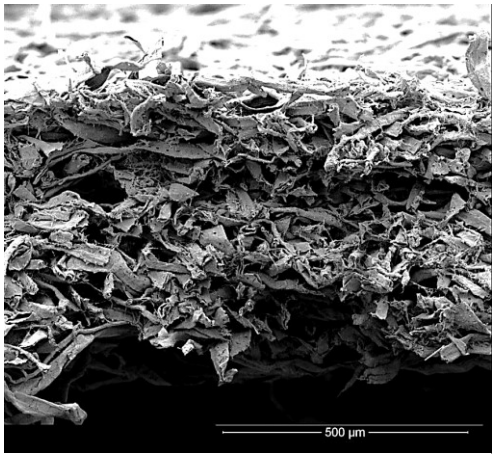

Figure 2.2-4: Z-Directional Break through a Freez-Dryed Paper Sample [26]

With its high amount of hydroxyl groups, cellulose is a hydrophilic molecule and thus contributing to wetting. The molecular structure, as well as the macromolecular arrangement within the fiber walls, will be described in detail in Chapter 2.3.2.1.3. The overall super-structure of the substrate with its multiple pores is creating an enormous void volume in which contact fluids could penetrate. Both factors contribute to the high

water absorption ability of paper sheets which are produced on the basis of natural cellulosic fibers.

2.2.4.1 Surface Wetting

One approach for the description of the phenomena occurring during the first contact between the fiber surface and the wetting fluid, is the Young's model from 1805 [27]. This model defines the wetting behavior by the three vectors of the surface energies at the interphases between liquid, solid and gas (γ_{SF}, γ_{SG}, γ_{FG}) and the resulting contact angle (Θ) (Figure 2.2-6). Furthermore, the theoretical approach by Young was put into mathematical form by Dupree (Equation 2.2-1). A further advancement of Young`s equation is the Young-Laplace equation (Equation 2.2-2) [28].

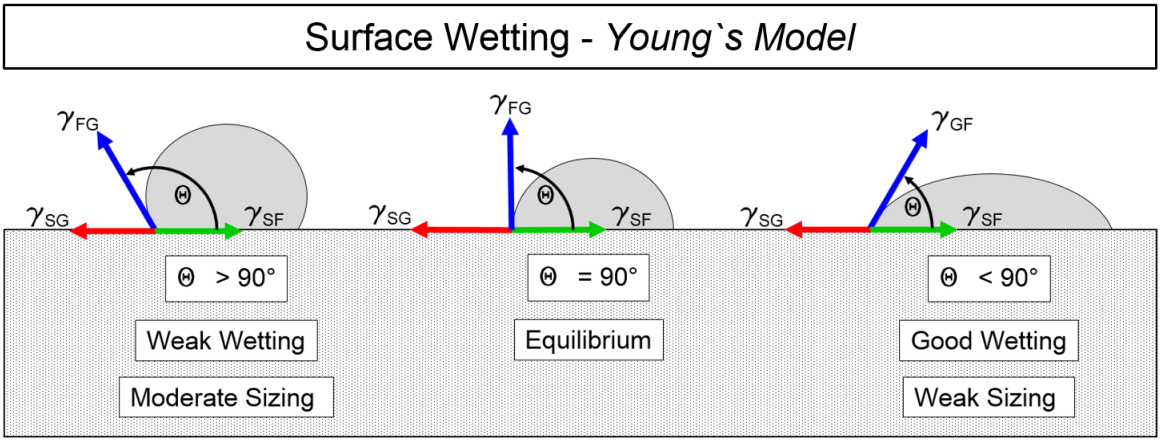

Figure 2.2-6: Surface Wetting according to Young`s Model

$$\gamma_{SF} = \gamma_{SG} - \gamma_{FG} * \cos\Theta$$

Equation 2.2-1: Young's Equation

Θ = *Contact Angle*
γ_{SF} = *Surface Energy at Interphase Solid/Fluid*
γ_{SG} = *Surface Energy at Interphase Solid/Gas*
γ_{FG} = *Surface Energy at Interphase Fluid/Gas*

$$p = \frac{2 * \gamma * \cos\Theta}{r}$$

Equation 2.2-2: Young-Laplace Equation

p = *Capillary Pressure*
γ = *Surface Tension of Liquid Phase*
Θ = *Contact Angle*

This states that the capillary pressure rises with an increase in surface tension of the wetting fluid and a decrease of the capillary radius. The displayed equation derivate furthermore includes the factor $\cos\Theta$ for a specific contact angle at a certain state of wetting. For a contact angle of < 90° the liquid penetrates

spontaneously into the substrate. If the contact angle is = 90° the capillary pressure turns to zero and no penetration will occur and the drop will only spread to the extent until the hydrostatic pressure generated by the drop weight equals the counteracting capillary pressure. When the contact angle exceeds a value of 90°, no spontaneous wetting will occur, because the capillary pressure will turn negative. In this case, pore penetration is only possible by the application of external pressure, which is higher than the capillary pressure.

2.2.4.2 Liquid Penetration

The phenomenon of liquid penetration is described in the following via two approaches which are both based on Young's model, but consider the penetration dynamics. The first approach is the Lucas-Washburn Equation (Equation 2.2-3), which defines the filled pore volume $(\mathrm{V_p})$ after time (t) in respect to the total pore area $(\mathrm{N_p} * \Pi \mathrm{r}^2)$, the liquid surface tension $(\mathrm{r}\gamma_{\mathrm{fl}})$, the contact angle (Θ) and viscosity (η). This means, the higher the surface tension and penetration time, and the lower the contact angle and liquid viscosity, the more liquid enters into the void volume of a single pore.

$$V_p = N_p * \Pi r^2 \sqrt{\frac{r\gamma_{fl} * \cos\Theta * t}{2\eta}}$$

Equation 2.2-3: Lucas-Washburn Equation

V_p = *Filled Pore Volume*
N_p = *Number of Pores*
Πr^2 = *Pore Cross Section Area*
$r\gamma_{fl}$ = *Surface Tension*
Θ = *Contact Angle*
t = *Time*
η = *Liquid Viscosity*

$$\dot{V} = \frac{\pi * p * \mathrm{r}^4}{8 * \eta * l}$$

Equation 2.2-4: Hagen-Poiseuille Equation

$\dot{V}$ = *Volume Flow*
p = *Capillary Pressure*
r = *Capillary Radius*
l = *Capillary Length*
η = *Liquid Viscosity*

The second presented approach is based on the Hagen-Poiseuille equation (Equation 2.2-4). This equation defines the capillary volume flow $(\dot{\mathrm{V}})$ by the capillary pressure (p), capillary radius (r), the penetration liquid viscosity (η) and the capillary length (l). As a result, it can be deducted that the volume flow increases with bigger pores and increasing capillary pressure, lower penetration liquid viscosity and shorter capillaries [11, 22].

Importantly it needs to be stated at this point that all displayed approaches to wetting and penetration are just approximations to the cellulosic system [29]. The formulas do not take into account that cellulose as substrate is not static, nor does it equal any idealized system. The most important features that are not taken into account by the displayed approaches are:

- the fiber surface is rough, not perfectly smooth,
- the pores are no ideal cylinders,
- most of the pores cross other pores,
- the fibers swell during water contact,
- the surface energy is area dependent (crystalline and amorphous regions),
- the surface energy changes during swelling (water cluster formation),
- the pore diameter changes during swelling,
- and the penetration liquid's surface tension changes by picking up salts, extractives and polymers from the fiber surface.

Nevertheless, these formulas are well suitable approximations, which are capable of displaying the main principles [11].

Since, the above-mentioned physical explanations of surface wetting and liquid penetration show quite different approaches, they can only be suited in two ways (Figure 2.2-7) for the implementation in paper sizing.

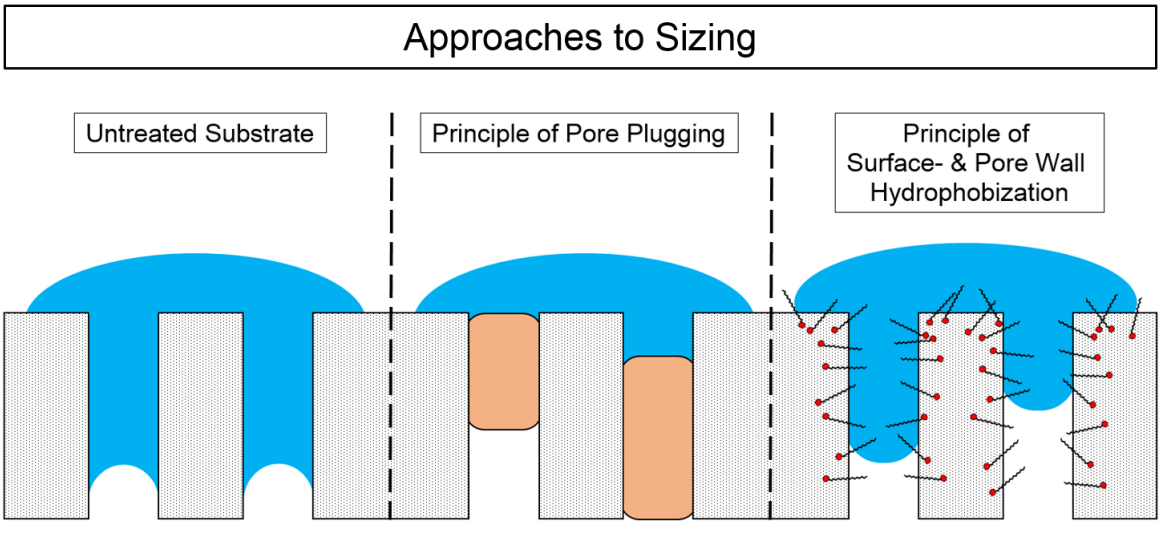

Figure 2.2-7: Approaches to Sizing

The first and traditional approach from the early days of papermaking is the reduction of water absorption by the principle of pore plugging. The use of early

animal- or plant glues caused nothing else, but filling up the substrate voids and pores during tub dipping [30]. This is also valid for sizing by the application of waxes. If the pores are plugged, both penetration equations show that no liquid can imbibe the substrate's structure, and hence, no water is able to penetrate [31, 32]. This is also a phenomenon, which can be observed during the surface treatment with starch, where the sizing degree can also increase [33].

The second and modern approach is the hydrophobization of the surfaces and pore walls by modern sizing agents. During this approach, the surface energy of the solid phase is decreased by the hydrophobic sizing agents to such an extent, that the contact angle between solid and liquid phase exceeds 90°. This means that firstly the laws of the two mentioned surface wetting equations and secondly, as a result of this, both penetration equations are applicable [22, 28, 34].

2.2.5 **Surface and Internal Sizing**

Depending on the final use of the produced grades, the available machinery and the applicable sizing systems, the manufacturer is free to size the paper internally or on the surface. Internal sizing gives a high and very homogeneous hydrophobicity to the paper (Figure 2.2-8). This application is required for grades, which are expected to have longer and more intensive contact to water such as packaging grades, liquid packaging board or copy paper. Even though the substrate shows a comparably higher sizing degree, internal sizing shows some drawbacks. Compared to surface sizing, more sizing agent is required, because less than 100% are retained on the fibers, and the whole stock has to be treated. An additional share is made ineffective by the interaction with other process or functional chemicals. Typical sizing agents for internal application are AKD, ASA and rosin size [11, 35].

If the final product will only be in contact with the penetration fluid for a very short time during processing, surface sizing is sufficient. With surface sizing, the paper is made hydrophobic in the outer layers (Figure 2.2-8) via z-directional sizing agent penetration in a sizing unit such as a size press, a metered size press or a puddle size press. The advantages of surface sizing are the lower required amount of sizing agent, almost no losses, no impact on the effluent quality and significant positive impacts on the substrate's strength properties. A disadvantage is the need

for an additional sizing unit in the paper machine, which leads to higher acquisition costs and to a higher drying energy demand. The typical sizing system used for surface sizing is based on PSAs. Some exotic applications use ASA or AKD [10, 36, 37].

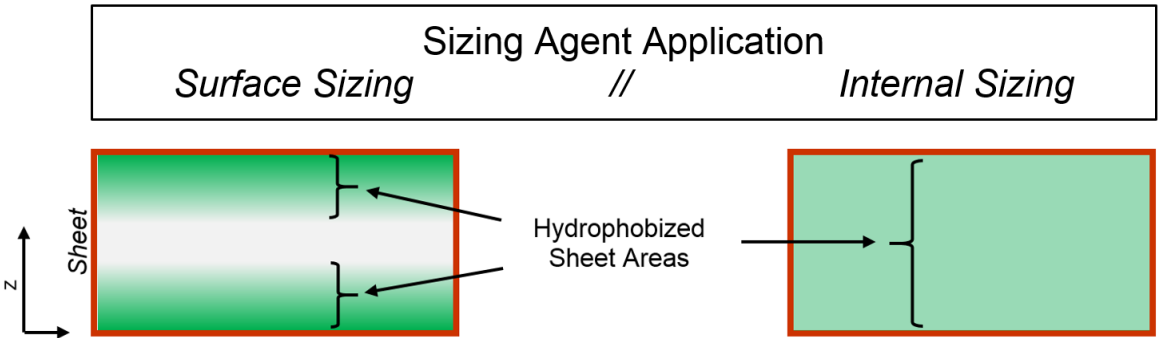

Figure 2.2-8: Surface and Internal Sizing

It is also a common measure to combine the systems of internal and surface application if the product or the process require so [38].

2.2.6 **Sizing Agents**

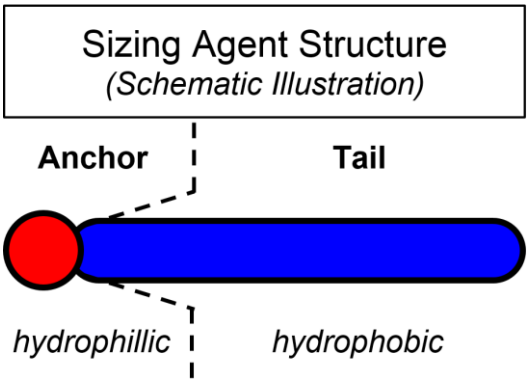

Figure 2.2-9: Sizing Agent Structure (Schematic Illustration)

As stated in Chapter 2.2.4, all modern sizing systems are working on the principle of surface energy reduction, which causes higher contact angles with the penetration fluid water, and therefore, lower liquid penetration. To fulfill this requirement, sizing agents have to have a tenside-like structure, with a hydrophilic anchor and a hydrophobic tail (Figure 2.2-9). Once in contact with the cellulosic system, the sizing agents are supposed to orient with their hydrophilic anchors towards the hydrophilic cellulose and with their hydrophobic tail towards the gas or liquid interface, causing the mentioned reduction in interface energy. The working mechanisms of the main sizing agent groups are explained in detail in the subsequent Chapters. Altogether, in order to fulfill the modern industry's needs, the respective sizing systems should show the following features [23]:

- highly hydrophobic character, once attached to the substrate,
- finely dispersible to provide homogeneous distribution,
- fast and controllable development of sizing performance,
- high degree of self-retention,
- good anchoring on the substrate (covalent, electrostatic or steric),
- low tendency to concurring reactions with water, fillers or additives,
- and high degree of robustness against interaction (e.g., anionic trash, tensides).

2.2.6.1 Alkenyl Succinic Anhydride (ASA)

The sizing agent Alkenyl Succinic Anhydride (ASA) will only be mentioned within this chapter. As the central sizing agent, contributing to this thesis, Chapter 2.3. will describe in detail ASA's basic structure, production, mechanistic reaction models and ways of application.

2.2.6.2 Rosin Sizes

The first step from single sheet tub sizing with animal glues or vegetable gums towards the internal sizing of the whole stock prior to sheet forming was done by Illig in 1807 [39]. He discovered and patented a sizing system, where rosin size was dosed to the stock and afterwards fixated on the fibers with alum. This was the state of the art sizing system for more than one century [40] and the first step to the rise of modern, continuous papermaking. Rosin is a natural product, which has its origin in either gum resins, wood resins or tallol resins. Gum resins are harvested by tapping trees, mostly pines, and collecting the bled out resins. Wood resins are produced by the steam distillation of tree stumps and roots, and tallol resins by processing black liquor from mostly softwood kraft or alkaline processes [11, 21].

All rosin resources share their composition of the same natural rosin acids, which in general belong to the group of tricyclic di-terpene acids as displayed in Figure 2.2-10 [11]. These rosin acids are extracted and purified during processing, and by this separated from terpenes and other lower molecular components. In order to enhance their performance and applicability, the resins are treated via various approaches to make them suitable for the use as a modern sizing agent [21].

Nowadays, the most commonly used approach to increase the rosin acids' performance, is the so-called fortification. During this step, the rosin acids are reacted with mostly fumaric or maleic acid via Diels-Alder reactions at elevated temperatures of ~ 200 °C (Figure 2.2-11). The benefits of fortified rosin are a enhanced processability during saponification, an increased dispersion stability, and a higher sizing performance, all triggered by the increased amount of carboxylic acids or acid anhydrides. This beneficiation step is usually conducted to an extent of 10% - 25% fortified rosin [21].

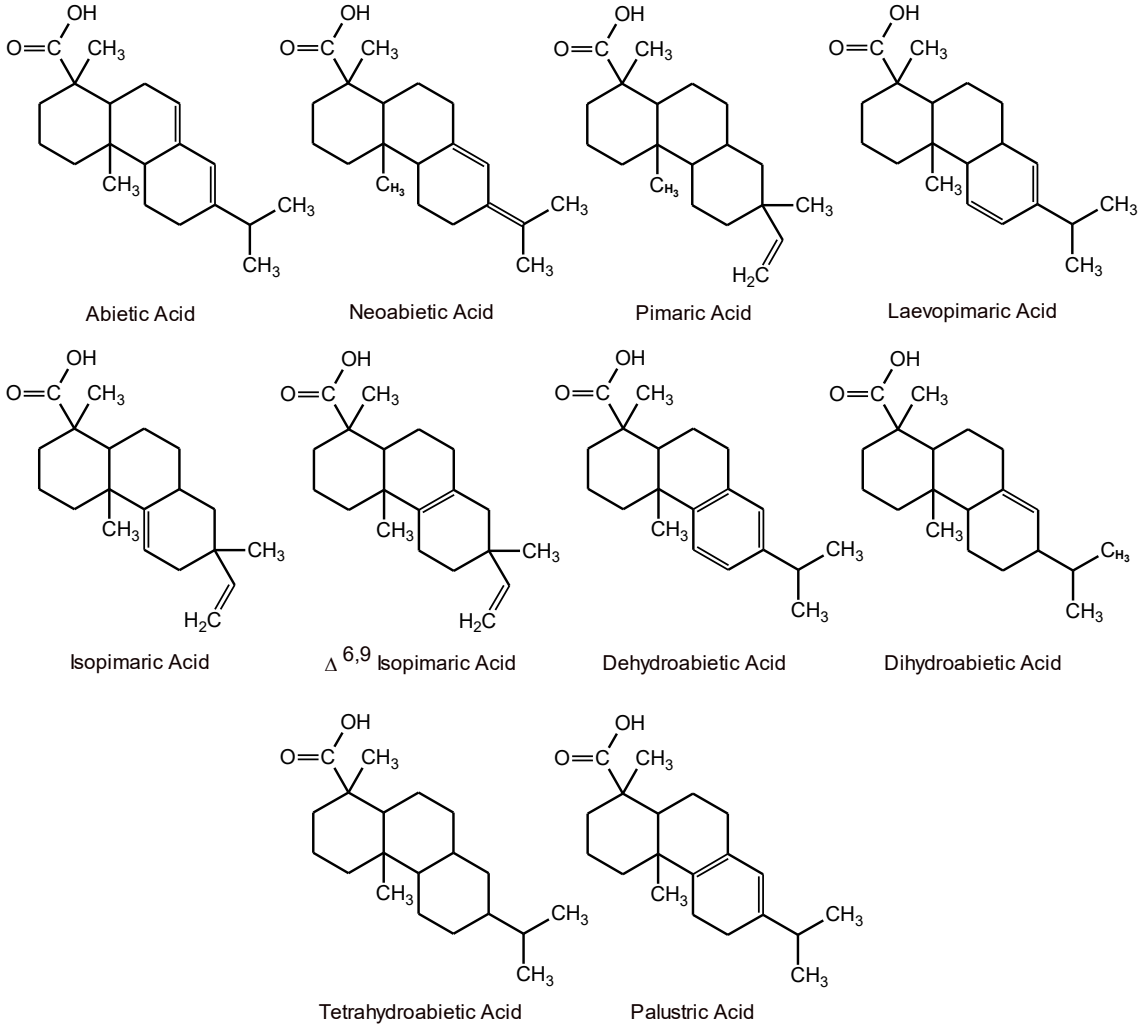

Figure 2.2-10: Rosin Acids

Being a water insoluble solid material, the rosin products need to be transferred into an industrial applicable form, i.e., soaps and dispersions. Rosin soaps, the traditional form of rosin sizes, are produced by the alkaline reaction of rosin acids with potassium or sodium hydroxide (Figure 2.2-12) [21, 41, 42]. This so-called saponification is never conducted completely, because a residual amount of rosin

acids guarantees better sizing performance. Rosin soaps are hydrophilic and water soluble and can thus be applied to the stock as aqueous solutions [41].

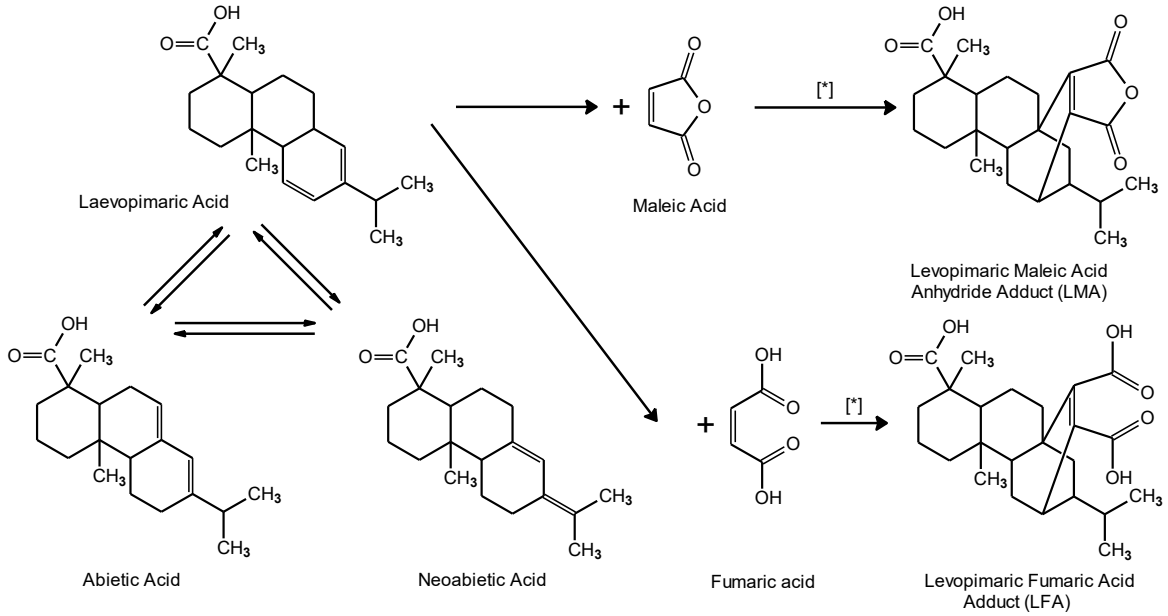

Figure 2.2-11: Rosin Fortification

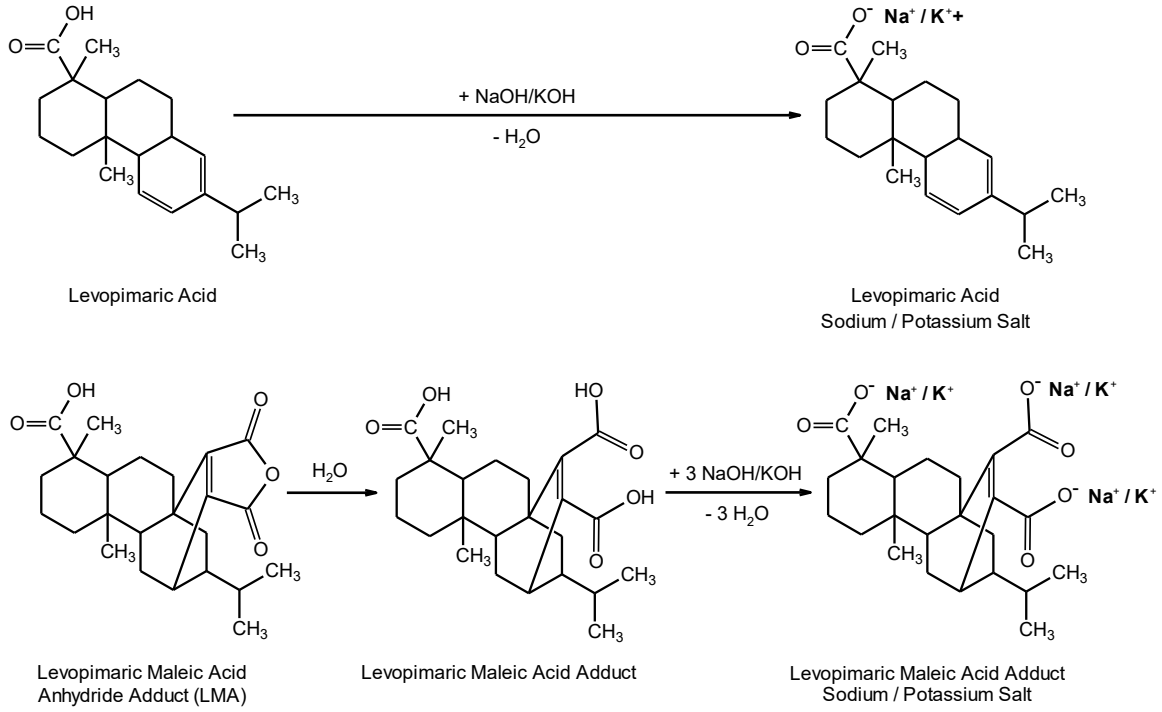

Figure 2.2-12: Rosin Saponification

The other approach, and recently most common, is not based on the chemical modification of the rosin acids, but on their already above-mentioned dispersion. During this step, the rosin acids are emulsified at elevated temperatures and

stabilized by e.g., casein, starch, surfactants or polymers as protection colloid. Emulsification is described by the example of ASA in Chapter 2.3.1.3.1.

The benefit of this procedure, on the one hand, is a higher sizing performance [21], and on the other hand, the possibility to adjust the surface charge of the protection colloid by the choice of stabilizer. On this basis, the rosin dispersions can be modified either anionic, cationic or nonionic, contributing to the paper manufacturing process needs [43, 44].

Rosin Sizing Mechanism
(Schematic Illustration)

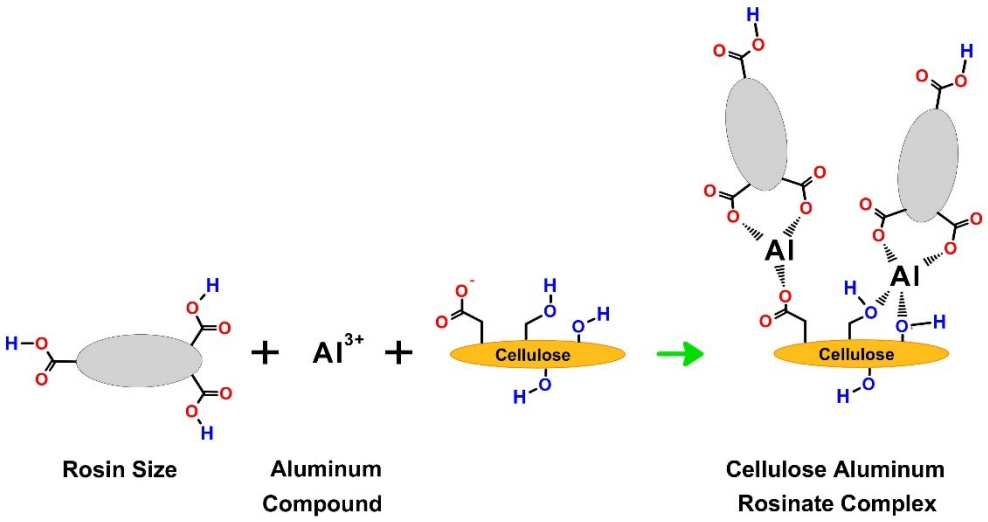

Figure 2.2-13: Rosin Sizing Mechanism (Schematic Illustration)

As already mentioned by Illig [39], rosin sizes require fixation on the cellulose [45]. The traditional fixation system was based on the use of alum ($Al_2(SO_4)_3$) at acidic conditions (pH 4 – pH 5.5). For papermaking at higher pH values (pH 5 – pH 7.5), alum could not be used anymore, caused by its structural switch to $Al(OH)_3$ and the along going loss of cationic charge. Therefore, it needed to be substituted by polyaluminum compounds like PAC or PAN. The schematic sizing mechanism of rosin sizes with aluminum ions as mordants is displayed in Figure 2.2-13.

Some other papers did also mention the fixation potential with polyamine, polyethylenimine-epychlorhydrin, metal ions in combination with polyethylenimine, ferric and ferrous mordants, or even without mordants [46-50]. The actual development of sizing performance happens in the drying section of the PM. Starting at a dry content of 60% to 65% and temperatures between 90 °C and 105 °C the rosin particles begin to melt and spread over the cellulose`s surface.

While spreading, the rosin molecules bind to alum or poly aluminum compounds (or other applicable mordants) and develop a so-called aluminum-rosinate-complex [10]. This complex builds up a proper and stable layer on the cellulose and with its hydrophobic properties it develops the degree of sizing [21]. This sizing system is a non-reactive system. That means that no covalent bonds are formed between the rosin particles, the alum and the cellulose.

2.2.6.3 Alkylketen Dimer (AKD)

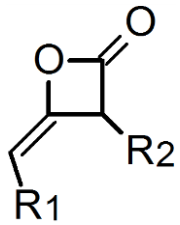

Figure 2.2-14: Basic AKD Structure

AKD (alkylketene dimer) was initially developed in the 1930s for the hydrophobization of textile fibers and fabrics. It was first mentioned in the 1950s for the sizing of paper [51, 52], and thus became the first additive of the group of reactive paper sizing agents. Until the 1970s, the major change from acidic to neutral papermaking, AKD had significant problems establishing on the market, because its sizing process in acidic conditions was hard to control. The rise of AKD happened, when the first production systems changed to alum free production and to neutral or alkaline conditions. AKD showed its advantages for the sizing of GCC or PCC filled paper grades, making it indispensable for modern papermaking [21, 53-55].

In principle, AKD sizes show the chemical structure displayed in Figure 2.2-14, which is, as described in Chapter 2.2.2 & 2.2.6, of a tenside-like nature [56]. Its basic components are the hydrophilic anchor, a reactive ß-keto lactone ring and the aliphatic, hydrophobic rests, composed of two hydrocarbon chains, with a chain length of 7 to 22 carbon atoms. The longer these rests are, the higher the hydrophobic character of the AKD molecule is as such. AKD sizes are traded in three major product groups,

- standard AKD, composed of a mixture of C16 and C18 rests, with the origin of palmitic and stearic acid. These types are the ones used most for commodity sizing.
- liquid AKD, composed of a mixture of C16 to C18 unsaturated olefin rests, with the origin of isostearic or isopalmitic acid. The hydrolysis products of these types show a lower migration tendency within the paper and cause less

debris on the PM. The drawback is a lower sizing efficiency compared to standard AKD products.

− high melting point AKD is composed of a mixture of higher aliphatic rests in the range C18 to C22. They have their origin in stearic and behenic acid, which show a very high sizing performance for special paper grades, but therefore require high drying temperatures [10, 54-57].

The above-mentioned fatty acids, the raw materials for the production of AKD, derive with no exception from natural sources like waxes or animal fats. The fatty acids are first extracted from the raw materials by lipolysis and afterwards transformed into AKD via the principle displayed in Figure 2.2-15.

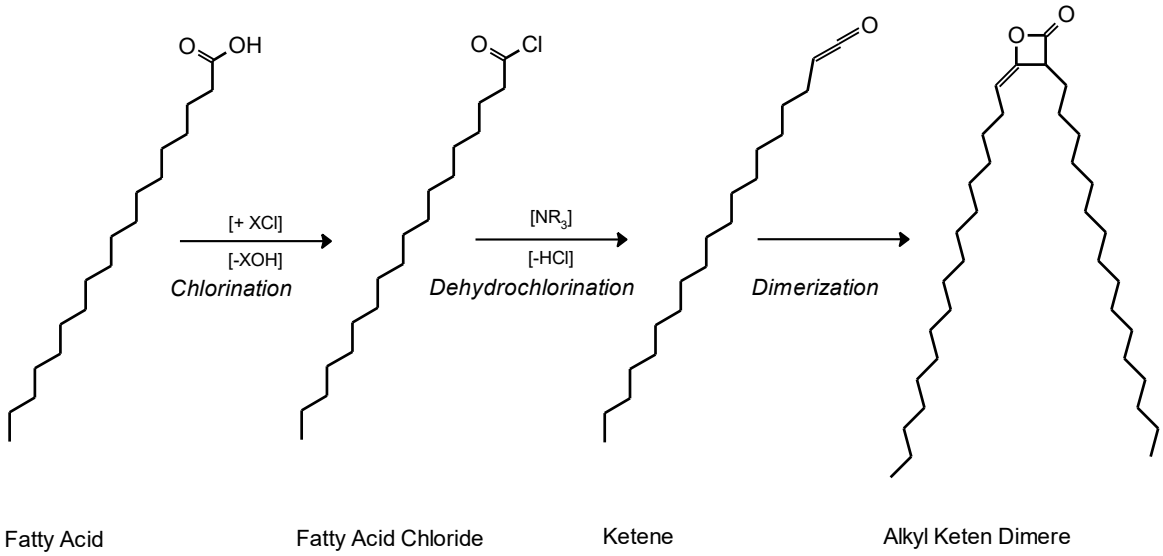

Figure 2.2-15: AKD Production

The fatty acids are at first chlorinated into their respective fatty acid chloride, and subsequently dehydrochlorinated by a tertiary amine (NR_3). The resulting Ketene is instable and dimerizes autonomously into an alkylketene dimere. The fatty acid chloride dimerization was commonly conducted under solvent atmosphere, e.g., toluene or organochlorides. In order to use AKD products for food and beverage packaging grades as well, a solvent free method was invented in the mid 1990s [11, 21, 51, 54, 56].

With the exception of liquid AKD, which is an oily substance at room temperature, all AKDs are hydrophobic, waxy substances with melting points between 40 °C and 65 °C. Driven by their insolubility in water and their high reactivity toward water (hydrolysis), AKDs need to be emulsified and stabilized prior to use, in order to

enable a successful addition to the stock. Modern AKDs are mostly stabilized by cationic starches [54, 55]. The emulsification process and the emulsion details are explained in on the example of ASA in Chapter 2.3.1.3.1.

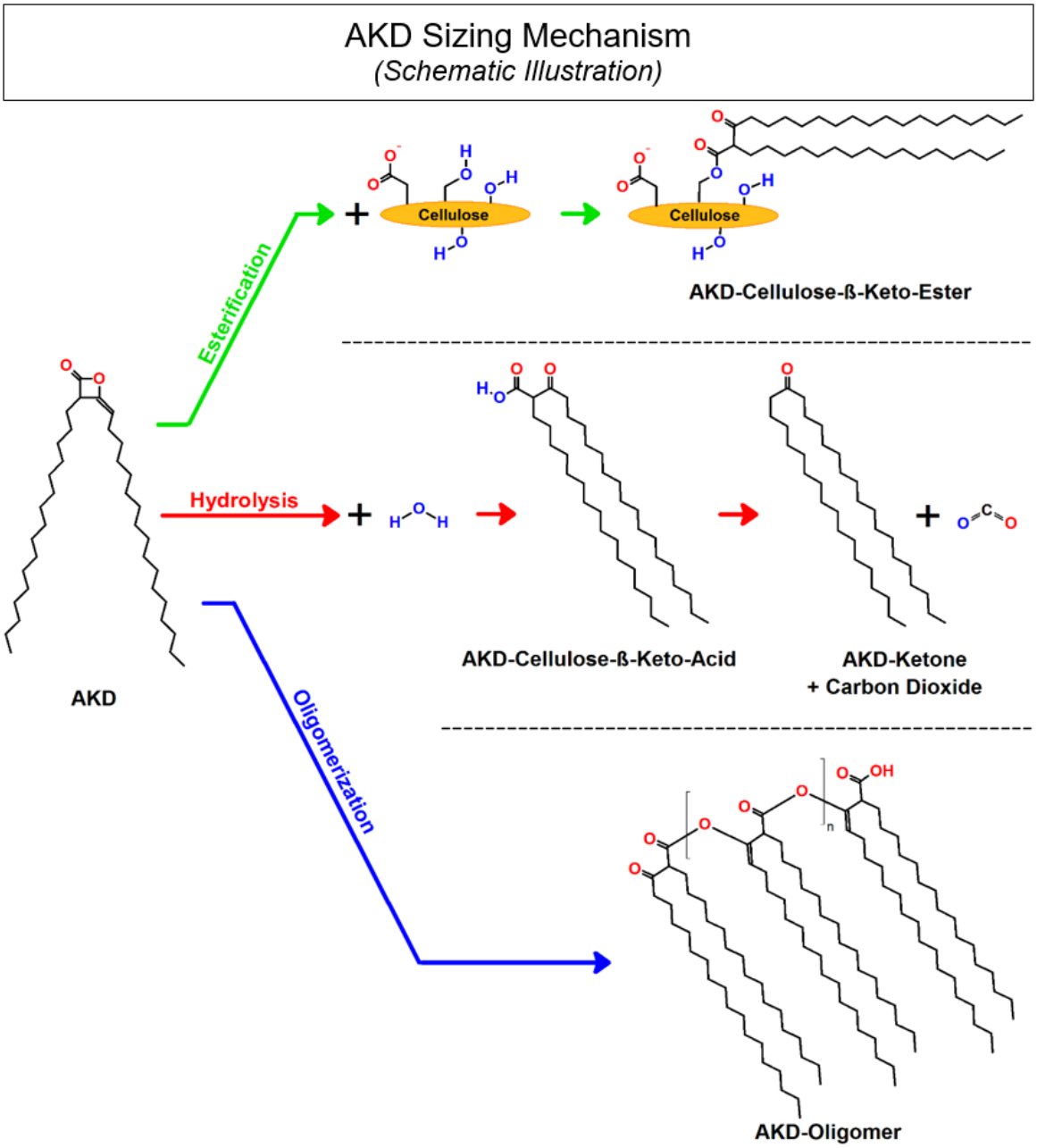

Figure 2.2-16: AKD Reaction Mechanisms (Schematic Illustration)

Ever since the first publications, the reaction mechanism of AKD (Figure 2.2-16), as so-called reactive sizing agent, is in the focus of controversial discussions [23, 55, 58-60]. The traditional reaction model states that the hydrophobizing performance of AKD is based on the generation of ester bonds between the AKD molecule and the celluloses' hydroxyl groups [55, 57, 61-63]. The product of this reaction, an AKD-Cellulose-ß-Keto-Ester, is, from the model point of view, capable

of generating a high extent of hydrophobicity by shielding the cellulose surface with its aliphatic rests. Even though this approach is quite plausible from a theoretical point of view, several papers have shown that the ester bond does only occur to a minor, or to no share, and by this, a different principal mechanism model based on a higher share of AKD ketones and AKD oligomers has to be taken into account [64-67]. The current mechanism models, which are based on the findings of the recent years, describe the sizing process with AKD via the steps of retention, spreading and chemical reaction [55]. During the retention step, the AKD particles which are finely dispersed and either anionically or cationically stabilized, are retained on the fiber/filler surface either by self-retention or by retention aids. The spreading step starts after pressing in the dryer section. Beginning at temperatures ranging from 50 °C and 60% dry content, the protection collide breaks open and releases the fine AKD droplets, which begin to melt and spread over the cellulose surface, driven by capillary and interface forces. The better and more homogeneous this spreading happens, the better is the final sizing performance. The last step, which begins at a dry content of 80%, is supposed to be the generation of covalent bonds. The major part hydrolyzes to ketones and oligomers and remains on the cellulose unbound. The final sizing degree is said to be directly related to the amount of bound AKD and the orientation of the unbound AKD-ketones and oligomers. If these orient with their hydrophilic anchor away from the celluloses, the sizing degree is significantly decreased [54, 55, 57-60, 62, 64-75].

2.2.6.4 Polymeric Sizing Agents (PSA)

Polymeric sizing agents are macromolecular substances especially designed for surface sizing applications. Their focus of use lies within applications, where conventional sizing additives cannot be used. This is the generation of very hard sizing degrees, which can only be obtained by the combination of internal and surface sizing, as well as the sizing of systems which are not sizeable with conventional sizing systems. Examples for the second case could be a too high system conductivity or trash load, a production pH out of the operation window of standard internal sizing agents, the requirement for instant on/in machine sizing degree development, or just the need to prevent any typical interactions known from standard sizing systems. PSAs are usually applied in combination with starch in aqueous solutions via a sizing unit. The benefit of surface sizing with PSAs is

that it does not only lead to a hydrophobization of the paper`s surface, but also to advanced strength properties caused by the starch [36, 37, 76].

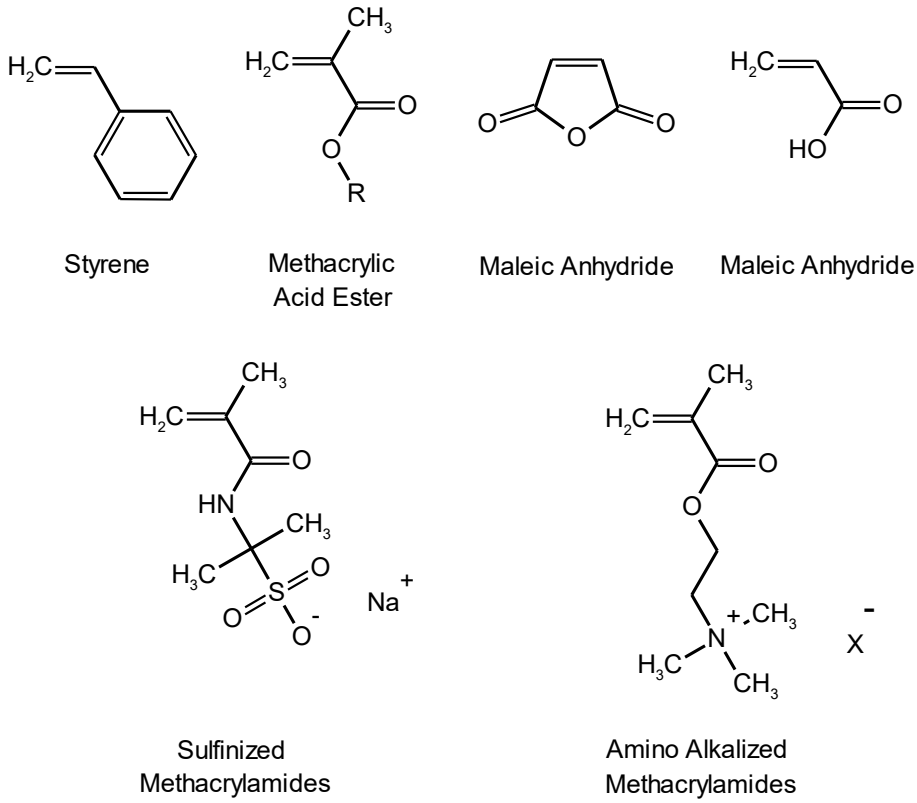

Figure 2.2-17: Main PSA Monomers

Contributing to their main chemical structure, synthetic polymeric sizing agents can be clustered into the following groups:

- Styrene Maleic Acid Anhydride Solution Polymers (SMA) and Styrene Acrylic Acid Solution Polymers (SAA)
- Styrene Acrylate Emulsion Polymers (SAE)
- Poly Urethane Micro Dispersions (PUD)

For the production of the sizing active polymers out of the group of SMAs, SAAs and SAEs, the following, unsaturated modified olefins are required (Figure 2.2-17) [36, 76-78]. Due to their minor importance, polyurethane based PSA compounds are not displayed within this thesis. Monomers, such as styrol or methacrylic acid ester, give the hydrophobic character to the polymer, while anionic or cationic monomers, such as sulfonated methacrylamides or amino alkalized methacrylamides, give the hydrophilic character and the anchoring ability. The sizing mechanism of PSAs can be understood as displayed on the example of a

cationic modified polymer in Figure 2.2-18. PSAs are added to the paper sheet via a sizing unit as aqueous dispersion of very small particle size (<< 1 µm). These dispersion droplets break up during the subsequent drying steps, whereas the polymers spread over the fiber surface. Their active charge centers interact during spreading either with the anionic surface charge of the cellulose or with additionally induced mordants [79]. The final substrate hydrophobization is a result of the surface coverage by the PSAs and of the orientation of the hydrophobic polymer sections. A typical application field for PSAs is the production of copy paper. Copy paper is mostly sized internally by AKD, ASA or rosin and then additionally on the surface by PSAs to provide sufficient printability [28, 36, 37].

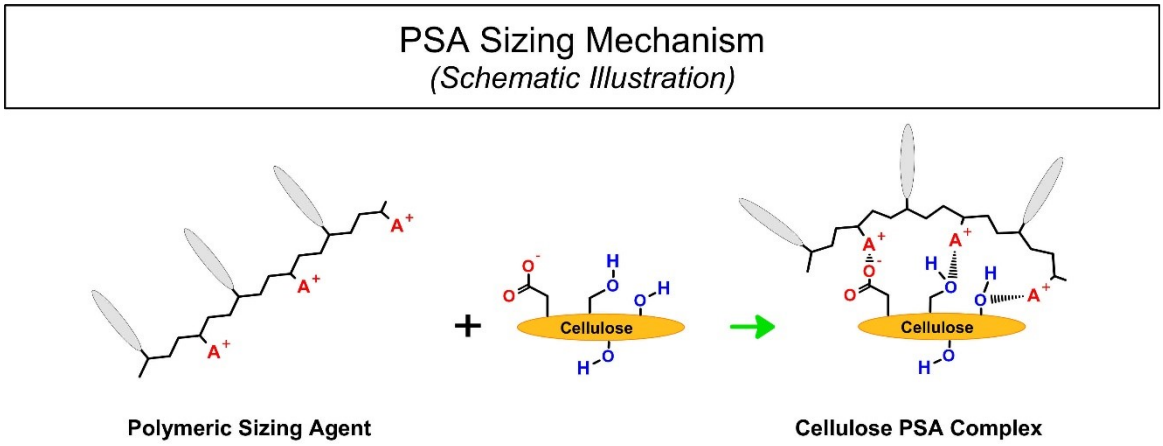

Figure 2.2-18: PSA Reaction Mechanism (Schematic Illustration)

2.2.7 **Determination of the Sizing Degree (Performance Analysis)**

The final sizing degree, as explained in Chapter 2.2.4, can be described as a time-dependent sum parameter of liquid adsorption and absorption. Therefore, this sum parameter has to be defined and controlled, in order to fulfill either the converting or final product demands. Several methods based on different principles for the measurement of the ad-/ absorptive substrate properties have evolved over the ages of paper sizing. Due to the dynamics and the dens interlock, none of the available methods is capable to definitely differentiate between surface wetting and penetration. The most important ones will be described during the following, whereas the methods of contact angle measurement, Cobb water absorption and ultra sonic penetration analysis will be described in detail, as they were used during the practical part of this thesis.

2.2.7.1 Cobb Water Absorption

The most widely used method for the determination of the sizing degree in the industry is the Cobb method. The sizing degree is defined by this method as the substrate's water pick up per area over a defined contact time. The measurement area for Cobb testing is circular with a size of 100 cm². For the measurement, the sample is wetted with 100 ml of water in a measurement cylinder from one side. This amount of water generates a water column of 10 mm, causing a constant hydrostatic pressure, which is prerequisite for comparable water pick up results. It is important to mention that this method is only suitable for the determination of the sizing degree of a specific paper side, and thus it is prerequisite that the water does not penetrate the paper sheet completely. If full penetration occurs, the contact time has to be minimized. After the water contact time (e.g., 30 s, 60 s, 120 s, 300 s or 1800 s) has elapsed, the extent of surface water is removed by filter paper and the weight difference between the wet sample and the dry sample is measured. This weight difference is then calculated to an area of 1.0 m² and announced as g/m² (Chapter 4.2.1.1).

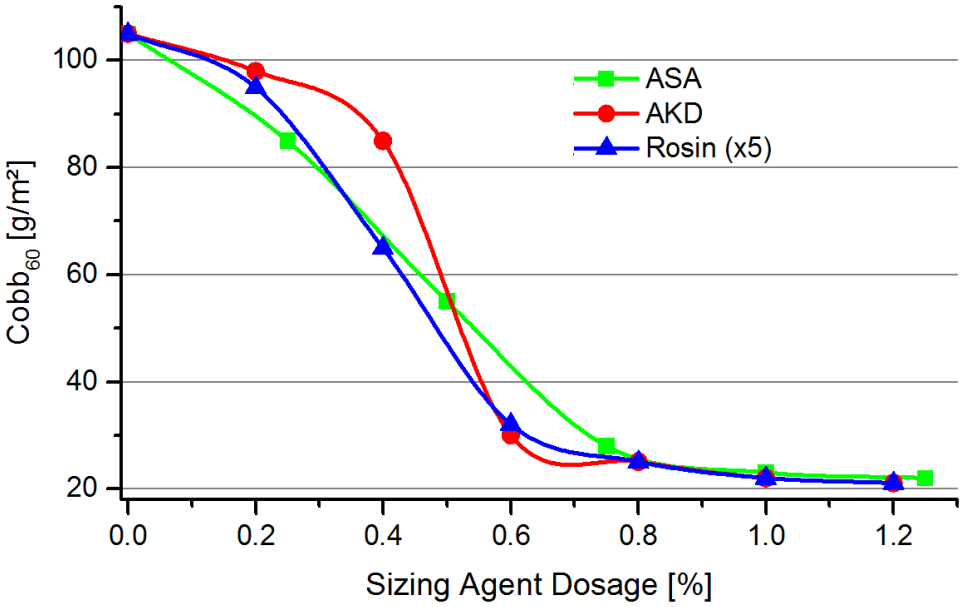

Figure 2.2-19: Cobb Sizing Profiles at Neutral Conditions (values originate [82])

The exact measurement principle as well as the measurement devices, are described by the regulation DIN EN ISO 535 [80] and by the Tappi Test Method T 441 om-98 [81]. Typical values for $Cobb_{60}$ measurements can reach from 15 – 20 g/m² for hard sized grades, up to the extent of the sample's base weight or even beyond for soft or unsized grades. $Cobb_{60}$ values for printing grades

(e.g., copy paper) range in the area of 20-30 g/m². Figure 2.2-19 [82] displays typical Cobb sizing profiles at neutral conditions for the sizing agents ASA, AKD and Rosin at a base weight of 70 g/m².

In order to fit the curves on one graph, the rosin dosages were divided by factor 5. The raw material for the displayed trials was based on virgin fibers, with 15% GCC, 0.8% starch and compozil as retention system.

2.2.7.2 Contact Angle Measurement

Contact angle measurement is a modern optical analysis method, which is suitable to determine the adsorption and absorption behavior during the first seconds of liquid contact [29, 83, 84]. The measurement principle for paper as substrate is described in the Tappi Test Methods T 458 0m-04 [85] and T 558 om-97 [86]. For analysis, a purified water droplet of defined volume is applied onto the surface of the substrate. From the very moment of the first contact, a camera is taking pictures of the droplet, capturing its shape and the penetration behavior into the substrate. An implemented software is calculating the contact angle and the droplet volume based on the drop outline and the paper surface as displayed in Figure 2.2-20.

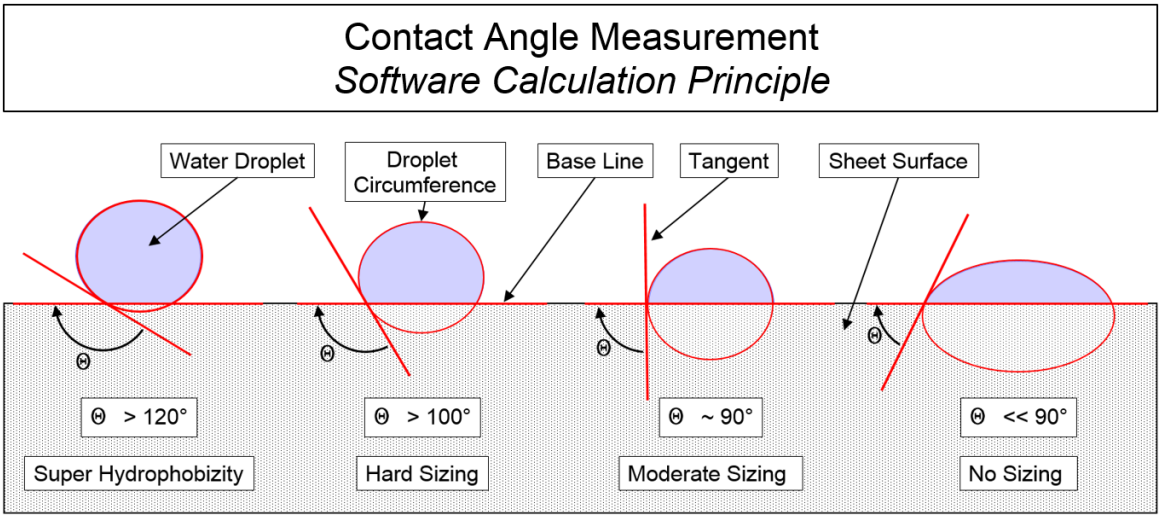

Figure 2.2-20: Contact Angle Measurement

The contact angle can be measured either statically or dynamically. The static measurement is either done by capturing a single image right after the drop has touched the surface, by including a short delay time, in order to minimize measurement deviations by drop vibration, or after a defined contact time. The results of the direct measurement provide a good foundation for the interpretation

of the substrate's surface hydrophobicity, and can thus be properly implemented for the determination of printing properties. Static measurements after a defined delay time deliver values, representing the time dependent penetration rate. More commonly used is the combination of both above-mentioned approaches by dynamic contact angle measurement over a variable contact time. This method on the one hand, gives results for the substrate's initial surface hydrophobicity and therefore on its wetting behavior, and on the other hand values for the fluid penetration over the contact time. It has to be considered during dynamic analysis and longer contact times that for low contact angles, and thus higher penetration rates, the substrate swells. This causes a substrate build-up under the drop with an along going position change of the actual base line. This position change cannot be respected by the calculation software, which can cause contact angle deviations or even false values.

Initial contact angle values can vary from << 90° for low or unsized grades, over 90° - 100° for moderate sized grades, up to > 100° for hard sized grades. Samples exceeding values over 120° are considered as super hydrophobic and shall not be confused with sized grades. Super hydrophobicity can only be obtained by special surface treatment [87-89].

2.2.7.3 Penetration Dynamics Analysis

Penetration dynamic analysis (PDA) is a modern sizing degree evaluation method, based on time-dependent sound wave attenuation in liquid phase through a fibrous substrate. The measurement principle relies on the structural losses of a cellulose-based substrate, once in contact with water. These losses are caused by water penetration and fiber swelling, and their evolution, as well as their extent, are highly dependent on the sizing degree.

For the measurement, a paper sample is taped onto a sample holder plate and then rapidly shot into a chamber with distilled water. In this chamber an ultrasonic sender unit fires high frequency (2 MHz) and low energy sound waves through the paper sample, which is positioned between sender and receiver unit (Figure 2.2-21). While being forced through the paper sample the sound waves are attenuated by reflection, absorption and scattering. The measured intensity at the sensor is highly dependent on the degree of water penetration. The penetration-

time depending results of the US-measurement are analyzed by software, allowing a differentiation between surface wetting and penetration.

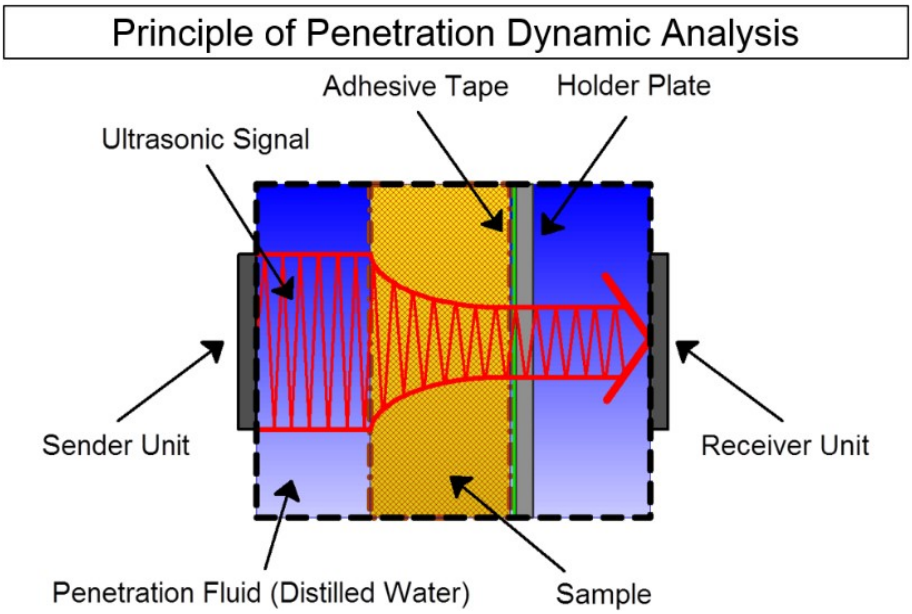

Figure 2.2-21: Principle of Penetration Dynamics Analysis

Looking at an idealized PDA measurement curve of a moderately sized substrate (Figure 2.2-22), it is visible that the curve can be divided into two sections.

The first, a section of signal intensity increase, stands for the process of surface wetting. During this time, water suppresses the entrapped air from the sample surface. By this suppression, the contact area of water and substrate is increased and the damping properties of the surface air are reduced. This causes an increase in signal strength. The moment the surface wetting reaches its maximum is the moment of highest signal intensity, and thus a measure for the surface hydrophobicity. The longer the duration until the maximum value is reached, the higher is the surface hydrophobicity. This is caused by higher interactions between the hydrophobic sheet surface and the hydrophobic air, making it harder for water to suppress the air. The point of maximum intensity is defined as t_{max} value and measured in seconds. The second section is dominated by water penetration and an along going intensity loss. Water penetration causes fiber swelling, a loosening of fiber bond energy, and by this, a more flexible substrate structure. This leads to a higher extent of signal attenuation, driven by weaker sound conductivity of the now more elastic substrate structure. The degree of sizing defines the amount of water that is able to penetrate the structure per time unit and hence also the degree

of signal attenuation. The value used for the determination of the substrate's structural hydrophobicity is the time until a 40% signal intensity loss has occurred (t_{60} [s]) [90-92].

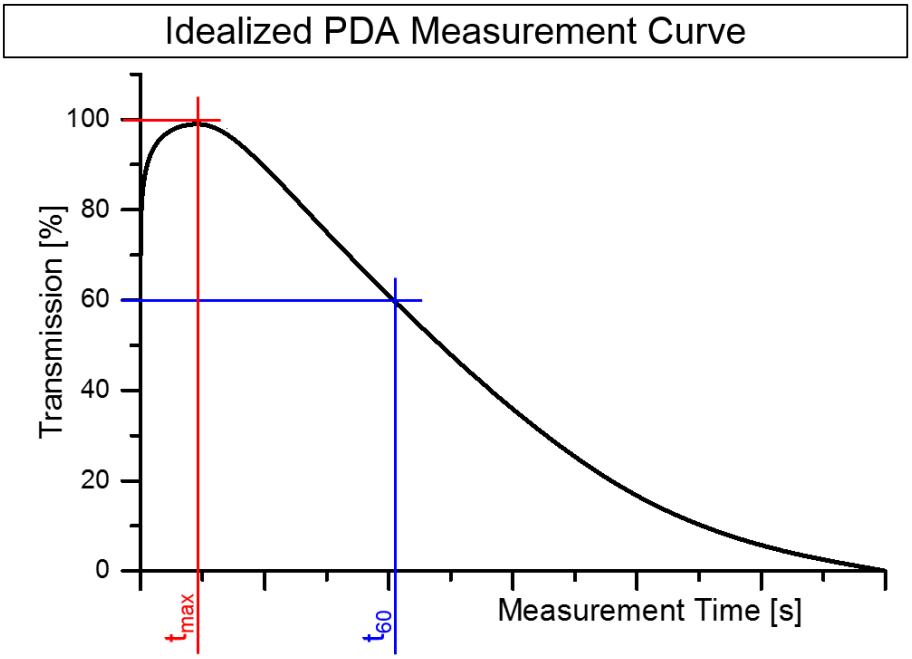

Figure 2.2-22: Idealized PDA Measurement Curve

2.2.7.4 Further Qualitative Analysis Methods

Further qualitative analysis methods for the determination of the sizing degree that are available and commonly used, but of no importance to this thesis are e.g.:

2.2.7.4.1 *Ink Stroke*

The ink stroke method is one of the oldest and most basic sizing degree analysis methods. For measurement a hash shaped symbol, consisting of four single strokes with four crossings, is drawn on the paper surface by a standardized feather. The stroke thickness is set to 1/100 of the sample's base weight in mm and the ink used is a blue standard ink. Sizing analysis is carried out based on personal observation, whereas the paper is considered as sized, when the ink does not strike through after 24 hours of storage. The detailed procedure and the device are described in the German standard DIN 53126 [93].

2.2.7.4.2 *Immersion Test*

The immersion test is suitable when the total water pick up capacity, when submerged in water completely, needs to be analyzed. For testing, the specimen

is submerged in water for 10 minutes ensuring that no air bubbles are entrained. The analysis is done, by comparing the dry weight with the wetted specimen weight, after removing the surplus of water with blotting paper. A total submersion respects the penetration of water not only from the top- and backside, but also from the cutting edges, which can be of highest importance for some specific grades such as photo paper or liquid packaging board. The detailed procedure is described in the Tappi Test Method T 491 om-95 [94].

2.2.7.4.3 *Floating Test*

Even though it is still widely used, the floating test is a very basic, not standardized method. For analysis, a square-shaped paper vessel is put on a water surface, with the side to measure in water contact. Analysis is carried out by measuring the time until a certain percentage (usually 50%) of the vessel bottom is soaked with water. For special products like plaster board liner, the floating test can be conducted under elevated temperatures (~ 90 °C) to simulate the hot water resistance of the product.

2.2.7.4.4 *Hercules Sizing Tester (HST)*

The Hercules sizing tester is a device which optically measures a substrate's penetration resistance against a standardized acidic ink. This device is most commonly used in the North American market. The measurement principal is based on a reflectance measurement which is calibrated to 100% for the untreated paper sample. As soon as the ink penetrates, the paper shade gets darker and the reflectance is reduced. The device measures the time elapsed, until a certain degree of reflectance (e.g., 50%) is reached. The detailed measurement principle as well as the measurement device are described in the Tappi Test Method T 530 om-96 [95].

2.2.8 Sizing Agent Detection (Qualitative Analysis) and Determination of the Sizing Agent Content (Quantitative Analysis)

For the analytical approach to sizing agent detection, a series of different measurement principles and multiple approaches are available. The plain detection of a substance, in this case a sizing agent of well-known chemical structure, is a basic analytical approach. Nevertheless, it is only possible to give information on the exact amount of sizing agent in the sheet structure with previous calibration, making the approach a lot more complex and therefore time consuming. The most common methods for sizing agent detection and quantitative analysis are listed in the following, separated by destructive and non-destructive methods.

2.2.8.1 Destructive Methods

The most common destructive analysis methods which are used for sizing agent detection, are extraction based. These are high performance liquid chromatography (HPLC) [31, 75, 96-100], nuclear magnetic resonance spectroscopy / ^{14}C labelling [57, 60, 62, 68, 101-103], gas chromatography (GC) [104-106], liquid chromatography – mass spectroscopy (LC-MS) [60, 98, 107], x-ray photoelectron spectroscopy (XPS) [29, 74, 108, 109], gas chromatography – mass spectroscopy (GC-MS) [97, 110], inverse gas chromatography (IGC) [29] or photometric titration [111].

Further destructive methods which are based on the principle of thermal disintegration, are pyrolysis – gas chromatography (Py-GC) [101, 109, 112, 113] and pyrolysis – gas chromatography – mass spectroscopy (Py-GC-MS) [114, 115]. These methods do not require a previous extraction step and can thus be directly conducted with the sample to be analyzed.

Specially available semi destructive analysis methods are time of flight - secondary ion - mass spectroscopy (ToF-SIMS) [116-119], which can also be implemented for xy-mapping issues, and direct analysis in real time – mass spectroscopy (DART-MS) [120]. These methods are considered semi destructive, because the sample as such remains undestroyed, but the sample's surface undergoes chemical and physical changes by the removal of surface molecules during electron treatment.

2.2.8.2 Non Destructive Methods

Nondestructive approaches to sizing agent determination are with no exception of optical nature. Their measurement principle is based on the absorption/transmission spectra or specific molecular groups, which are representative for the analyzed substances. The most common approaches are infrared - / Fourier transformed infrared spectroscopy (IR/FTIR) [74, 97, 101, 121, 122], near infrared spectroscopy (NIR) [31, 110, 123] and Raman spectroscopy [124-126].

2.3 Alkenyl Succinic Anhydride (ASA)

Alkenyl Succinic Anhydride is, as stated in Chapter 2.2, the most important sizing agent nowadays and key sizing agent to the content of this thesis. The following Chapter will therefore give an overview over ASA's historical background, its production, chemical mechanism models, application and processing, causes for interactions during the sizing process as well as the most important physico chemical aspects during sizing. ASA, whose basic structure is shown in Figure 2.3-1, was first mentioned for the hydrophobization of cellulose based textiles in 1959 [127], and finally implemented as paper sizing agent in 1963 [128].

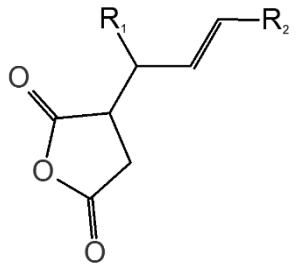

Figure 2.3-1: ASA Basic Structure

Today about 1/3 of the globally produced sized paper & board grades contribute to ASA [10]. During the first years of use, ASA had severe establishment problems caused by its complicated application and its sensible chemical structure [82]. ASA's success story began with the switch to neutral/alkaline papermaking, beginning in the 1970ies to 1980ies [129]. In fact, ASA and AKD were the triggers for this switch, because they enabled a sizing process in neutral conditions, which

was at that point of time not possible by the use of rosin [11]. In comparison to rosin and AKD, ASA shows advantages and drawbacks displayed in Table 2.3-1.

Table 2.3-1: Advantages and Drawbacks of ASA Sizing Systems [10, 23, 82, 129-132]

Advantages:
− Applicability over a wide pH-range (also valid for AKD) − High reactivity and thus on machine sizing − Easy adjustable sizing degree (compared to AKD) − Low dosage amounts (compared to rosin) − Neglectable impact on physical paper properties − Robust sizing performance − High degree of aging resistance
Drawbacks:
− On machine emulsification / high investment and running costs − High hydrolysis tendency − Very low storage stability − Danger for tacky deposit formation − Oily deposits in the dryer section

2.3.1.1 Chemical Composition and Production of ASA

ASA is a synthetic sizing agent and liquid at room temperature with an amber shade and the basic chemical structure as displayed in Figure 2.3-1. It consists of two main components. On the one hand, the reactive succinic anhydride, which provides the anchoring ability to cellulose, and on the other hand, the alkenyl rest, consisting of an iso-olefin with chain lengths from C16 to C22, which provides the required hydrophobicity. The basic chemical and physical properties of ASA are displayed in Table 2.3-2. The production of ASA is conducted via three main steps, as displayed in Figure 2.3-2. The first step is the petrochemical polymerization of a-olefins from ethylene, while only the ones with chain lengths from C16 to C22 are of importance. These make up a total share of about 10% and are separated from the olefin mixture by distillation. The terminal position of the double bond within the a-olefins is moved via a catalytic isomerization towards the molecule center within the second step. The result of this isomerization is a mixture of linear olefins of identical chain length, but with randomized double bond position.

Table 2.3-2: Basic Chemical and Physical Properties of ASA [82, 133, 134]

Visual properties	Transparent, light amber to brown oil
Odor	Weak to none
Density	~ 950 kg/m³
Solubility	- < 1% in water (pH 7) - Dispersible in water - Soluble in organic solvents
Viscosity	10 °C: >500 mPas 25 °C: <250 mPas
Melting point	< 5 °C
Flash point	190 °C
Toxicity	Xi

These iso-olefins are reacted with maleic anhydride within the third step. During this so-called En-reaction, the double bonds of maleic anhydride and the iso-olefin react in an addition of the maleic anhydride, resulting in the desired alkenyl succinic anhydride. The final reaction product consists, due to the iso-olefins random double bond positions, of multiple (> 300) [135] structural isomers. [23, 82, 136].

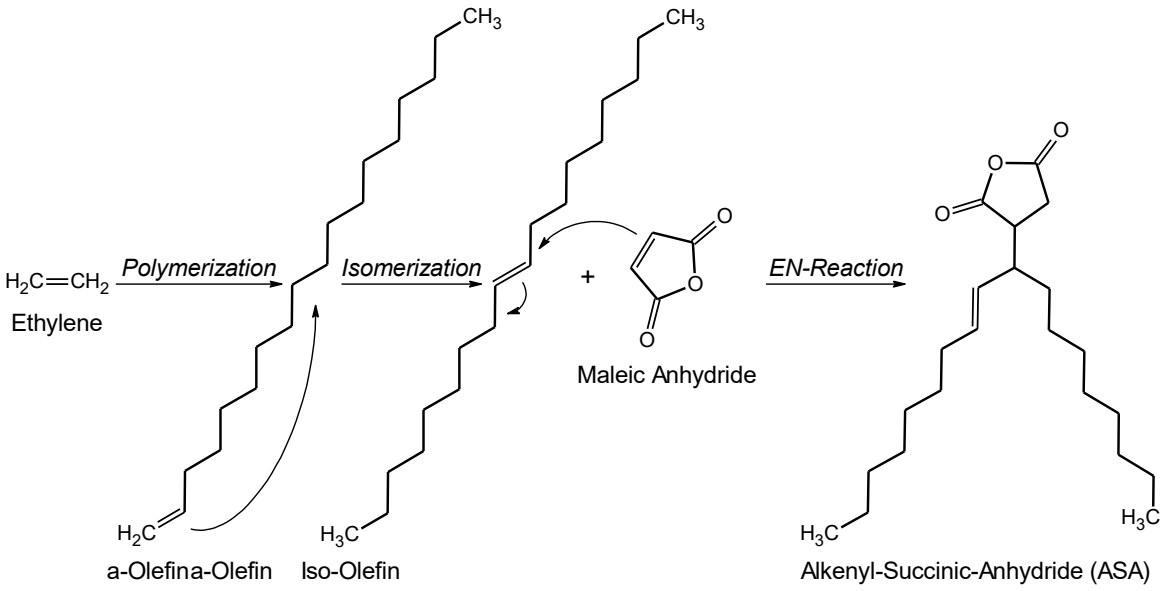

Figure 2.3-2: ASA Production Steps

Next to the above-mentioned standard ASA products, a variety of alternative ASA products is meanwhile available on the market. These are based on natural resources such as sunflower oil and oleic acids [136-139], in order to substitute crude oil based ASA products, or in order to minimize ASA specific problems such as hydrolysis and deposits. The benefits, drawbacks and the competitiveness of

these products was discussed in several publications, stating that they show a high degree of suitability for industrial-scale paper sizing [140-147]. Nevertheless, they still have only a neglectable share on the global ASA market.

2.3.1.2 Mechanistic Reaction Models

ASA is an alkaline reactive sizing agent with on-machine sizing performance. This means, that it is applicable at a wide pH range [130] from acidic to slightly alkaline with an optimum between pH 7.5 and pH 8.4 [148] and that its sizing performance reaches almost its maximum before the size press. This rapid performance evolution is supposed to be based on ASA's high chemical reactivity [11, 149], deriving from the cyclic anhydride group [150-152]. Nevertheless, the reaction mechanisms of ASA and cellulose, which finally lead to hydrophobization, ever since ASA's introduction to the paper industry, are subject to intense discussions. Generally, two approaches (Figure 2.3-3) are implemented for the description of the occurring phenomena, whereas one is chemically based and the other physically.

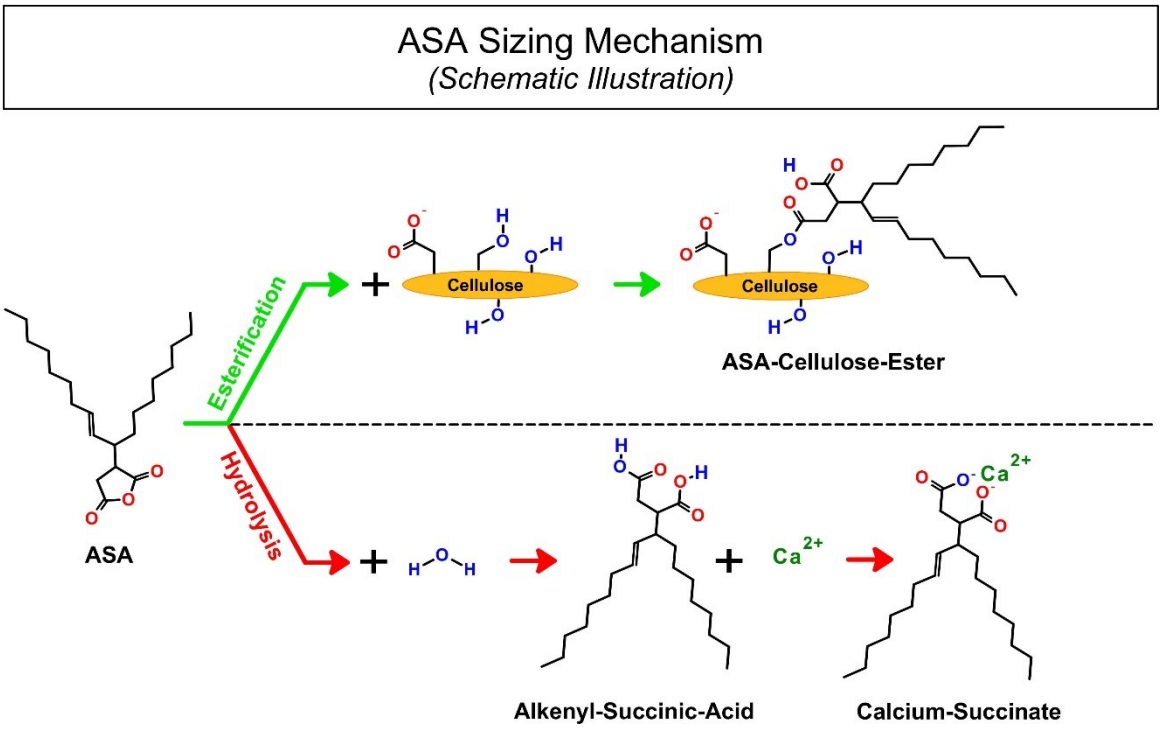

Figure 2.3-3: ASA Reaction Mechanism (Schematic Illustration)

The traditional, chemical approach states that the sizing performance of ASA is based on an esterification between the ASA's succinic anhydride and the

cellulose's hydroxyl groups [127, 128, 153]. The second, physical approach states, that the sizing performance has to be based on the distribution and orientation of unreacted, hydrolyzed and/or succinated ASA, by taking into account, that only a minor part of the present ASA is bound to the cellulose [31, 101, 154, 155]. The chemical reactions which are the foundation of both approaches, are summarized in Figure 2.3-3, while their details and backgrounds will be described in the following. The chemical background on the esterification reaction between ASA and cellulose is based on the high carbonyl activity of the ASA's anhydride group and additionally supported by the cyclic anhydride ring tension [156]. These properties make ASA a quite reactive electrophile for reactions with nucleophiles of any kind. In the case of an esterification reaction with cellulose, the respective nucleophiles are the cellulose's hydroxyl groups. Within this first-order reaction ASA and cellulose undergo an irreversible, exothermic nucleophilic addition (esterification) which goes along with a ring opening and the formation of a free acid group. This acid group dissociates correspondingly to the present pH [150, 157] (Figure 2.3-4 and Figure 2.3-5).

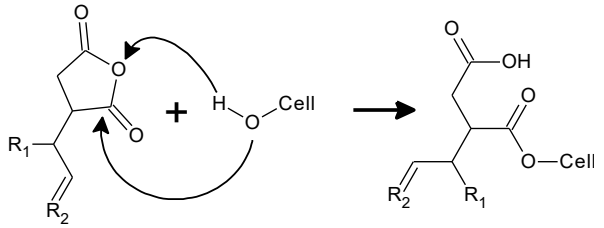

Figure 2.3-4: ASA-Cellulose Esterification

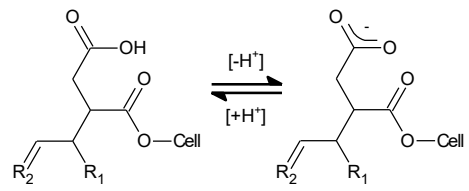

Figure 2.3-5: ASA-Cellulose Ester / Dissociation

The result of the described reaction is an ASA-cellulose half ester, which is due to the molecular sterics, a plausible cause for hydrophobization. The hydrophobic alkenyl rest is forced to orient away from the cellulose, shielding the surface, and thus hydrophobizing the structure [130, 148, 153, 158].

The undesired reaction, described in these approaches, is ASA's reaction with water, the so-called hydrolysis. ASA hydrolyses once it gets into contact with water, a stronger and more available nucleophile than cellulose. This reaction happens under ring opening and the generation of two carboxylic acids which are free to dissociate in respect to the present pH value (Figure 2.3-6) [130, 148, 153, 158].

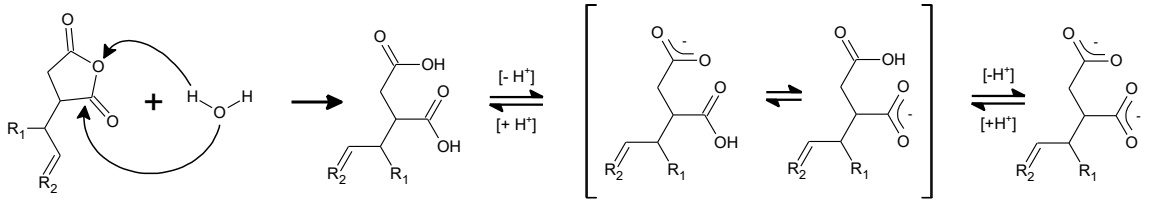

Figure 2.3-6: ASA-Hydrolysis / Dissociation Steps

A subsequent problem of hydrolysis is the formation of salts with metal ions, especially calcium and magnesium. The calcium salts, also well known as succinates (Figure 2.3-7), have the ability of forming tacky deposits, especially with filler particles, throughout the approach flow system and the wet end section, causing sever runnability and performance problems [82, 159-162]. Within the traditional mechanism models, the hydrolysis products of ASA, including the corresponding salts are said to show no sizing performance and to additionally decrease the sizing performance of the bound ASA [23, 82, 158].

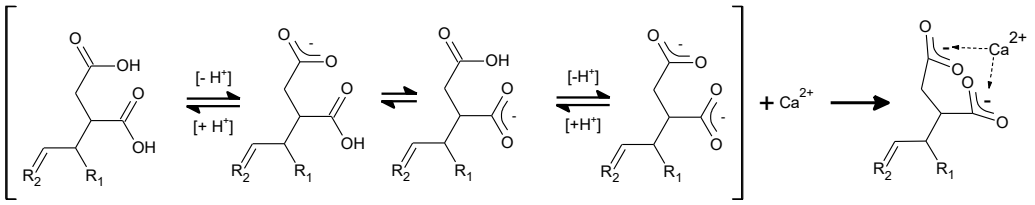

Figure 2.3-7: ASA-Succination

Contrary to this approach stand the findings of several researchers, showing that only a minor part of the ASA is bound to the cellulose structure [31, 101, 163, 164]. Some papers even state that there is almost no covalent bond formation (esterification) between ASA and cellulose at all and that its reactivity is only necessary for successful application [114, 165-168]. Founded on the evidence that the mentioned publications deliver, the hydrophobization of cellulose by ASA has to be based on other mechanisms than the pure esterification, and thus on the performance of the hydrolysis products. It is thought, that the key parameters to effective ASA sizing are quite the same as for rosin sizing. These are, at first, a high degree of retention, then a uniform distribution amongst the whole stock and then proper orientation during the drying and curing steps. This model does also consider the calcium succinates as substance, capable of giving sizing performance. Even though this model is not based on the esterification between ASA and cellulose, it is still an important factor that hydrolysis does not occur prior

to fixation on the fiber or filler surfaces. Hydrolysis prior to fixation causes emulsion instability and an along going agglomeration, charge reversal and thus a significant lower extent of fixation [31, 54, 101, 105, 112, 122, 162, 165, 167, 169, 170].

2.3.1.3 ASA Application

The key parameter to high performance ASA sizing, no matter which approach is used as argumentative foundation, is a successful application of ASA to the stock system [23, 31, 105, 112]. As ASA is an oily and hydrophobic liquid with a very low solubility in water, it needs to be converted into a processable and applicable form for papermaking [23, 82]. To reach these requirements, it is emulsified prior to application and subsequently applied to the production process via several ways. The following Chapters will describe the processes of emulsification and application with focus on modern high-performance systems.

2.3.1.3.1 *Emulsification*

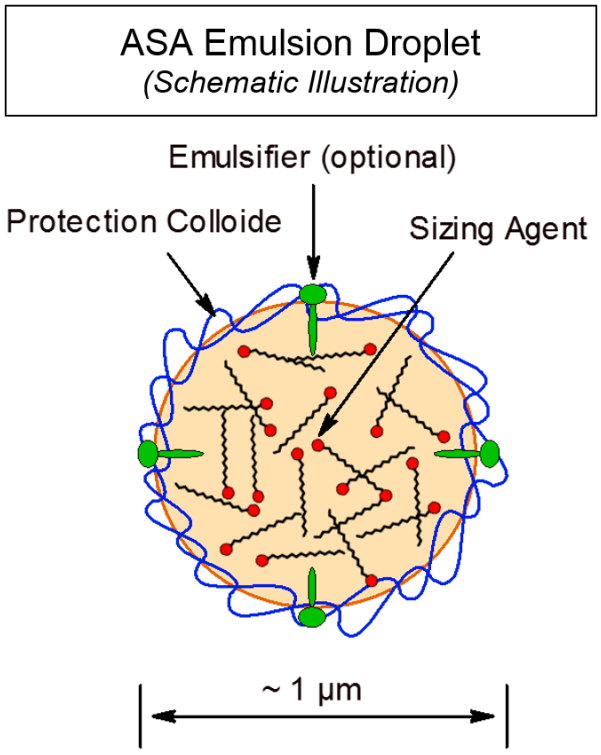

Figure 2.3-8: ASA Emulsion Droplet (Schematic Illustration)

The emulsification of sizing agents, in this case ASA, but also applicable for rosin sizes, AKD and PSAs, is the key process to successful high-performance sizing. To convert ASA into an applicable substance, it needs to be transformed into a water-soluble and fiber-affine form. This conversion is done by an emulsification step, resulting in an ionically or sterically stabilized oil in water emulsion. Due to ASA's high tendency towards hydrolysis and the resulting low emulsion stability, the emulsification step has to be conducted on sight. The typical emulsification agents, also known as protection colloids, are cationic, amphoteric or anionic starch [11, 23, 82, 171-175]. Some alternative applications implement polymers such as polyethylenimine [176], polyvinylamine [177], galactomannan

[178, 179] and modified/grafted platy minerals such as laponite or montmorillonite [124, 125, 180-185]. Special ASA types are modified to such an extent with special emulsifiers/surfactants, that they do not need any emulsification agent at all. These so-called instant ASA types [186-188] are niche products, and thus not established on the commodity market. Standard ASA types are a composition of pure ASA, mixed with up to 1% of emulsifier / surfactant, which optimizes the emulsification behavior, by means of a lower energy consumption to reach the required particle size [82]. The ideal ASA emulsion, as displayed in Figure 2.3-8, consists of stabilized particles with a size of approximately 1 µm in diameter and a high stability against coagulation and hydrolysis. The emulsion particles are made up of the sizing agent in the core, optional emulsifiers/surfactants on the oil/water interphase and a protection colloid, which encapsulates and stabilizes the sizing agent droplet. By this stabilization, the protection colloid properties are transferred upon the sizing agent droplet, making it water-soluble and giving it an ionic character. Most systems are based on cationic stabilization, in order to enhance the sizing agent's self-retention properties [21, 82, 132, 159, 160, 189]. Previous research, as well as industrial experience, have shown that the average emulsion particle size is an essential factor to sizing performance, stating that it should not be significantly bigger than 1 µm (d50). Emulsions with bigger particles show weaker sizing performance, while emulsions with smaller particles require an substantially higher energy input for their production [82, 130, 176, 190].

The already mentioned limited emulsion stability of ASA, which can be traced back to its high hydrolysis tendency, is the reason why ASA needs to be emulsified on sight with as low dead times upon dosage as possible. The emulsification is commonly done by the principle shown in Figure 2.3-9 [82, 159].

For processing, ASA is dosed as pure substance into the main volume flow of the emulsification agent (starch for the displayed case) and then emulsified in a high shear, high-pressure mechanical unit, which is usually equipped with a pressure controlled recirculation. The most widely used emulsification units are either turbine or cavitron systems [131]. The amount of emulsion which is treated multiple times by the recirculation set up, defines the energy input and thus the particle size and the particle size distribution. As several papers have shown, these properties are not only affected by the specific energy input, but also significantly by the

emulsification temperature, the ASA and emulsification agent consistency, the share between ASA and the emulsification agent, the emulsification agent viscosity and by the amount of emulsifiers/surfactants.

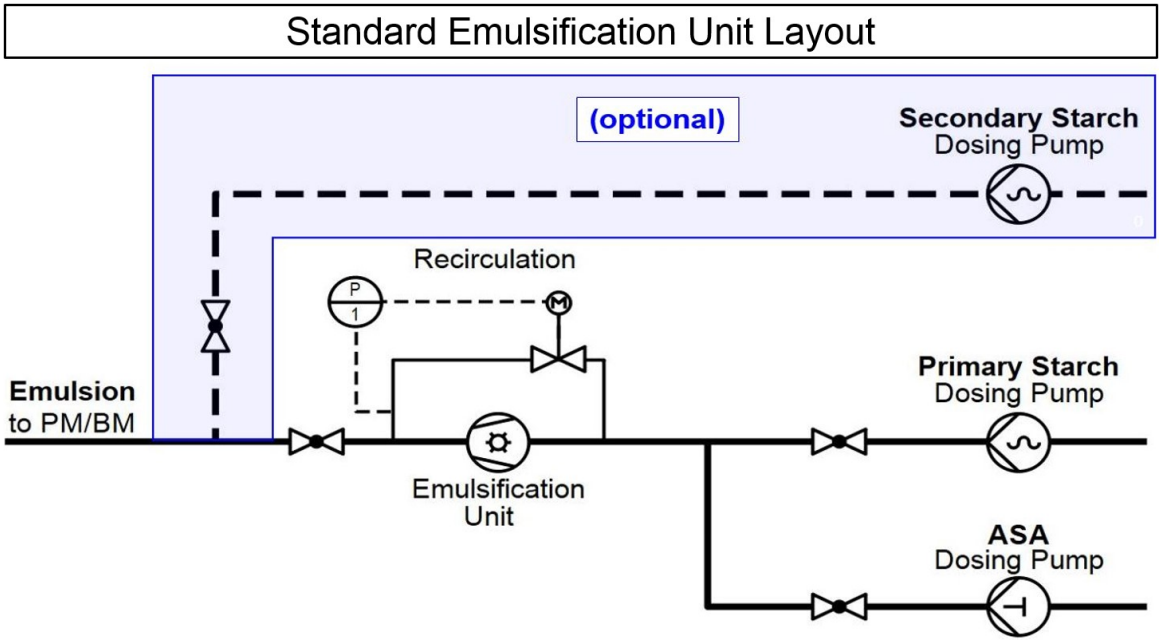

Figure 2.3-9: Standard Emulsification Unit Layout

The emulsion stability is most dominantly controlled by the protection colloid, the particle size, the temperature and the pH value. This is why the emulsions are usually cooled down after emulsification and in some cases acidically stabilized [11, 21, 82, 171, 190-192]. An option after emulsification, which is not so often implemented anymore, is an additional application of secondary-starch to the emulsion, to achieve further stabilization and higher degree of self-retention and thus better sizing performance. The benefit of this approach is that only a share of the starch needs to be emulsified, which has the advantage of lower energy consumption and a smaller required emulsification unit [11, 82, 159].

2.3.1.3.2 *Dosing*

The consecutive detrimental step toward successful high performance sizing is the dosing procedure. All sizing agents are generally dosed within the approach flow system, meaning at consistencies between 3 - 4% (mixing chest, machine chest) down to 0.5 – 1% (short circulation between white water chest and head box). Traditional systems, with basic dosing units follow the trend of ASA dosing at higher consistencies, further away from the head box, in order to enable proper

mixing and enough dwell time for the emulsion particles to retain on the fiber. These systems have the advantage that they are very simple in their implementation and quite economical in their operation. Nevertheless, these systems also show some significant drawbacks, contributing to too high dwell times and improper mixing. The dosage of ASA, as well as AKD, far away from the head box increases the contact time to water and thus the potential for hydrolysis and emulsion instability. An additional problem is that the conventional dosing units work only with a low degree of dilution, causing low turbulences and small contact area between the sizing agent and the stock at the point of dosage. This is why production systems which are implementing this dosing principle, are often prone to ASA- and AKD specific problems such as deposits, weak retention and a relatively weak sizing performance. Modern, more advanced dosing systems work on the principle of high dilution rates and “last-minute” dosing very close to the head box. Two of these systems are displayed in Figure 2.3-10 [193, 194].

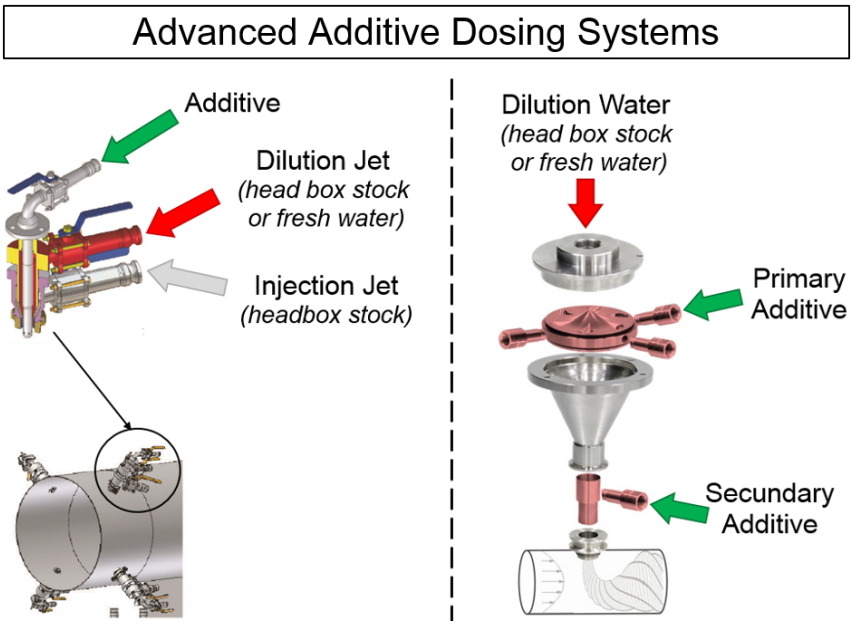

Figure 2.3-10: Modern Additive Dosing Systems / Trump Jet® (left) [193] & ecowirl (right) [194]

The advantages of these are a very high dilution rate and thus high turbulences at the dosing point, low dwell times to dewatering, with the additional possibility of dosing more than one additive with the same unit at a time. Based on the very large contact area between the sizing agent and the stock during dosing, the sizing agent has the possibility to retain on the fibers uniformly and properly. Trials have shown that it is possible to minimize not only the required sizing agent content by the

implementation of such a system, but also to minimize the sizing agent related problems [132, 159, 191, 193-196].

2.3.1.4 Mechanistic Steps of ASA Sizing

Once the ASA is dosed and homogeneously distributed to the system as stable emulsion, the sizing process undergoes its most important steps toward a successful substrate hydrophobization. These steps, also known as fixation, emulsion break-up, spreading and curing, are illustrated in Figure 2.3-11 [197] in correlation to the along going production steps. The following model is referring to the use of ASA. Nevertheless, the steps described are also valid for the application of AKD and dispersed rosin sizes.

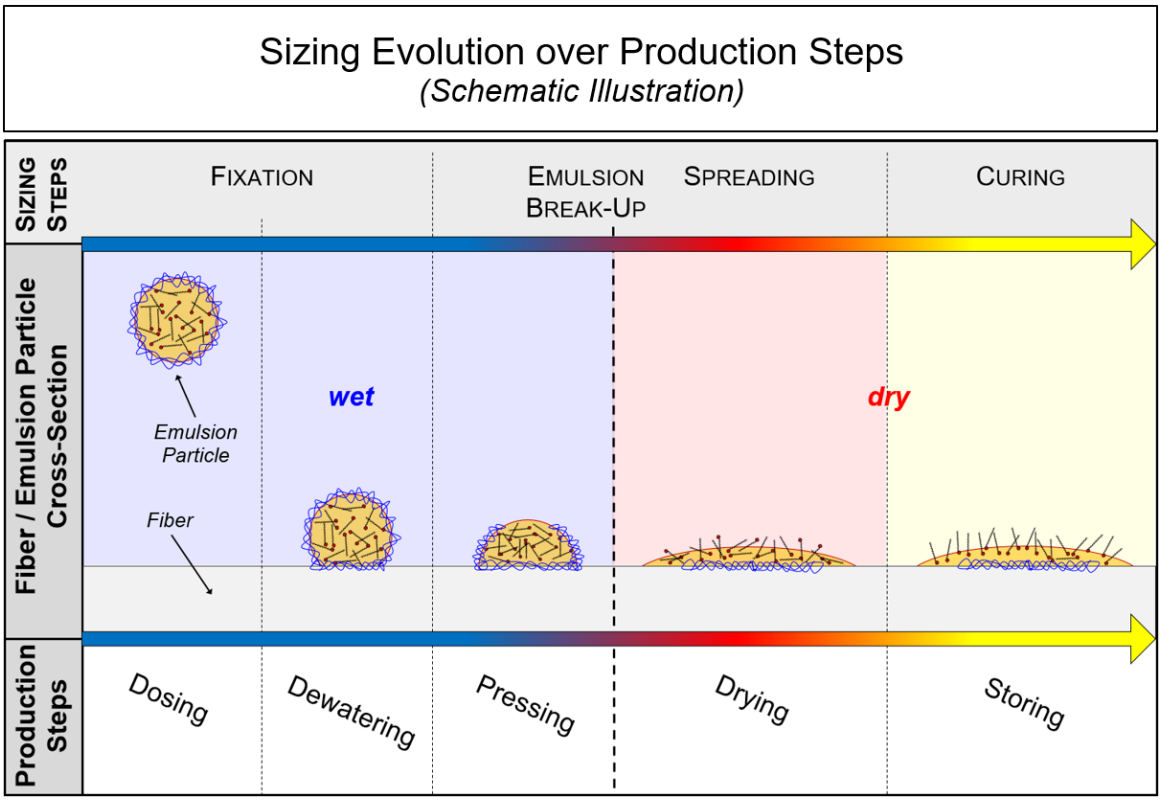

Figure 2.3-11: Sizing Evolution over Production Steps [197] (Schematic Illustration)

The first step is the sizing agent fixation on the fiber or filler particles, either by self-retention or by the help of retention aids or fixatives. Self-retention is driven either by electrostatic/ionic interactions between the fiber surface (anionic) and the protection colloid (cationic) or by steric circumstances (filtration). The fixation via retention aids or fixatives is done by the known retention principles (bridging model, patch model or complex flocculation). Key parameter to proper fixation is a homogeneous distribution of the ASA emulsion particles over all solids in the stock.

Only proper fixation can prevent a separation in high shear production steps such as approach flow screening, head box passage and the dewatering within the forming and press section. The higher the degree of fixation is, the higher is the sizing agent's retention, enabling a sufficient and dosage-correlated sizing performance. In optimized industrial-scale systems, ASA retention values of up to 95%, in lab scale even beyond, are possible [23, 31, 112, 130, 158, 197-200].

The second step, after the paper sheet is formed, is the emulsion brake up. This phenomenon occurs while the paper sheet is dewatered/pressed in the press section to a solid content of approx. 50% and afterwards heated up by the first dryer cans. The break up is driven by three factors. First, the decreasing water content causes emulsion instability, which is driven by reduced distances from the emulsion particle to the fibers. Second, the press section induces a huge extent of shear forces into the sheet structure. The third factor is the increasing temperature, which reduces the ASA's viscosity and the emulsion stability, which in combination with the other mentioned factors, in turn promotes the emulsion collapse [23, 54, 132, 197, 200].

The third step is the spreading of ASA over the solids' surfaces within the drying section. This process happens very fast for ASA, driven by its very low viscosity at elevated temperatures. During spreading, the ASA covers the surfaces of the substrate's components and orients itself to some extent by the help of fixatives and retention aids with its hydrophilic anchor towards the cellulose. This process reduces the substrate's surface energy and thus increases hydrophobicity [23, 153, 197, 200].

The whole process from dosing, to fixation, break up and spreading until the paper passes the size press or ends up on reel, does usually not take any longer than 30 seconds to 5 minutes for modern paper machines.

The last step that ASA sized paper or board grades undergo, is the curing step, which is defined by an increase in substrate hydrophobicity over a short term of storage (few hours to few days). This additional performance increase is so far explained by an ongoing distribution and orientation process [23, 197, 200, 201].

2.3.2 **Physico-Chemical Aspects during ASA Sizing**

ASA has been shown to only react with cellulose to a minor extent. Despite this fact, it still needs to be clarified why the esterification reaction does hardly happen and what the consequences of a high unbound, hydrolyzed ASA share are. The following Chapter will combine the state-of-the-art knowledge and focus on the one hand on the physico-chemical aspects that lead to a neglectable extent of esterification, and on the other hand, on the consequences of the high amount of hydrolyzed ASA.

2.3.2.1 Reaction Plausibility

The first step toward a sufficient explanation of the occurring physico-chemical aspects during ASA sizing is the consideration of the reaction plausibility between ASA and cellulose. This consideration includes the educt-product balance, the kinetics, the reaction energetics and sterics.

2.3.2.1.1 *Educt-Product Balance / Kinetics*

Esterification and hydrolysis are two reactions of second order, which occur simultaneously and stand in direct competition. The reactions can be described via the educt-product balance described in Equation 2.3-1 [156]. This balance might lead to the assumption that the reaction kinetics of ASA within the stock systems follow quite simple rules. In fact, the system is a lot more complicated and hence cannot be considered via this simple one-dimensional approach. For a holistic picture, the process needs to be observed within two steps. The first step, the application stage, where ASA is stabilized as emulsion, and the second, where it spreads over the more or less dry cellulose surface.

Esterification:	$\mathrm{A} + \mathrm{C}$	$= \mathrm{AC}$
Hydrolysis:	$\mathrm{A} + \mathrm{W}$	$= \mathrm{AW}$
Combination:	$\mathrm{A} + \mathrm{C} + \mathrm{W}$	$= \mathrm{AC} + \mathrm{AW} + \mathrm{C} + \mathrm{W}$

Equation 2.3-1: Concurrent Reactions between ASA-Esterification & Hydrolysis [156]

$A = \mathrm{ASA}$ $C = \mathrm{Cellulose}$ $W = \mathrm{Water}$
$AC = \mathrm{ASA\text{-}Cellulose\ Ester}$ $AW = \mathrm{Hydrolyzed\ ASA}$

During the emulsion step, ASA is exposed to an excessive amount of water, due to the emulsification agent being an aqueous solution (e.g., starch with ~ 3%). This causes direct hydrolysis on the surface of the emulsion droplets, while the reaction follows the stoichiometric formula (Equation 2.3-2),

$$C_{18}H_{32}C_4H_2O_3 + H_2O \rightarrow C_{18}H_{32}C_4H_2(COOH)_2$$

Equation 2.3-2: ASA-Hydrolysis

and the following kinetics (Equation 2.3-3):

$$v = -\frac{d[A]}{dt} = -\frac{d[W]}{dt} = k_h * [A] * [W]$$

Equation 2.3-3: Kinetics of ASA-Hydrolysis

v = Reaction Speed k_h = Reaction Rate Constant
$[A]$ = Concentration of Available ASA $[W]$ = Concentration of Available Water

If it were not for the emulsification agent (protection colloid), this reaction would proceed until no unreacted ASA is left. The stabilization of the status-quo after some of the ASA is hydrolyzed happens by the principle visualized in Figure 2.3-12.

Partially Hydrolyzed ASA-Emulsion Particle
(Schematic Illustration)

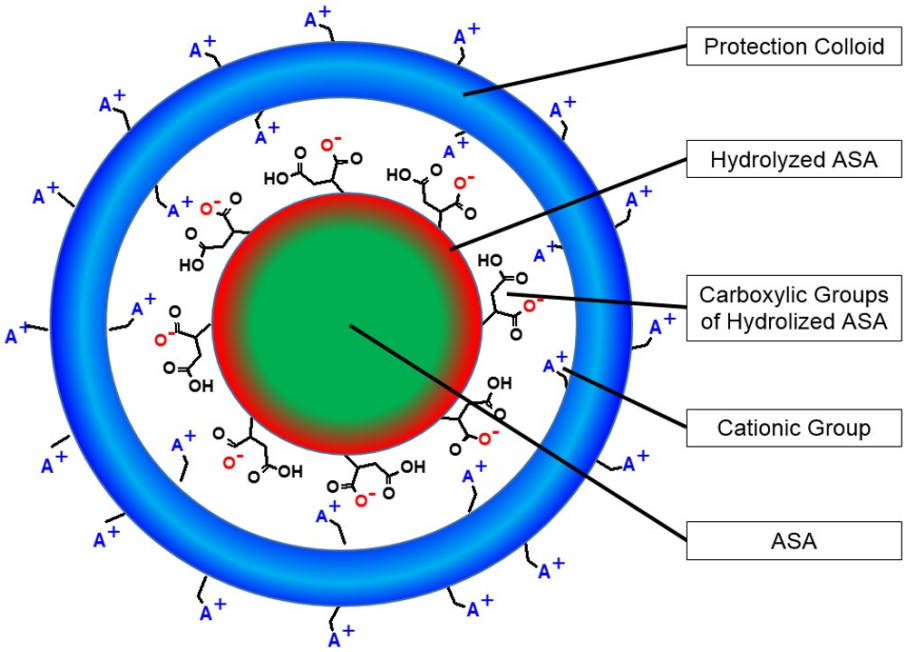

Figure 2.3-12: Partially Hydrolyzed ASA-Emulsion Particle (Schematic Illustration)

The ASA molecules on the surface of the emulsion droplet hydrolyze and partly dissociate, generating a negative surface charge. This surface charge then is directly neutralized by the cationic charge of the protection colloid. This charge neutralization coincides with strong electrostatic and ionic attraction forces, creating a stable compound and causing an immobilization of the hydrolyzed ASA particles on the droplet surface. The layer of stabilized hydrolyzed ASA serves somehow as a barrier against rapid water penetration into the core of the emulsion droplet where the unreacted ASA is located. It also prevents unreacted ASA from

reaching the water/droplet interface. However, this stabilization does not stop hydrolysis at all; it only slows the reaction down. The reaction kinetics (Equation 2.3-3) are negatively influenced by a significant reduction of available ASA $[A]$ and available water $[W]$, caused by the hydrolyzed ASA layer after stabilization. The comparatively lower emulsion stability of ASA to AKD is based on two facts, which can be best described by the reaction kinetics. First, the reaction rate constant k_h of ASA is about 80 times higher, compared to the one of AKD. Second, the concentration of available ASA $[A]$ is also higher compared to the one of AKD. This is based on the melting point. AKD is a waxy substance at room temperature, preventing any molecule mobility within the emulsion droplet after emulsification, and thus the possibility for AKD molecules to reach the water / droplet interface. ASA is liquid at room temperature, meaning that within the droplet Brownian motion and convection, drive at least a few molecules to the water / droplet interface, keeping the concentration of available ASA $[A]$ on a certain level, up to the point, where all ASA is hydrolyzed. Once the emulsion droplet is retained in the sheet structure and the sheet is dewatered, the emulsion breaks open at dry contents of ~ 60%, exposing the unreacted ASA to the surrounding water and to the cellulose. Keeping in mind that the fibers are surrounded by a stable cluster of water molecules at elevated moisture contents, it needs to be considered that the ASA molecules are only in contact with water molecules until high levels of dryness at the end of the dryer section are reached. As a result of this, the reaction kinetics after the emulsion breaks open follow the ones of ASA hydrolysis (Equation 2.3-3), while the concentration of available water $[W]$ is infinite (pseudo first order reaction) and the concentration of available ASA $[A]$ stands in direct correlation to the present amount of ASA, causing the highest rate of hydrolysis in all of the production process.

If any unreacted ASA is left at the end of the dryer section, where the water content is so low that, it allows contact between ASA and the hydroxyl groups of the cellulose, the possible reaction follows the stoichiometric formula (Equation 2.3-4),

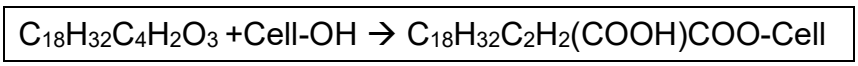

Equation 2.3-4: ASA-Esterification

and the following kinetics (Equation 2.3-5):

$$v = -\frac{d[A]}{dt} = -\frac{d[C]}{dt} = k_e * [A] * [C]$$

Equation 2.3-5: Kinetics of ASA-Esterification

v = Reaction Speed k_e = Esterification Reaction Rate Constant

$[A]$ = Concentration of Available ASA $[C]$ = Concentration of Available Cellulose

The comparatively higher reactivity of ASA compared to AKD, once in contact with cellulose is also based on two facts. First, the viscosity of ASA is significantly lower compared to the one of AKD, enabling faster and wider spreading. This influences the kinetics, by a quicker generation and higher amount of available cellulose $[C]$. Second, the reaction rate constant k_e of ASA is about three times higher, compared to the one of AKD.

A point that was not taken into account so far is the mass balance between ASA, water and cellulose. As can be seen in Equation 2.3-4 and Equation 2.3-2, one Mol ASA requires each one Mol water or one Mol hydroxyl groups for its reaction. Expressed in reactant mass, with the fictive assumption that all cellulose hydroxyl groups are available, it can be stated that 1 gram ASA (M: 351 g / C18) requires 0.051 g of water (M: 18 g) or 0.154 g of cellulose (M: 162 g / anhydroglucose / 3 OH-groups) for hydrolysis or esterification. If this fact is respected and transferred to the paper making process with the knowledge that only a minor share of the cellulose is effectively accessible for chemical reactions, it can be stated that a residual moisture content in the sheet structure of 0.01% would be sufficient to hydrolyze the complete present ASA for a sheet sized with 0.2% ASA. Considering the fact, that the normal moisture content at reel is between 3% and 12%, and that the water forms stable clusters or monolayers on the cellulose surface, it is obvious that there is always an excessive amount of water available for hydrolysis [142, 156, 157, 168, 202-204].

2.3.2.1.2 *Energetics*

An important parameter when looking at reaction plausibility is the consideration of the respective energetic states before and after reaction. To take this into account, the bond energies were considered and compared, without respecting the reaction entropy. The bond energy change for the esterification reaction was set as reference ($\Delta H_{rel.}$ = 0 kJ/mol).

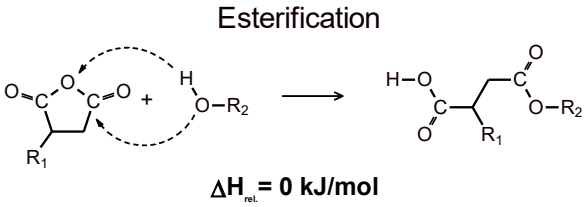

Figure 2.3-13: ASA Esterification Reaction Enthalpy

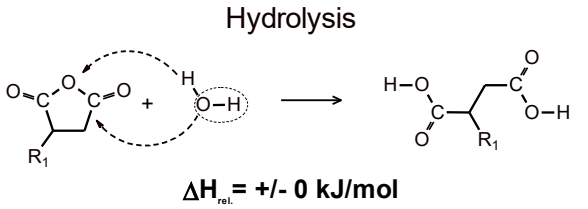

Figure 2.3-14: ASA Hydrolysis Reaction Enthalpy

This approach shows, that esterification and hydrolysis are, from an energetic point of view, reactions of equal plausibility. Both show the energetic values $\Delta H_{rel.}$ = 0 kJ/mol, as the same covalent bonds are opened and/or reconnected during these reactions. The di-acid as hydrolysis product, once dissociated and stabilized by metal ions, is even of higher stability compared to the ester, which can be hydrolyzed under acidic or alkaline conditions [150, 151, 156].

2.3.2.1.3 *Sterics*

A further important point when defining the plausibility of concurring reactions is their steric background. The reaction between ASA and cellulose can happen on five positions over the cellulose molecule (Figure 2.3-15). The first two positions are the terminal hydroxyl groups in position 1 and 4. Considering the fact that every cellulose macromolecule is in average made up of at least 10,000 glucose molecules, only one hydroxyl group out of 15,000 is in terminal position. This is why they can be neglected. The important hydroxyl groups are the ones in position 2, 3 and 6, while some of the ones in position 6 are oxidized to carboxylic acids and thus not reactive. The calculation in Chapter 2.3.2.1.1 has shown that from a theoretical point of view, only 0.154 g of cellulose are required for the complete esterification with 1 g of ASA. This approach, which indicates that all hydroxyl groups are available, does by far not meet the real circumstances. The single cellulose chains are not dissolved in water during the paper production process. The macromolecules are clustered to fibers with amorphous and crystalline regions

that are more or less penetrated by water (swelling) and thus already occupied by water molecules prior to sizing agent contact. The only positions where the sizing agent can get into contact with the cellulose is from the fiber lumen or the fiber surface, while still the fact that the cellulose surface is covered by more than a molecular water film during the production has to be taken into account (3% – 12% residual moisture content). These conditions promote the fact, that driven by steric hindrance, the concentration of available cellulose [C] is by far not as high as the actual concentration of cellulose in the system [205-207].

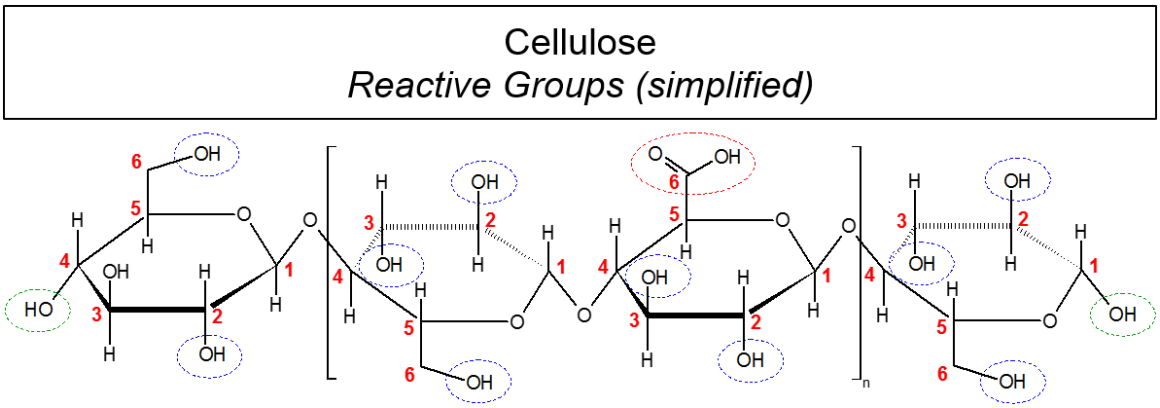

Figure 2.3-15: Cellulose' Reactive Groups (simplified)

2.3.2.2 Phenomena based on Sizing Agent Mobility

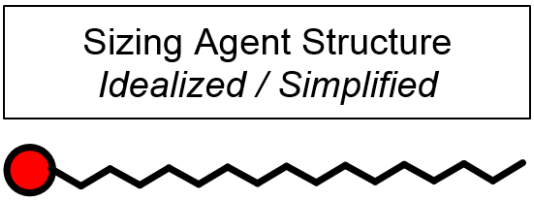

Figure 2.3-16: Simplified Sizing Agent

Theoretical investigations and practical approaches have proven that the major part of the retained ASA is present in the sheet structure in hydrolyzed form. During an optimal production process, the hydrolyzed ASA gets well distributed and well oriented among the substrate surface. By this, even the unbound ASA is able to perform as hydrophobizing substance. Looking at some well-known interactions, it must be considered, that the hydrolyzed share is somehow stabilized via electrostatic or ionic interactions by either metal ions (Ca^{2+}, Mg^{2+}, Al^{3+}) or by polymeric cationic groups deriving from the protection colloid, fixatives or retention aids. The fixation is due to its electrostatic or ionic nature reversible and can thus be significantly influenced by external factors, such as relative humidity or temperature, resulting in possible molecule mobility. That means that the hydrolyzed ASA share is free to move within, or even out of the cellulosic structure, creating new entries to the

explanation of ASA sizing. The following Chapters will describe the molecule mobility based processes occurring in ASA sized sheets, including possible ways of orientation, agglomeration, migration, size revision and size reactivation. As these approaches are applicable for hydrolyzed AKD as well, the sizing agent (Figure 2.3-16) is illustrated in simplified form within the models (except for the model of intra molecular orientation).

2.3.2.2.1 *Sizing Agent Orientation*

The orientation of the sizing agent molecules on the substrate surface is, as already stated, the major factor influencing the sizing performance. In general, two orientation extremes with an intermediate state can be reached (Figure 2.3-17.) The first stage (left) shows the optimal situation. All molecules are oriented with their anchor in the direction of the cellulose surface, thus decreasing the surface energy and boosting the sizing performance. This state is promoted by homogeneous sizing agent distribution and proper fixation.

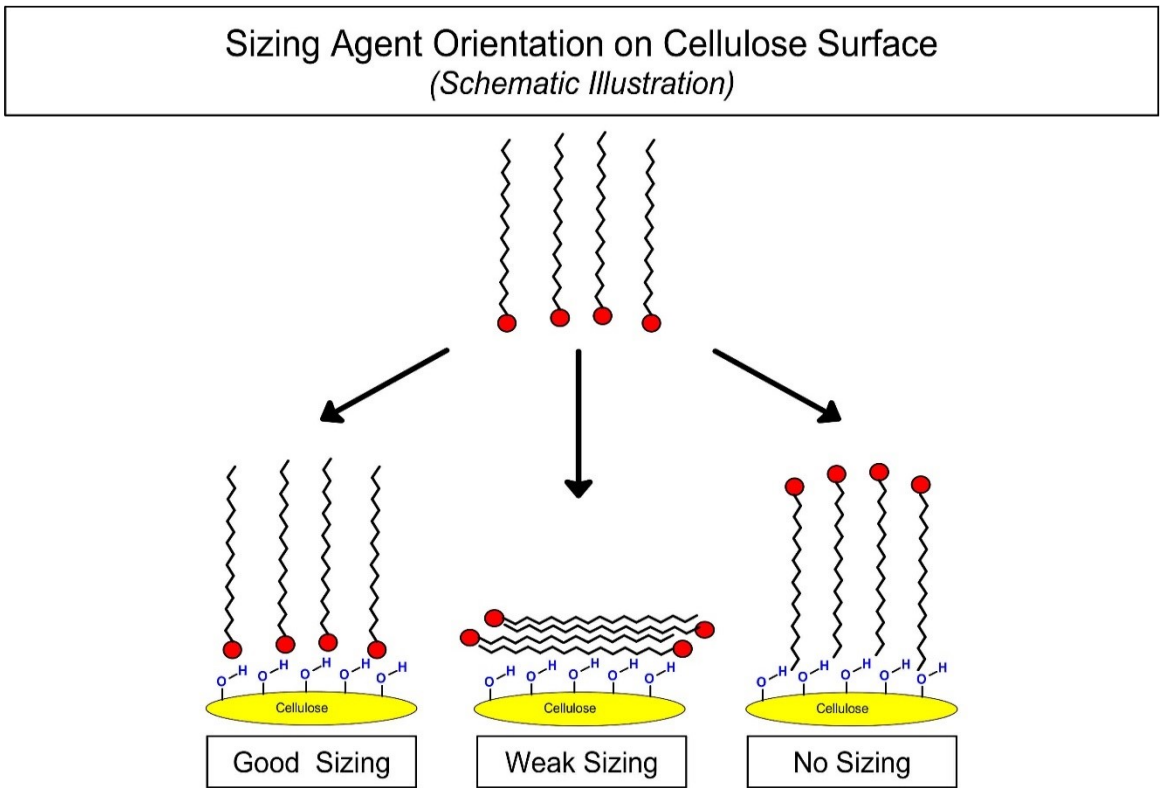

Figure 2.3-17: Sizing Agent Orientation on Cellulose Surface (Schematic Illustration)

State two (center) shows random orientation. The major part of the particles is neither oriented with the anchor to the cellulose, nor away from it. That leads to a minor decrease of surface energy and by this to a weaker sizing performance. The

third state (right) describes an orientation with the olefin rests in the direction of the cellulose. This scenario triggers the highest degree of surface energy, hence causing the weakest sizing performance. For real life scenarios, the orientation states will never occur in extremes, but thermodynamically driven as equilibrium. The way of orientation (equilibrium) is supposed to be very sensible to retention, distribution and fixation, as well as to the drying intensity [31, 66, 73, 147, 154, 208].

2.3.2.2.2 *Intra-Molecular Orientation*

Looking at the molecular structures of ASA, a further orientation possibility comes into consideration. This so-called intramolecular orientation results from the different structural isomers of ASA and the possibilities for the saturated part of the alkenyl rest to rotate freely. Figure 2.3-18 displays different orientation states of one specific structural isomer.

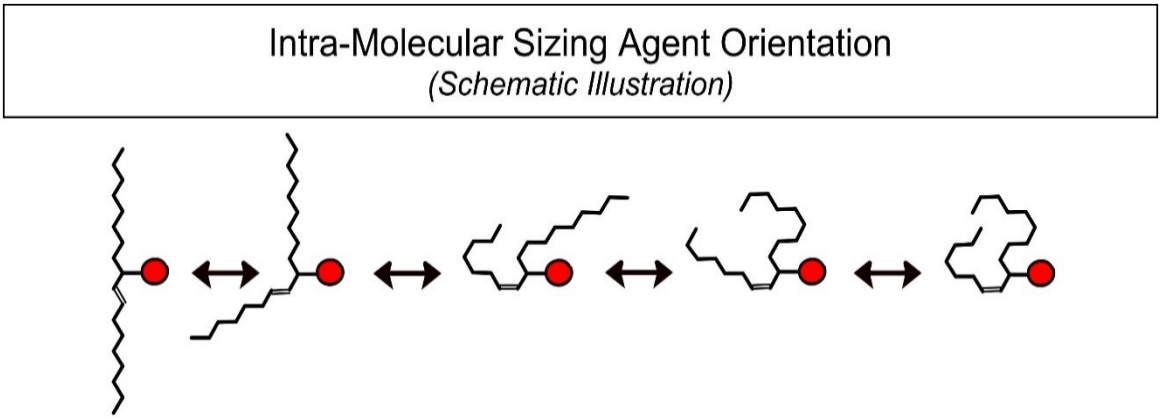

Figure 2.3-18: Intra-Molecular Sizing Agent Orientation (Schematic Illustration)

The state displayed on the left shows no degree of entanglement, while the one on the right shows the maximum degree. From a theoretical approach, the possible extent of surface energy reduction is related to the degree of entanglement, meaning the more spread out the molecule is, the better its shielding performance and hence its hydrophobizing properties are. Due its two alkyl-rest with chain lengths of C16 to C22, AKD has even more degrees of freedom for entanglement, affecting it even more by intramolecular orientation processes [209, 210].

2.3.2.2.3 *Sizing Agent Agglomeration*

Sizing agent agglomeration is an effect which results directly from the molecular mobility on saturated surfaces. The type of agglomeration mentioned in this section

should not be confused with the agglomeration phenomena occurring in aqueous phases, e.g., the ones that lead to emulsion instability. The described agglomeration phenomena refer to the processes occurring in the dry paper web (Figure 2.3-19). This theory says that there are two major possibilities the hydrolyzed sizing agent molecules could arrange. One is the formation of hydrophobic micelles / agglomerates. Here, the hydrophilic anchors orientate in one central direction, so a spherical structure with hydrophobic character is created. Agglomerates of this kind show low surface energy and high hydrophobicity. Agglomerates, which are made up the other way around, show quite different properties. For these, the olefin rests point to the center, creating an agglomerate with a very high surface energy and by this a hydrophilic nature [103, 191, 211, 212].

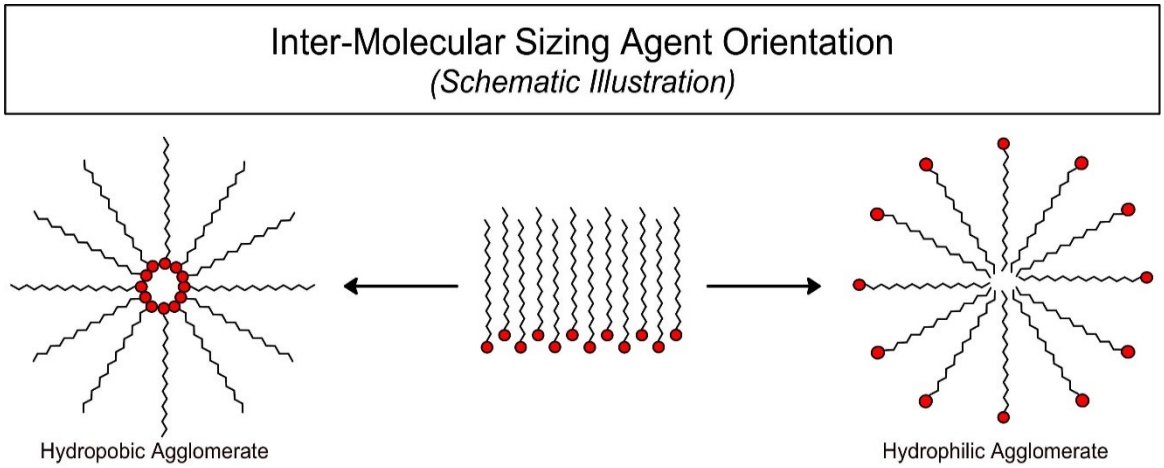

Figure 2.3-19: Inter-Molecular Sizing Agent Orientation / Agglomeration (Schematic Illustration)

2.3.2.2.4 *Fugitive Sizing / Sizing Loss / Size Reversion*

The processes that cause a decrease in sizing performance are also known as size reversion, sizing loss or fugitive sizing [31, 46, 55, 57, 60, 70, 75, 213-215]. All these phenomena have, from a theoretical point of view, other triggers, but result in the same molecular processes, which in fact are a combination of sizing agent migration, orientation and agglomeration. The occurring events can be explained via a three-phase model (Figure 2.3-20).

The first phase defines the properties at the beginning of aging time right after production, where the whole sizing agent is distributed equally, but mostly in hydrolyzed form, within the paper sheet. The molecules are free in their mobility, but absorbed and fixated on the surface of filler particles or cellulose fibers. Only a

very small share is covalently bound to the cellulose. Driven by the natural molecular hydrophobicity in combination with their fixation driven orientation, the paper shows a sizing agent dosage correlating sizing performance.

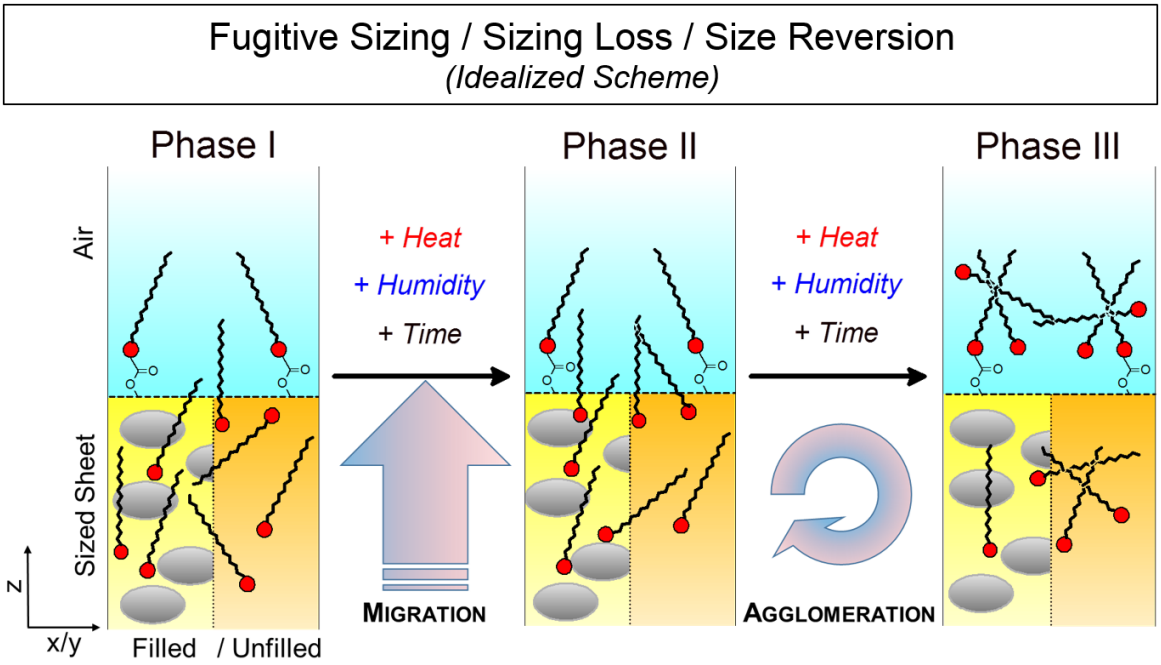

Figure 2.3-20: Fugitive Sizing / Sizing Loss / Size Reversion (Idealized Scheme)

The second phase defines the first stage of aging, also known as curing time. Driven by external factors, such as relative humidity and temperature, the molecules start migrating within the sheet structure. Once they reach the interphase between cellulose and air, the molecules orientate with their olefin rest away from the paper surface, while decreasing the surface energy. This process causes an increase in sizing performance. The end of the second phase is reached, when the maximum substrate-specific surface saturation is reached.

Phase three starts at the point, where the maximum degree of saturation is exceeded, and the molecules begin to agglomerate. That means that they form bundles or micelle-like structures and lose their sizing performance. These agglomerates are formed either within the sheet structure or on the surface, while some can also include covalently-bound ASA molecules and thus weaken their sizing performance as well. This process of agglomeration-driven sizing decrease can proceed up to a total loss of sizing performance, while the speed rises with increasing relative humidity and temperature [215].

2.3.2.2.5 *Sizing Agent Migration*

Sizing agent migration is a topic that has come to discussion during the recent years. This process describes the molecular mobility of hydrolyzed ASA (di-acid) and AKD (ketone) beyond the sheet structure. Several approaches have shown that the molecules are capable of leaving the initially sized substrate and to migrate onto or into surrounding substances, by either direct contact or vapor-phase transport. This process is especially known to AKD sized paper under the name of ketone migration, a phenomenon causing severe problems in copy machines by depositions [31, 55, 57, 60, 73, 74, 129, 131, 216-220]. It is also supposed to be the trigger for the AKD-typical significant friction coefficient reduction [60].

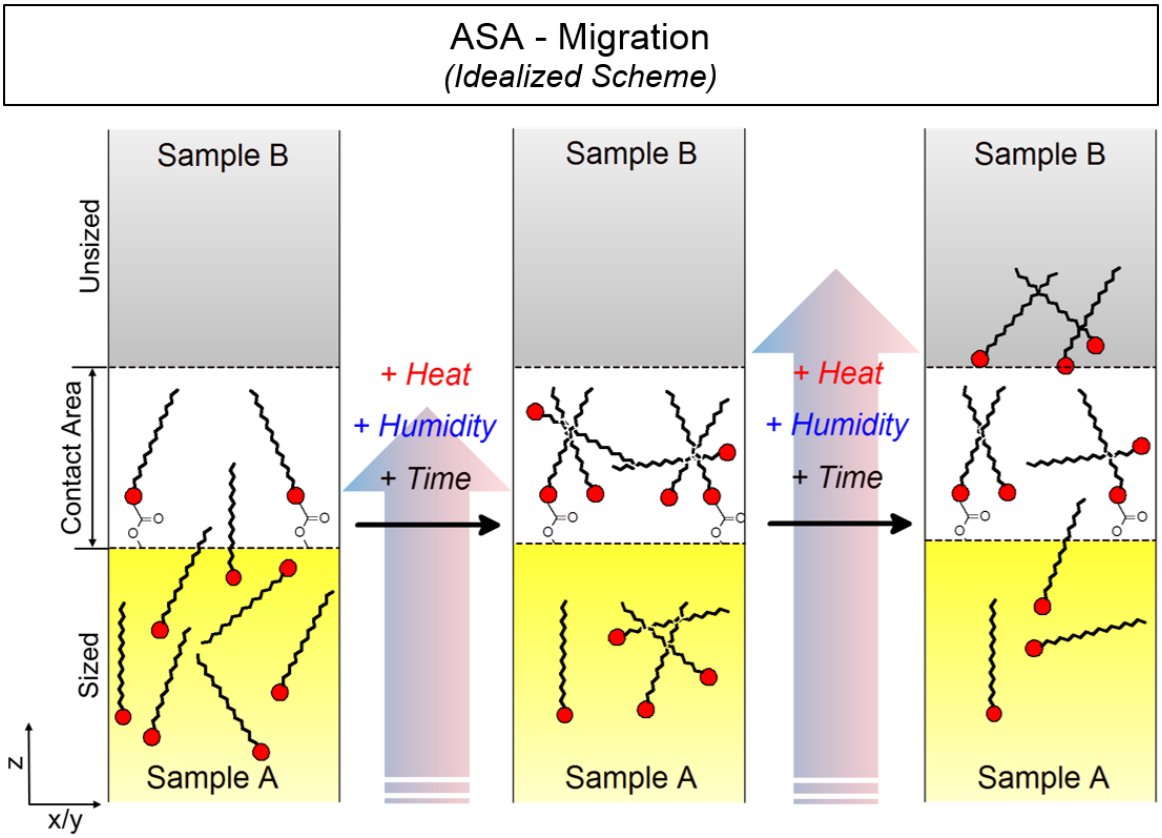

Figure 2.3-21: ASA-Migration (Idealized Scheme)

ASA migration from sized to unsized paper samples was observed, by proving very high extents of migration. Migration processes are of highest importance for paper & board products which are in direct or indirect food or beverage contact. The maximum rate of migrated sizing agents is therefore defined by national regulations, such as “XXXVI Empfehlung des Bundesinstitut für Risikobewertung”

[221] or the “Code of Federal Regulations, Title 21 by the U.S. Department of Health and Human Services” [222].

The migration processes can be described as displayed in Figure 2.3-21. Accelerated by high relative humidity and ambient temperatures, the hydrolyzed sizing agents start to migrate within the sheet structure, in order to find the optimal energetic state. The migration of the sizing agent onto another surface, or into another substance can be driven by two main factors. One is the plain concentration gradient, as it is applicable for migration processes between sized and unsized papers. The other factor contributes to the properties of the contact substance/material as solvent or adsorbent. If the substance is less polar and more hydrophobic than cellulose, such as butter or oil, the sizing agent is a lot more likely to migrate compared to a polar substance, such as water or cellulose.

2.3.2.2.6 *Sizing Reactivation / Sizing Agent Reorientation*

A further phenomenon, which underlines the high degree of molecule mobility of hydrolyzed ASA, is a possible reactivation of the sizing performance by the application of Alum [31]. It was observed that paper samples that were contaminated with migrated (hydrolyzed) ASA and did not show any initial sizing performance, showed significant sizing performance after a treatment with aqueous alum solutions and subsequent drying. These trials prove that it is possible to redistribute and reorient agglomerated ASA molecules by substrate vaccination with Al^{3+} ions. The principle that describes this process is displayed in Figure 2.3-22.

The reactivation process starts with either an aged paper sample or a sample which is contaminated with migrated ASA, while it does not matter if it is filled or not. When these sheets are treated with aqueous solutions of $Al^{3+,}$ or cationic aluminum derivates, the water and the aluminum cause a disintegration of the agglomerates and a fixation of the ASA molecules to the cellulosic structure. The reorientation, which is the trigger for the sizing performance regain is induced by subsequent drying. The chemical principle, which is supposed to be the trigger for the reactivating properties of alum, is the secondary formation of ASA-cellulose-aluminates [223], as schematically displayed in Figure 2.3-23. The fixation principle follows the basic mechanistics of rosin fixation (Chapter 2.2.6.2).

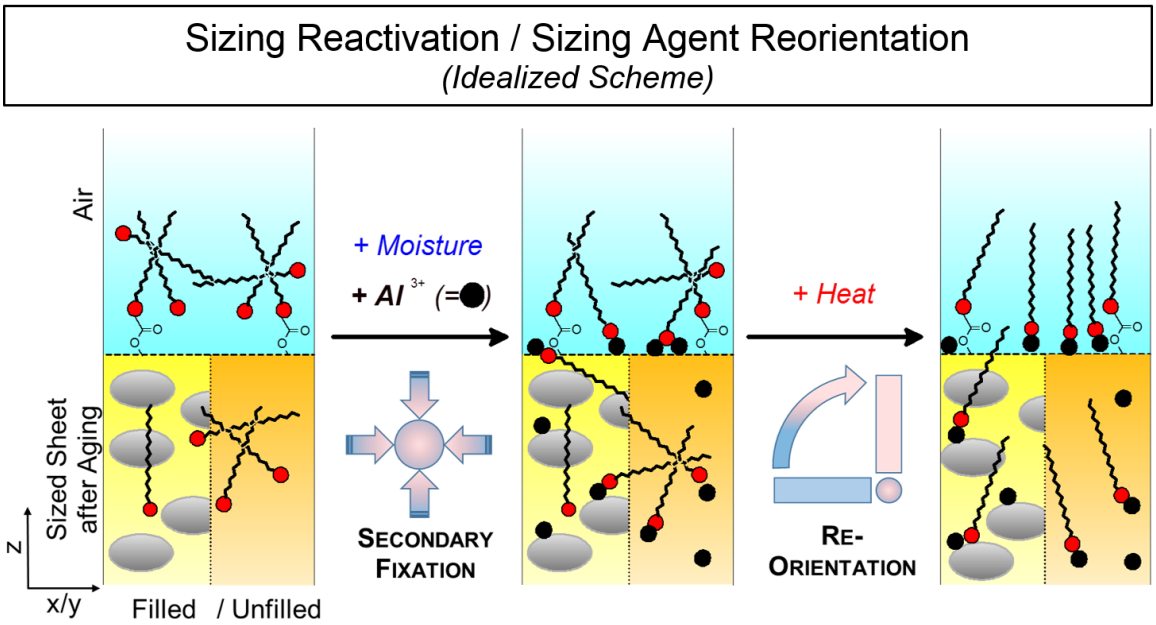

Figure 2.3-22: Sizing Reactivation / Sizing Agent Reorientation (Idealized Scheme)

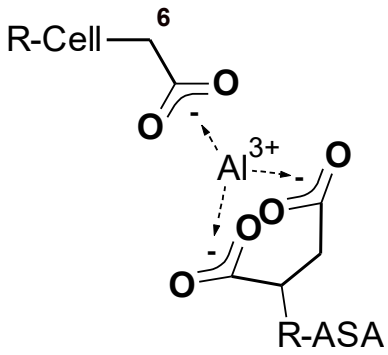

Figure 2.3-23: ASA-Cellulose Aluminate

2.3.3 **Causes for Interactions during ASA Sizing**

The production step of paper sizing as such, no matter if rosin, AKD or ASA is used, is subject to a number of internal and external factors that are capable of causing interactions during the sizing process. These interactions can be of negative, but also of synergetic nature, and thus be undesired or favorable. The following Chapter will briefly focus on the well-known interactions during paper sizing with ASA as sizing agent. However, based on their similar molecular composition and mechanism of action, the gross content of these interactions can be transferred to AKD and rosin as well.

2.3.3.1 Process Parameters

ASA's sizing performance is most dominantly affected by the process parameters pH, water hardness and temperature. The observable interactions are based on the strong impact on the hydrolytic stability of the ASA emulsions. It can be seen from the following figures that increasing pH, hardness and temperature significantly affect the hydrolysis rate, and thus the emulsion stability [131, 160, 168]. The direct result is a decreasing sizing performance. Figure 2.3-24 [31] displays the dependency of the sizing performance on the evolution of emulsion hydrolysis. This approach shows that successful sizing is not possible with a hydrolysis rate beyond 25% [31], even though the actual present amount of ASA in the sized sheet remains unchanged. The mentioned process parameters are, next to their negative impact on the hydrolytic stability of ASA, capable of changing the fiber properties, in terms of swelling and surface charge [224]. This can also affect the fixation/retention behavior of ASA on the fibers and thus the sizing performance.

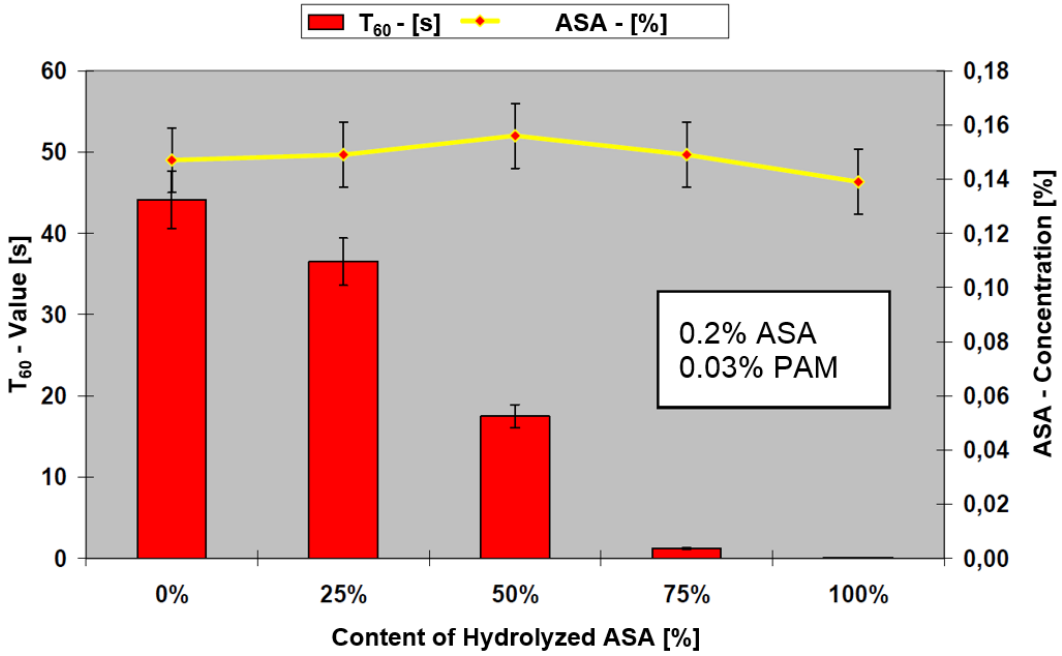

Figure 2.3-24: Impact of ASA-Hydrolysis Rate on Sizing Performance (translated from original [31])

2.3.3.1.1 *Temperature*

The kinetics of chemical reactions are most dominantly affected by the ambient temperatures [156]. A rule of thumb states that a temperature increase of 10 °C doubles the reaction speed, resulting in an exponential impact factor. This

correlation is visualized in Figure 2.3-25 [31], showing a rapid hydrolysis rate in a process-typical temperature range between 50 °C and 70 °C.

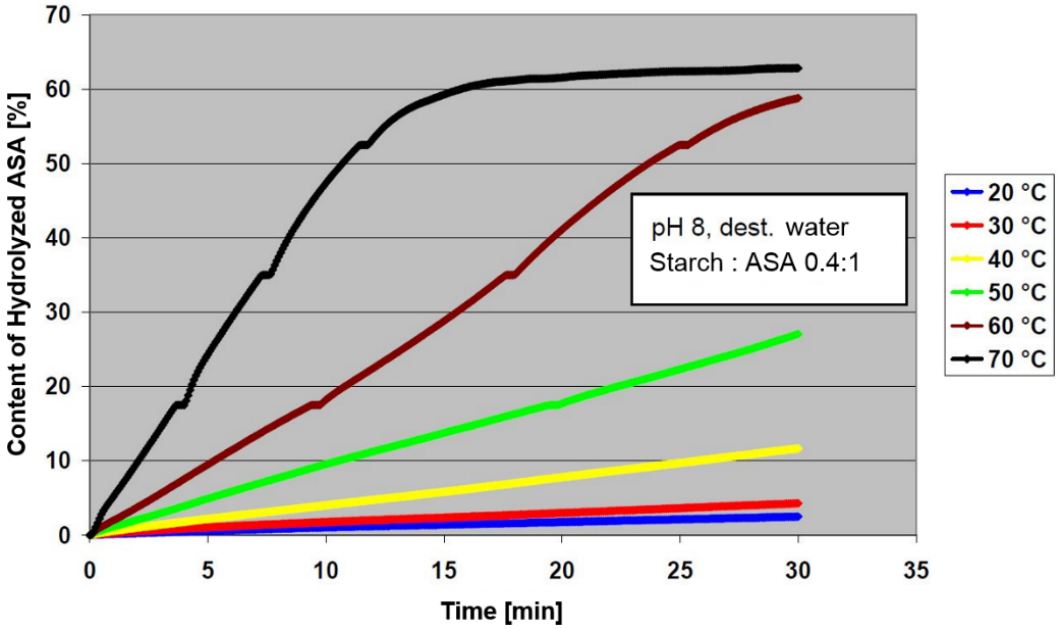

Figure 2.3-25: Impact of Temperature on ASA-Hydrolysis Rate (translated from original [31])

The hydrolysis rate published in this paper is nevertheless significantly higher compared to other publications [130, 131, 198], where a progress of 50% hydrolysis was reached after 1.5 - 4 hours. This might be due to the implemented, consecutive titration method with NaOH at pH 8. This method can be considered as hydrolysis promoting and thus is only capable of delivering relative values. To prevent extraordinary hydrolysis rates in industrial-scale upon dosage, the readymade ASA emulsions or the emulsion starches are usually cooled down with heat exchangers. This is necessary, because it is quite common that the emulsions are transported or stored a few minutes after emulsification, before being added to the stock [82].

2.3.3.1.2 *pH-Value*

The ambient pH value is also considered as one of the most emulsion stability influencing factors throughout the production process (Figure 2.3-26 [31]). Several attempts have shown that a switch from acidic to alkaline conditions is boosting the hydrolysis rate [130, 131, 198]. This phenomenon is based on the nucleophilic properties of water and on the acidic stabilization of ASA acid. The nucleophilic properties of water increase with increasing pH value, due to a higher

concentration of OH^-, and thus promotes the reaction speed of the anhydride ring-opening reaction. Driven by a stabilization of the chemical equilibrium, ASA can be properly stabilized by acidic conditions, slowing down the hydrolysis speed. For the case that the acid is deprotonated by high pH values, it is free to form succinates or salts with other suspension components, which causes precipitation and an along going hydrolysis-promoting change of the reaction equilibrium [168].

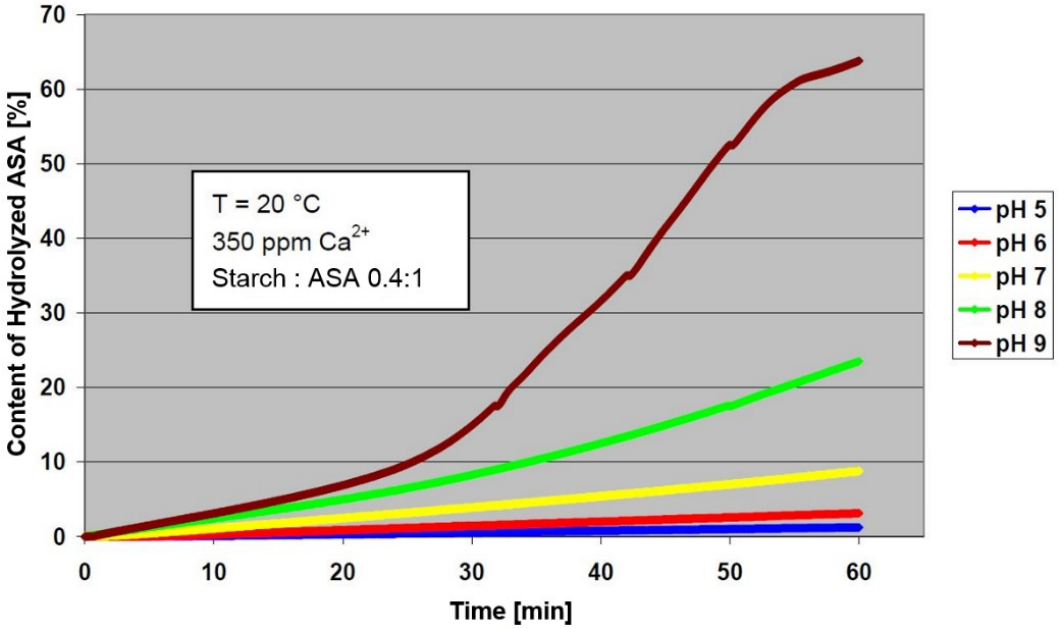

Figure 2.3-26: Impact of pH on ASA Hydrolysis Rate (translated from original [31])

To avoid pH triggered hydrolysis within industrial-scale ASA processing, either the used starches are acidically stabilized, or the whole emulsion is brought to acidic conditions upon dosage [191].

2.3.3.1.3 *Water Hardness*

The water hardness, what is the concentration of the divalent cations Ca^{2+} and Mg^{2+}, shows a significant impact on the hydrolytic stability of ASA (Figure 2.3-27 [31]). Even though the impact is not as dominant as the factors pH and temperature, it still has to be considered [31]. As mentioned in the previous Chapter, the increase in hydrolysis by increasing water hardness can be explained by salt formation. Once the ASA molecule is hydrolyzed, it is, depending on the ambient pH value, partially or fully deprotonated and subsequently stabilized by cations in terms of salt formation. The salts have a comparably low water solubility, which causes them to precipitate [162]. Even though the water hardness is a sum parameter for the concentration of Ca^{2+} and Mg^{2+}, it is well known that Ca^{2+} has

the highest impact on ASA hydrolysis and thus on the resulting sizing performance [31, 225].

This high sensitivity of ASA emulsions towards water hardness is respected in industrial-scale by only using fresh water for starch cooking, emulsification or dilution issues within the emulsion preparation steps.

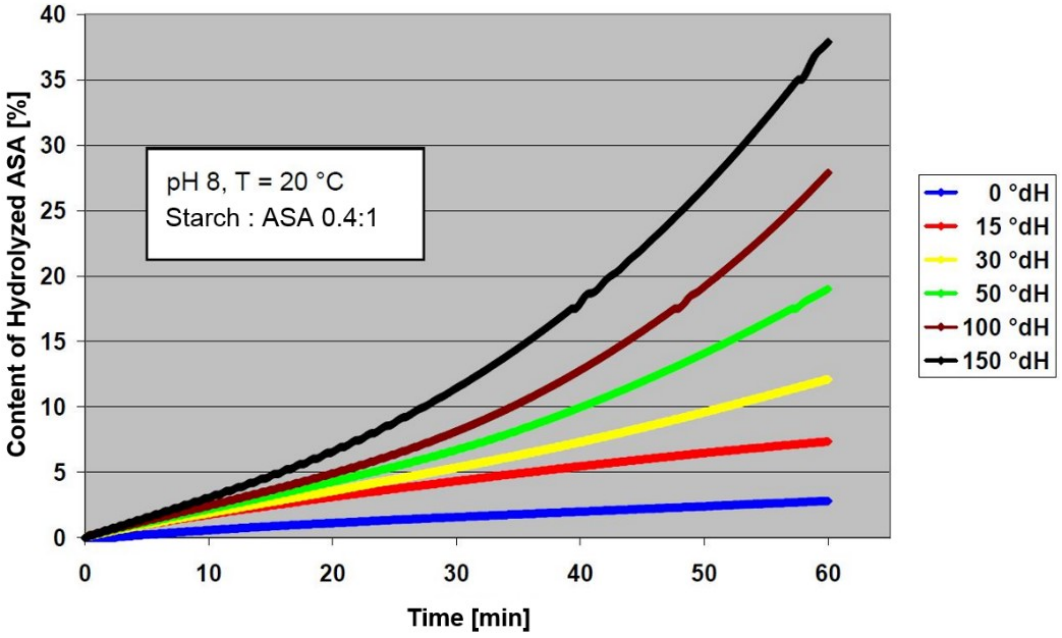

Figure 2.3-27: Impact of Water Hardness on ASA Hydrolysis Rate (translated from original [31])

2.3.3.2 Fiber Types

Even though there is a lack of scientific proof, it is well known to the suppliers, as well as to the paper & board producers that sizing with ASA is prone to the same stock impact factors than AKD [191]. This is why these factors are explained and visualized using the example of AKD. Figure 2.3-28 [195] shows the following global tendencies. First, hardwood fibers show a higher size-ability compared to softwood fibers. Second, unbleached pulp is better to size compared to bleached pulp. Third, sulfate/kraft grades show a higher size-ability compared to sulfite grades. The last observation that has been made, is that secondary fiber grades (OCC, DIP), in general show weaker size-ability compared to virgin grades [195, 226, 227].

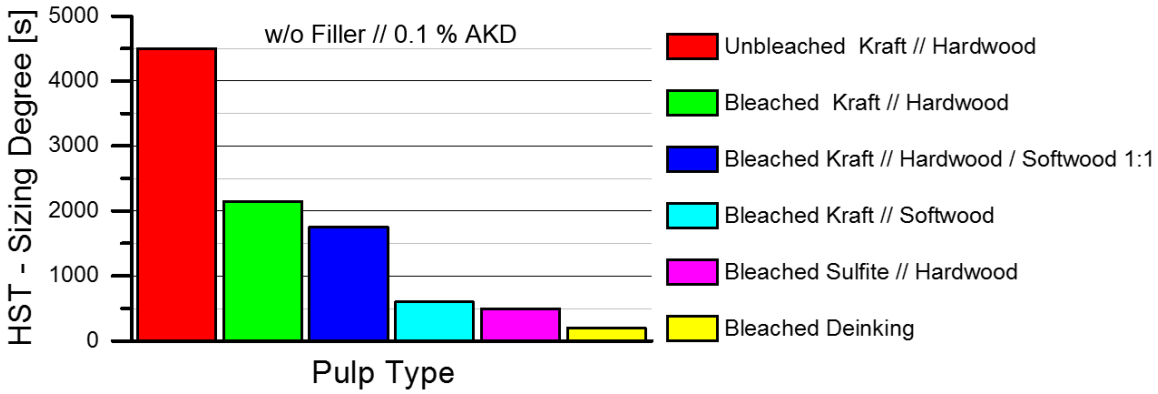

Figure 2.3-28: Impact of Pulp Type on AKD-Sizing Performance [195]

2.3.3.3 Filler Types

As the production of unfilled paper or board grades only represents a minor share of the globally produced grades, the impact of fillers on the sizing performance of ASA has to be taken into account as well. The impact of different commonly used filler types is displayed in Figure 2.3-29 [31].

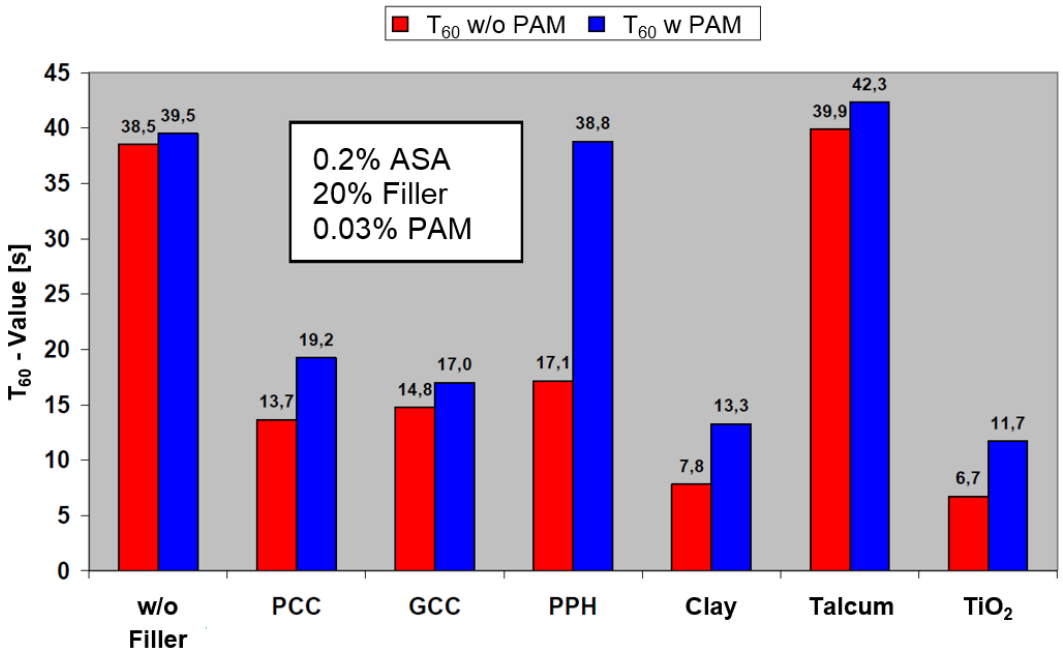

Figure 2.3-29: Impact of Filler Type on ASA-Sizing Performance (translated from original [31])

This graph, as well as other publications state that the sizing performance is significantly influenced by the type of filler used and by the content in the paper sheet [35, 225]. The mostly negative impact of fillers on the sizing performance is based on two main factors. The first is the comparably low first-pass retention of filled systems compared to unfilled ones. A decreasing first-pass retention

decreases also the retained amount of ASA in the sheet and thus causes undesired hydrolysis of the unretained fraction. The second factor is the very high specific surface area and the surface charge of some filler types. This is why especially fine filler types, such as PCC, GCC and TiO_2 are affecting the sizing performance explicitly negative [195]. The most negative observable impact is caused by clay, when used as filler and not as pigment [31]. It is possible to compensate the negative side effects of high filler dosages by the modification of their surface properties, as it is done with PPH (Pigment Polymer Hybrid) [228].

2.3.3.4 Cationic Additives

Cationic additives are key components to successful ASA sizing. Their synergetic effects have widely been analyzed and are therefore well known. Next to the use of cationic emulsion polymers, other cationic additives, like starches, wet strength resins, retention aids, fixatives and aluminum compounds are known to promote ASA's sizing performance [35, 112, 169, 208, 223]. For these additives it can be observed, that an increase in their dosage does not only promote the sizing performance, but also increases the ASA retention. This is based on the retention promoting properties of most cationic additives. Figure 2.3-30 [31] displays the synergetic effect of cationic internal starch on the sizing performance.

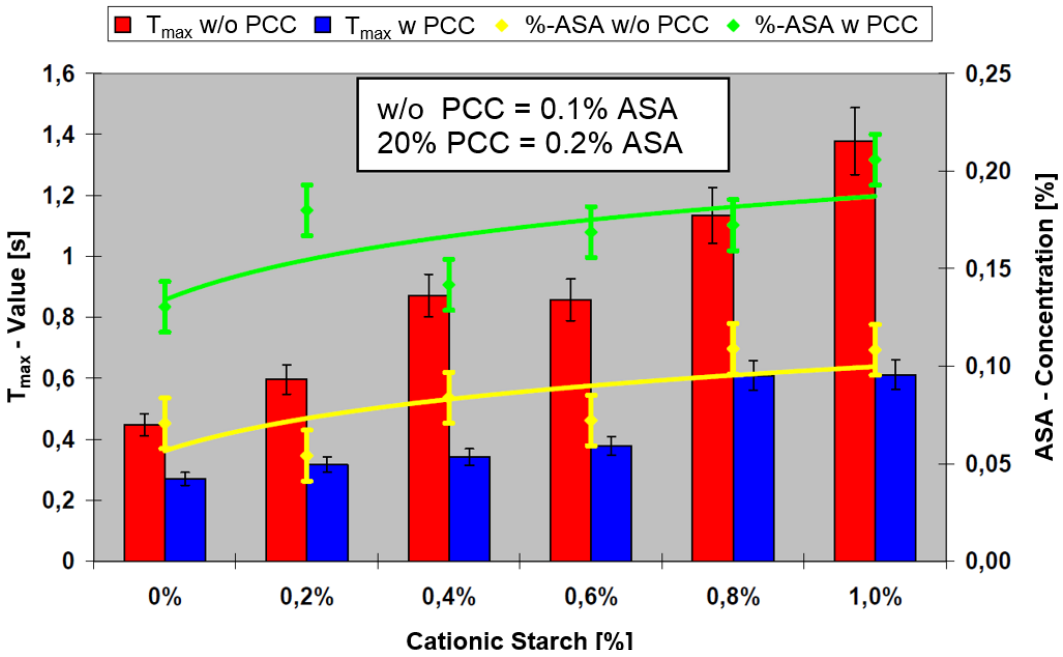

Figure 2.3-30: Impact of Cationic Starch on ASA-Sizing Performance (translated from original [31])

A further synergetic effect, that has been observed are the sizing promoting properties of aluminum compounds. These are not only supposed to increase the ASA retention, but to also promote the ASA fixation and orientation after sheet forming. This synergetic effect is displayed in Figure 2.3-31 [31] on the example of alum [31].

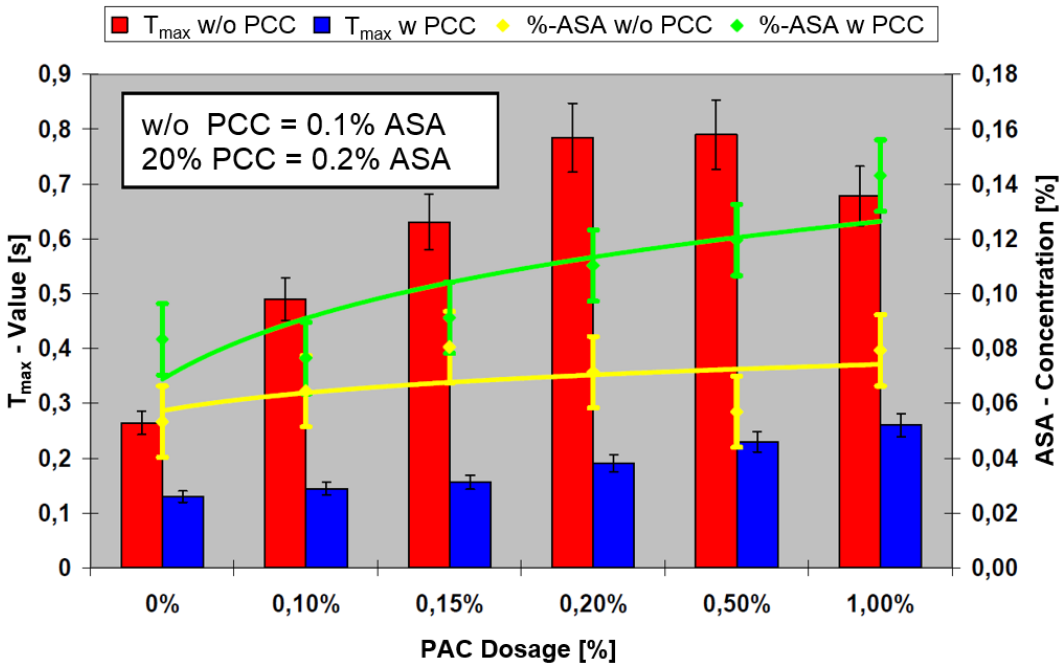

Figure 2.3-31: Impact of PAC Dosage on ASA-Sizing Performance (translated from original [31])

2.3.3.5 Anionic Additives

The presence of free anionic additives, such as dispersing or optical brightening agents is a trigger for several negative interactions with cationic additives such as retention aids, starches or emulsified sizing agents. Anionic molecules, also known as anionic trash, if not adsorbed to the fiber/filler surfaces, cause either a passivation or an agglomeration of cationic additives. As a result, their self-retaining properties are significantly minimized and by this, their way of action. The negative impact of free dispersing agent is displayed in Figure 2.3-32 [31], showing that an increasing content of anionic charge in the system is decreasing the ASA retention and subsequently the sizing performance [31]). This is why it is of highest interest within industrial paper & board production to dose anionic additives earlier in the process chain and as far as possible away from the dosing positions of cationic additives. If some undesired free/unbound anionic additives should remain

in the suspension at crucial points, they are fixated/flocculated with fixatives, which are also known as anionic-trash catchers (e.g., PAC, alum, polymeric fixatives) [11, 35, 229].

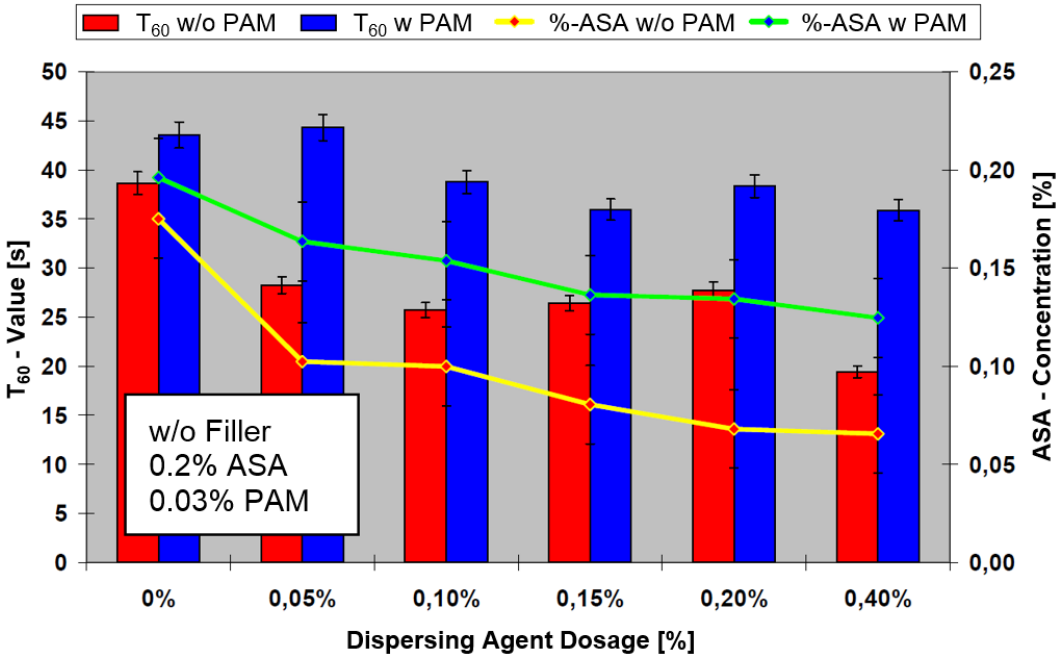

Figure 2.3-32: Impact of Anionic Dispersing Agent Dosage on ASA-Sizing Performance (translated from original [31])

2.3.3.6 Surface-Active Additives

Surface-active additives have the same chemical superstructure as sizing agents from a basic point of view, meaning hydrophilic and hydrophobic groups within one molecule. They serve the issue to decrease the interphase phenomena between two substances, by a decrease of surface energy, just as sizing agents do. The two main groups of surface-active additives, which are used for the production of paper & board, are defoamers and deaerators. Investigations have shown, that some product classes, especially defoamers such as fatty acid ethoxylates and fatty acid polyether, have the highest negative impact on the sizing performance (Figure 2.3-33 [31]). However, not only defoamers or deaerators which are dosed to the process continuously in order to maintain a certain process stability, are triggers for interactions, based on surface-active phenomena. Products, such as cleaners/tensides, which might remain in the system after a boil-out, or extractives from the pulp production process can cause quite similar interactions [31, 35, 230, 231].

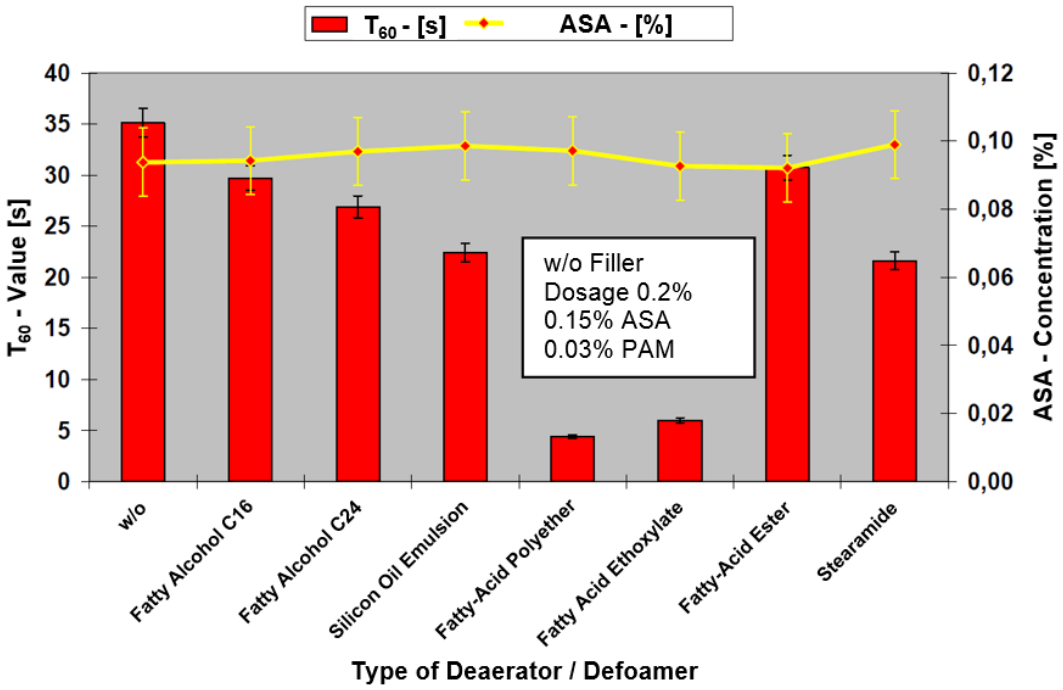

Figure 2.3-33: Impact of Defoamer / Deaerator Type on ASA-Sizing Performance (translated from original [31])

This well-known negative impact is thought to be based on interactions between the surface-active additives and the ASA-hydrophobized sheet surface once the sheet is dried. The mechanism is based on a surface energy increase of the sized paper surface by a misagglomeration of the surface-active molecules on the outermost layers of the interphase, causing a reduction of sizing performance.

2.4 Limitations of State-of-the-Art ASA-Sizing Analysis

Considering the state-of-the-art knowledge on reactive sizing with ASA, which was described in the previous Chapters, it becomes obvious that one existential link towards a holistic description of the sizing mechanisms is missing. As sizing agents are from their basic nature surface active additives which are added to the cellulosic system in order to decrease the surface energy, they do not only have to be present in the sheet structure, but they also have to be present equally distributed on the interface between cellulose and water. This interphase is the water-accessible surface of fibers and fillers within the sheet structure.

This background was elaborated by the author in a model which describes ASA sizing as a sum parameter that is based on three pillars (Figure 2.4-1 [232]). This sum parameter, which is representative for the final sizing result, is measurable via sizing performance analysis (Chapter 2.2.7) and based on the sizing agent quality,

the sizing agent quantity and the sizing agent localization. How these pillars are defined within this model will be described in the following.

Figure 2.4-1: The Foundation of Reactive Sizing with ASA [232]

The first pillar, the sizing agent quality, is defined as the type of ASA, its composition and its processing. This includes the length of the aliphatic rest (C16 or C18), the share between the lengths of the aliphatic rests, the amount and type of emulsifier used, the type and charge density of the protection colloid as well as the emulsification parameters (particle size, dilution rate, share of protection colloid/ASA, etc.). The magnitude of impact of these factors has widely been analyzed and optimized during the recent years (see Chapter 2.3) and can therefore be considered as well known.

The second pillar, the sizing agent quantity, describes the effective amount of ASA in the sheet structure after manufacturing. This amount is determinable via several quantification approaches, as described in Chapter 2.2.8. A series of approaches which have connected the amount of sizing agent in the sheet structure to the sizing performance, have shown that on the one hand, the sizing agent retention is a crucial factor, but on the other hand, the amount of sizing agent in the sheet structure cannot always be linked to the sizing performance (Chapter 2.3.2.2 & Chapter 2.3.3).

The third pillar, which defines the sizing agent localization within the sheet structure, is the yet still insufficiently known factor. As mentioned above, it is crucial for the sizing agent as surface-active additive to be positioned equally distributed among the whole surface/interface, in order to provide sufficient surface energy reduction. So far, none of the above-mentioned performance, qualitative or quantitative analysis methods are capable of analyzing this micro-scale distribution behavior within the sheet structure. This problem is due to either a required sample destruction (e.g., combustion by using Py-GC/MS), sizing agent extraction (e.g. HPLC), a far too big measurement area (e.g., NIR-Spectroscopy), or even a too low sensitivity toward sizing agents (e.g., Raman-, FTIR-Spectroscopy).

In order to holistically understand the mechanisms that lead to the sizing performance of ASA, it is considered as necessary to better understand the phenomena of sizing agent localization, which are supposed to be the missing link. As it is not possible to determine the exact localization of the sizing agent in a microscopic scale away from model substrates with the existing methods, it was necessary to develop a method which is capable of filling the existent gaps within the field of ASA localization in real life sheet structures.

2.5 Optical ASA Localization

2.5.1 **General Background**

The localization of ASA or its reaction products within the sheet structure is a topic of interest ever since it became common knowledge that ASA hardly reacts with cellulose. Contributing to this interest, one approach has shown that it is possible to trace the calcium salts (succinates) within the sheet structure by electron scanning microscopy [167]. However, no other paper states a potential measurement method for the microscopic analysis of the sizing agent distribution within the paper/board sheet.

Parallels to the field of bioscience have shown that it is a state-of-the-art analysis method to conduct destruction free and real time confocal microscopy analysis in the sub-micron range for the purpose of e.g., cell analysis [233]. Further investigations led to the conclusion that confocal microscopy might be a suitable tool for ASA distribution analysis, as it was already implemented for paper research

as a tool for topographical analysis [234, 235] and in one known special application for the tracking of marked PAE in the sheet structure [236].

The principles of confocal microscopy, with its benefits and restrictions and the focus on ASA localization are explained in the subsequent Chapters.

2.5.2 **Confocal Microscopy**

2.5.2.1 Principle

Confocal microscopy is an advanced derivate of conventional light or fluorescence microscopy. Even though it is possible to analyze samples at high magnification rates, conventional microscopy is suffering some drawbacks which influence the image quality significantly. One major problem is a picture blurriness deriving from out-of-focus planes, which causes undesired obscuring phenomena, especially when analyzing samples of higher thickness and when the desired focus planes are within the sample. This problem is based on the illumination of the whole sample thickness during conventional microscopy and the correlated light reflection of areas above and below the focus planes, resulting in reduced contrast values and thus in a lower obtainable resolution. This drawback is eliminated by the use of confocal microscopy, for which the physical set-up of the microscope suppresses the interference of reflection/blurriness of out-of-focus planes. This specific set up is displayed schematically on the example of confocal white light microscopy in Figure 2.5-1. As it can be seen, the set-up of diaphragms, dichroic mirror (beam splitter), and objective lens defines three points of focus, which are all in optical crucial positions *(confocal, Latin for point of same focus).* One is in the illumination pinhole, one on the focal plane and one in the confocal pinhole. This arrangement allows only reflected light from the focal plane (indicated as black lines) to enter through the confocal pinhole, preventing that any light rays from out of focus planes (indicated as red lines) cause interferences at the detector. Enabled by these features, pictures taken by confocal microscopy are defined by a very high resolution and a comparably low extent of interference. The depth of the focal plane, the achievable lateral and axial resolution are defined by the numerical aperture of the objective, the wavelength of the light source and the diameter of the pinholes. The lower this diameter, the higher the confocal effect. The depth of the focal plane and the maximum achievable lateral and axial

resolution are defined by the formulas (Equation 2.5-1, Equation 2.5-2, Equation 2.5-3 and Equation 2.5-4) [237-240].

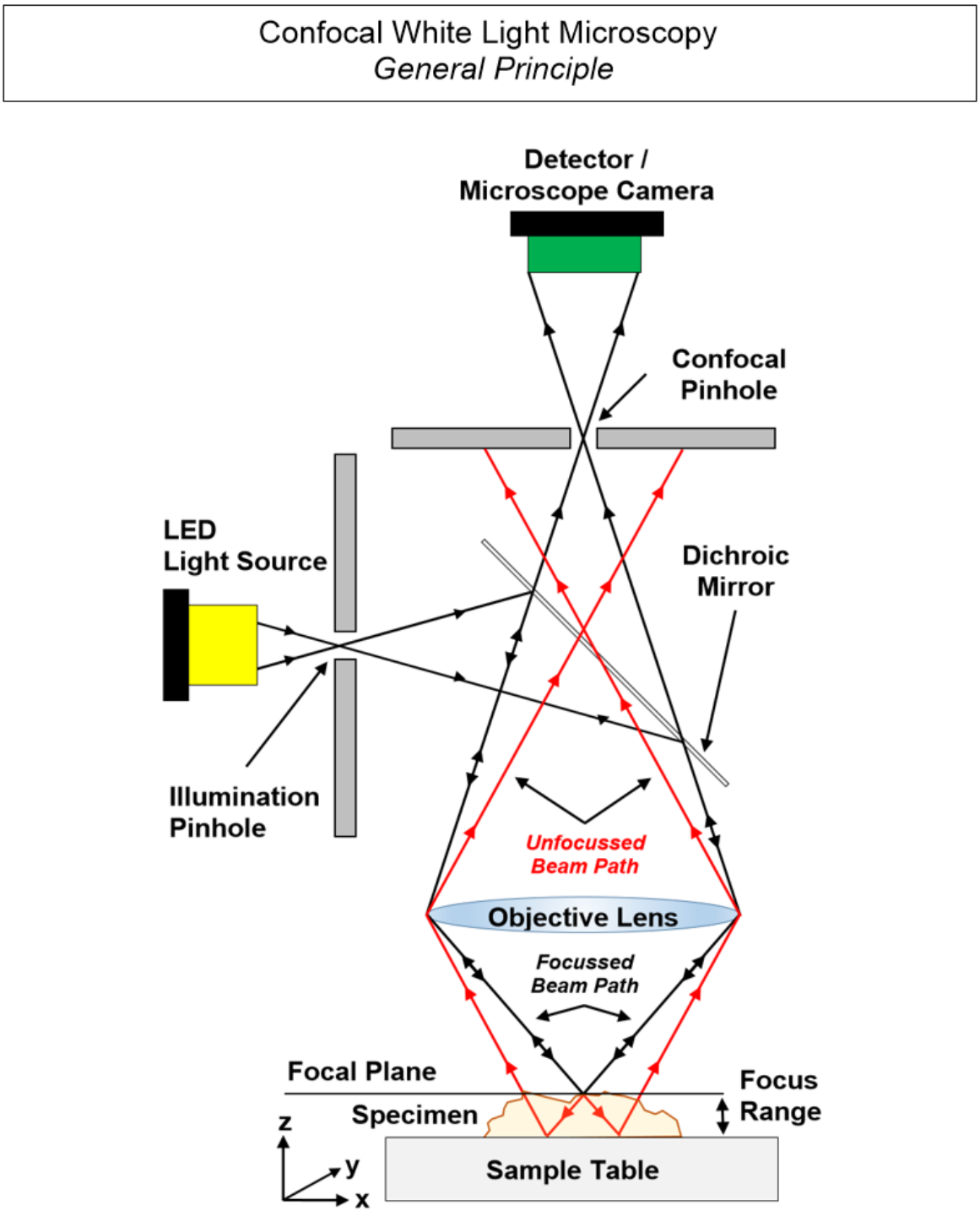

Figure 2.5-1: Principle of Confocal White Light Microscopy

$$d_{min} = \frac{\lambda_0}{NA_{obj.} + NA_{cond.}}$$

$$d_{min} = \frac{\lambda_0}{2 * NA_{obj.}}$$

Equation 2.5-1: Microscopy // Lateral Resolution / Abbe Diffraction Limit [237]

d_{min}= Minimum Resolvable Lateral Spacing between two Lines [nm]

λ_0 = Wavelength of Light

$NA_{obj.}$ = Numerical Aperture of the Objective

$NA_{cond.}$ = Numerical Aperture of the Condenser

while for confocal microscopes $NA_{obj.} = NA_{cond.}$

$$r_{Airy}\ or\ d_{Rayleigh} = 0{,}61\ \frac{\lambda_0}{NA_{obj.}}$$

Equation 2.5-2: Microscopy // Lateral Resolution / Airy Diffraction Limit [237] or Rayleigh Criterion [240]

r_{Airy}= $d_{Rayleigh}$ = Minimum Resolvable Lateral Spacing between two Reflecting Spots [nm]

λ_0 = Wavelength of Light

$NA_{obj.}$ = Numerical Aperture of the Objective

$$z_{min} = \frac{2 * \lambda_0 * \eta}{(NA_{obj.})^2}$$

Equation 2.5-3: Microscopy // Axial Resolution / z-Diffraction Limit [237]

z_{min}= Minimum Resolvable Axial Spacing between two Reflecting Spots [nm]

λ_0 = Wavelength of light

η= Refractive Index of Object Medium

$$\delta = \frac{1}{4} * ({z_{min}}^{+} - {z_{min}}^{-})$$

Equation 2.5-4: Microscopy // Depth of Filed [237]

δ= Depth of Field [nm]

z_{min}^{+}= First Axial Minima above central Maximum [nm]

z_{min}^{-}= First Axial Minima below central Maximum [nm]

2.5.2.2 Features, Advantage and Applicability for Paper-Component Analysis

The features and advantages of confocal compared to conventional microscopy can be summarized, as displayed in Table 2.5-1. Many different types of confocal microscopes are available on the market, all based on different working principles such as laser scanning, electron beam scanning, fluorescent light or white light. All of them have their advantages in respective fields of research. While analyzing the different microscopy types, it turned out that the principle of white light confocal microscopy could be of highest interest not only for topographical analysis of paper, but also for the analysis of paper components. Its principle is based on the sample illumination with a light source that delivers light of all wavelengths throughout the

visible area. This results in the advantage of microscopic pictures that do not only deliver the above-mentioned advantages of general confocal microscopy, but also deliver real color information of the examined specimen.

Table 2.5-1: Advantages of Confocal vs. Conventional Microscopy

Advantages of Confocal vs. Conventional Microscopy
− Reduction of blurriness deriving from light reflection / scattering of out-of-focus planes. − Optimized signal-to-noise ratio. − Increased effective / minimal resolution. − Enabled examination of voluminous, light scattering samples (e.g., paper). − Possibility to conduct real 3-D analysis by x-y-z mapping. − Low extend of stray light and photo bleaching by only a very small illuminated sample spot.

The implementation of an optical analysis method always requires an optical differentiability of the substance to be analyzed from the surrounding substances that are of no interest. If the substance does not deliver these properties in terms of shape or shade/color, it is necessary for it to be marked. This is usually done by a staining/dying step. The most implemented procedure is fluorescent staining, while using fluorescent microscopy approaches (e.g., in biosciences). For the case of white light confocal microscopy a fluorescent staining step is of no advantage, because these types of microscopes are neither equipped with either the right light source for fluorescence excitation, nor with filter units for the isolation of the emitted light. Therefore, it is necessary to dye/stain the substances of interest with dyes that absorb and emit light in the visible wavelength area. An additional requirement is a high color intensity of the marked substance, which enables the examiner to properly differentiate the substance of interest from the background [237, 240, 241].

2.5.3 **Dying / Staining**

Transferring the above-mentioned information on the application of confocal white light microscopy in order to trace ASA within the cellulosic sheet structure, it needs to be taken into consideration that ASA is a translucent liquid with a slight amber shade, which is hardly differentiable from cellulose. This states the clear need to dye or stain ASA prior to analysis.

This requirement is also valid for the analysis of proteins, DNA, RNA, lipids or any other substances of interest within the field of biosciences. To fulfill these requirements a typical staining principle is implemented. As these approaches mostly deal with the optical analysis of substances that are already in the specimen, it is necessary to also dye the substance of interest within the specimen. In the field of biosciences, this dyeing step is usually done under solvent (water, alcohol, etc.) atmosphere, while the dyes adsorb on or bind to the substances of interest [236, 242, 243]. By choosing highly selective dyes, it is possible to mark selectively, transferring the fluorescent properties of the dye to the substance of interest and by this visualize it during microscopic analysis [237].

As the mentioned staining methods require dye application under solvent atmosphere, it is, due to the volatile mobility of ASA, not possible to implement these, as they would change the distribution behavior of ASA within the sheet structure. This is why an alternative approach of ASA dyeing/staining has to be implemented. This step has to include the dyeing of ASA prior to the contact with the specimen, making it from the basic principle similar to 13C labeling [102], during which labelled ASA is induced to the system and later analyzed with a specific method (NMR). While following this approach, several aspects have to be considered in order to avoid undesired interactions or deviations once ASA is dyed. As the method is supposed to suit the description of ASA's distribution and mobility behavior within the sheet structure, it has to be of highest importance, that the dye does not have any impact on ASA's crucial properties. Therefore, it is necessary to consider possible changes in ASA's chemical or physical properties, as well as the mixing and de-mixing properties, in order to confirm that the sizing mechanisms of conventional ASA are reconstructable with D-ASA.

An additional point of importance is the color of the suited dye and the optical discriminability of D-ASA from cellulose. It is therefore necessary, that the dye transfers a very deep shade onto ASA. This is supposed to increase the contrast between ASA and cellulose and minimize optical confounding between the D-ASA and native cellulose components.

3 Discussion of Results

The following section of Chapters will describe the development of the implemented approaches, their conduction as well as the generated results. The first section will describe the development and verification of an optical analysis method based on confocal white light microscopy for the determination of ASA within the sheet structure. This Chapter will be followed by a section on the determination of the main performance-impacting factors for ASA sizing. The most important impact factors on the sizing performance will subsequently be analyzed by the developed localization method, in order to determine and quantify the correlation between the sizing performance, the localization behavior and external factors. In a subsequent step, the results of this correlation analysis will be transferred into an emulsion-modification-based optimization approach, which combines the gained knowledge of both, the sizing performance and the localization behavior analysis. The last step explained will be the transfer of the elaborated optimization approach onto industrial-scale production with the focus on significant sizing agent savings.

3.1 Localization of ASA within the Sheet Structure

The development of a comparably simple and reliable method for the localization of ASA or its derivates within the sheet structure was a main goal of this thesis. Based on the advantages explained in Chapter 2.5, it was decided to follow a localization approach via confocal white light microscopy, as this method enables yet unknown possibilities in terms of resolution and applicability for paper. The following Chapters on the localization of ASA within the sheet structure will describe the path from the determination of boundary conditions, such as ASA dyeing and microscope set up, the analysis of gained data, to the determination of repeatability and correlations with other papermaking parameters.

3.1.1 **Choice of Dyes**

ASA is an amber, translucent liquid, which can be discriminated by no chance from the cellulosic structure, by the use of confocal white light microscopy, without a dyeing or staining step. As explained in Chapter 2.5.3, ASA needs to be dyed prior to application in order to enable an unaffected representation of its behavior within

the sheet structure. To conduct this dyeing step without affecting ASA's chemical or physical behavior, some important facts have to be taken into consideration. The dye properties, required for a successful ASA staining procedure are listed in Table 3.1-1.

Table 3.1-1: Required Staining Dye Properties

Required Staining Dye Properties
− very deep shade for maximum contrast during analysis. − a color that cannot be confounded with other paper ingredients. − high solubility in ASA, without the tendency of de-mixing at the given circumstances (temperature, presence of water, pH, etc.). − no reaction with ASA (esterification, hydrolysis, etc.). − no effect on ASA's physical properties (viscosity and mobility). − no effect on ASA's processability nor sizing performance. − no affinity toward water and/or cellulose.

3.1.1.1 Dye Type

To fulfill the above-mentioned requirements, the selection of possible dyes had to be conducted very carefully, starting at the molecular structure of candidate substances. The most important aspect that was considered was the need of a "non-impact dyeing" step, meaning that ASA is not affected in any of its properties. This feature can only be reached by the use of dyes, which have a similar chemical structure to the one of ASA. The first criterion that had to be fulfilled was a predominantly hydrophobic structure, with the need to contain at least one polar group. This feature is supposed to increase the solubility in ASA and in addition to meme ASA's tenside-like structure, without being too hydrophilic. The second requirement was a molar weight in the range of ASA ($M_{ASA\ C18}$ = 351 g) in order to provide a similar molecular mobility. The third requirement was the need of a low possibility of chemical reactions between ASA and the dye, meaning a high degree of chemical inertness, as a reaction would not only change the chemical, but also the physical properties of the mixture. The last requirement was a dye melting point above process-typical temperatures, in order to ensure that the dye is dissolved and not melted in ASA. Table 3.1-2 and Figure 3.1-1 list the properties of five dyes that were selected as potential substances according to the given requirements, including one fluorescent dye which was used for a verification step, utilizing fluorescent light microscopy.

Table 3.1-2: Dye Specifications

Dye Type	IUPAC-Name - Formula -	Molar Weight	Reactive Groups	Melting Point
Sudan Red 7B [244]	N-ethyl-1-((4-phenyldiazenyl-phenyl)diazenyl)naphthalen-2-amine - $C_{24}H_{21}N_5$ -	379g	1 x 2nd amine	130 °C
Sudan Blue II [245]	1.4-bis(butylamino)anthracene-9, 10-dion - $C_{22}H_{26}N_2O_2$ -	350g	2 x 2nd amines	105 °C
Sudan Red III [246]	1-(4-(phenyldiazenyl)phenyl)-azonaphthalen-2-ol - $C_{22}H_{16}N_4O$ -	352g	1 x hydroxyl	199 °C
Sudan Black B [247]	(2.2-dimethyl-1.3-dihydroperimidin-6-yl) -(4-phenylazo-1-naphthyl)diazene - $C_{29}H_{24}N_6$ -	458g	2 x 2nd amines	120 °C
Nile Red [248]	9-diethylamino-5-benzo[α]phenoxazinone - $C_{20}H_{18}N_2O_2$ -	318g	none	205 °C

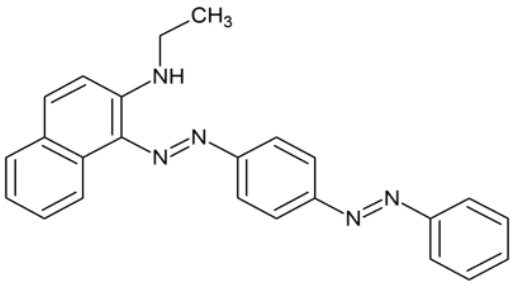

Sudan Red 7B

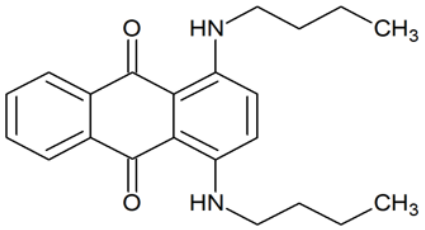

Sudan Blue II

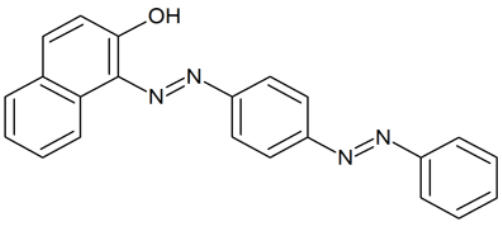

Sudan Red III

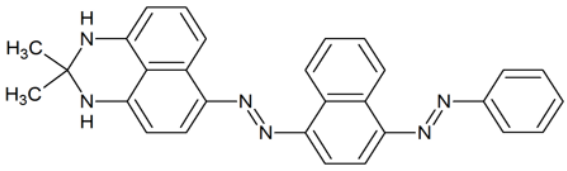

Sudan Black B

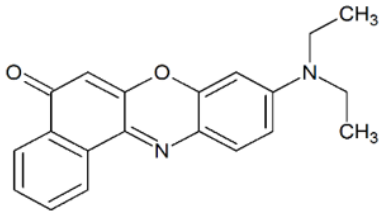

Nile Red

Figure 3.1-1: Selection of Dyes for ASA

3.1.1.2 Evaluation of Dye/ASA Mixtures

Subsequently to choosing these dye types, which were suitable from a theoretical point of view, it was necessary to analyze their behavior, once mixed with ASA. Within these trials, the maximum soluble dye content and the possible existence of reaction products of dye and ASA were analyzed.

ASA and the dyes were mixed within a standardized procedure, during which the dye was added to ASA at 70 °C under steady agitation for 10 minutes mixing time under exclusion of ambient air (petri-film seal). The properties of the mixture were analyzed after 24 h storage at ~ 10 °C (fridge) and subsequent warming to room temperature. The goal of this procedure was the determination of possible occurring temperature-triggered recrystallization effects.

3.1.1.2.1 *Maximum Soluble Dye Concentration*

As the optical determinability of ASA in the sheet structure will mainly be based on its contrast with the fiber-background, it is of highest importance to transfer a shade, as deep as possible on ASA. Therefore, the dye concentration has to be adjusted to a maximum level, while it still needs to be ensured that the dye does not recrystallize. The determination of the maximum soluble dye content was carried out via the analysis by conventional microscopy of dye-ASA mixtures of different concentrations. An excerpt of the captured images is displayed in the following figures (Figure 3.1-2).

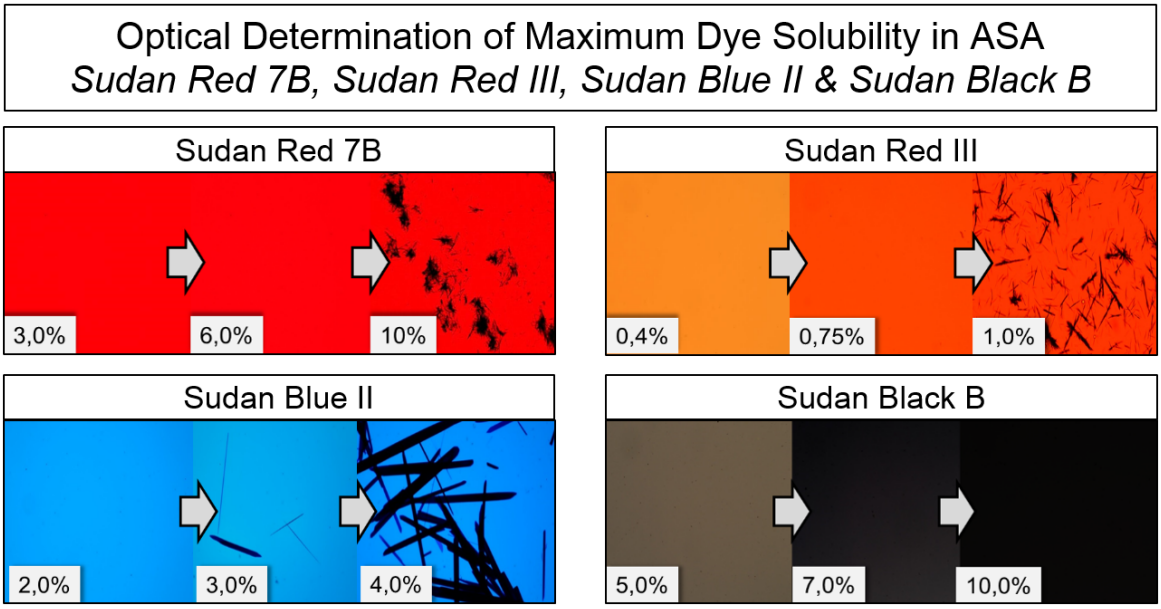

Figure 3.1-2: Optical Determination of Maximum Dye Solubility in ASA Sudan Red 7B, Sudan Red III, Sudan Blue II, Sudan Black B

The maximum soluble content of Nile Red in ASA was not analyzed by this approach, because the required amount of Nile Red for fluorescent staining was determined to range at 0.1%, which is far beyond the maximum solubility. As it can be seen from the microscopic pictures, the dyes tend to recrystallize at quite different concentrations. The determined values for each dye are listed in Table 3.1-3, while the concentrations for possible trials were chosen to be 2/3 of the maximum non-crystallizing concentration. This was done to provide some safety during the trials, in order to prevent unforeseen interactions, which could cause recrystallization effects at respectively lower concentrations.

Table 3.1-3: Maximum Soluble Dye Content

	Sudan Red 7B	**Sudan Blue II**	**Sudan Red III**	**Sudan Black B**	**Nile Red**
Maximum Non-Crystallizing Concentration	7.5%	2.5%	0.75%	10%*	n.V.**
Trial Concentration	5%	1.67%	0.5%	6.67%	0.1%

* *an evaluation above 10% was not possible, because of total light absorption by Sudan Black B.*

** *maximum soluble dye content was not determined, as there was no need.*

The results of the maximum soluble dye content determination lead to the conclusion that Sudan Red 7B (SR7B) is the dye of choice for the development of the desired optical analysis method. Sudan Red III and Sudan Blue II were excluded at this point of development, as their maximum soluble dye content and thus the degree of shading is significantly lower compared to SR7B. An additional factor for their exclusion is their comparably higher reactivity toward ASA. Sudan Black B was excluded even though its shading performance was the highest, because its black shade could be confounded with shadows within the microscopic pictures. This bears the possibility of the generation of false values, and thus had to be eliminated.

3.1.1.2.2 *Thin Layer Chromatography*

In order to ensure that ASA does not react with the dyes, the mixtures of ASA and SR7B, as well as the one with Nile Red (NR), were analyzed via thin layer chromatography (TLC). The mobile phase of choice was chosen to be a 1/1 mixture of toluene and ethyl acetate, as it showed the best separation values for the analyzed substances. Figure 3.1-3 displays the results of the TLC trials, while it

can be seen that it was not possible to find any reaction products of ASA with either SR7B or NR. An interesting additional outcome of these trials was that SR7B did split into two frontiers during TLC, proving that the used substance was as declared by the vender not of 100% purity, but contaminated with some additional substance. This substance (SR I) which appeared during the analysis of SR7B, as well as during the analysis of the mixtures, showed a specifically lower mobility.

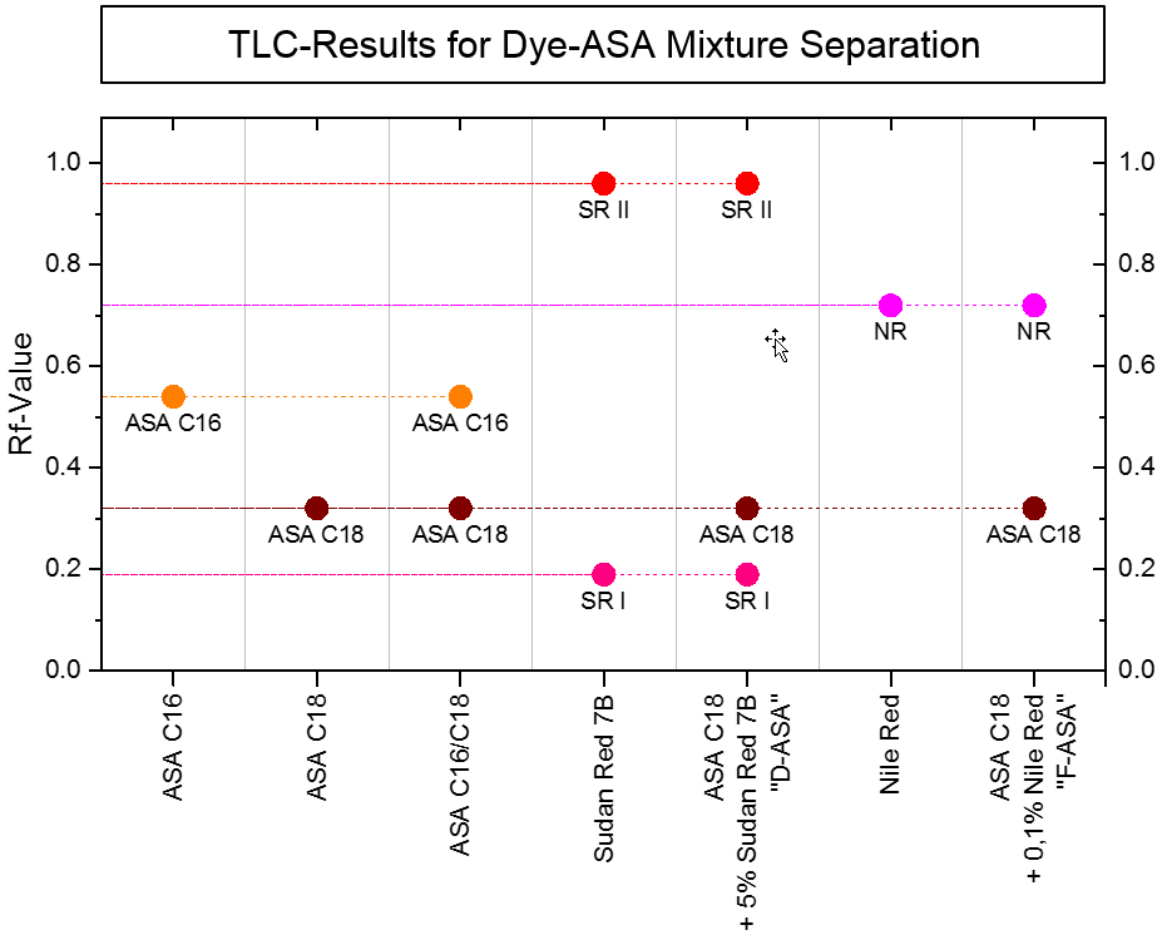

Figure 3.1-3: TLC-Results for Dye-ASA Mixture Separation

3.1.1.2.3 *FTIR-Spectroscopy*

For the verification of the TLC results, FTIR spectra of ASA and the mixtures in hydrolyzed and unhydrolyzed form were taken (Figure 3.1-4). The goal of this approach was to make sure that, from a molecular point of view, no reaction between the substances occur which were not determinable by TLC. If there were to be a reaction, new molecular bonds would be formed, which trigger differing molecular-group specific absorption spectra during FTIR analysis. The references for these analyses were the absorption spectra of ASA C18, partly hydrolyzed ASA

C18 and fully hydrolyzed ASA C18. The analysis of the mixtures was consequently conducted by spectra subtraction and the determination of the resulting peaks. For the evaluation of the ASA and SR7B mixture (D-ASA), the formation of amide bonds between the ASA and the secondary amine of SR7B could be observed. Even though this reaction is very unlikely to occur, as the secondary amine's nucleophilicity is comparably low [156], a reaction would create an additional absorption maximum. The product of this reaction would be a tertiary amide, which has its absorption maximum at 1670 cm^{-1} to 1630 cm^{-1}. This maximum could not be found in the unhydrolyzed and hydrolyzed mixtures and consequently a possible reaction of ASA with SR7B could be excluded.

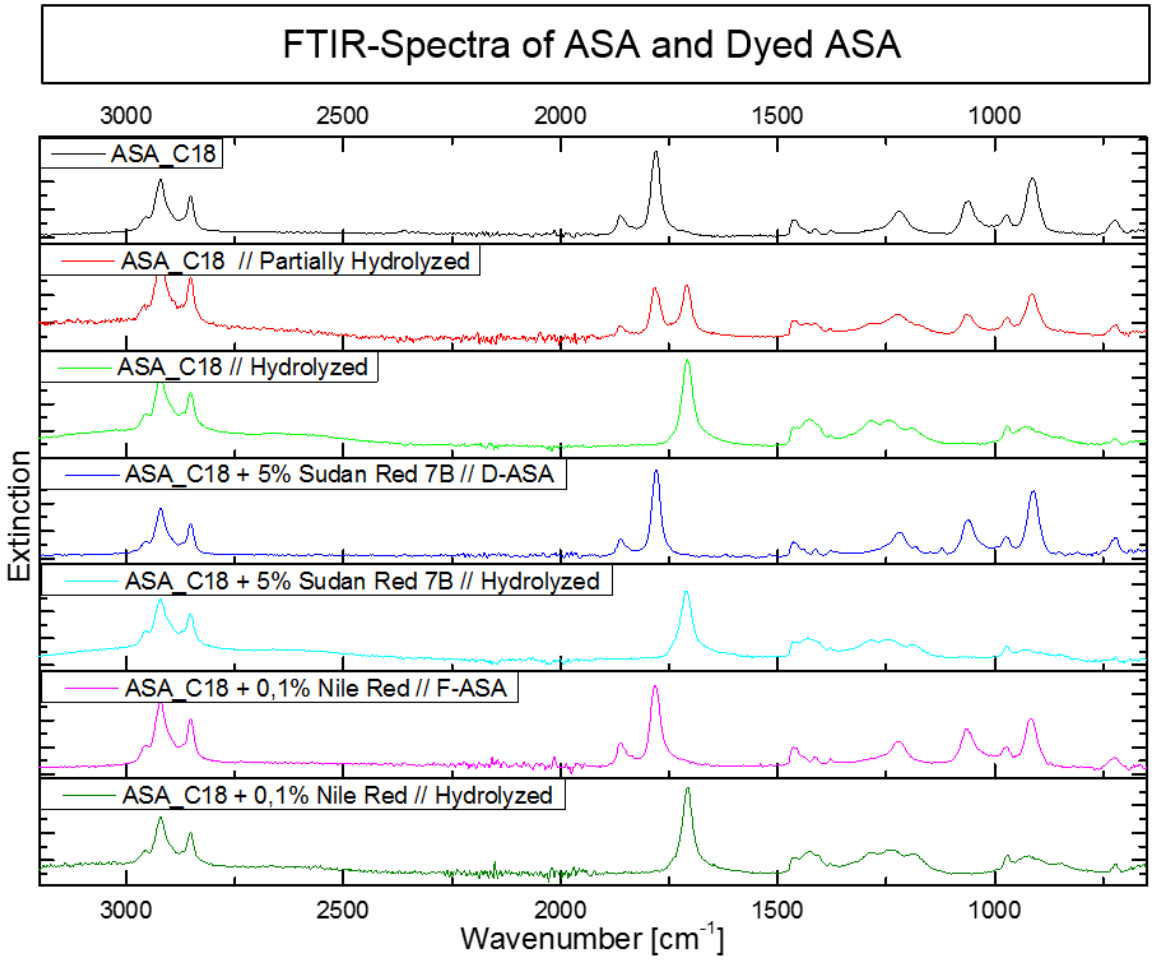

Figure 3.1-4: FTIR-Spectra of ASA and Dyed ASA

FTIR analysis of ASA and NR (F-ASA) mixtures were only conducted, in order to see if any unexpected structural changes appear after mixing, as NR shows no reactivity toward ASA at all. The unhydrolyzed and hydrolyzed mixtures behaved just as the reference ASA samples, which proved that no reaction occurred.

This trial, in combination with the TLC results displayed that either SR7B or NR are suitable substances for the purpose of ASA dyeing from a chemical point of view, as they properly dissolve in, and not react with ASA.

3.1.1.3 Evaluation of the D-ASA Emulsion

The next step towards a possible applicability of the D-ASA mixtures as full-value sizing agents was the determination of their processability. The most important step during ASA processing within sizing applications is the emulsification step. Keeping in mind that the particle size, as well as the emulsion stability, do have a major impact on ASA's sizing performance, it was of highest interest to analyze the impact of the dyes on the emulsion properties. This was done by particle size measurements directly after emulsification and after 10 minutes of storage at high dilution. Respecting the fact that the emulsification result is highly dependent on the sizing agent viscosity, it was assured prior to the subsequent trials that the mixtures had no significantly differing viscosity values from pure ASA.

The particle size distribution (Figure 3.1-5 [24]) of pure ASA and the mixture directly after the emulsification step can almost be considered as congruent. The main peaks of both substances are located between 2 µm and 3 µm, while the distribution of the mixture is slightly wider with a higher share in the range below 1 µm. This tendency might be based on possible emulsifying, or shear thinning properties of SR7B. Due to the neglectable impact on the particle size distribution, no further investigations were conducted concerning this tendency.

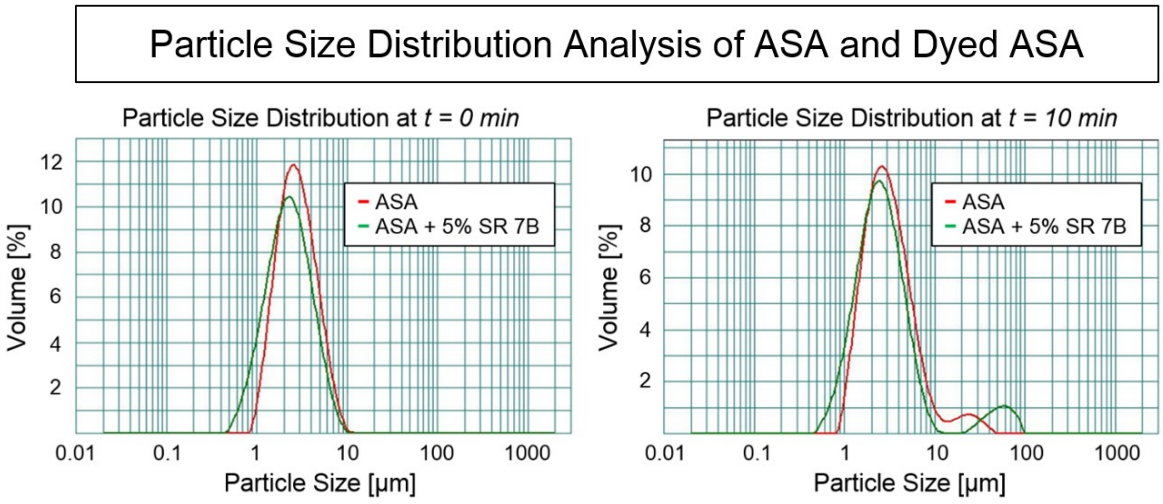

Figure 3.1-5: Impact of Dyeing on the Particle Size Distribution after 0 min and 10 min [24]

The situation after 10 minutes does not show significant changes. Both distribution curves are almost unchanged in the range < 10 µm, while each curve shows a small additional peak in the range from 10 µm – 100 µm. This peak is typical for shortly aged samples, as it indicates on the one hand the normal emulsion instability (agglomeration) and on the other hand, the typical deviations caused by air entrainment over longer measurement times.

The particle size distribution of the mixtures with NR did not show any deviations compared to those of pure ASA. This might be based on the comparably low Nile Red content of only 0.1%.

3.1.1.4 Paper Chromatography with D-ASA & F-ASA Emulsions

The first approach to analyze the behavior of D-ASA and F-ASA once in contact with cellulose was conducted via a simple paper chromatographical approach. For this approach, a RK paper sample made of virgin fibers (400 g/m² reference stock system, Chapter 4.3.1.1) was put into a 0.2% solution of D-ASA or F-ASA Emulsion. The goal of this approach was to prove that the dye stays with the ASA while travelling through the cellulose. This was an essential feature to further develop the optical analysis method development. Following the procedure of conventional paper chromatography, the measurement was conducted by letting the emulsion travel upwards through the paper sample until the waterfront reached about 90% of the sample's height. Sampling was aborted by a subsequent contact-drying step at 120 °C for 5 minutes.

During analysis of the dried samples, it was observable that two frontiers were visible (Figure 3.1-6 [24]), one for the water front and one that marked the travelling distance of the dye. The samples were subsequently analyzed along the travel direction of the emulsion by contact angle analysis for sizing performance evaluation and by iodine test for starch determination. The results are indicated in Figure 3.1-6, while it was observable that both tests turned negative on the edge of the dye boundary. This states that ASA (positive contact angle test), starch (positive iodine test) and the dye (color appearance / UV for F-ASA) travelled the exact same distance through the sample, which is proof that the dye remains with the stable emulsion within ASA and does not show any differing mobility properties.

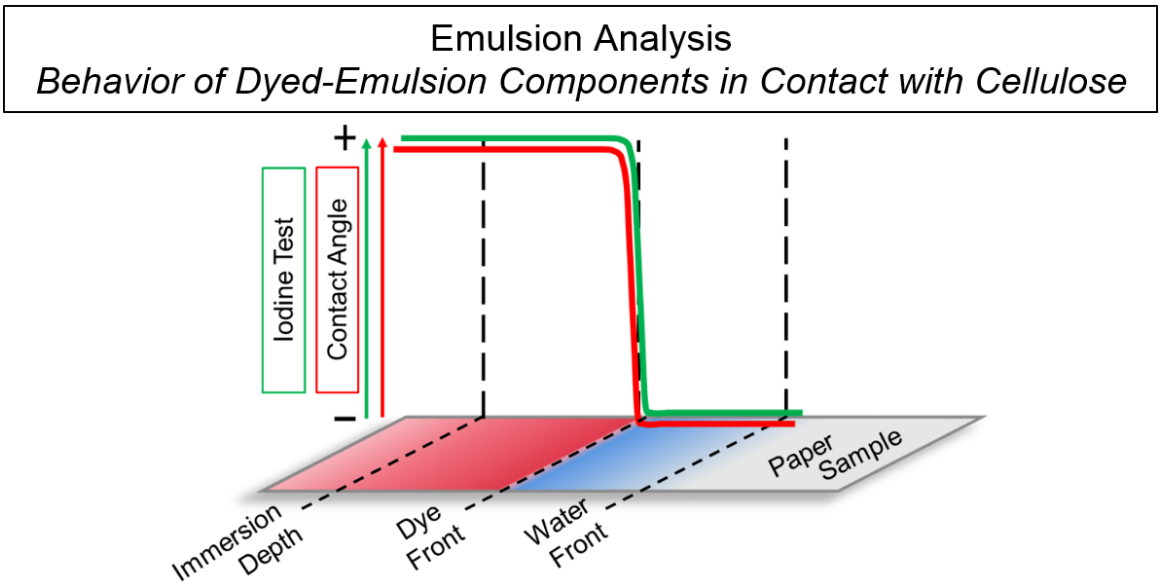

Figure 3.1-6: Emulsion Analysis - Behavior of Dyed-Emulsion Components in Contact with Cellulose [24]

3.1.1.5 Evaluation of the D-ASA Emulsion's Sizing Efficiency

The final step in the evaluation chain for the applicability of D-ASA as full-value sizing agent was the determination of the impact of the dye content on the sizing performance. This impact was analyzed by a trial set up, during which on the one hand the share of D-ASA to standard ASA was varied and on the other hand the sizing agent dosage. This approach was supposed to give answers on the impact factor of D-ASA over the whole sizing agent dosage range. Figure 3.1-7 displays the dye impact on the example of SR7B, where the values for t_{max} are displayed on the left and the ones for t_{60} on the right.

The discrimination between t_{max} and t_{60} was done, in order to see, if the presence of dye rather affects the surface or the substrate hydrophobicity. The results of this trial show that the sizing performance of ASA is not reproducibly affected by the presence of SR7B over the whole dosage range, neither in terms of surface nor substrate hydrophobicity. Trials with NR showed no impact on the sizing performance as well.

These results verify the ASA systems dyed with SR7B or NR as full value sizing agents, enabling the subsequent development of the achieved optical localization method.

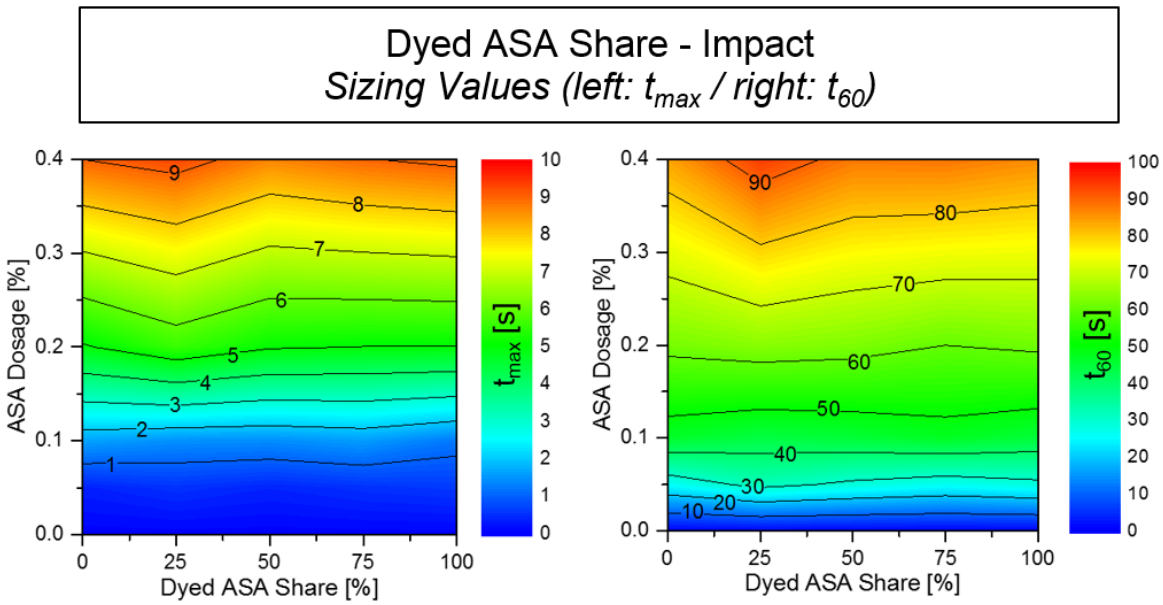

Figure 3.1-7: Impact of SR7B Content on ASA-Sizing Performance

3.1.2 **The Localization Method**

From their first appearance, the paper samples sized with D-ASA had a very homogeneous shade, which ranged from very light pinkish for lower dosages to intense pink at high dosages (Figure 3.1-8).

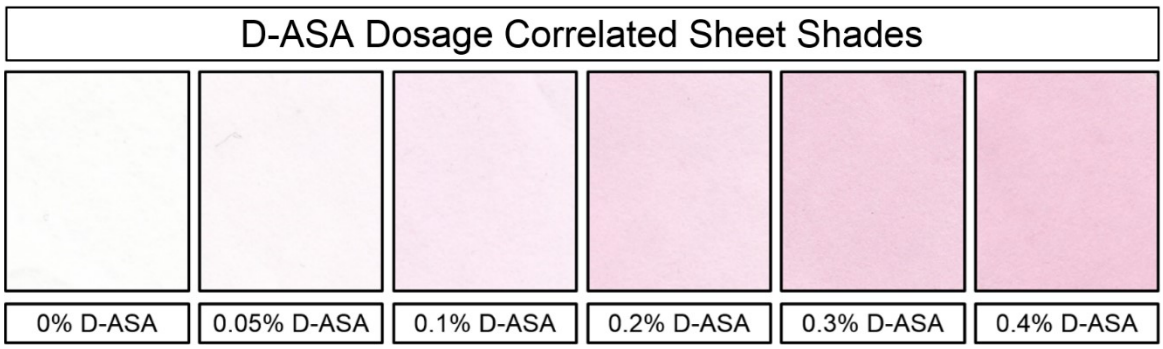

Figure 3.1-8: D-ASA Dosage Correlated Sheet Shades

As their initial optical appearance showed a very homogeneous shading and hence a homogeneous D-ASA distribution, it was crucial to analyze, whether the distribution behavior in microscopic scale is as homogeneous as it seemed in the macroscopic scale.

Figure 3.1-9 shows that the ASA distribution behavior turns more and more heterogeneous and random, the higher the chosen resolution is. Further, it became obvious that it is only possible to analyze the distribution behavior at an optical

magnification of factor 100, as only then agglomerates with a size below 1 µm² became visible.

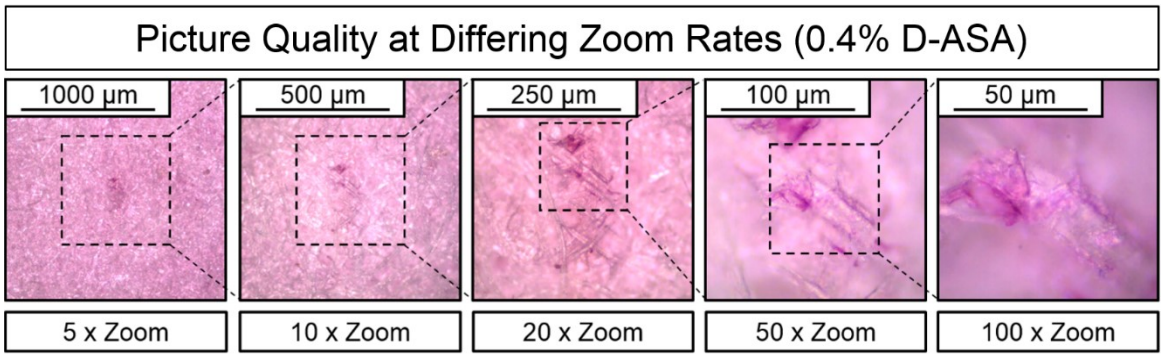

Figure 3.1-9: Picture Quality at Differing Zoom Rates (0.4% D-ASA)

The overall deduction that came along with the analysis of the first pictures was that ASA is heterogeneously distributed on a microscopic scale, while it shows the tendency to form agglomerates on the fiber surface. Facing the limitation of not being able to state, if ASA is also present out of the structures of the agglomerations, the subsequent step was the analysis of the agglomeration behavior. This approach was conducted in order to see, whether the agglomeration behavior is affected by external factors, and if it is possible to draw any conclusions concerning a correlation between the agglomeration behavior and the respective sizing performance.

3.1.2.1 The Correlation between ASA Distribution and Agglomeration

The heterogeneous distribution of ASA within the sheet structure, which was observed during the first analysis approaches, led to the conclusion that the optimal approach to distribution analysis is the indirect one via its agglomeration behavior. In the case of optimal ASA distribution, meaning same concentrations throughout the sheet structure, the color shade has to be uniform at all measurement points. If the distribution is heterogeneous, meaning that there are spots of different ASA concentration, the color density of these spots has to differ from its surroundings. This difference, especially for spots of respectively higher concentrations (agglomerates), can be discriminated via optical analysis and image processing, while the result can be directly correlated to the distribution behavior.

3.1.2.2 Measurement Settings

Even though the pictures presented in Figure 3.1-9 do show a heterogeneous distribution of ASA in the sheet structure, they cannot be taken as granted, as they only project the agglomerates in a single focal plane. To compensate this problem, the advantages of confocal microscopy were utilized, meaning the capturing of real color 3D pictures. The confocal microscopy system used for the presented trials and results was a module, type InfiniteFocus G3 by the Company Alicona GmbH. The microscope specific details are listed in Chapter 4.1.2.1.

The general specifications in terms of analyzed sample area and depth are displayed in Figure 3.1-10 [197], showing that the lateral dimensions of a single picture were 83.2 µm x 104 µm. The vertical component was defined by the highest and lowest focusable planes of the specimen, which correlated to the samples thickness.

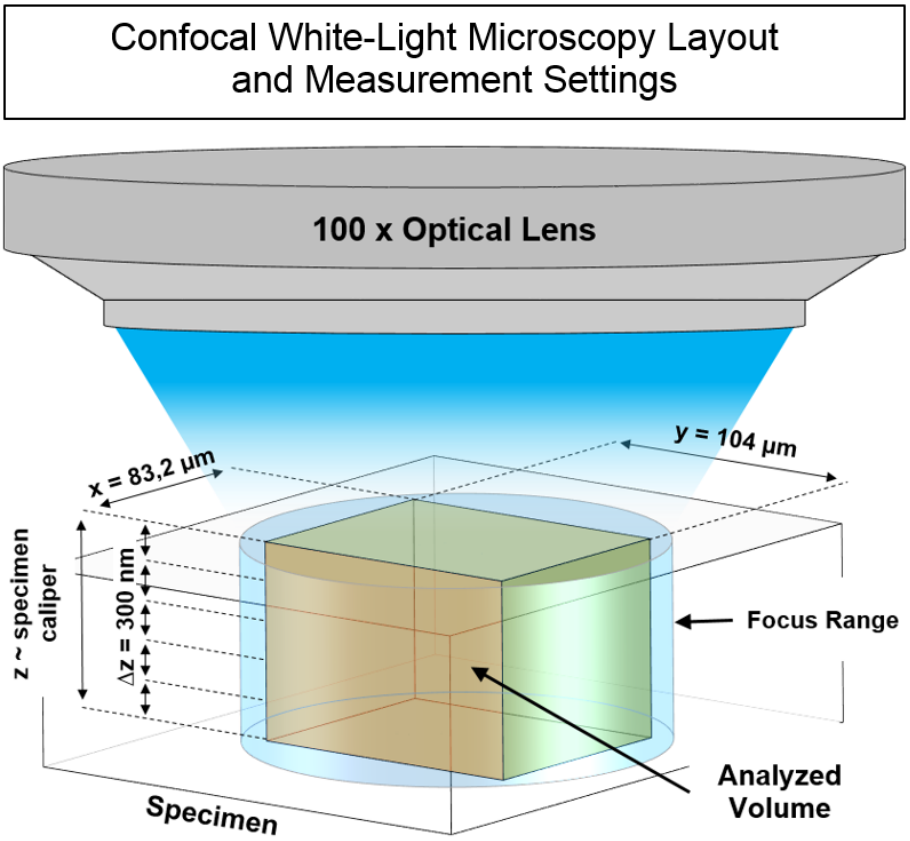

Figure 3.1-10: Confocal White-Light Microscopy Layout and Measurement Settings [197]

In order to gain optical information as dense as possible over the vertical planes, every 300 nm a picture was taken, resulting in ~ 500 single pictures for the analysis of a paper sample with a thickness of 150 µm.

The single pictures are automatically stacked into a 3D model of the sheet structure, which contains the agglomeration behavior over the whole sample depth. This 3D model of the sample volume is subsequently converted into a 2D top-view projection for simplified analysis (Figure 3.1-11).

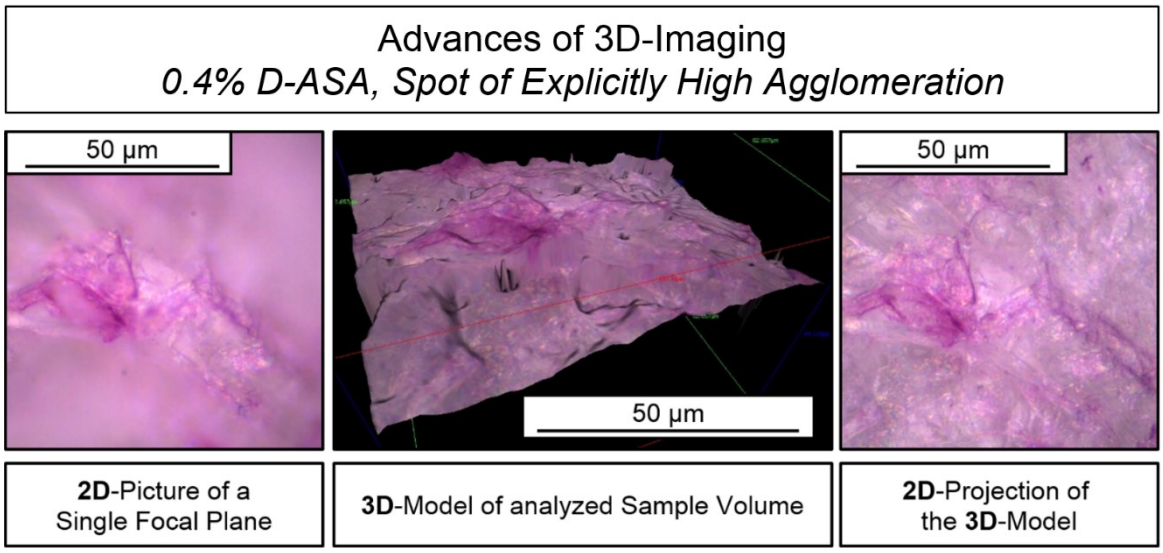

Figure 3.1-11: Advances of 3D-Imaging (0.4% D-ASA, Spot of Explicitly High Agglomeration)

3.1.2.3 Manual Analysis

The elaboration of a manual agglomeration-behavior analysis method was the foundation for a subsequent automization. It served the determination and development of the optimal microscope and measurement setting (Table 4.1-6 [24]), as well as the discrimination of boundary values for agglomerate identification. Initial imaging for manual analysis was conducted via field imaging, during which 3x3-image fields with the size of 280 µm x 220 µm were captured for analysis (Figure 3.1-12).

The analysis step was subsequently conducted with the software tool IF-MeasureSuite 4.2 (IFM), provided by the microscope supplier (Alicona), while every agglomerate was manually circled trice by a polygon (Figure 3.1-13 [24]). The average values for every agglomerate were refined and analyzed in a final step, giving values on the total agglomeration area (Aggl_A [%]), the number of agglomerates (Aggl_N [n/mm²]) and the average agglomerate size (Aggl_AV [µm²]). The IFM tool also provides the possibility to conduct 3D-analysis of isolated agglomerates, which supports the understanding of the agglomeration behavior (Figure 3.1-13 [24]).

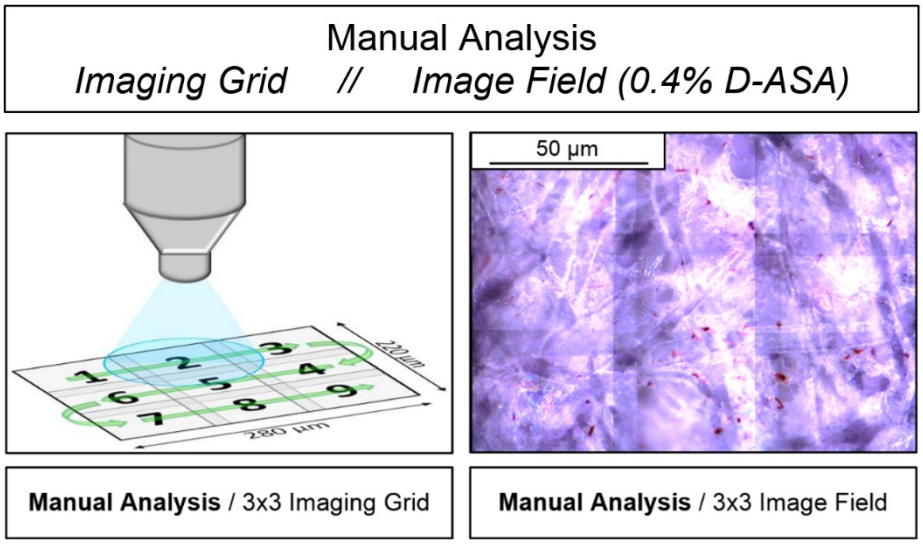

Figure 3.1-12: Manual Analysis / Imaging Grid (left) & Image Field (0.4% D-ASA) (right) [24]

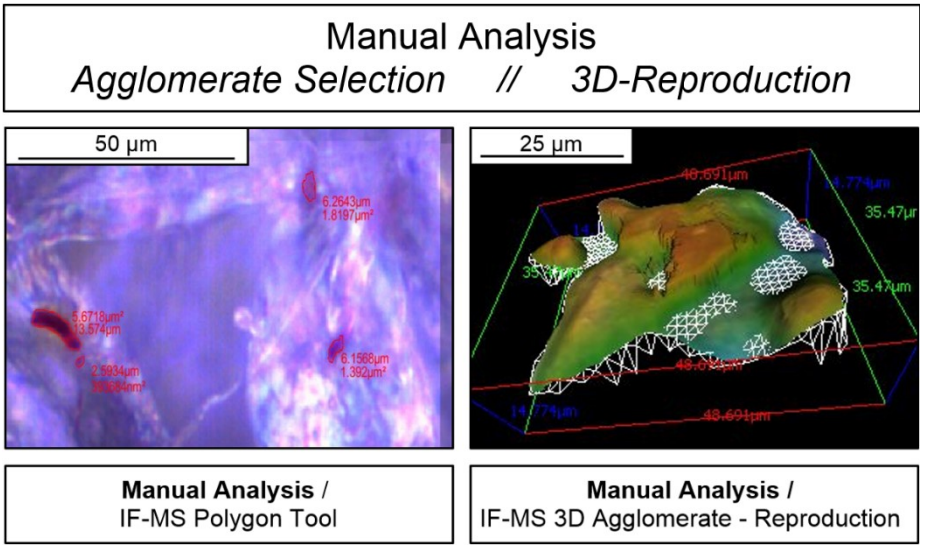

Figure 3.1-13: Manual Analysis / Agglomerate Selection (left) and 3D-Reproduction (right) [24]

The results of the trials analyzed by the manual method showed that it is possible to draw conclusions, concerning the correlation between the agglomeration behavior, process parameters and the sizing performance. These results are expressly designated as such and presented in Chapter 3.3 among those of the automated method.

Even though the manual measurement of the agglomeration behavior proved to be an applicable, reproducible and practical method, it showed some drawbacks in terms of time consumption and objectivity.

The first time affecting drawback was the image-field capturing mode. On the one hand, this required significant extra computing time for the image alignment after

capturing and on the other hand, was a lot more prone to malfunctions of the microscope. If only one picture of the whole 3x3-image set was defected, by e.g., vibrations, misalignment, the whole image set had to be recaptured. The second drawback in terms of time consumption was the manual analysis of the agglomerates. By circling every agglomerate trice with a polygon, in order to ensure statistical solidity, it was of no exception that it took 15 h – 20 h for a single image of a highly sized sample to be analyzed. The last drawback derived from the statistical analysis of the samples, which had to be done manually for every agglomerate, as there is no value export function embedded in the IFM.

The main drawback of this method was a possible lack of objectivity, as the agglomerates had to be circled manually by an individual. The circling of the agglomerates was supposed to be done on the exact boundary between the cellulose and the agglomerates. Aside of this definition is the position of this boundary, which derives from an optical contrast, affected by the individual's interpretation. This drawback was eliminated/minimized by the measure that all manual agglomerate measurements were conducted by a single individual, in order to provide comparability and repeatability within these trails.

3.1.2.4 Automated Analysis

Based on the fact that the manual localization measurement method delivered repeatable and significant results for the interpretation of the occurring mechanisms within the process of paper sizing with ASA, it was considered as a logical consequence to improve the measurement method towards full automization. The goal of this step was to get rid of the above-mentioned drawbacks, in order to improve the method in terms of time consumption, repeatability and robustness. The developed automated analysis method consists of two main steps, automated microscopy measurement and automated image processing, which are explained in the following.

3.1.2.4.1 *Automated Localization / Microscopy Measurement*

The software bundle provided with the Alicona IF-G3 microscope was equipped with some basic measurement automization script which was programmed for topographical serial analysis of paper samples. This script provides the basic settings required for the automated analysis of agglomerates, but as it was

designed for topographical issues with a maximum magnification of 20 x optical zoom, it had to be modified and adjusted to the given requirements. The detailed settings of this measurement script are listed in Table 4.1-6, while the basic steps can be explained as followed. Within one measurement, six different samples can be analyzed by the use of a six-windowed grid plate. During the measurement of one single sample, the microscope is programmed to take 12 individual 3D-pictures at random positions over the sample surface, which is about 35 mm x 35 mm in its dimensions. 3D-pictures are captured at 100 x optical magnification, following the settings explained in Figure 3.1-10. The focusing of the lowest and highest focal plane of each individual position is carried out via an autofocus step, ensuring that every single picture is in complete focus. By the implementation of this script, it is possible to analyze six different samples on all 12 positions, while each 3D-picture taken consists of 833 stacked frames (scan height 250 µm & 300 nm vertical resolution). The benefit of these settings are an autonomous measuring procedure, which delivers 3D-pictures of high optical density and statistical robustness in a comparably low required amount of time (~ 3.25 h / six samples). The individual pictures are automatically saved by the software in a 3D-formate and their respective 2D-projections (*.tiff* files).

3.1.2.4.2 *Automated Analysis / Image-Processing*

The second step of the automated ASA localization method consists of two individual image-processing steps, which are based on a primary filtering step with Adobe Photoshop (PS) and a subsequent vectorization step with Adobe Illustrator (AI). The goal of the image processing steps was the creation of crisp values out of the taken pictures in terms of total agglomeration area, number of agglomerates and average agglomerate size based on the optical information embedded in the 2D-projections of the pictures taken. To generate these crisp values it was necessary to develop specific filtering sequences for PS as well as for AI, while the results had to be adjusted to correlate with the values from manual analysis. The filtering sequences conducted by PS were made up of six action steps, consisting of 136 single filter actions, whose details are explained in Chapter 4.1.2.2.1, while their goal was the generation of a picture file that did only content the information of the determinable agglomerates. The results of each filter sequence are displayed using the example of the sample which was already

displayed in Figure 3.1-9 and Figure 3.1-11. This sample was chosen, because it contains an extraordinary high amount of agglomerates, making it especially suitable for the illustration of the filter sequences working principles. Figure 3.1-14 displays the results of each of the six filter sequences/actions.

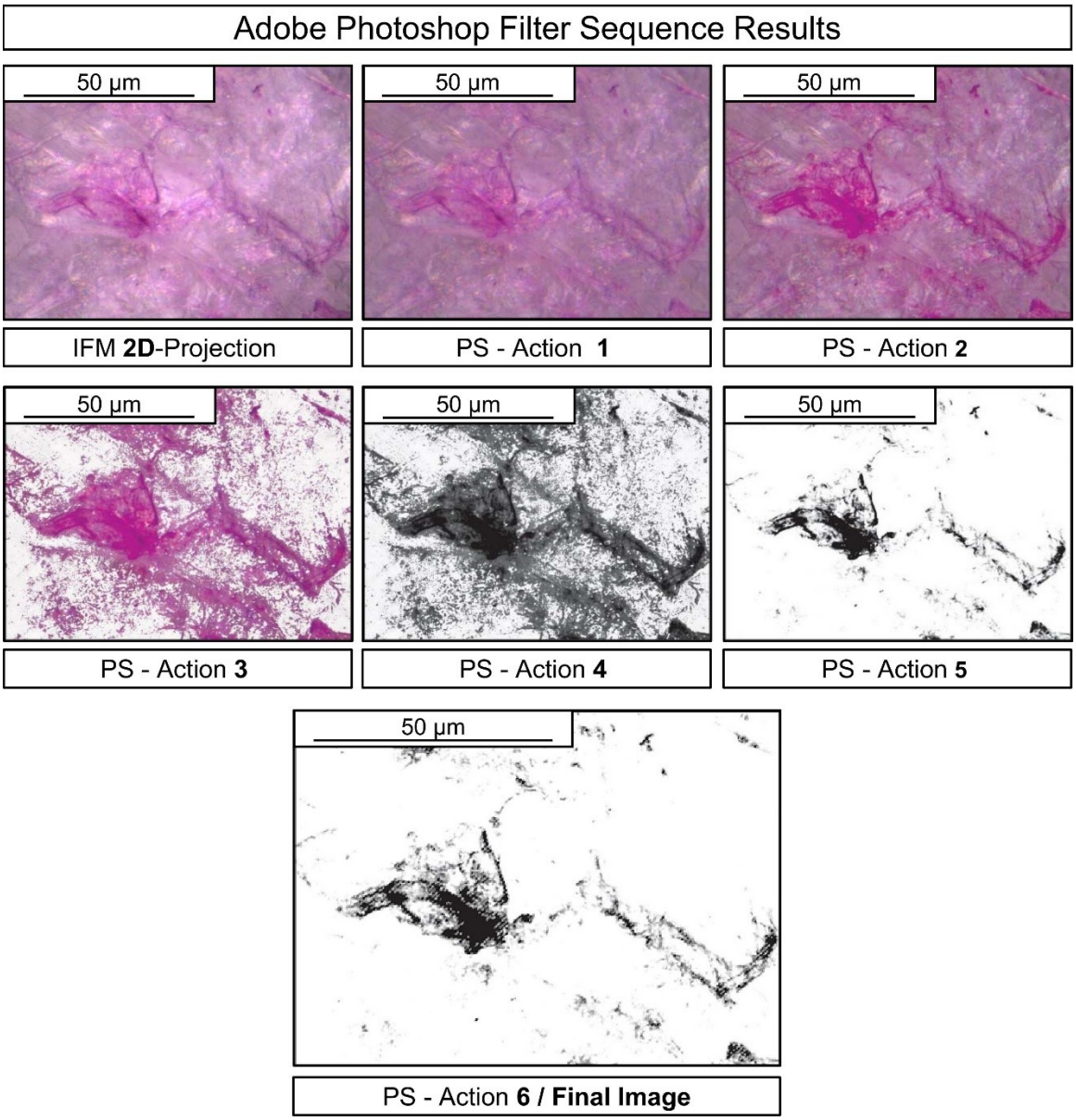

Figure 3.1-14: Adobe Photoshop Filter Sequence Results

During the first action, dark grey areas are lighted up, in order to avoid confounding with dark red shades in the RGB channel. The second action includes the three following sub-actions at once.

Firstly, dark grey and black areas are transferred to white. Secondly, the color channel is transferred from RGB to CMYK, in order to add a pure black channel.

Thirdly, the magenta information in the picture is enhanced to provide better contrast values. The third action replaces the color information of grays and light colored areas to white. The fourth action is the conversion of all color channels to black, resulting in a black and white image. The fifth action is the actual determination of the agglomeration area, by removing light grey areas and enhancing the color information of dark grey areas (initially areas of dark pink shade). The last action is a cropping step to standardized size and a removal of picture information that was embedded by the Alicona IFM (picture size, date, etc.). The result of these steps is a plain black and white picture of standardized size that contains the information of agglomeration area as black pixels and the area not affected by agglomeration as white pixels. At this stage of image processing, it would already be possible to give a crisp value for the total agglomeration area, by comparing the number of black pixels to the number of the whole images' pixels.

Due to the fact, that the plain information on the total surface covered by agglomerates was not considered as sufficient, an additional image-processing step by AI was implemented. AI is a program, which can be used for the vectorization of standard image files such as *.jpg* or *.tiff.*

Therefore, AI was implemented to vectorize the pictures deriving from the PS filtering sequences. By this step, which is explained in detail in Chapter 4.1.2.2.2, all connected black areas were combined into single areas and by this separated from the surrounding agglomerates (Figure 3.1-15).

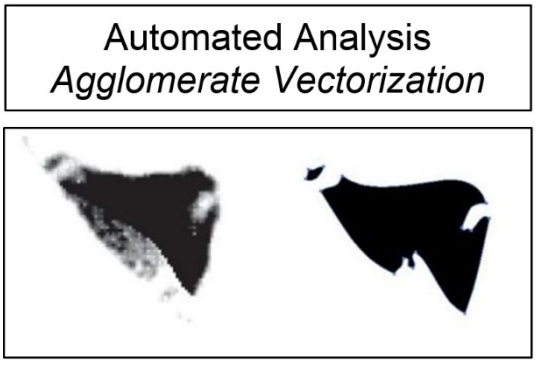

Figure 3.1-15: Automated Analysis / Detail of Agglomerate Vectorization

The overall action list conducted within AI consisted of three single actions, whose results are displayed in Figure 3.1-16. The first action is the selection of all black pixels. The second is the actual vectorization, as described above. Within the last

action, the individual agglomerates are counted and their total area share compared to the whole image area is calculated. Based on these two values, it is subsequently possible to calculate the average agglomerate area. The results of the automated analysis are listed in Table 3.1-4.

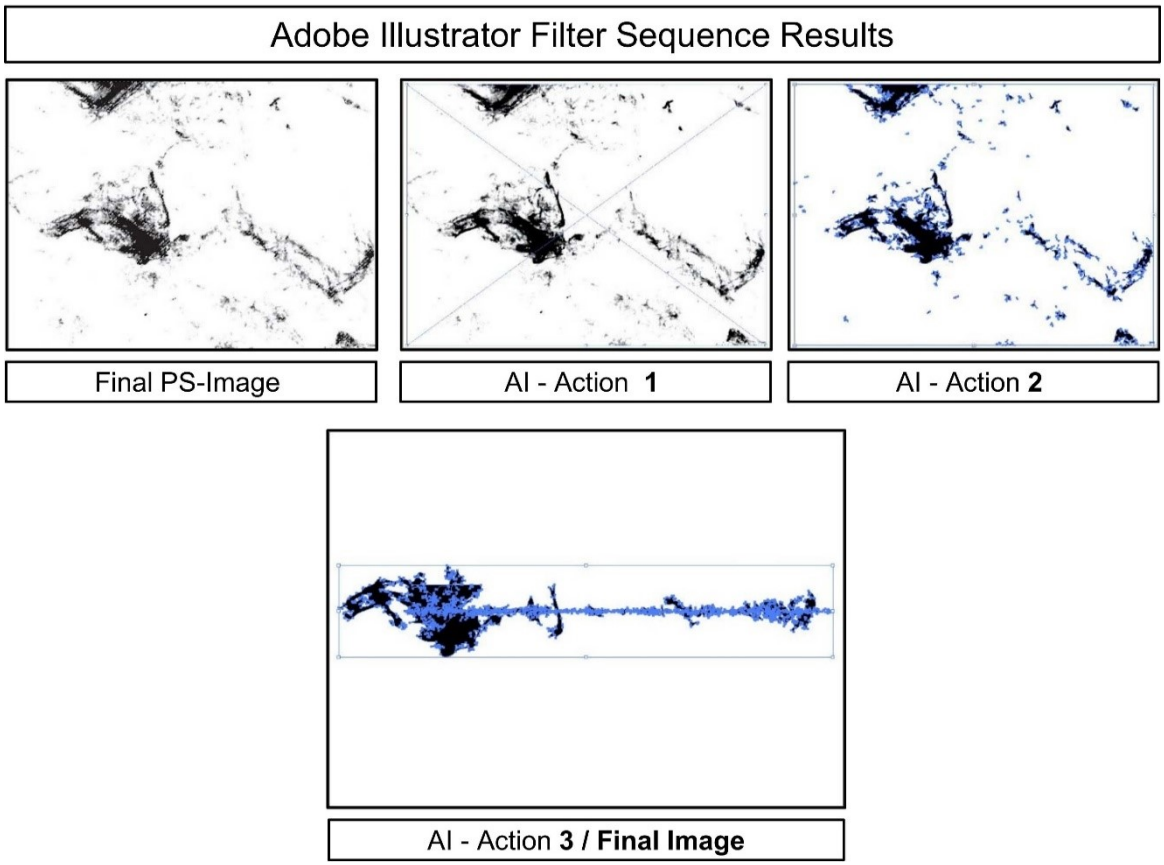

Figure 3.1-16: Adobe Illustrator Filter Sequence Results

Table 3.1-4: Results of Agglomeration Analysis

Value	Abbr.	Unit
Total Agglomeration Area	*Aggl_A*	*[%]*
Number of Agglomerates	*Aggl_N*	*[n/mm²]*
Average Agglomerate Size	*Aggl_AV*	*[µm²]*

3.1.2.5 Result Interpretation and Example Results

The pictures, which were presented in the previous Chapters, already showed that the agglomeration behavior does not necessarily follow a homogeneous pattern. This is why the presented analysis method is based on the statistical evaluation of the 12 individual pictures.

Figure 3.1-17 displays a typical value distribution behavior, as it can be observed for the analysis of moderately sized samples. It is visible that the values are spread over a wide range, which does not display a lack of analysis quality, but a distribution behavior of ASA, which turned out to be even more heterogeneous as it was initially considered. Typical values for moderately sized paper sheets are for Aggl_A ~ 0.1%, for Aggl_N 1000-5000 n/mm² and for Aggl_AV 0.2-1 µm².

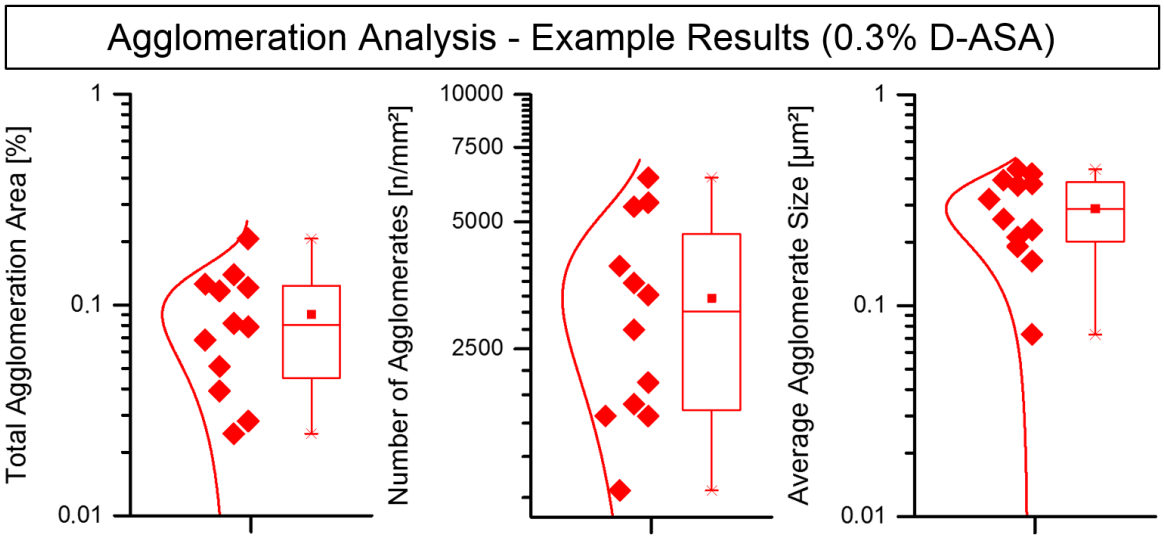

Figure 3.1-17: Agglomeration Analysis - Example Results (0.3% D-ASA)

3.1.2.6 Reproducibility

In order to prove that the wide spread distribution behavior is not based on a lack of analysis quality, but on the factual distribution of ASA agglomerates in the sheet structure, a series of reproducibility trials was conducted. Figure 3.1-18 displays the results of three individual measurement sets, which were conducted independently on random spots within one grid plate window on one specific sample. The analyzed sample was sized with 0.3% D-ASA and showed a typical agglomeration behavior.

The crisp results of the reproducibility trials, in terms of mean-values, median-values and standard deviations are displayed in the Appendix in Table 7.1-1, while they are split up into the individual trial sets (Set A, B and C) and the overall sum of all sets. The resulting standard deviations between the measured sets, calculated in [%] of the respective mean or median value, are displayed in Table 3.1-5. These show that the developed method for the localization and analysis of ASA agglomerates within the sheet structure is a tool that is capable of determining

ASA's agglomeration behavior with respect to its heterogeneous distribution with a high degree of reproducibility.

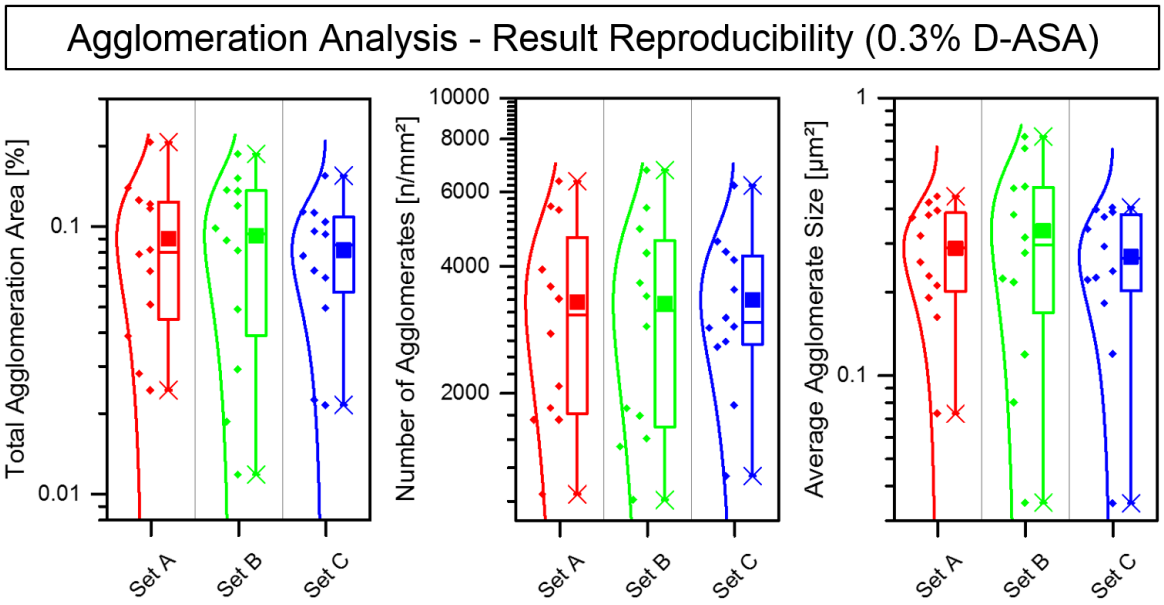

Figure 3.1-18: Agglomeration Analysis - Result Reproducibility (0.3% D-ASA)

Table 3.1-5: Variation Coefficients of Reproducibility Trials

Total Agglomeration Area [%]			
Mean	+/- 6.4%	***Median***	+/- 7.67%
Number of Agglomerates [n/mm²]			
Mean	+/- 0.93%	***Median***	+/- 3.14%
Average Agglomerate Size [µm²]			
Mean	+/- 11.16%	***Median***	+/- 5.7%

3.1.2.7 Sample Mapping

During the first approaches to measuring the agglomeration behavior of ASA and correlating these results to the present sizing performance, it turned out that these two factors correlate. Some simple trials, during which e.g., curing temperature or aging time were changed, have shown that the lower Aggl_A was at constant parameters, the higher the measurable sizing performance was. This information was subsequently transferred to a phenomenon occurring during the sizing of laboratory RK-hand sheets. Previous unpublished investigations by the author have shown that the sizing performance over the area of a RK sheet is differing to a high extent, even though it is supposed to be very homogeneous. Therefore, a mapping trial, in terms of sizing performance and agglomeration behavior over the

surface of a RK-sheet was conducted, in order to find out, if the deviating sizing performance stands in correlation to the occurring agglomeration behavior.

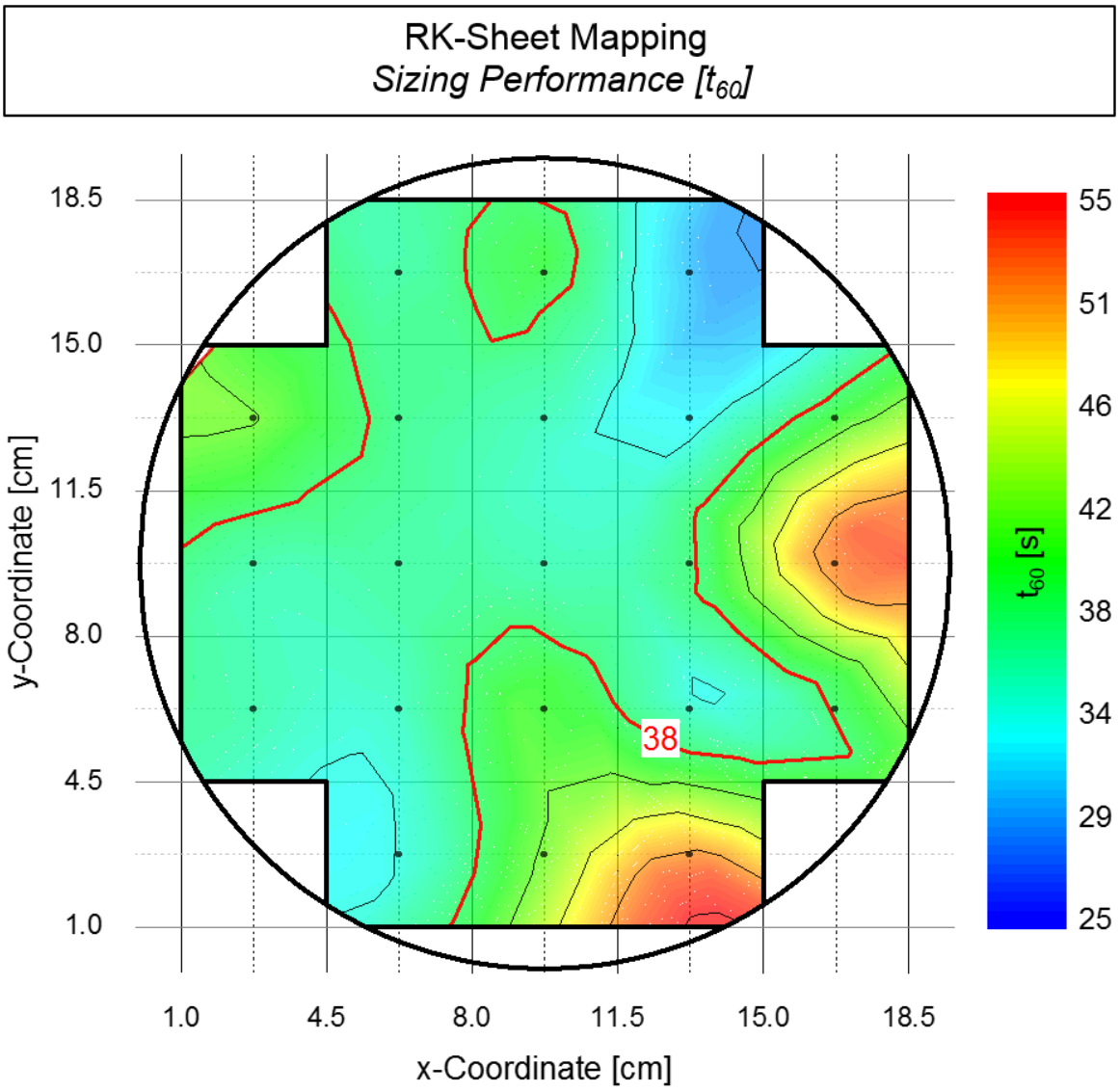

Figure 3.1-19: RK-Sheet Mapping / Sizing Performance Results (0.3% D-ASA) // t_{60} Top-Side Values [197]

For the analysis, the RK-hand sheet was cut into 21 samples, representing the grid displayed in the following contour plots. Every sample was fully analyzed by the localization method and by sizing performance analysis. Figure 3.1-19 [197], a sizing performance (t_{60}) contour plot over the surface of a RK-sheet, shows a very heterogeneous behavior. Within this contour plot, the circled area defines the RK-hand sheet outline, the colored area defines the respected measurement area, every black dot represents an imaginary measurement point and the color shade defines the sizing degree. On each of the 21 samples, two PDA measurements with reduced measuring spot (10 mm) were conducted.

Even though, the overall average of 38 s t_{60} is a typical value for a hand sheet sized with 0.3% ASA, the standard deviation is rather high with a value of 5.9 s. It is obvious that the sizing performance is peaking on the right hand side and on the bottom right hand corner. In addition, two areas of specifically low sizing performance are visible in the top right hand corner and in the bottom left hand corner.

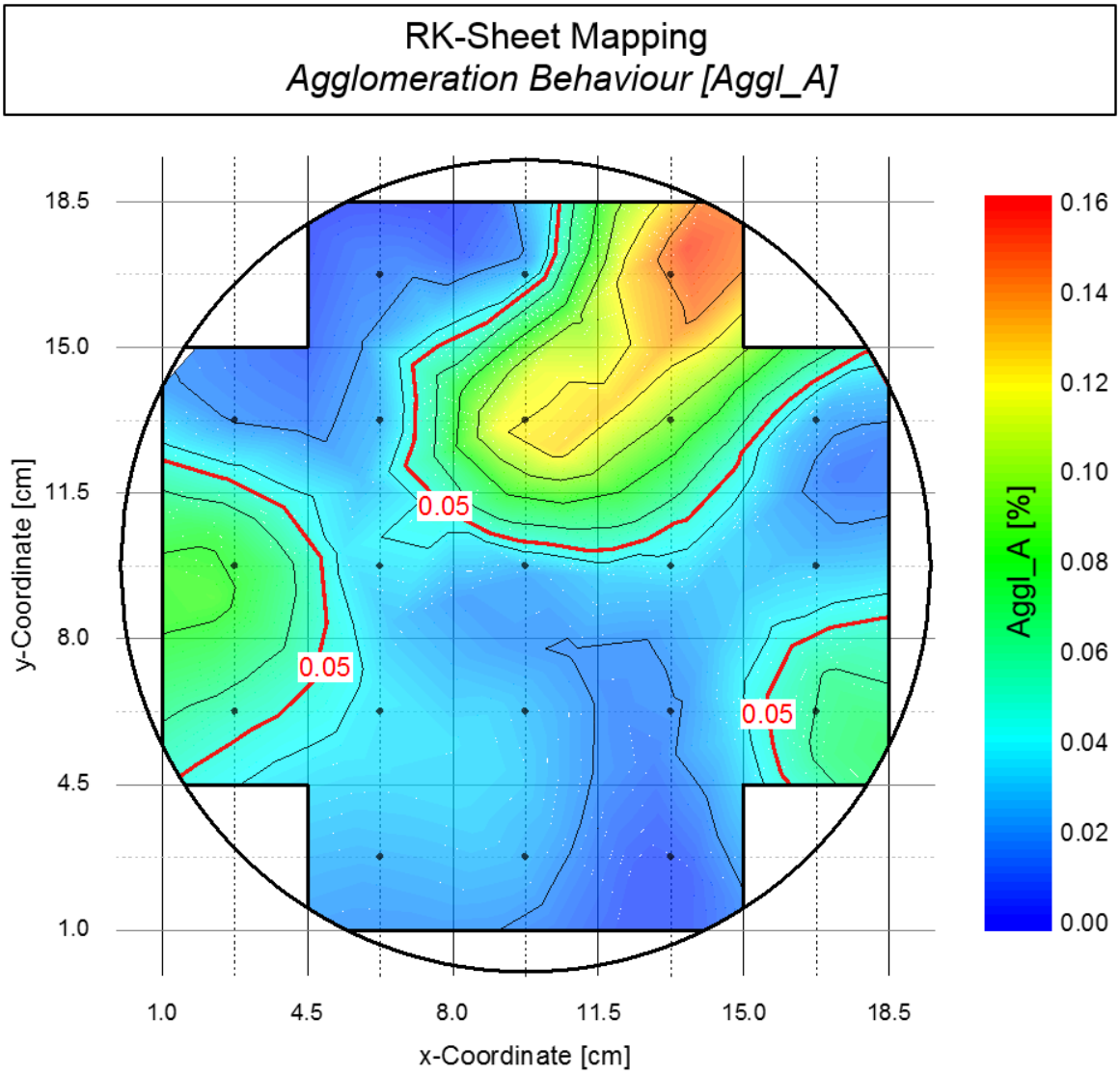

Figure 3.1-20: RK-Sheet Mapping / Agglomeration Behavior Results (0.3% D-ASA) // Aggl_A Top-Side Values [197]

Figure 3.1-20 [197], the agglomeration behavior (Aggl_A) contour plot over the surface of the very same RK-hand sheet, also shows a very heterogeneous distribution behavior. Compared to the overall average of the total agglomeration area of 0.05%, the standard deviation of 0.04% is even higher, compared to the one of the sizing performance. It is also obvious that the agglomeration behavior

shows three peaks over the measurement area. These peaks, in the top right corner, on the left hand side, and on the lower right hand side fall into the areas, where the sizing performance had its lowest values.

In order to verify the link between the existing agglomeration behavior and the respective sizing performance within samples of equal raw material and same ASA Dosage, a correlation analysis was conducted, based on the results from the above-mentioned trials. For this analysis, the plain data was analyzed in unrefined form, showing the result in Figure 3.1-21. The position of each black dot is defined by the values of the total agglomeration area (Aggl_A), measured via 12 single measurements, as x-axis value, and by the sizing degree (t_{60}), measured twice per sample, as y-axis value. Each sample represents one of the 21 RK-sheet sub-samples. The results of the correlation analysis show a correlation between the two mentioned factors. The correlation of determination can be calculated as R^2=0.345, using a power-function trend line.

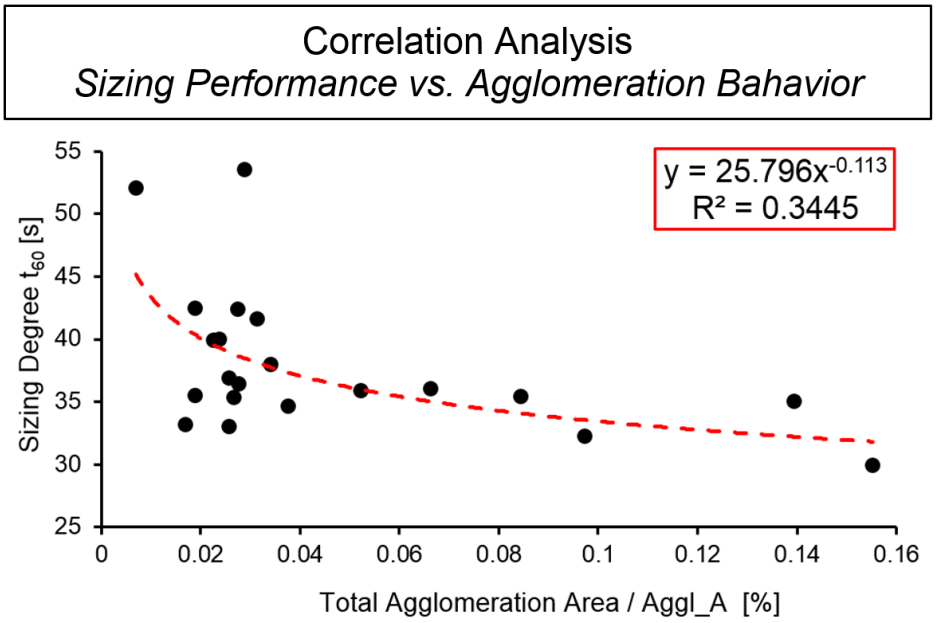

Figure 3.1-21: Correlation Analysis between Sizing Performance and Agglomeration Behavior

Considering the fact that the distribution behavior of ASA is very heterogeneous and that the PDA measurement is compared to the microscopic localization method a macroscopic analysis method, this correlation can be considered as significant.

3.1.3 **Approaches to Localization-Method Validation**

Even though the above-mentioned localization method was developed in order to fill the existing gaps within the available analytical methods, which could be used for sizing agent localization in microscopic scale, the following approaches were implemented with the focus on its validation.

3.1.3.1 Raman Spectroscopy

The first approach toward method validation was done by Raman spectroscopy. Therefore, paper samples dyed with 0.4% D-ASA, were analyzed in mapping mode in order to find deviations in ASA or in SR7B concentrations. The results of this approach turned out negative, as it was not possible to find any local peaks for ASA or for SR7B, even though it was possible to localize significant agglomerates within the measured area by the optical localization method. This result might be based on the one hand on the comparably low dosage of ASA (0.4%) and SR7B (0.02%), which is already on the edge or even below Raman spectroscopy's capabilities, and on the other hand on the absorption maxima of ASA, which are drowned by the ones of cellulose by overlapping phenomena.

3.1.3.2 Confocal Laser Scanning Fluorescent Microscopy

The second validation approach was based on confocal laser scanning fluorescent microscopy (CLSM). The dye of choice for these trials was Nile Red (NR), which was mixed with ASA at a concentration of 0.1% (F-ASA). The results showed that in general it is possible to mark ASA within the sheet structure by using NR. Even though it was not possible to differentiate between agglomerates and well-distributed ASA, the captured images gave some existential hints on the explanation of the occurring phenomena during sizing with ASA. By the use of two filter sets, one for a red channel at 572 nm - 642 nm and one for a green channel 505 nm - 545 nm, it is possible to analyze substances which emit light at different wavelengths and merge the resulting pictures, within one trial. The microscopy specifications are given in Chapter 4.1.2.1. Two representative pictures deriving from this trial are displayed in Figure 3.1-22.

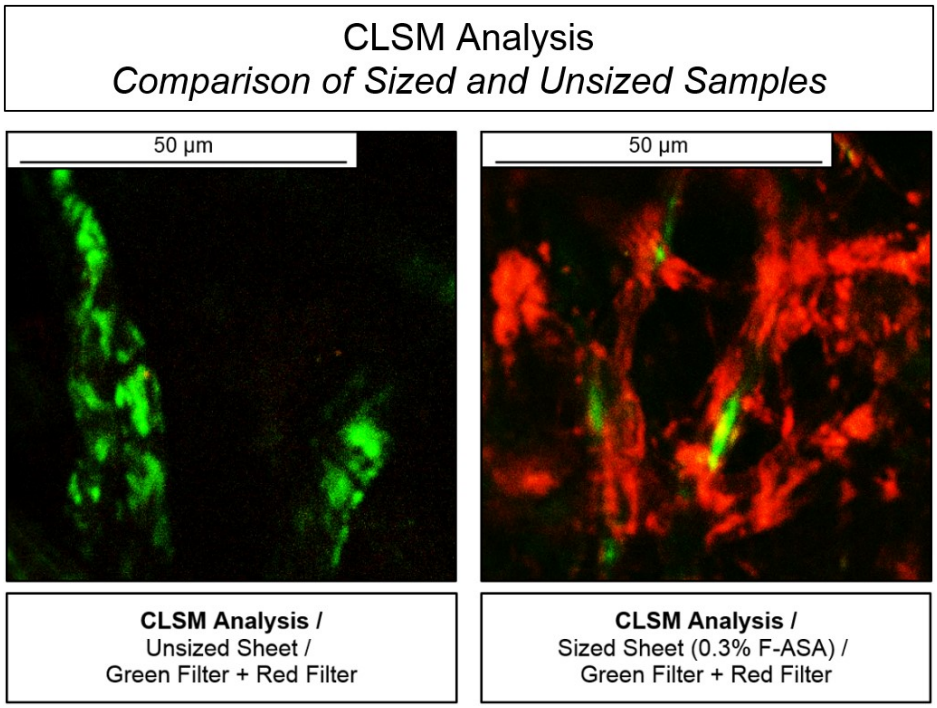

Figure 3.1-22: CLSM Analysis / Comparison of Sized and Unsized Samples

The left picture was taken during the analysis of an unsized paper sample. Even though the sample was analyzed by both filters and merged afterwards, it was only possible to capture the auto-fluorescence of the fiber's cellulose by the green filter. The right picture displays the fluorescence of a paper sample sized with 0.3% F-ASA measured with both filters. It shows the green autofluorescence of the fiber's cellulose and a strong red fluorescence, triggered by NR. Considering the fact that NR stays with ASA just like SR7B (Chapter 3.1.1), it has to be concluded that the red glowing regions on the fibers are regions covered with ASA. This picture indicates that ASA is not only present within the agglomerates, measurable with the developed optical localization method, but also as a very thin layer, distributed over the majority of the fibers surface.

3.1.3.3 Decolorization

The third approach implemented for method validation was based on the limited light fastness of SR7B. During the first trials of finding the optimal microscope and analysis settings, it was observed that dyed agglomerates lost their shade, once illuminated for an excessive amount of time. This fade of shade is based on light triggered (150 W illumination source focused on the area of ~ 150 µm x 150 µm) structural changes within the SR7B molecules, causing a loss of its color intensity

(photo bleaching). This feature was implemented in order to purposely decolorize agglomerates, with the goal of seeing what remains after they lose their shade.

Figure 3.1-23 displays the change that the agglomerates undergo during an excessive duration of light exposure. Starting with nicely visible and well defined agglomerates during initial illumination, the shade of the agglomerates consecutively decreases, leaving blurry, amber, film-building residues after 70 minutes of illumination. These residues were made up of ASA, which was initially the main component of the agglomerates, and forced to spread by the light induced heat during exposure. The possibility that the residues consisted of only the remains of the decolorized dye can be excluded, as there was not enough dye in the system (0.015%) to form massy structures as observed.

These results help to validate the localization method to the point that the agglomerates which can be found by microscopy, in fact consist of dyed ASA, and not of sole dye.

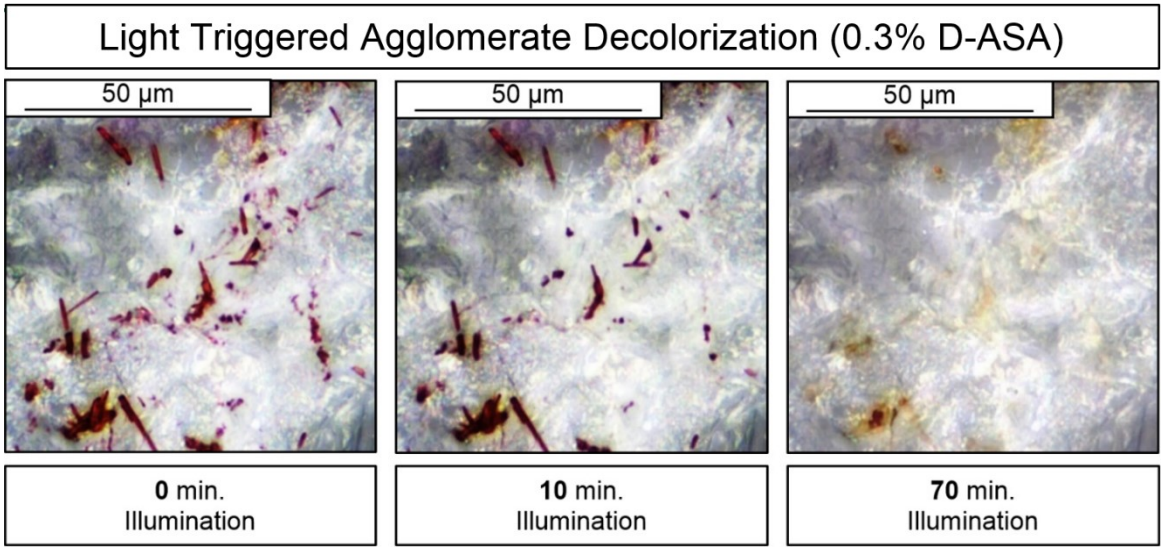

Figure 3.1-23: Light Triggered Agglomerate Decolorization (0.3% D-ASA)

3.2 Factors Impacting the Sizing Behavior of ASA

The first step toward a holistic understanding of the occurring phenomena and mechanisms during sizing with ASA is the determination of the factors which interact with the resulting sizing performance. In order to evaluate and determine the factors of significance, several trial sets were conducted. These include the impacts of the ASA type, emulsion parameters, stock parameters as well as

process parameters. If not stated differently, all presented trials were conducted, by using reference stock (Chapter 4.3.1.1), the standard RDA sheet forming procedure (Chapter 4.2.2.2) and subsequent PDA analysis (Chapter 4.2.1.5) for the determination of the sizing performance. The clear differentiation of the presented and discussed trial results from ones presented in theoretical part of this thesis (Chapter 2.3.3) is based on their full factorial design. Past research has only focused on impacting-factors at a constant ASA dosage, while the presented trials respect these factors over the whole ASA dosage-range, leaving linearity and entering into an space of interactions. The results are presented and discussed within the following chapters, while the focus of the discussion is on the physico-chemical mechanisms that lead to hydrophobization.

3.2.1 **ASA Type**

The impact of the ASA type on the sizing performance, in terms of chemical composition and emulsifier type is a topic of ongoing discussion (Chapter 2.3.1.1). In practical applications it has crystallized, that the use of tailored ASA compositions is a crucial step in order to successfully adapt to the given situation. This adaption is necessary, because the sizing performance of different ASA types is highly influenced by stock and process parameters [191]. The goal of the following trial was a comparison of available commodity ASA products in terms of their sizing performance within the implemented standardized methods. The analysis was done by using the sizing agents displayed Table 3.2-1.

The results of the conducted trials are displayed in the following four graphs (Figure 3.2-1), while the one on the top-left displays the results for pure ASA grades, the one on the top-right the results for ASA grades with emulsifier “A”, the one on the bottom-left the results for low shear ASA grades with emulsifier “B”, and the one on the bottom right side the results for a MSOHO-grade.

They show that the impact of the different ASA-types on the sizing performance is of a minor extent. The tendency that is visible throughout all three standard ASA sets, is that the sizing performance increases by a higher ASA-C18 share, making the pure ASA-C18 grades the ones with the highest sizing performance. The impact of the different emulsifier types is also within the occurring standard

deviations and can therefore as well be neglected. The MSOHO-type, which is based on renewable resources, showed a sizing performance compared to C18/C16 ASA-types with a higher share of C18. The comparably low impact of the ASA composition on the sizing performance can be explained by the interactions with the reference stock system.

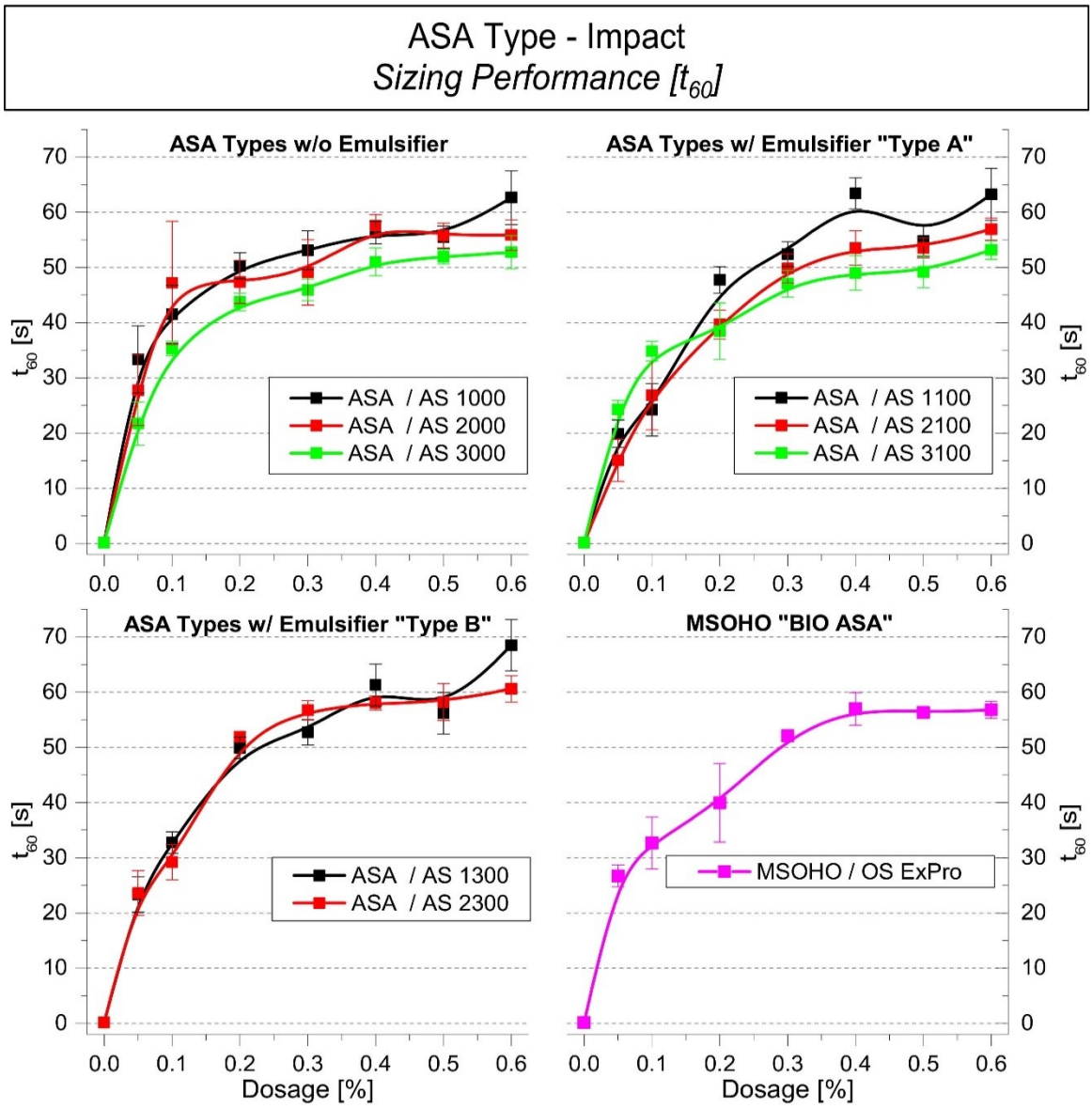

Figure 3.2-1: ASA-Type Sizing Performance Comparison

As the reference stock system is based on virgin fibers which are of lowest pollution by salts or other negatively interacting substances, every ASA-type can unfold its maximum sizing performance, resulting in equal sizing degrees over all types.

Table 3.2-1: Analyzed ASA-Types

ASA Type*	Composition	Emulsifier
AS 1000*	pure C18	none
AS 1100	C16/C18, shares ~ 65/35	none
AS 1300	C16/C18, shares ~ 35/65	none
AS 2000	pure C18	type A
AS 2100	C16/C18, shares ~ 65/35	type A
AS 2300	C16/C18, shares ~ 35/65	type A
AS 3000	pure C18	type B / low shear
AS 3100	C16/C18, shares ~ 65/35	type B / low shear
OS ExPro	C18 + MSOHO + FAA	type C

** all analyzed ASA types were sponsored by Kemira GesmbH*
*** Fennosize AS 1000 was the utilized standard ASA grade*

3.2.2 **Emulsion Parameters**

The following section will describe the impact on ASA's sizing performance by several factors, contributing to the group of emulsion parameters. These include the share of hydrolyzed ASA, the starch to ASA ratio as well the emulsion age. The emulsification process was conducted, following the standards displayed in Chapter 4.1.1.4, while the specific parameters, as mentioned for the different factors, were adjusted.

3.2.2.1 Hydrolyzed ASA Content

The impact of proceeding hydrolysis on the sizing performance is a factor that has widely been discussed, while all implemented approaches (Chapter 2.3.3.1) did only respect the impact of emulsion hydrolysis and not the impact of the hydrolyzed ASA content. Therefore, in order to really analyze the impact of the hydrolyzed share, ASA was mixed with its pure hydrolyzed form (Chapter 4.2.2.8) prior to emulsification, while the shares 0%, 25%, 50%, 75% and 100% were chosen. The mixtures were produced directly before emulsification under standard conditions, using cationic or anionic liquid starches (Chapter 4.3.3.2).

The results of these trials are displayed in Figure 3.2-2, where on the left, the results for cationic emulsification and on the right, the ones for anionic emulsification are displayed.

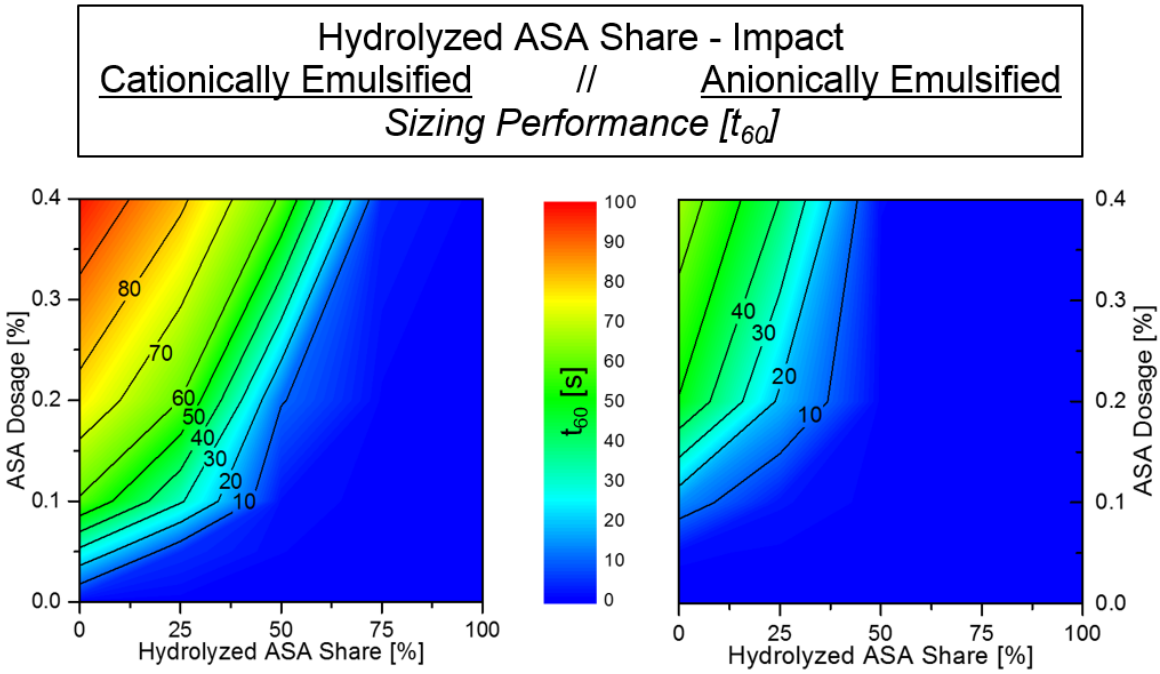

Figure 3.2-2: Impact of Hydrolyzed-ASA Share on Sizing Performance by Cationic (left) and Anionic (right) Emulsification

The emulsion particle size distribution was not analyzed during these trials. The two approaches by anionic and cationic emulsification were followed, because it was of interest, if ASA's containing a high share of hydrolysate and thus carrying a higher negative charge, might show a better performance if also anionically stabilized. The following graphs show that the sizing performance of ASA is significantly impacted by the initial content of hydrolysate. In the case of cationic emulsification, a content of 50% hydrolysate leads to a total sizing loss at ASA dosages up to 0.2%, while it causes a 50% performance reduction at an ASA dosage of 0.3%. Even at 0.4% ASA dosage it is not possible to generate any sizing performance if the hydrolysate content exceeds 75%.

The trial sets with anionic emulsified ASA show a 50% lower initial sizing performance, compared to the cationic emulsion. This is thought to be based on the different self-retention abilities of both emulsions. The cationic emulsion shows high self-retention, by strong attraction to the fiber surface, while the anionic emulsions usually need fixatives for good retention. The use of a fixative (retention aid) was denied, as this would have induced a further unknown factor to the trials.

The impact of the hydrolysate content on the sizing performance of anionically emulsified emulsions is even more dominant compared to trials with cationic starch. A hydrolysate share of 25% does already cause a sizing performance

reduction of 30%, when sized with 0.4% ASA, while no sizing performance is left at 50% hydrolysate content.

These results promote the common knowledge to keep the degree of hydrolysis on a minimal level, in order to provide an optimal sizing performance. In addition, it was possible to show that the sizing performance is not only affected by emulsion hydrolysis and the triggered emulsion instability, but by the content of hydrolysate in the stable emulsion. Further, this promotes the thesis that the reactive structure of ASA is, even though it hydrolyzed in the sheet structure, the key factor to successful application [167].

3.2.2.2 ASA/Starch Ratio

An important point toward successful ASA emulsification and application is the optimal starch-to-ASA ratio. This ratio defines the stability of the emulsion, which is as stated above of highest importance, and the overall charge character of the emulsion droplet. This charge character defines the self-retention abilities of the emulsion with respect to the furnish and dosage point used. The following graph (Figure 3.2-3) displays the trial results, where the ratio between ASA and the standard emulsification starch was varied (1/4, 1/2, 1/1, 2/1, 4/1), in order to find the optimal set-up for the furnish of choice (reference stock system).

Throughout all ASA dosages the trial results show that an ASA/starch ratio of 1/1 delivers the best sizing performance. This impact is especially dominant for low dosages (0.05%), where it boosts the sizing performance for more than 100%.

Considering the fact that emulsions prepared with the standard emulsification starch show optimal particle size and stability properties at an ASA-to-starch ratio of 1/0.37 [31], it has to be concluded that not only do these factors play a role for the development of an optimal sizing performance, but also the over-all charge potential. This is transferred by the choice and amount of protection colloid and needs to be adjusted to the system by varying the ASA-to-starch share, in order to not only reach optimal emulsion properties, but to also optimize the emulsion’s self-retention behavior on the furnish.

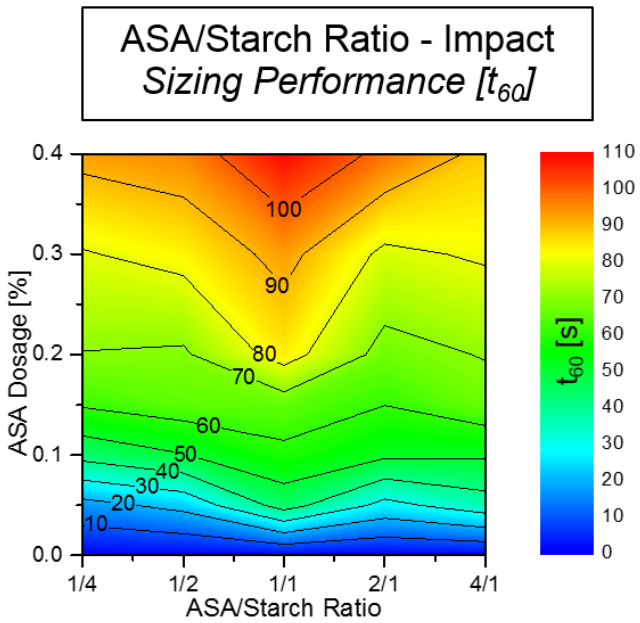

Figure 3.2-3: Impact of ASA/Starch Ratio on ASA Sizing Performance

3.2.2.3 Emulsion Age

The age of the emulsion prior to dosage in combination with the along going progress in hydrolysis and emulsion instability is supposed to have a significant negative impact on the sizing performance. This is why the impact of the emulsion's age prior to dosage was analyzed within the following trial, while the emulsion age was defined as the elapsed time after emulsification and storage under diluted conditions (1.0% / Chapter 4.1.1.4).

The results in Figure 3.2-4 show that the most dominant impact on the sizing performance by aging happens within the first 20 minutes for low and high ASA dosages, while the moderate dosages (0.1% & 0.2%) remain unaffected. In the subsequent aging period between 20 minutes and 120 minutes, the dosages of 0.05% and 0.1% remain unaffected, while the higher dosages undergo some ups and downs. This indicates that sizing performance is not directly correlating to the emulsion age within the presented trials. This fact might be based on the emulsification and storage in deionized water at room temperature, which significantly decreases the hydrolysis tendency and promotes the emulsion's stability. Nevertheless, the negative effect by excessive storage time seems neglectable under the given boundary conditions, the emulsions for the conducted trials within this thesis were renewed at least every 5 sheets or at least every 20 minutes to guarantee emulsions of highest quality.

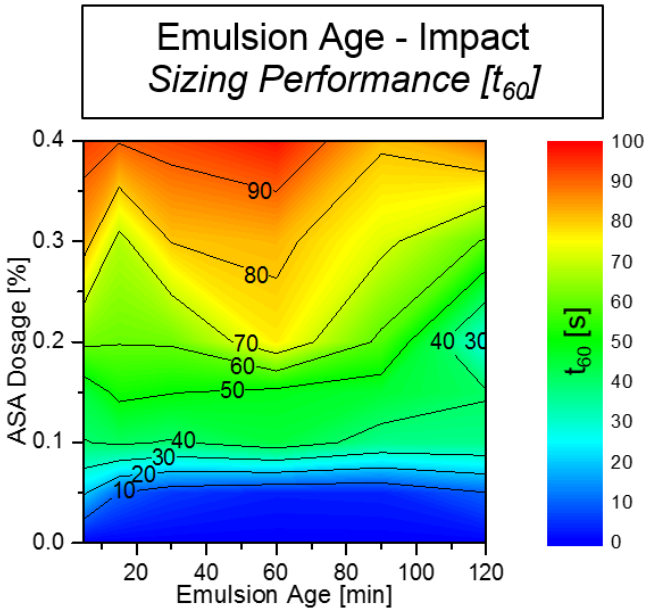

Figure 3.2-4: Impact of ASA-Emulsion Age on ASA Sizing Performance

An influence as neglectable as observed during this trial will not be observable during industrial-scale application, as it is hardly realizable from a cost factor point of view, to emulsify and store the ASA emulsions with/in deionized water. However, it should be of main interest for those mills who use ASA, to utilize water of highest purity, as this is a comparably uncomplicated measure, which has a significant effect on ASA's processability and sizing performance.

3.2.3 **Stock Parameters**

The following subchapters will focus on analyzing and discussing the main stock parameters which are supposed to influence the sizing performance of ASA. These include, the share between long and short fibers, the furnish type (virgin fibers, OCC and DIP), the degree of refining, as well as the filler type (GCC, PCC and clay) and dosage.

3.2.3.1 Long Fiber/Short Fiber Ratio

Virgin fiber furnishes for the production of paper & board are in most cases composed of a mixture of long and short fibers. As many of these virgin fiber based grades are sized with ASA, it was of interest during this thesis to analyze how a difference in shares between long and short fiber is capable of affecting the sizing performance. Within the following trial, a bleached eucalyptus kraft (EUKA) grade and a northern bleached softwood kraft (NBSK) grade were compared with respect

to their sizeability. For trial conduction, fiber suspensions were prepared with differing shares of long fiber (NBSK) compared to short fiber (EUKA), while the shares were 0%, 25%, 50%, 75% and 100% and the ASA dosages between 0% and 0.4%. After adjusting the fiber type shares, the mixtures were beaten in a valley beater (Chapter 4.2.2.2) to SR 30.

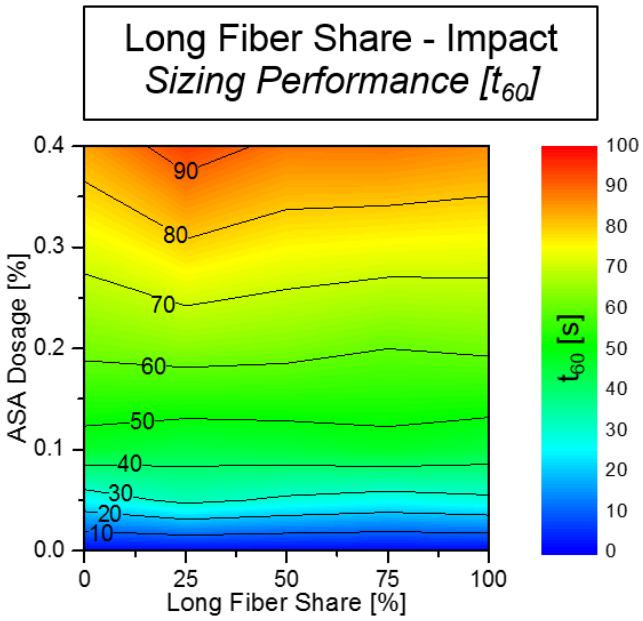

Figure 3.2-5: Impact of Long Fiber Share in Furnish on ASA Sizing Performance

The correlating trial results are displayed in Figure 3.2-5, making visible that an increasingly long fiber share has almost no impact on the sizing performance. The only tendency that can be derived from these results is that a long fiber share of 25% slightly contributes to the sizing performance. Based on these results, the impact of the long fiber to short fiber ratio can be neglected for trials within this thesis.

3.2.3.2 Furnish Type

To analyze the influence of different furnishes on the sizing performance of ASA, two trial sets were conducted, where the reference stock furnish was compared to an OCC and a DIP furnish. The reference furnish, consisting of 80% bleached eucalyptus kraft pulp (EUKA) and 20% northern bleached softwood kraft pulp (NBSK) combined refined to SR 30, is a system that shows a high degree of sizeability, as its degree of contamination is very low and the cellulose accessibility high (Chapter 4.3.1.1). As OCC and DIP furnishes (Chapters 4.3.1.2 and 4.3.1.3) are anything but comparable to virgin fiber based furnishes, it was the focus of the

following trials to evaluate their impact on the sizing performance. For trial conduction, fiber suspensions were prepared with differing shares of DIP or OCC compared to reference stock, while they were set to 0%, 25%, 50%, 75% and 100%. For better comparability to industrial systems, the suspensions were prepared with tap water instead of deionized water. Due to the expected negative impact of DIP and OCC, the ASA dosages were adjusted from 0% to 0.8%.

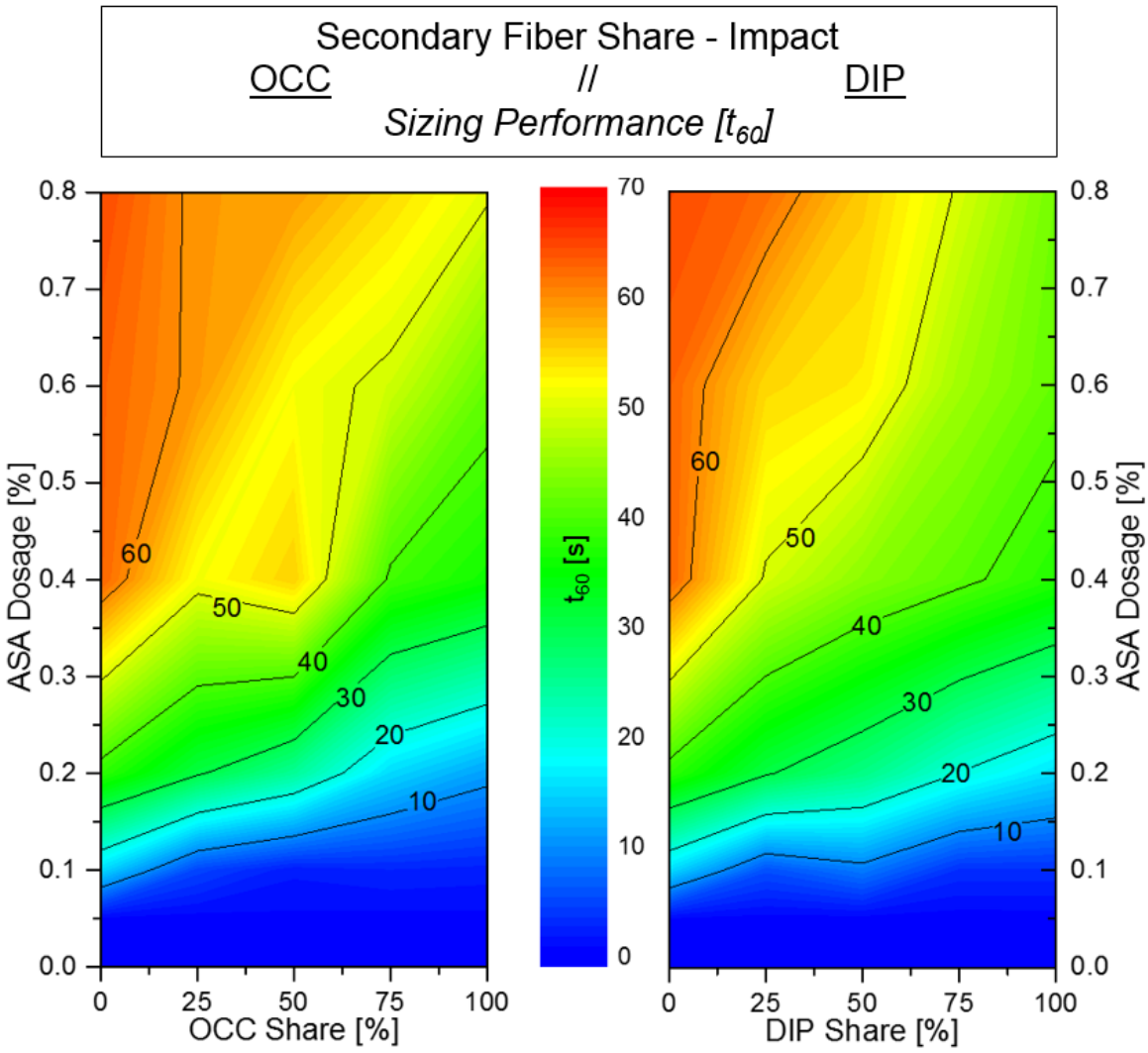

Figure 3.2-6: Impact of Secondary Fiber Share in Furnish on ASA Sizing Performance OCC (left) // DIP (right)

The results for OCC are displayed in Figure 3.2-6 on the left. It is visible that an increasing OCC share has a negative impact of almost linear nature throughout the whole ASA dosage range. Comparing the required amount of ASA to size the reference stock and the OCC furnishes, it is obvious that twice the amount of ASA is required to reach the equal sizing performance when the OCC furnish content is increased from 0% to 100%.

The results for DIP are displayed in Figure 3.2-6 on the right. It is visible that they show an almost identical behavior compared to the ones of the OCC trial. The main difference between the OCC and the DIP trial is that the sizing performance of lower dosages is not as negatively affected by DIP as by OCC, while higher ASA dosages are more negatively affected by DIP compared to OCC.

The negative impact of OCC and DIP can be explained by three secondary fiber specific features. The first feature is a high degree of hornification, caused by the recycling process [249, 250], which somehow inactivates the fiber surface and decreases its negative surface charge. This feature, as such, is capable of decreasing ASA's self-retention on the fiber surface, and thus the resulting sizing performance. The second feature is a comparably high content of negatively interacting substances, which are entrained in secondary fiber furnishes. These derive from e.g., printing inks, coating colors, glues or process chemicals, such as tensides for deinking and are thus capable of decreasing, on the one hand, the ASA's self-retention (anionic trash, Chapter 2.3.3.5) and, on the other hand, its sizing performance (surface-active additives, Chapter 2.3.3.6). The third feature is the natural ash content of OCC and DIP furnishes, which derives from the raw materials for the recycling process. This ash content is a cause for weak retention in general and, as a consequence, for ASA retention as well (Chapter 2.3.3.3). This might be considered as the main trigger for the highly decreasing sizing performance by increasing DIP or OCC shares.

3.2.3.3 Degree of Refining

The impact on the sizing performance by a variation of the degree of refining and an along-going morphological change of the sheet structure has so far not been described in the literature. Based on the principles of wetting and penetration (Chapter 2.2.4), which define the sizing performance not only by the hydrophobicity of the sizing agent, but also by the morphology of the stock, the degree of refining has to have an impact on the sizing performance from a theoretical point of view. This is the reason, why the following trial for the evaluation of the morphological impact was conducted. For analysis, a mixture of 80% EUKA and 20% NBSK was beaten in a Voith valley beater (Chapter 4.2.2.2) from an unbeaten state (SR 17.5) over three intermediate steps (SR 27.5, SR 40, SR 49) to a highly beaten state

(SR 62), while samples from every state were sized with 0% - 0.4% ASA. The results of this trial, in terms of sizing performance, are displayed in Figure 3.2-7 on the left. These show that the degree of refining has an extraordinarily high impact on the sizing performance. Throughout all ASA dosages, the increase of the SR value from 17.5 to 62 boosts the sizing performance by ~ 1000%, which represents the strongest impact factor determined within this thesis.

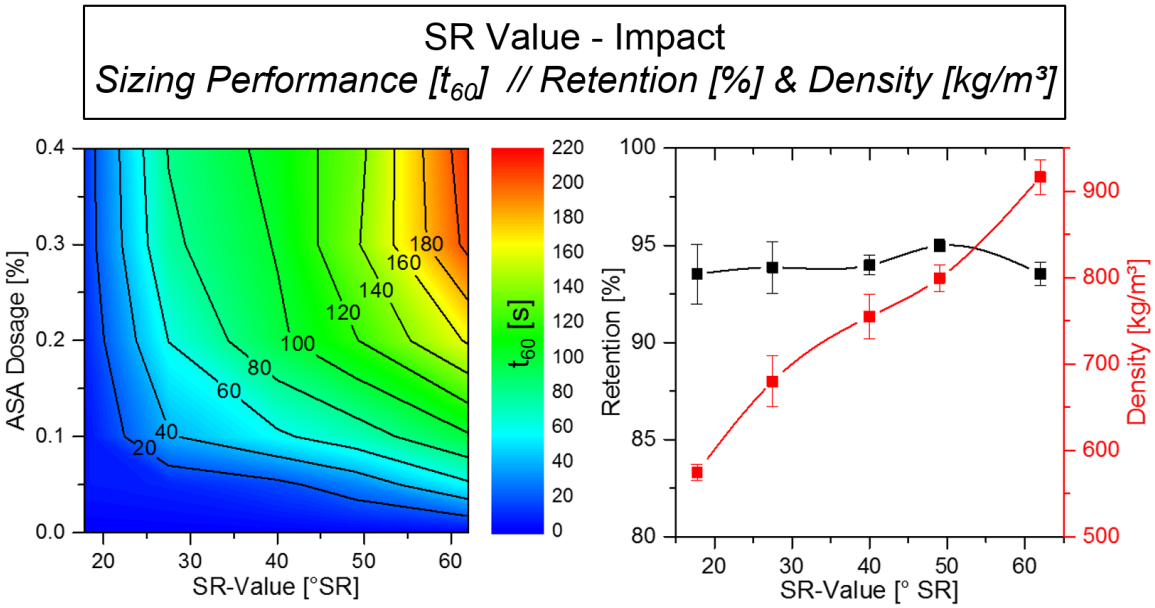

Figure 3.2-7: Impact of Refining Degree on ASA Sizing Performance (left) & Retention and Sheet Density (right)

This strong synergetic effect can be explained by two arguments. The first argument is based on the fines' content, which is generated by refining. A common theory states that sizing agent emulsions retain rather on the high surface area of accessible fines (active fine content), than on coarse fiber fractions [174, 251]. If these fines are retained in the sheetstructure during sheet forming, the sizing performance is promoted by a higher fines content. As it can be seen in Figure 3.2-7 on the right, the overall retention for the produced paper samples remains unchanged over an increasing degree of refining, thus stating that the mentioned argument can be considered as valid.

The second argument is based on the structural changes the sheet undergoes by refining. The higher share of fines, as well as the increased fiber flexibility during refining, enable a higher degree of packing density during sheet forming and as a consequence a higher sheet density (Figure 3.2-7 / right). This means by implication that the void volume, as well as the pore sizes, decrease with ongoing

refining, generating less interphase area between air and cellulose. As the sizing agent is located on this interphase, its relative concentartion on the interphase increases by ongoing refinig, resulting in a higher degree of hydrophobization (Chapter 2.2.4).

3.2.3.4 Filler Type/Content

The last important stock parameter that has a major impact on ASA's sizing performance is the presence of fillers. Fillers have a very high surface area on which sizing agents can adhere. First, this causes a weak sizing agent retention as a consequence of a low natural filler retention, and second, a weak sizing performance. The comparably weak sizing performance is not only based on the reduced retention, but also on the increase in interphase area, which is triggered by the fillers' high surface area (Chapter 2.3.3.3). As a result, more sizing agent is required to reach the same degree of hydrophobization. In order to analyze the impact of different filler types and dosages, the following three trial sets were conducted. These respect the sizing performance over the filler types (GCC, PCC and clay), filler dosages (0%, 15% and 30%), the presence of retention aid (0% or 0.03% PAM) and ASA dosages from 0% to 0.4%. The filler specifications are displayed in Chapter 4.3.2, while all types are typical minerals for internal application. The results for GCC are displayed in Figure 3.2-8.

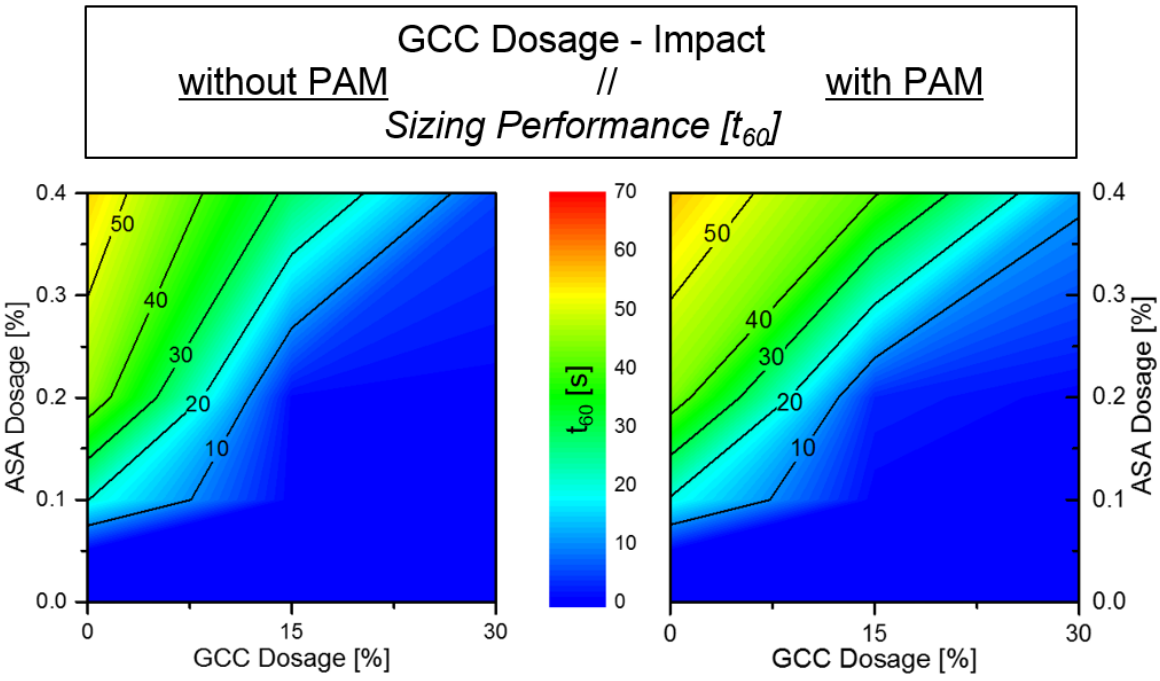

Figure 3.2-8: Impact of GCC Dosage on ASA Sizing Performance w/o PAM (left) and w PAM (right)

These results display the highly negative impact of GCC, showing that the sizing performance almost decreases linearly by an increasing GCC content. The results also show that almost no sizing performance can be generated if only small amounts of GCC are present at ASA dosages of up to 0.1%. A GCC content of 15% causes a total sizing loss at 0.2% ASA dosage, while it decreases the sizing performance by 50% for a dosage of 0.4% ASA. At GCC dosages of 30%, no sizing performance could be generated at all. The filler retention evolved during the trials without PAM from 30% at 0% ASA dosage to 56% at 0.4% ASA dosage. This increase is based on the retention-promoting properties of the cationic ASA emulsion. The presence of PAM, as displayed in the right graph, only slightly improves the sizing performance of high ASA dosages, while the performance of low dosages remains unaffected. During the trials with PAM, the GCC retention values remained unchanged at a level of ~ 86%.

The results displayed in Figure 3.2-9 represent the negative impact of PCC on ASA's performance. These show that the sizing performance is linearly affected by an increasing PCC content without PAM, while the sizing performance levels after 15% PCC dosage for the trials with PAM.

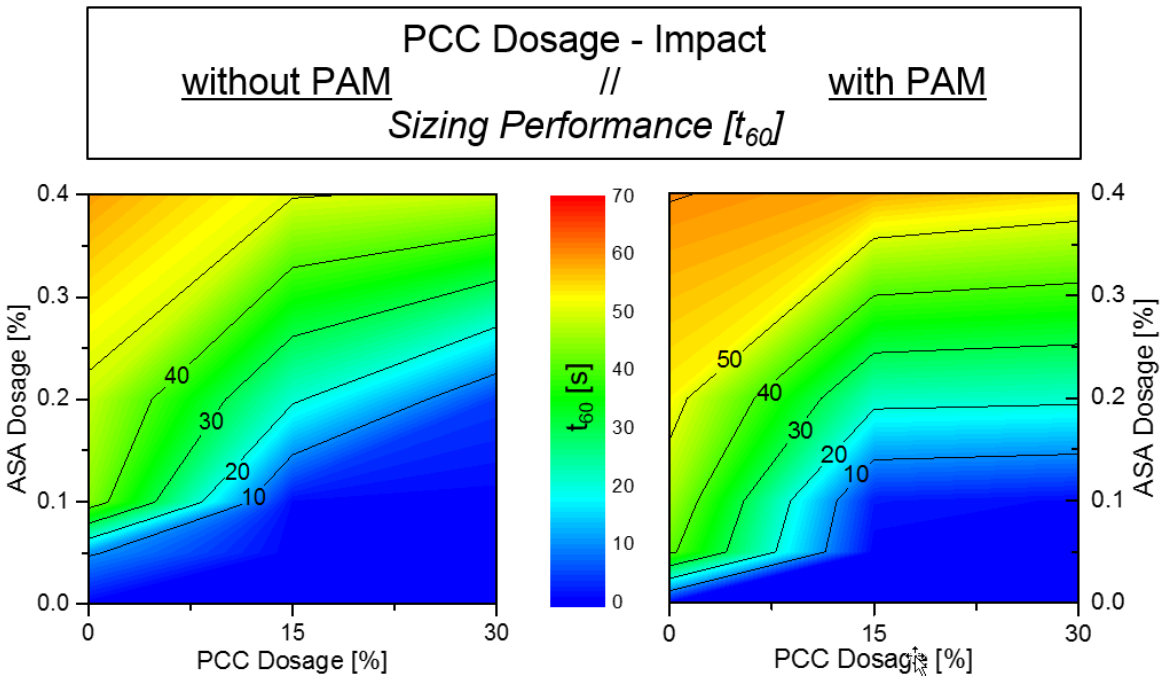

Figure 3.2-9: Impact of PCC Dosage on ASA Sizing Performance w/o PAM (left) and w PAM (right)

The overall sizing performance is in general not as negatively affected compared to using GCC. The results show that almost no sizing performance can be

generated in the system without PAM if only small amounts of PCC are present at ASA dosages of up to 0.1%. This tendency is significantly decreased by the use of PAM, enabling some sizing performance at low PCC dosages. By the use of PAM, the total sizing values increase by about 10%, while the point of significance is visible at PCC dosages over 15%. Here, the sizing values remain stable, enabling moderate sizing values from ASA dosages of 0.2% even at PCC levels of 30%. During the trials without PAM, the filler retention evolved from 18% at 0% ASA dosage to 63% at 0.4% ASA dosage, while, during the trials with PAM, it evolved from 67% at 0% ASA dosage to 76% at 0.4% ASA dosage. This indicates that even though the retention values of PCC remained lower compared to the ones of GCC, PCC does show a significantly higher sizeability.

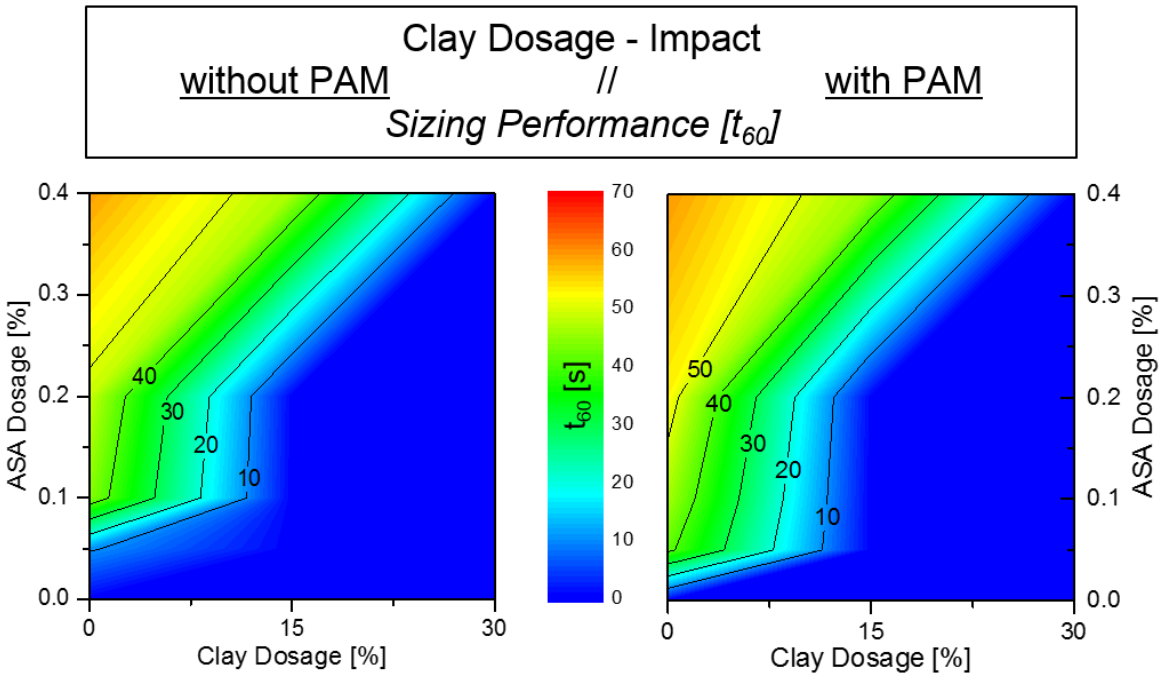

Figure 3.2-10: Impact of Clay Dosage on ASA Sizing Performance w/o PAM (left) and w PAM (right)

The results for clay as filler are displayed in Figure 3.2-10, where it is visible that the negative impact is almost identical to the one of GCC. The results show that only slightest amounts of clay are capable of significantly influencing the sizing performance, and that it is not possible to generate any sizing performance at 30% clay at 0.4% ASA dosage, even if PAM is used. The sizing performance does increase more by the use of PAM compared to GCC, while it is also not possible to minimize the negative effects on the sizing performance. The clay retention did evolve during the trials without PAM from 31% at 0% ASA dosage to 63% at 0.4%

ASA dosage, while it increased during the trials with PAM from 67% at 0% ASA dosage to 83% at 0.4% ASA dosage.

The overall conclusion that can be drawn from the trials with GCC, PCC and clay, is that the negative effects of fillers on the sizing performance of ASA can only be compensated by an increase in ASA dosage, while it is possible to additionally enhance the sizing performance by the use of retention aids (PAM). The trials did also show that the most significant negative impact on the sizing performance amongst all ASA dosages was triggered by GCC and the smallest by PCC, standing in conversion to common knowledge (Chapter 2.3.3.2). A factor which was not mentioned by the literature so far, is the strong impact of the cationic ASA emulsions on the over-all and filler retention behavior. This positive effect has to be considered while planning and designing ASA systems, as this synergetic effect could create significant benefits during industrial-scale production.

3.2.4 **Process Parameters**

The following subchapters will describe and analyze a row of trials that were conducted, in order to evaluate the impacts of different process parameters on the sizing performance of ASA. These include the sheet forming temperature, the sheet forming pH-value, the stock conductivity, the stock water hardness, the sheet forming shear rate, the ASA dwell time, the dosing position and dosing order, the drying type and intensity as well as sample aging.

3.2.4.1 Temperature

A factor which was identified within previous research (Chapter 2.3.3.1.1) as harmful to sizing performance, is the emulsion temperature, as it significantly promotes emulsion hydrolysis. A point that was not evaluated so far, is the impact of the stock and sheet forming temperature on the sizing performance of ASA. Therefore, the following trial, during which the sheet forming temperature was changed from 20 °C, over 30 °C, 40 °C, 50 °C to 57 °C, was conducted with ASA dosages from 0% to 0.4%.

The results displayed in Figure 3.2-11 show that the sizing performance is slightly positively affected by an increasing sheet forming temperature. This behavior can be explained, on the one hand, by a temperature dependent decrease in surface

tension, which allows the emulsion to penetrate deeper into the fiber structure, providing better anchoring during dewatering and pressing, and on the other hand, by the possibility that the emulsion particles attach to the fiber surface more rapidly, as the molecular mobility within the stock system is increased by higher temperatures.

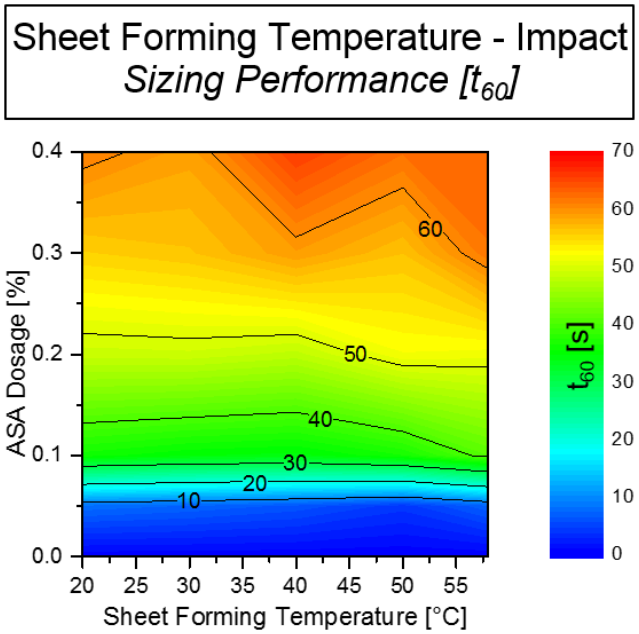

Figure 3.2-11: Impact of Sheet Forming Temperature on ASA Sizing Performance

Altogether, these results do not indicate that they are controversial to the ones discussed during the theoretical approach (Chapter 2.3.3.1.1), but as they access the factor of temperature from another point of view, they give results, showing different tendencies.

During this approach, it was not possible for the elevated temperatures to have any negative impact on the emulsion properties, as the contact time with the “hot” stock until dewatering was 30 seconds, which is not enough to cause excessive hydrolysis or emulsion instability. Therefore, this trial only displays the slightly positive impact on the sizing performance by elevated stock temperatures.

3.2.4.2 pH-Value

ASA is a so-called alkaline sizing agent, which is supposed to show its optimal sizing performance in the neutral to slightly alkaline process conditions (Chapter 2.3). It is of common knowledge during laboratory and industrial ASA application that pH-value changes are capable of influencing ASA’s hydrolytic

stability and consequently significantly influencing the sizing performance (Chapter 2.3.3.1.2). Yet there are no publications available, stating the sole influence of the stock pH-value on ASA's performance. This is why the influence of the pH value over a range from pH 4, over pH 5.5, pH 7, pH 8.5 to pH 10 was analyzed for samples sized with 0% to 0.4% ASA. The pH value was adjusted prior to sheet forming with 0.1 N hydrochloric acid (HCl) and 0.1 N caustic soda (NaOH). Figure 3.2-12 shows the impact of the pH value over the complete analyzed pH-range on the left, while the graph on the right side focusses on the section from pH 6 to pH 8, the operation window for paper manufacturing. The graphs indicate that the switch from acidic to alkaline has a major negative impact on ASA sizing performance, showing that it is possible to get moderate sizing performance at pH 5 with only 0.05% ASA, while it is not possible to give the same sizing performance at pH 10 with an ASA dosage of 0.2%. The most significant change happens within the operation window for paper production from pH 6 to pH 8. This switch has its most extreme impact on soft-sized grades with ASA dosages of 0.1% and below, where the ASA demand increases by 300% to reach the same sizing degree at pH 8 as for pH 6. This tendency is not as drastic for higher ASA dosages, but still in between 150% and 200%.

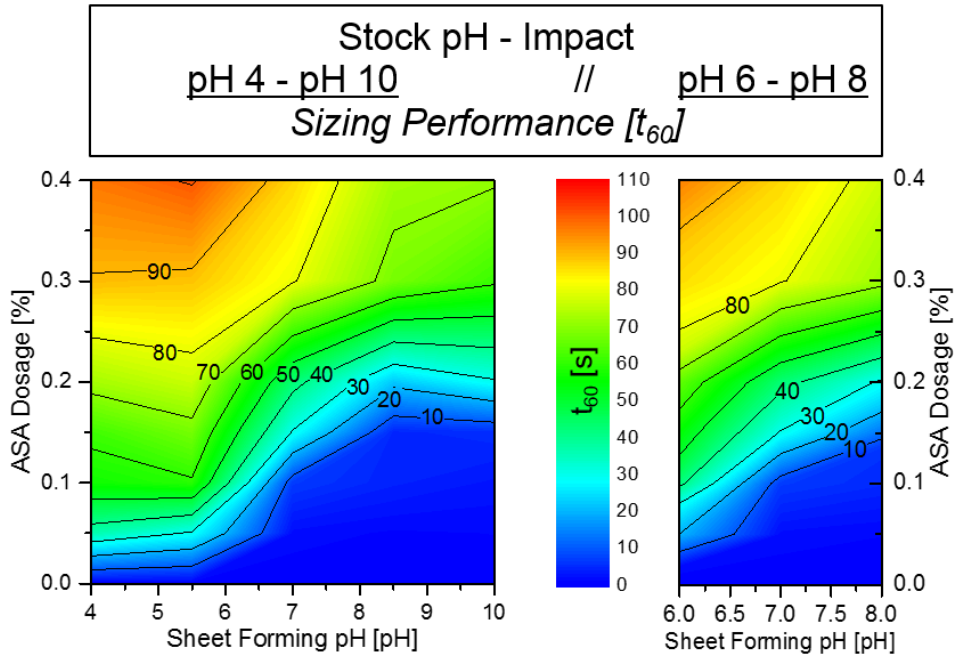

Figure 3.2-12: Impact of Sheet Forming pH on ASA Sizing Performance

Lacking of publications, describing the exact mechanisms which are leading to the observed decrease in sizing performance, the following hypothesis on the

explanation is stated. The observed negative impact on the sizing performance might be based on rapid ASA hydrolysis, but not in the aqueous phase, but already within the formed sheet structure. The time for emulsion hydrolysis is too short to have any impact during the implemented standard sheet forming procedure, as only 30 s elapse from dosage to sheet forming. Thus, high pH-values hydrolyze the ASA within the sheet structure before spreading, while low pH-values stabilize the emulsion comparably longer, leading to a lower extent of pre-spreading hydrolysis. Based on the high tackiness and high viscosity of ASA hydrolysate, high pre-spreading hydrolysis would lead to a significantly reduced spreading performance, resulting in less and more heterogeneous surface coverage and, as a consequence, in a lower sizing performance.

3.2.4.3 Conductivity

Process water conductivity is a factor, which is interacting with the majority of all wet end chemicals. As these mostly develop their way of action by electrostatic or ionic interactions with the fibers or other protagonists, high values of conductivity are capable of significantly interacting with the chemicals' charge centers, masking these, and by that inactivating the chemicals' performance. Due to the fact that ASA also fixates on the fiber surface by electrostatic and ionic interactions, high process conductivity values also interfere with ASA's performance. To evaluate this interaction, the following trial was conducted, for which the stock conductivity was varied from 0.2 µS, over 625 µS, 1250 µS, 2500 µS, 5000 µS to 10000 µS by the addition of NaCl, while the ASA dosages were varied from 0% to 0.4%. The results of this trial are displayed in Figure 3.2-13.

It can be observed, that an increasing stock conductivity has a negative impact on ASA's performance throughout all dosages, while high dosages are more robust against the negative impact. The sizing performance of 0.1% ASA decreases by 50% with a conductivity increase from 0.2 µS to 5000 µS, while it collapses completely at conductivity levels between 5000 µS and 10000 µS. The performance of 0.4% ASA is decreased by 30%, when reaching 5000 µS and by an additional 40% when reaching 10000 µS.

These results indicate that an increase in process water or stock suspension conductivity interferes with ASA's sizing performance throughout all dosages and

therefore has to be considered, when trials are conducted or systems adjusted. Especially the occurring difference between results, gained during laboratory trials with deionized water (~ 0.2 µS) and tap water (625 µS / Munich), have to be considered during sizing system analysis.

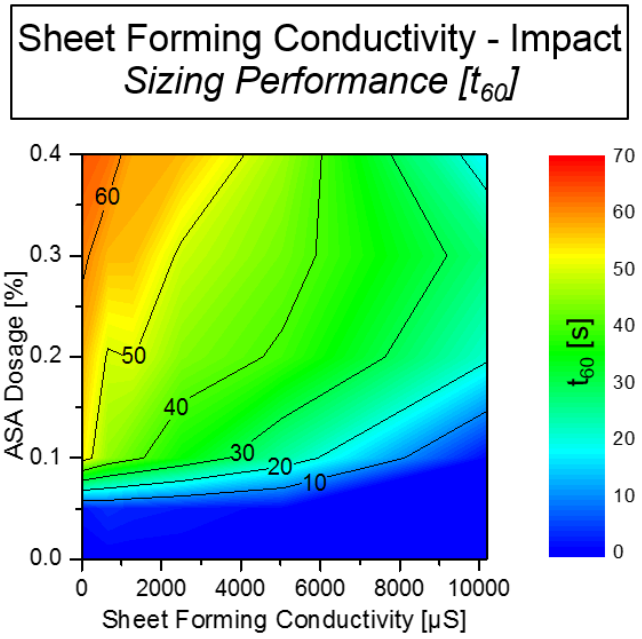

Figure 3.2-13: Impact of Sheet Forming Conductivity on ASA Sizing Performance

However, the results do not allow a clear distinction, whether the decreasing sizing performance is based on reduced retention or on interferences of other nature. At this point, it is hypothesized that it is a combination of both factors.

3.2.4.4 Water Hardness

The last factor contributing to process water and stock suspension properties is the water hardness, which is defined by the concentration of Ca^{2+} and Mg^{2+}. Just like other ions, these ions are, on the one hand, capable of interfering with process chemicals, by interacting with their active charges, and on the other hand, of special harm to ASA, as they form stable salts with ASA hydrolysate. To evaluate the influence of increasing hardness values on the sizing of the reference stock system, the following trial was conducted. The stock suspension was adjusted to water hardness values from 0 °DH, over 5 °DH, 25 °DH, 50 °DH, 100 °DH to 500 °DH by the use of $CaCl_2$, while the samples were sized by 0% to 0.4% ASA. Figure 3.2-14 displays the results of this trial.

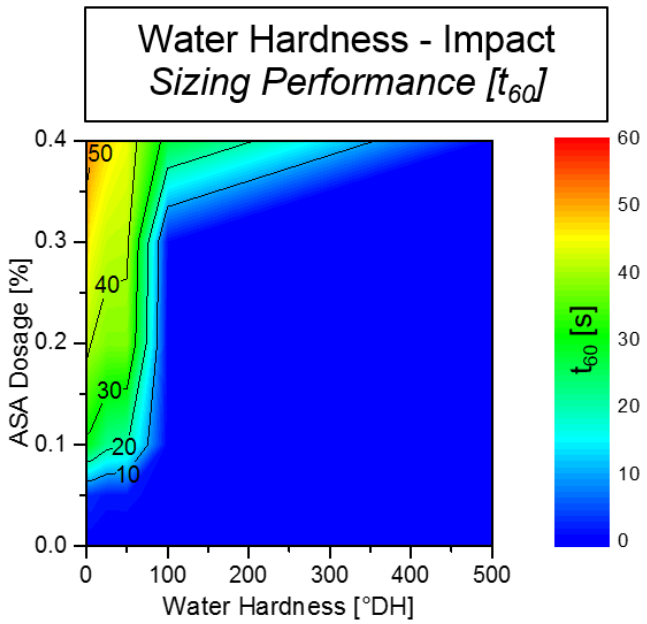

Figure 3.2-14: Impact of Sheet Forming Water Hardness on ASA Sizing Performance

These show that the negative impact of an increasing water hardness is of devastating nature. The sizing performance completely collapses for ASA dosages up to 0.3%, before reaching hardness values of 100 °DH. For an ASA dosage of 0.4% the sizing performance collapses at slightly higher water hardness values between 100 °DH and 500 °D.

This negative influence can be explained, implementing two approaches. One is based on the above-mentioned (Chapter 3.2.4.3) decreased ASA retention, which is triggered by negative interactions between the protection colloid and the ions responsible for water hardness.

The other is based on excessive hydrolysis before the ASA spreads. Similar to the hypothesis, which was stated for the explanation of the negative impact triggered by high pH values, hydrolysis prior to spreading could be the reason for the experienced weak sizing performance. Ca^{2+} promotes ASA hydrolysis to a very high extent [31], leaving the possibility that Ca^{2+}-triggered hydrolysis occurs in the instances after sheet forming, causing the formation of Ca^{2+}-Succinates, which are very tacky and thus not able to spread during the drying process. This would result in a significantly decreased surface coverage and sizing agent orientation and thus in a weaker sizing performance.

3.2.4.5 Shear Rate

Motivated by the fact that ASA is applied to the stock as cationically charged emulsion, which adheres to the fiber or filler surface by electrostatic or ionic interactions (Chapter 2.3.1.4), it was of interest to figure out, how this fixation is sensitive to shear force. This is why the following trial sets were conducted on the impact of shear forces during sheet forming.

The sheet forming shear forces were adjusted by differing the RDA stirring speeds from 250 rmp, over 500 rpm to 750 rpm. In addition to this adjustment, the impact of 25% GCC as filler, as well as, the impact of PAM or PEI as retention aids were analyzed. The ASA dosages for these trials were adjusted from 0.05% to 0.4%.

Figure 3.2-15 displays the results of these trials, while within this chart, the top left graph displays the results for plain ASA, the one on the top right the results for ASA and GCC, the one in the middle left, the results for ASA with PAM, the one in the middle right, the results for ASA and GCC with PAM, the one on the bottom left the results of ASA with PEI and the one on the bottom right side the results for ASA and GCC with PEI. The results for the trials without GCC show that plain ASA shows a very high shear sensitivity especially for a dosage of 0.05%, while it almost vanishes for dosages above 0.1%. The addition of PAM improves the shear sensitivity of 0.05% and equalizes the one of the higher dosages, while only slightly improving the sizing performance over all. The addition of PEI increases the shear sensitivity of 0.05%, while it has no impact on the shear sensitivity of the residual dosing amounts. The overall performance is decreased by the presence of PEI.

The results for the trials where GCC was added to the stock system, show quite different tendencies. As already mentioned during the discussion of the impact of GCC (Chapter 3.2.3.4), it can be observed that the sizing performance is significantly decreased with GCC present. Along with this negative impact, the shear force impact increases slightly. The sizing performance is not positively affected by either the presence of PAM or PEI. In fact, it is slightly decreased, while the shear force impact increases as well.

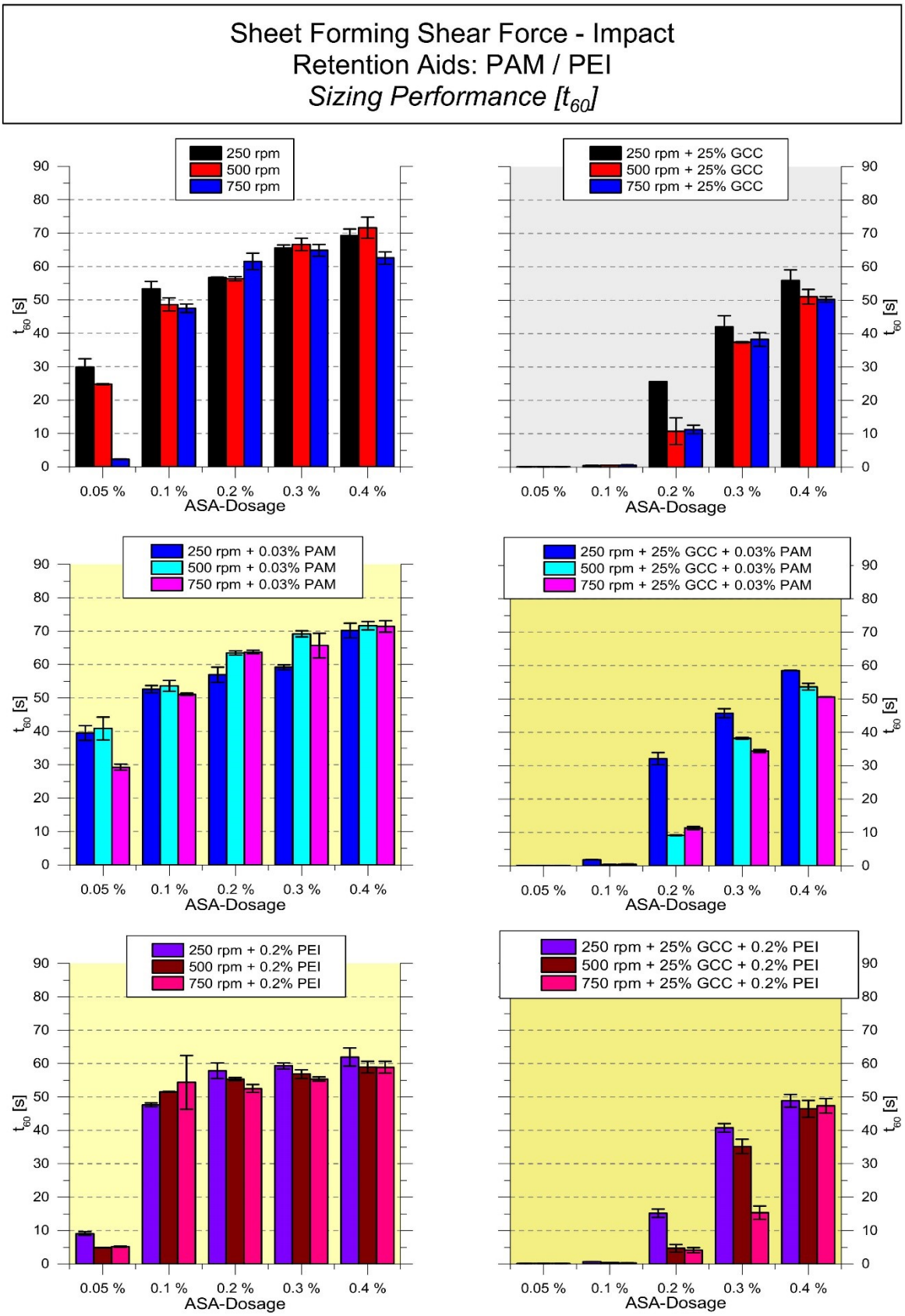

Figure 3.2-15: Impact of Sheet Forming Shear Rate with PAM and PEI on ASA Sizing Performance

In addition to the graphically presented results, the overall and filler retention values were analyzed during this trial. These show that the retention values are boosted by the addition of PAM and PEI, while the increase in filler retention accounts the most to the total retention increase. However, the sizing values can remain unchanged. This phenomenon can only be explained by an equal ASA distribution amongst all stock components and not by a favored adhesion to the filler particles in the system. Only if the distribution among all ingredients is equal, can the sizing performance remain unchanged by lower retention values.

This explanation is only applicable for systems without filtrate (white water) recirculation, because the unretained ASA would subsequently hydrolyze and cause negative interactions once recirculated and again in contact with stock.

The impact of shear force can be neglected for unfilled systems, while filled systems show certain sensitivity, especially if retention aids are present. This might be based on the retention aids' ability to retain ASA also on the filler particles, which are retained worse at higher shear forces. By this, the relative ASA amount in the sheet decreases, leading to lower sizing performance.

3.2.4.6 Dwell Time

Following the current trend to move the ASA dosing position closer to the head box (Chapter 2.3.1.3.2), the question about the required dwell time for ASA to unfold its maximum performance rises. This question was respected during the following trial where the ASA dwell time, meaning the time between dosage and sheet forming, was adjusted from 5 s over 15 s, 30 s, 60 s, 150 s to 300 s. This influence was analyzed at ASA dosages from 0% to 0.4%. The trial results are displayed in Figure 3.2-16.

The trial results show that the sizing performance of ASA within the application at the reference stock system is hardly affected by changes in dwell time. The full sizing performance is already developed after 5 seconds, stating that the emulsion's adhesion process to the fiber requires almost no time. The increase in dwell time of up to 300 s (5 min) did not influence the sizing behavior significantly under given conditions. The only observable impact was recognized for high ASA dosages of 0.3% and 0.4%, during which the sizing performance decreased by 5% - 10% over a dwell time of 300 s. These results, in combination with the shear

rate impact results, enforce the argument that in unfilled systems, the ASA emulsion adheres to the fiber surface very quickly by a strong interaction, which is very shear force and dwell-time resistant.

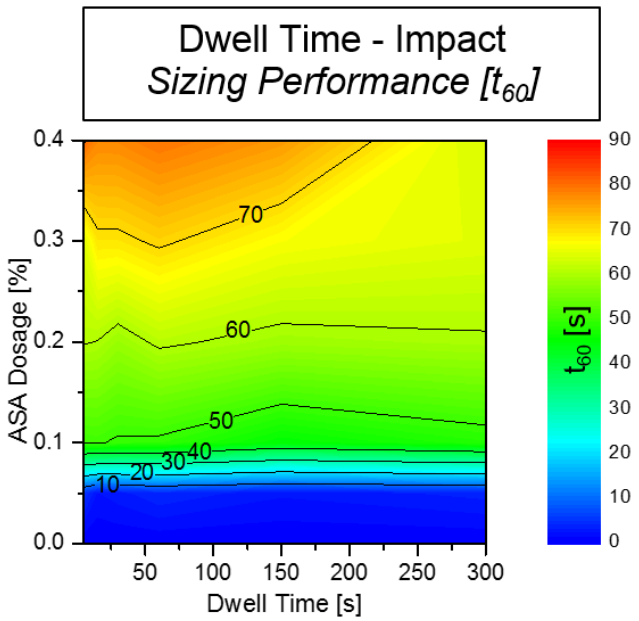

Figure 3.2-16: Impact of Dwell Time on ASA Sizing Performance

3.2.4.7 Dosing Position & Dosing Order

The previous trials, contributing to the factors of shear force and dwell time, evaluated the two factors in an isolated environment. As this is not overall applicable to continuous paper or board production, a trial paper machine (TPM, Chapter 4.2.2.9) trial was conducted, in order to analyze these factors during realistic production conditions with 10% GCC as filler and 0.03% PAM as retention aid. Therefore, the ASA dosing position was varied from the HC-stock pump (pos. ①), over the head box pump (pos. ②) to the head box (pos. ④). The exact locations of the dosing positions are displayed in the TPM RI-scheme (Figure 4.2-7). This change does not only influence the dwell time, but also the shear forces the ASA has to undergo, as it has to pass the head box pump, the ultraturax and the head box. GCC was dosed via a separate nozzle in position ① and PAM in position ③, while both positions were kept static during this trial. The selected ASA dosages were 0%, 0.1%, 0.2%, 0.3% and 0.4%. The TPM parameters were adjusted according to the settings described in Chapter 4.2.2.9.

The trial results (Figure 3.2-17) display that the impact of the dosing position does not significantly affect the sizing performance of ASA dosages up to 0.2%. The impact becomes visible at dosages of 0.3% and 0.4%, while the maximum sizing performance for all dosage points is reached at 0.3% ASA. The weakest sizing performance is reached for the dosage in position ④ at the head box, after GCC and PAM. The highest sizing performance is reached for dosing position ② at the head box pump, in between GCC and PAM.

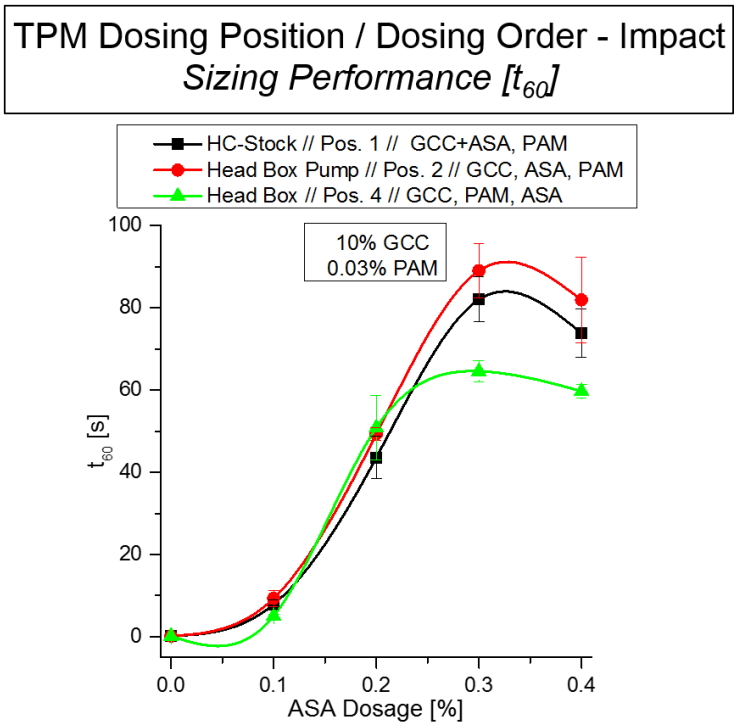

Figure 3.2-17: TPM - Impact of Dosing Position and Dosing Order on ASA Sizing Performance

These results display that a dosage too close to the head box (pos. ④) is not beneficial for the sizing performance. This might be based on two facts. The first is a very short dwell time of not more than 2 seconds before sheet forming, which might be too short to provide proper mixing and adhesion. The second point is the dosage after PAM. This means that the ASA is dosed in a stock suspension, where PAM has already formed flocs and occupied the celluloses' charge centers. This might be a reason for a significantly influenced ASA's performance, as the possible spots of adhesion are blocked.

The reason why ASA shows a higher sizing performance, if dosed at the head box pump (pos. ①), compared to a dosage at the HC-stock pump (pos. ②), is interpreted as a combination of both, dwell time and shear force impact.

The last important information that can be withdrawn from this trial is that the sizing performance at 0.4% ASA is comparably lower than the one of 0.3% ASA. This is a typical indicator for overdosage, showing that it is only possible to reach a certain degree of hydrophobization at given conditions (Chapter 2.2.4).

3.2.4.8 Drying

Since the development of the sizing performance is significantly influenced by the spreading performance of ASA, it was of highest interest to analyze the impact of the drying procedure, which is the factor that influences spreading the most. During the following presented trial sets, it was the goal to evaluate the impact which is generated by differing RK-drying temperatures and times, as well as, the ones of subsequent curing by hot air or contact curing.

Figure 3.2-18/1 shows the results of the trial set which was conducted by plain RK-sheet drying (Chapter 4.2.2.3) at temperatures of 60 °C, 80 °C, 100 °C and 120 °C, while the drying times had to be adjusted correspondingly to 40 min, 20 min, 10 min and 7 min to reach a dryness level of 95%. Figure 3.2-18/2 displays the results of a sample set, which was produced similarly to set 1, but additionally treated by a contact-curing step within a photo-drying machine for 5 min at 140 °C (Chapter 4.2.2.5). Within Figure 3.2-18/3, the contact-curing step is replaced by a hot air curing step which was adjusted to 15 min at 105 °C (Chapter 4.2.2.6).

The results of the three trial sets show that the sizing performance is significantly influenced by the drying and curing procedure. The ones from Figure 3.2-18/1 indicate that the final sizing degree after RK sheet drying is significantly boosted by the implementation of low drying temperatures and high drying times. It is especially visible that the dosages below 0.1% ASA are significantly boosted by low temperatures and long drying times.

Figure 3.2-18/2 and Figure 3.2-18/3 indicate that the sizing performance can be further promoted by a subsequent curing step, while contact curing showed a potential of ~ 10% performance increase and hot air curing a potential of ~ 20%.

It can be concluded from the overall results that the sizing performance development which is triggered by the drying procedure, is not only based on the actual drying temperature, but rather more on the total energy input. Further, it can

be stated that ASA does not necessarily need high temperatures to spread and unfold its sizing performance.

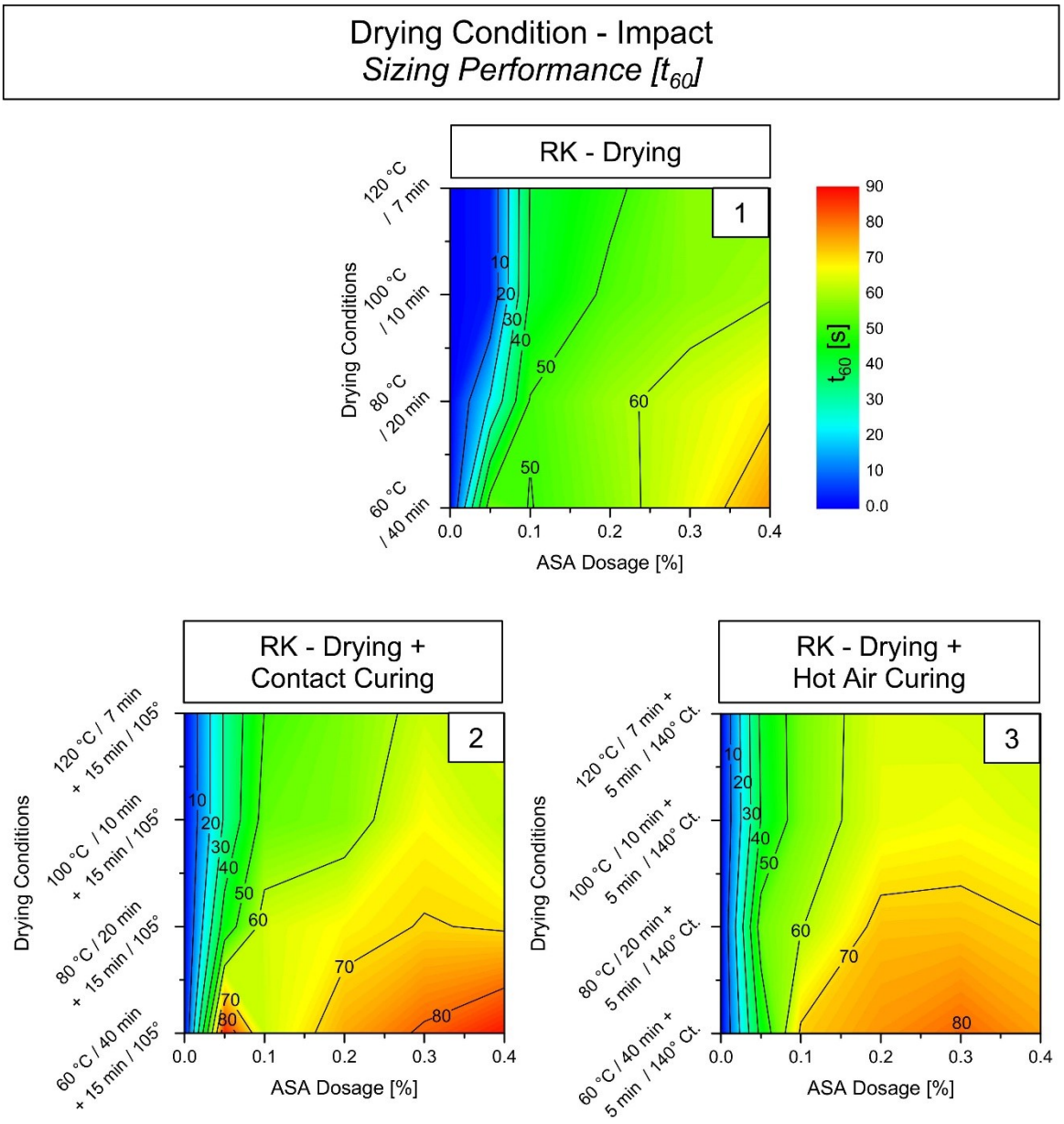

Figure 3.2-18: Impact of Drying- and Curing Conditions on ASA Sizing Performance

3.2.4.9 Aging

The post-production sizing degree cannot be considered as a static value, as it shows significant sensitivity toward humidity, temperature and aging time. The extent of this sensitivity was observed in industrial applications to be dependent on the paper or board grade and on the ASA dosage. In order to evaluate the impact of aging on the paper samples produced within this thesis, the following aging trial was conducted. Due to a lack of space in the climate cabinet, the aging trial was

conducted with samples, sized with 0.4% ASA. The parameters for this trial were set to a temperature of 80 °C, a relative humidity of 65% and an aging duration of 22 days (Chapter 4.2.2.7).

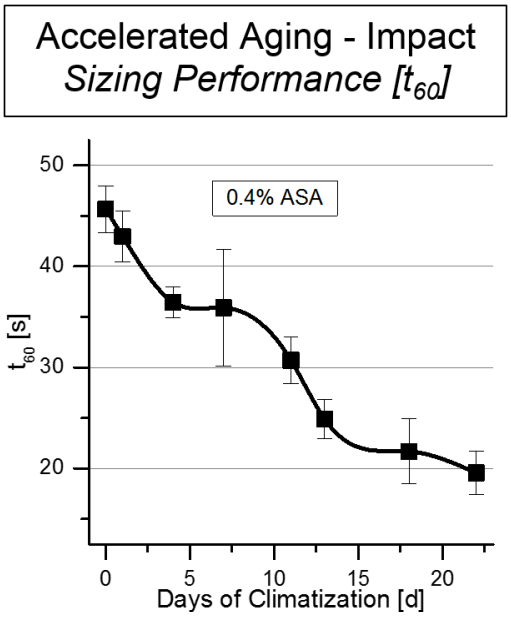

Figure 3.2-19: Impact of Accelerated Aging on ASA Sizing Performance

The trial results (Figure 3.2-19) show that a progress of sample aging has a dominant negative impact on the sizing performance of ASA. Within this trial, the sizing performance decreased almost linearly for more than 50% over the aging time of 22 days. These results further promote the theories of internal molecular mobility or ASA migration, to be the main trigger for the phenomena that influence the sizing performance (Chapter 2.3.2.2).

3.3 Factors Impacting the Localization Behavior of ASA

The approaches and results from the above-noted chapters on the factors which interfere with ASA's sizing performance, have displayed that ASA is very sensitive to some external factors. As it is the goal of this work to evaluate, analyze and describe the mechanisms behind these interactions, an excerpt of these factors will subsequently be analyzed in accordance to their effect on ASA's agglomeration behavior. The information gained by these results shall help to uncover more puzzle pieces which are still missing for a holistic understanding of reactive paper sizing with ASA. The results that are presented within the following trials were gained by combining the above-mentioned novel localization method (Chapter 3.1) with the respective sizing performance of the analyzed samples.

3.3.1 **Degree of Refining**

As it has crystallized during the evaluation of the different stock parameters which influence the sizing performance of ASA, the degree of refining turned out to be the factor of highest significance. The following graphs display the agglomeration behavior (Figure 3.3-1), as well as, the respective sizing performance

(Figure 3.3-2), measured over the degrees of refining from SR 27.5 over SR 40 and SR 49, to SR 62, while the ASA dosages were set to 0.1%, 0.2%, 0.3% and 0.4%.

The results, displayed in logarithmic scale, show that the agglomeration behavior in terms of total agglomeration area, is very positively influenced by the increasing degree of refining, on the one hand, and, on the other hand, by the increasing ASA dosage. The total agglomeration area grows on the example of 0.1% ASA over the increase of the degree of refining from SR 27.5 to SR 62 by ~ 200%, while it grows by the step from 0.1% to 0.4% ASA for SR 27.5 by ~ 400%. It increases for an ASA dosage of 0.4% over the degree of refining from SR 27.5 to SR 62 by ~ 250%, while it increases by the step from 0.1% to 0.4% ASA dosage for SR 62 by ~ 210%.

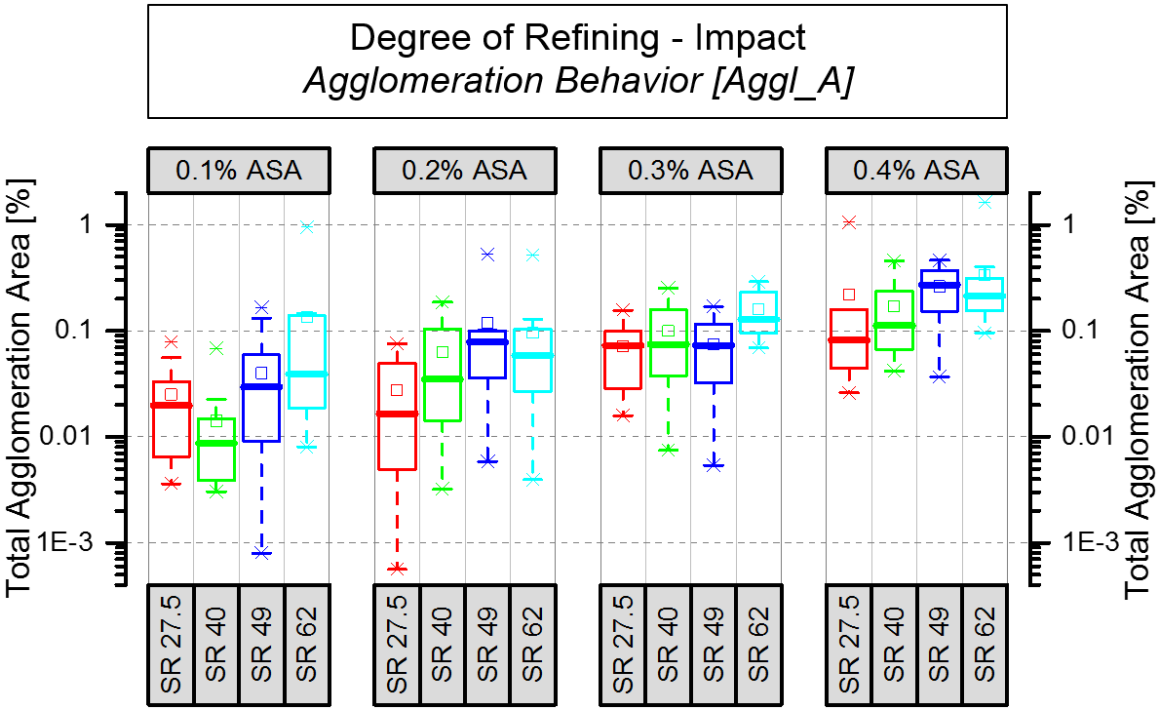

Figure 3.3-1: Agglomeration Behavior – Degree of Refining Impact (Automated Analysis)

The results of the sizing performance analysis, which are also displayed in logarithmic scale, show a similar outline. The increase of the degree of refining as well as, the ASA dosage, have a significant positive impact on the sizing performance. The total sizing performance increases on the example of 0.1% ASA over the increase of the degree of refining from SR 27.5 to SR 62 by ~ 200%, while it grows by the step from 0.1% to 0.4% ASA for SR 27.5 by ~ 400%.

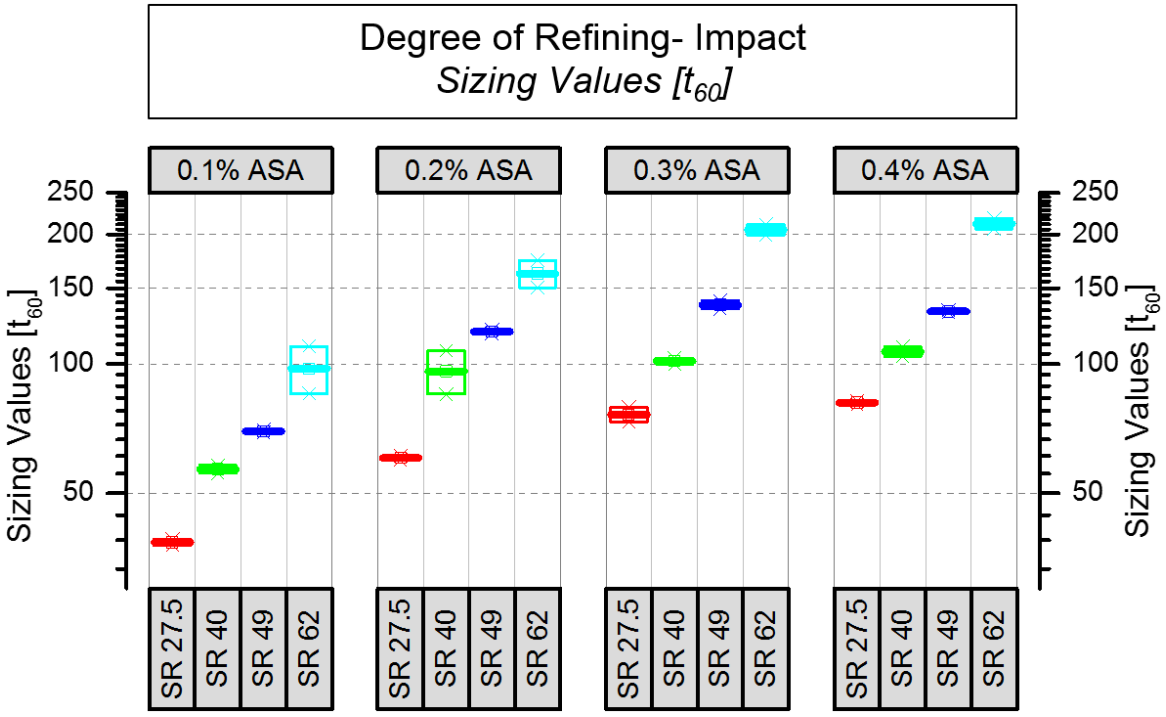

Figure 3.3-2: Sizing Performance – Degree of Refining Impact

The explanation for the increasing total agglomeration area can be delivered by utilizing the same approach that is applicable for the increase in sizing performance. On the one hand, the increasing sizing agent dosage increases the sizing agent content in the sheet, leading to a higher surface saturation and thus to an increasing total agglomeration area. The agglomeration behavior is on the other hand boosted by the morphological changes, the sheet structure undergoes by refining. An increasing degree of refining leads to a higher packing density in the sheet structure, leaving less void volume and a lower residual surface area. As ASA naturally locates on the interphase between cellulose and air, which is the fiber surface, the concentration of ASA on the surface increases in direct correlation to the packing density. This leads to oversaturation phenomena and thus to a higher extent of agglomeration.

This trial as such indicates a significant correlation between the total agglomeration area and the sizing performance. A detailed correlation analysis has resulted in a power-function based correlation of determination of R^2=0.61, proving a significant correlation.

3.3.2 **Sheet Forming Conductivity**

The first suspension-defining process parameter to be analyzed within this correlation analysis is the sheet forming conductivity, as it is an important process parameter and one of the factors impinging ASA's sizing performance most significantly. In order to facilitate the comparison between the agglomeration behavior and the sizing performance, only the values for 0.3% ASA dosage are displayed as representative values (Figure 3.3-3).

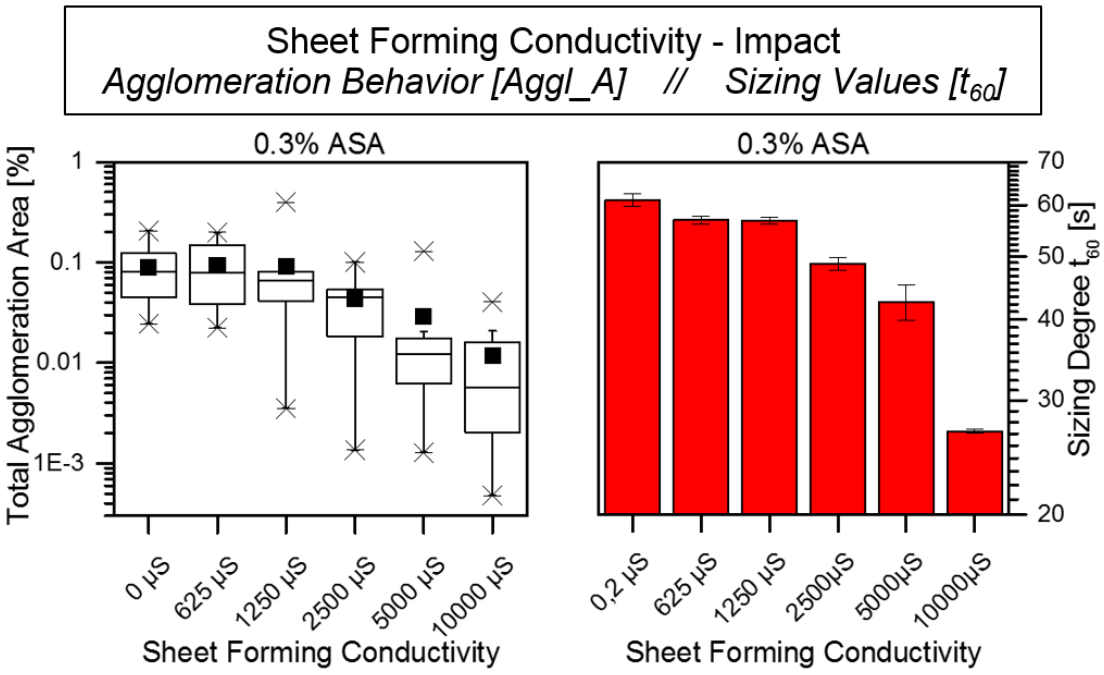

Figure 3.3-3: Agglomeration Behavior vs. Sizing Performance - Conductivity Impact (Automated Analysis)

The analysis was conducted on the samples which were also utilized for the interpretation of the conductivity's impact on the sizing performance (Chapter 3.2.4.3) The conductivity steps are therefore 0.2 µS, 625 µS, 1250 µS, 2500 µS, 5000 µS, 10000 µS. In order to provide a higher degree of comparability, both result values, the total agglomeration area and the t_{60} sizing performance, are logarithmically scaled. As it can be seen from the results, both show a significant, highly correlating decrease over increasing conductivity. The median agglomeration values remain static on a level of 0.08% up to 625 µS, before they decrease to 0.0056% for 10000 µS. The sizing values remain rather unchanged at ~ 60 s up to a level of 1250 µS, before they collapse down to 26 s at 10000µS. The correlation of determination of the median agglomeration values and the sizing

performance was determined to show an exponential behavior with a value of R^2=0.94.

These results show that ASA's sizing performance highly correlates on its agglomeration behavior, even though they do not explain, why the sizing performance, as well as, the agglomeration behavior, are that negatively influenced by increasing conductivity values. An observation that was made was that the sheets lost their red color intensity over conductivity increase, while the sheet forming filtrate became simultaneously redder. This is an observation which promotes the theory that ASA's retention is significantly decreased by increasing conductivity values.

3.3.3 **Water Hardness**

The second suspension defining process parameter that was analyzed in accordance to evaluate the correlation between the agglomeration behavior and the sizing performance, was the impact of the process water hardness. As for the above-mentioned correlation analysis for process water conductivity, for this trial the same samples, as for the evaluation of the impact on the sizing performance (Chapter 3.2.4.4), were used. The results are also displayed in logarithmic scale, where the agglomeration values and the respective sizing performance for an ASA dosage of 0.3% are displayed (Figure 3.3-4). The water hardness levels of choice were 0°DH, 5°DH, 25°DH, 50°DH, 100°DH and 500°DH.

The results show a highly negative impact on the sizing performance, as well as, on the agglomeration behavior by increasing process water hardness. The median agglomeration values decrease immediately with increasing water hardness, resulting in an agglomeration area reduction of 75% by the step to 5°DH, and a 99% reduction by the step to 500°DH. The sizing performance remains rather static at a value of ~ 45 s to a level of 50°DH, before it decreases to almost zero by the step to 500°DH. The correlation of determination of the median agglomeration values and the sizing performance was determined to show an exponential behavior with a value of R^2=0.60, still indicating a significant correlation.

During this trial, the same observation was made as for the conductivity impact trial. The sheets lost their red color intensity over water hardness increase, while

the sheet forming filtrate became redder, indicating that weakened ASA retention is the trigger for the decrease in sizing performance and total agglomeration area.

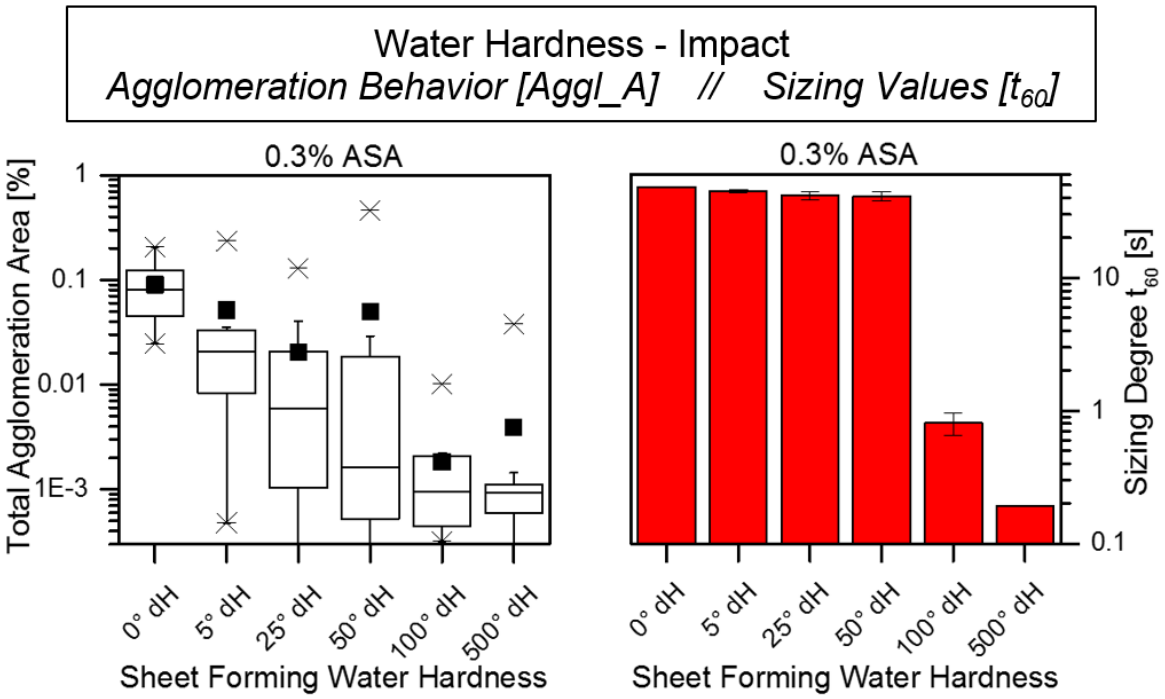

Figure 3.3-4: Agglomeration Behavior vs. Sizing Performance – Water Hardness Impact (Automated Analysis)

3.3.4 **Retention Aid (PAM)**

The synergetic effect of retention aids on the sizing performance of ASA is a well-known factor and shall therefore be analyzed by the example of PAM within the following correlation analysis. Even though the sizing performance analysis within the above-mentioned approach (Chapter 3.2.4.5) has shown that PAM has no significant impact on the sizing performance within the reference stock system, its impact on the agglomeration behavior is of interest, as the results could help to explain the mechanisms on which PAM's synergetic effects are based.

Therefore, the following trial was conducted, where the PAM dosage was varied from 0%, over 0.015% to 0.03% and the ASA dosages from 0% over 0.1%, 0.2% to 0.3%. This trial was planned and analyzed by Modde, using a full factorial design with a PLS fit. The model fit for the total agglomeration area and the sizing performance (t_{60}) is displayed as contour plot in Figure 3.3-5, while the model specifications are listed in the appendix (Table 7.2-1). The fit results show that the agglomeration behavior is linearly positively affected by an increasing ASA dosage, whereas it slightly decreases by the dosage of PAM. The sizing behavior shows

the same tendency in terms of a performance increase by ASA dosage increase, but an inverse tendency over the dosage of PAM. Here, the performance is slightly increased by the presence of PAM.

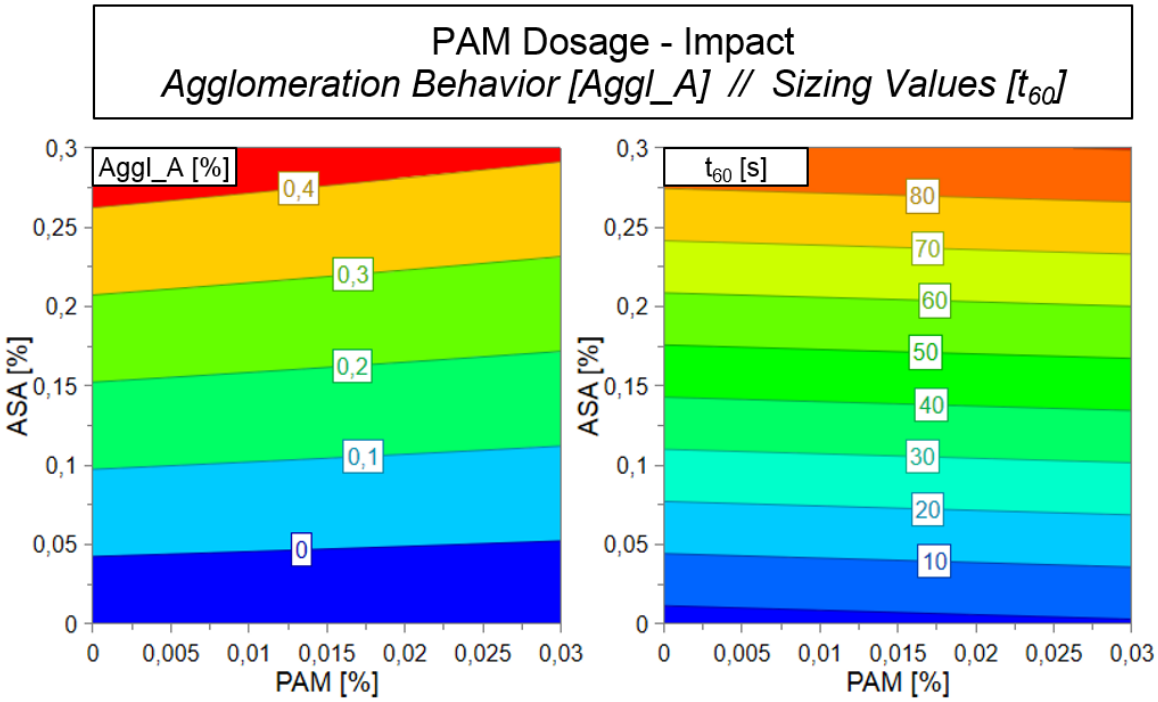

Figure 3.3-5: Agglomeration Behavior vs. Sizing Performance – Retention Aid (PAM) Impact // DOE / Full Factorial Design / Model Fit: PLS Manual Analysis, verified by Automated Analysis

This result indicates that a relative decrease of the agglomeration area at constant ASA dosage and constant stock and process parameters, leads to higher hydrophobization. This phenomenon is interpreted as a PAM promoted, comparably higher ASA distribution uniformity, which leads to improved surface coverage and thus to better sizing performance.

3.3.5 **Contact Curing**

The trials within Chapter 3.2.4.8 showed that the drying process has a significant impact on the sizing performance of ASA. In order to analyze the correlation between the synergetic effect of contact curing and the agglomeration behavior, the following trial was conducted. This trial is, as well, based on a full factorial design of experiments which was fitted by a PLS model. The factors were the ASA dosage, which was varied from 0% over 0.1% and 0.2% to 0.3% and the contact curing temperature, which was set to 100 °C, 120 °C and 140 °C. The contact curing time remained static at 5 minutes. The two models, displayed as contour

plots, are embedded in Figure 3.3-6, while the agglomeration behavior is displayed on the left and the sizing performance on the right. The model specifications are listed in the appendix (Table 7.2-2).

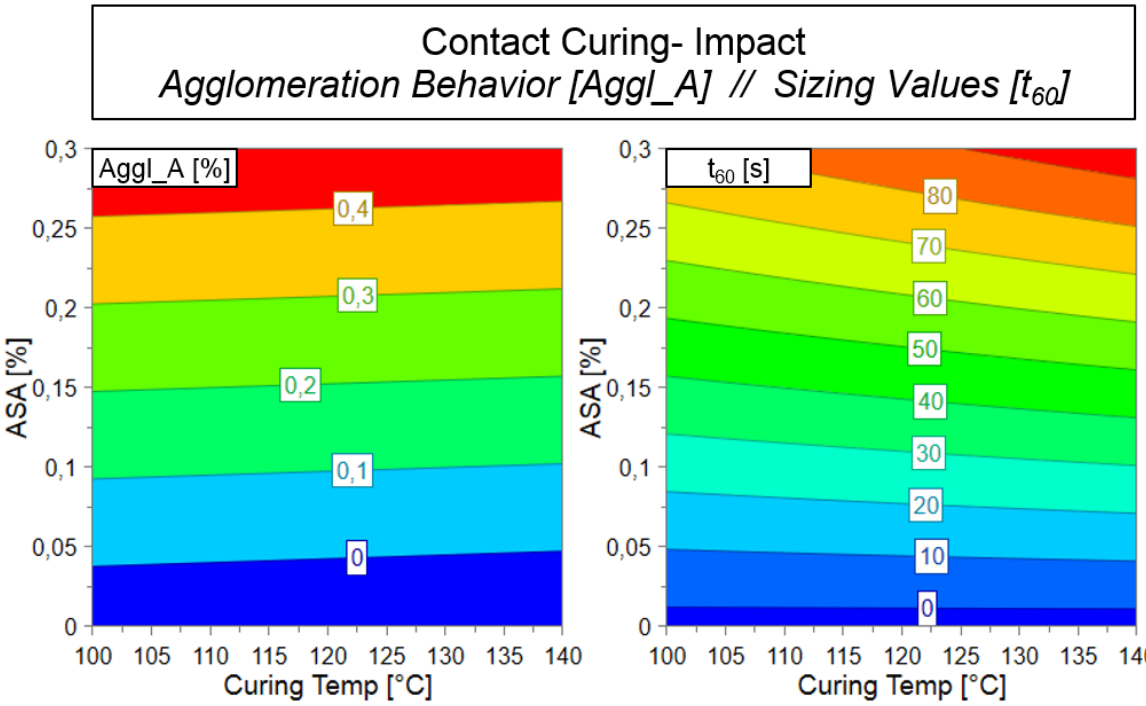

Figure 3.3-6: Agglomeration Behavior vs. Sizing Performance – Contact Curing Impact // DOE / Full Factorial Design / Model Fit: PLS Manual Analysis, verified by Automated Analysis

The results of this trial show that the total agglomeration area is positively affected by an increasing ASA dosage, while it slightly decreases over rising curing temperatures. The sizing values show a synergy toward both factors, the ASA dosage and the curing temperature, while the impact of the curing temperature is considerably lower, compared to the one of ASA dosage. These results indicate that the performance increase during contact curing is based on similar mechanisms as applicable for PAM. Higher curing temperatures lead to enhanced post-sheet-forming spreading phenomena, which cause an optimized ASA distribution and surface coverage, and by this, less observable agglomerates and thus an increasing sizing performance.

3.3.6 **Accelerated Aging**

The last factor that is analyzed within the determination of agglomeration influencing factors is the impact of accelerated aging. The impact of aging on the sizing performance was already explained during Chapter 3.2.4.9 on the example

of paper samples sized with 0.4% ASA and 22 days of aging time, showing a significant linear negative impact. The following trial was conducted by aging of samples sized with 0%, 0.05% and 0.1% ASA over a time of 7 days. The comparably low ASA dosages were chosen to create a higher sensitivity toward the impact of aging, in order to evaluate the resulting mechanisms within a shorter period of time. This trial is based on a full factorial design of experiments which was fitted by a PLS model. For interpretation, a third contour plot is introduced, visualizing the respective average agglomerate size. The resulting models, displayed as contour plots, are embedded in Figure 3.3-7, while the agglomeration behavior is displayed on the top left, the average agglomerate size on the top right and the sizing performance on the bottom. The model specifications are listed in the appendix (Table 7.2-3).

The results of the aging trial show that all three result-values, the total agglomeration area, the average agglomerate size, as well as, the sizing performance are positively influenced by an increasing ASA dosage. The tendencies over increasing aging time show different outlines. The measurable total agglomeration area decreases with proceeding aging time of 7 days by ~ 50%, while the sizing performance decreases by ~ 20%. The difference between their behaviors is that the total agglomeration area decrease is of quadratic nature, while the one of sizing performance is, as experienced during Chapter 3.2.4.9, of linear nature. The average agglomerate size shows the tendency toward the formation of bigger agglomerates over aging time, resulting in a quadratic increase of ~ 35% for 7 days of aging.

These results can be concluded via an approach based on the molecular mobility of ASA molecules within the sheet structure. Driven by heat and moisture-promoted mobility phenomena, the ASA molecules tend to form big, voluminous agglomerates by the inclusion of many small agglomerates into several big agglomerates. This causes a reduction of the total agglomeration area and the number of agglomerates, while the residual agglomerates gain in size and volume. This leads to a reduced and more heterogeneous surface coverage of the fibers, and thus to a reduced sizing performance.

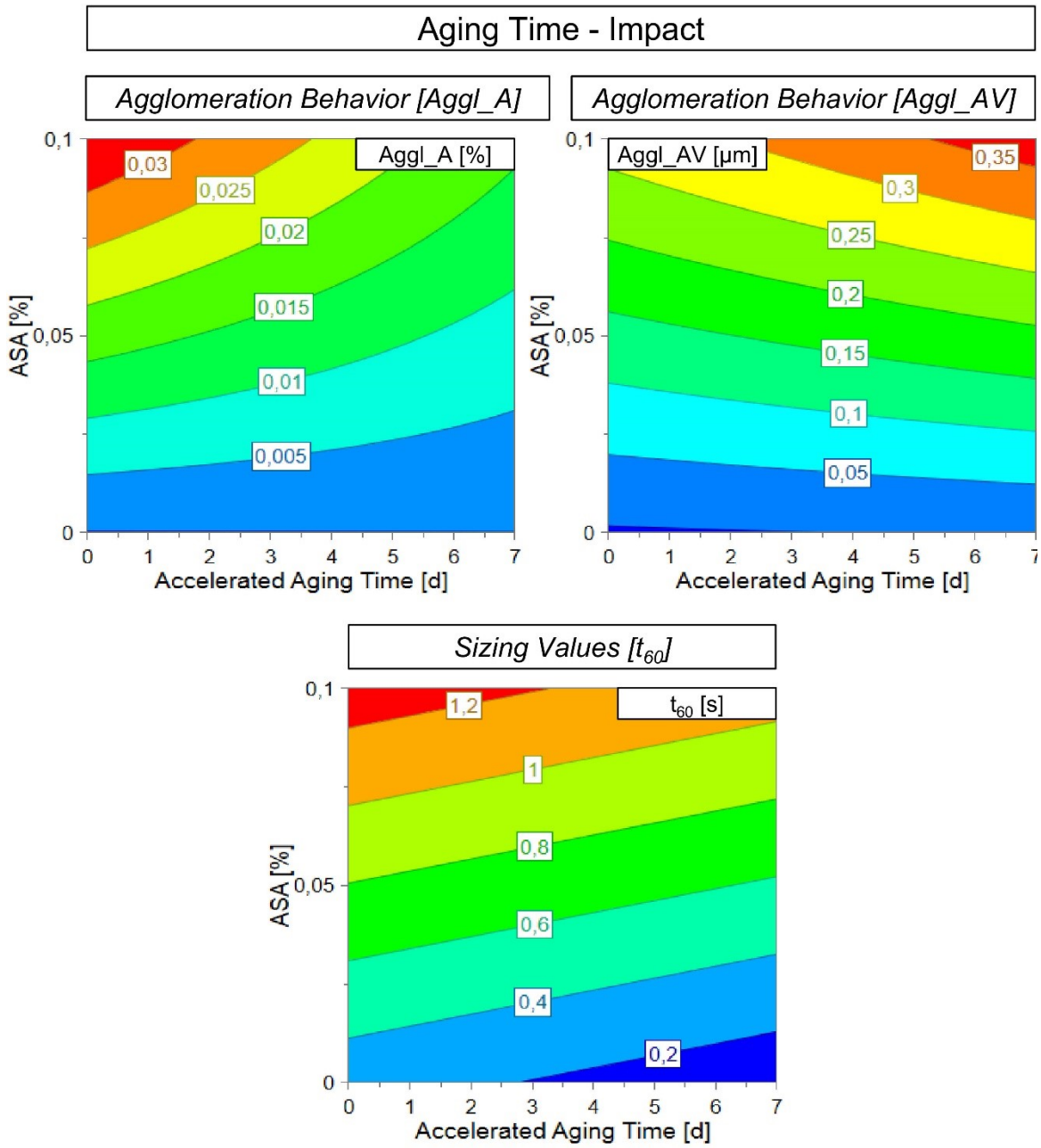

Figure 3.3-7: Agglomeration Behavior vs. Sizing Performance – Accelerated Aging Impact // DOE / Full Factorial Design / Model Fit: PLS Manual Analysis, verified by Automated Analysis

3.4 Main Optimization Approach

The objective goal of this thesis was an industrial-scale sizing performance optimization by a methodology, based on the results which were gained during the determination of the sizing performance and agglomeration behavior interfering factors. As the results from Chapter 2, Chapter 3.2 and Chapter 3.3 have shown, an optimal sizing performance of ASA is significantly depending on four factors.

These are:

- An optimal fixation to the stock and subsequent high retention, to provide a high share of active ASA in the sheet structure.
- A minimized extent of pre-spreading hydrolysis, either as emulsion or in the sheet structure, to avoid emulsion instability at first and a reduced spreading performance at second.
- A high degree of spreading during the drying and curing process, to provide maximum surface coverage with as little as possible spots of oversaturation (agglomerates).
- Finally, an optimized molecular anchoring and orientation, to guarantee a maximum of surface energy reduction and thus a high sizing performance.

In order to optimize the overall sizing performance of ASA, one or a combination of the above-mentioned factors have to be optimized.

3.4.1 **Optimization of ASA Sizing Performance Characteristics**

The first step toward a successful optimization approach was to gain a holistic understanding of ASA's current performance characteristics, as only this could reveal possible optimization approaches. Based on the gained data throughout all conducted trials within this work, the following model for ASA's performance characteristic was developed (Figure 3.4-1).

Within this model, the relative sizing performance of ASA is indicated on the y-axis, while the relative dosage is indicated on the x-axis. ASA's performance characteristics are split into four representative sections.

The first is the activation section, where a certain amount of ASA has to be dosed in order to experience any resonance in sizing performance. The amount for first resonance was determined to be 0.05% ASA for the reference stock system. This region of activation is described by a minimal required amount of fiber surface saturation by ASA in order to hydrophobize enough surface to have an impact on the wetting and penetration behavior.

The second section is defined by a linear increase of the sizing performance over an increasing ASA dosage. This linear gain is explained by an increasing surface coverage by ASA and thus an increase in hydrophobized fiber surface, leading to higher sizing performance.

The third section describes the region of saturation, which is defined by a more or less static sizing performance, even though the ASA dosage is increased. The reason for this static behavior is based on a maximum surface saturation and coverage of the cellulose by ASA.

The last section is representative for an ASA overdosage, where the sizing performance decreases over an ASA dosage increase. This response is based on surface oversaturation phenomena and along-going hydrophobicity and surface energy inversions, which lead to a reduction of the sizing performance.

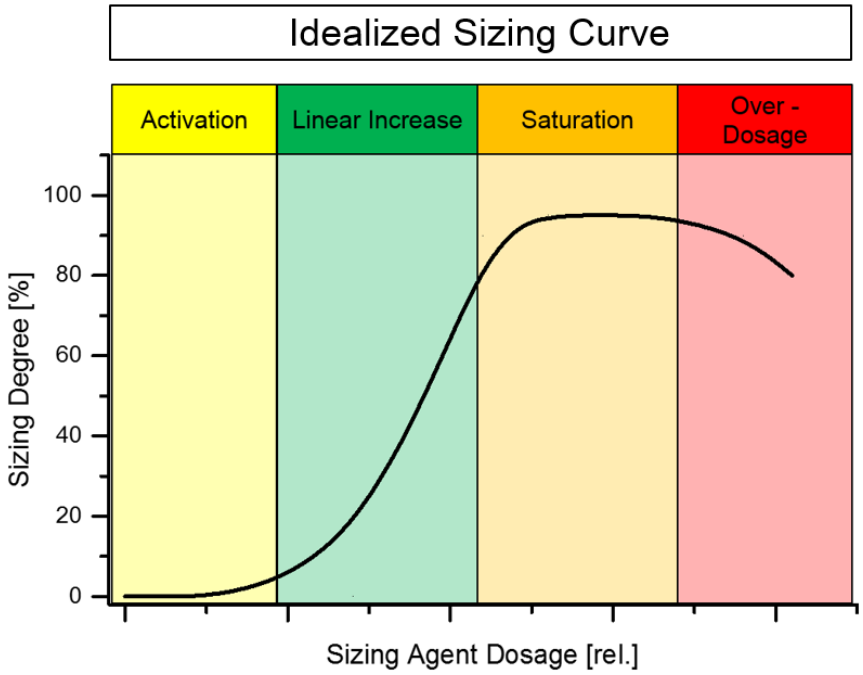

Figure 3.4-1: Sizing Performance Characteristics - Idealized Sizing Curve with Specific Sectors

The approach that was followed within the scope of performance optimization is displayed in Figure 3.4-2. The fictive performance characteristic curve is displayed in green shade, indicating that the main difference to the standard performance characteristic is the quenched activation section and a switch of the whole curve toward lower dosages. This optimization was supposed to be realizable by improved ASA fixation in terms of a higher degree of homogeneity, anchoring and orientation, leading to improved sizing performance at lower dosages.

It is also visible, that the approach does not consider a significant improvement of the total hydrophobicity. This is based on the already gained results which show that the maximum degree of hydrophobicity is highly correlating to the stock parameters and the stock morphology, which are not supposed to be changed

within the implemented approaches. The third important feature about the optimized sizing curve is an expected overdosage, which will be reached at lower dosages compared to the standard process. This is based on global oversaturation phenomena, which do occur earlier, as the surface is initially more homogeneously covered by ASA.

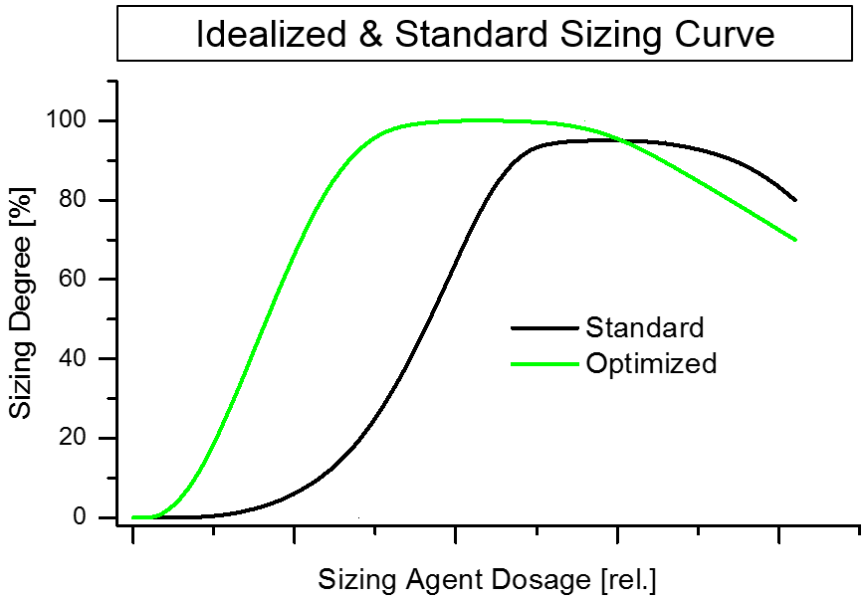

Figure 3.4-2: Sizing Performance Characteristics - Optimized Sizing Curve

3.4.2 **Emulsion Modification**

The results of the conducted trials, as well as intense theoretical considerations, have brought up the approach of sizing performance optimization by emulsion modification via cationic mordants. This consideration is based on the principle displayed in Figure 3.4-3.

The standard emulsion particle which is stabilized by cationic starch, shows a high degree of self-retention as such and thus proper adhesion to the fiber surface, leaving not much room for improvements. The point where improvements could be done is during the spreading process. As the cationic emulsification starch has a very high molecular weight and the ability to form strong interactions with the cellulose by its cationic charge, it only shows a minor extent of mobility after the emulsion break up. Resulting from this, the ASA flows over the starch covered fiber surface during the spreading process. Due to the starches ability to act as fixative, anchor and orientation help, the ASA out of the starch-covered area suffers by not having a benefit of this feature. This leads to a comparably weaker orientation and

distribution of the ASA that is not in contact with starch, enabling only sizing performances below the possible maximum.

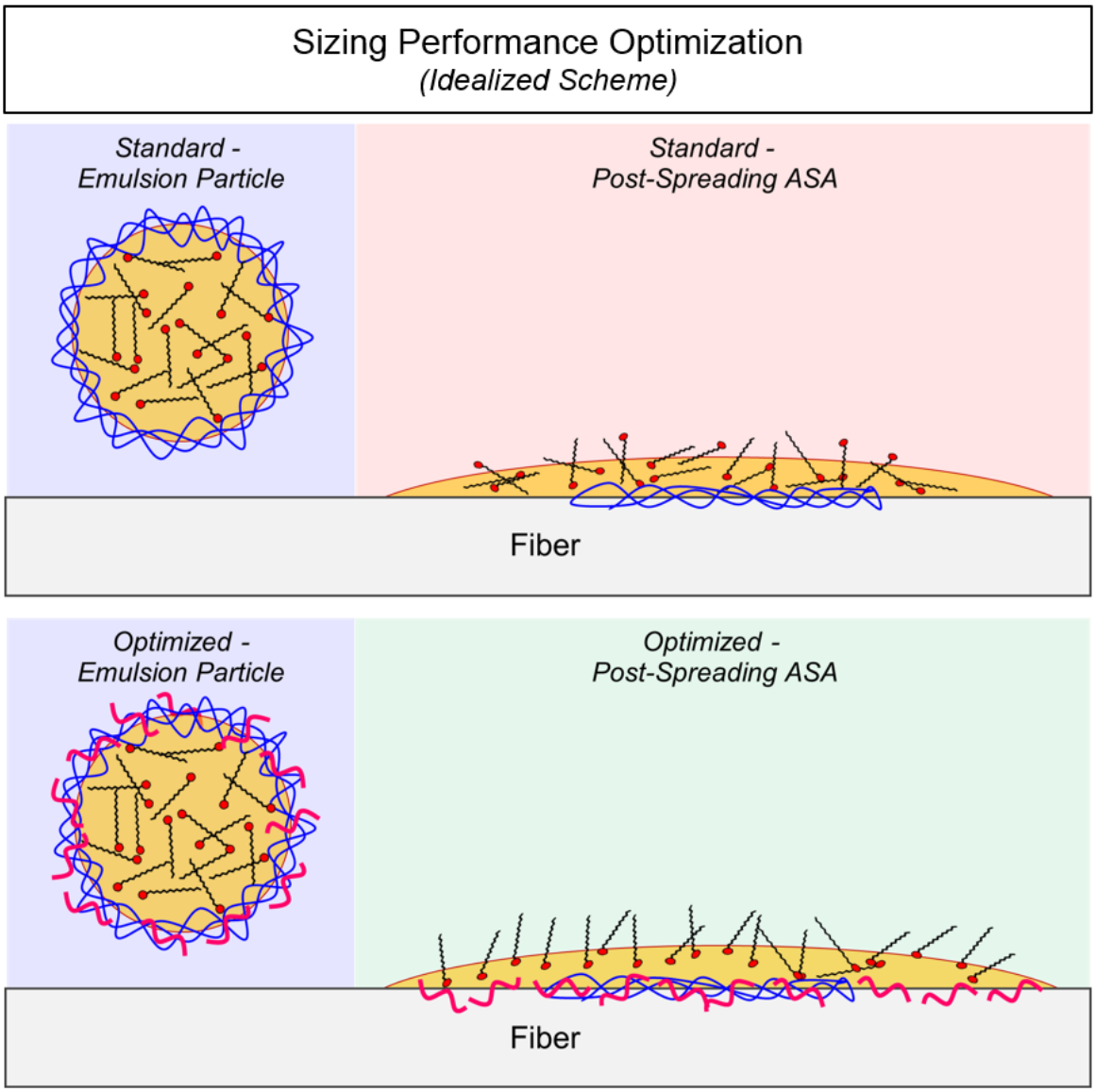

Figure 3.4-3: Sizing Performance Optimization by Emulsion Modification (Idealized Scheme)

This drawback is supposed to be overcome by the induction of cationic mordants into the protection colloid during the emulsification process. This process step triggers an immobilization of the mordants in the protection colloid, which would lead to the benefit that they travel with the emulsion droplet to the area on the fiber where they are needed. The way of action is supposed to be based on a higher mobility of the mordants, compared to the emulsification starch. This would enable the mordant molecules to travel with the ASA on the still water carrying cellulose interphase during the spreading process, generating orientation anchors among

the whole ASA-covered surface. This would lead to a more homogeneously distributed ASA and to a promoted orientation, resulting in comparably higher sizing performances.

The mordants of choice for this trial approach were poly aluminum chloride (PAC, Chapter 4.3.3.5), poly aluminum nitrate sulfates (PANS, Chapter 4.3.3.5) and poly amidoamine epichlorhydrin (PAAE, Chapter 4.3.3.4). The synergetic effect of these additives to ASA sizing is well known, but only if applied to the system as isolated additive, and not in direct combination with ASA (Chapter 2.3.3.4). The supposed benefit of the emulsion modification approach is that the mordants have no chance to react with other process ingredients, such as fibers or anionic trash. For the following discussion of the conducted optimization trials and their respective results, only the ones where PAAE was used are described. The results for PAC and PANS are skipped during the following, while stating that both additives did deliver equal performance boosting properties as PAAE.

The evaluation of the optimization potential was conducted through three steps, starting with laboratory RDA sheet-forming trials with reference stock, over laboratory trial paper machine (TPM) trials by simulating an industrial OCC based system, to the implementation in industrial-scale board production, including the necessary process adjustments.

3.4.2.1 Lab Trials / RDA Sheet Forming

The following trial describes the optimization potential generated by the induction of PAAE as additional additive within the protection colloid. PAAE was therefore mixed with the emulsification starch prior to emulsification (Chapter 2.3.1.3.1), with subsequent standard dosing and sheet forming. The percentage with which PAAEs dosage is announced during the following trials indicates the dosage compared to ASA, meaning that a 50% PAAE dosage indicates a total PAAE content (active matter) in the emulsion, which is 50% of the one of ASA. Figure 3.4-4 displays the results of the trial which was conducted for the evaluation of PAAEs impact as emulsion additive on the sizing performance. Within the following graph, the x-axis indicates the ASA dosage, which was varied from 0.05%, over 0.1%, 0.2%, 0.3% to 0.4%, the y-axis indicates the sizing performance (t_{60}), while the curve colors indicate the different PAAE dosages of 0%, 5%, 10%, 25% and 50%.

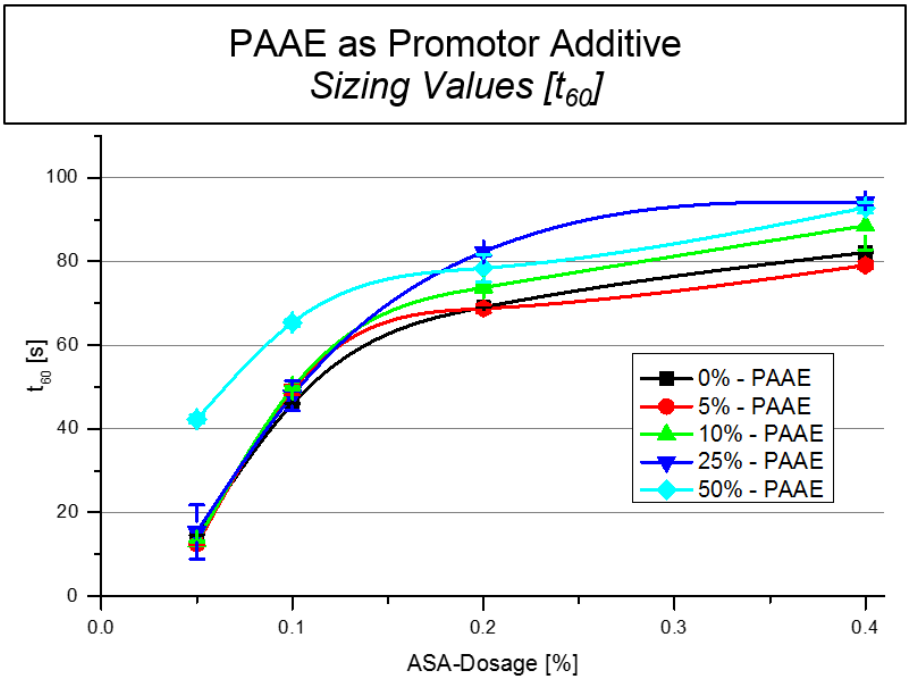

Figure 3.4-4: Impact of PAAE as Promotor Additive on ASA Sizing Performance // RDA / Reference Stock

The results show, that a PAAE dosage of 5% does not deliver any advantages, while the dosages of 10% - 25% have a positive impact on the sizing values in the saturation sector, resulting in ~ 10% performance improvement. The desired quenching of the activation sector was only possible by the dosage of 50% PAAE. For this dosage value, the performance is especially promoted in the linear section, indicating a possible ASA reduction of up to 50%. The overall sizing performance in the saturation sector is additionally boosted by 7% - 10%. These results indicate a significant potential for PAAE as emulsion additive for ASA sizing performance optimization.

3.4.2.2 TPM Trials

As the initial laboratory RDA sheet forming trial results were of highly promising nature, the emulsion optimization approach was transferred on continuous trial paper machine production (TPM) within a real life industrial OCC system (Chapter 4.3.1.2). The utilized trial paper machine which is located at MUAS was provided by IVP e.V.. The paper machine's specific details are listed in Chapter 4.2.2.9. The OCC system was simulated during this trial by the utilization of fresh OCC stock as well as the corresponding board machine white water. The ASA dosages were adjusted to 0%, 0.2%, 0.4% and 0.6%, while the PAAE

dosages were adjusted to 0%, 25%, 50% and 100%. The comparably high dosage of PAAE was chosen in order to evaluate a further optimization potential beyond the one presented in Figure 3.4-4. During this trial (Figure 3.4-5), in order to properly simulate the industrial-scale production process, wet strength resin (WSR), PAC and retention aid (RET) were dosed with a fixed amount. As their dosage values are of sensitive nature, these are not displayed within this thesis. The dosing positions for all additives were set as following: ① WSR, ② PAC, ③ ASA, ④ RET (Figure 4.2-7).

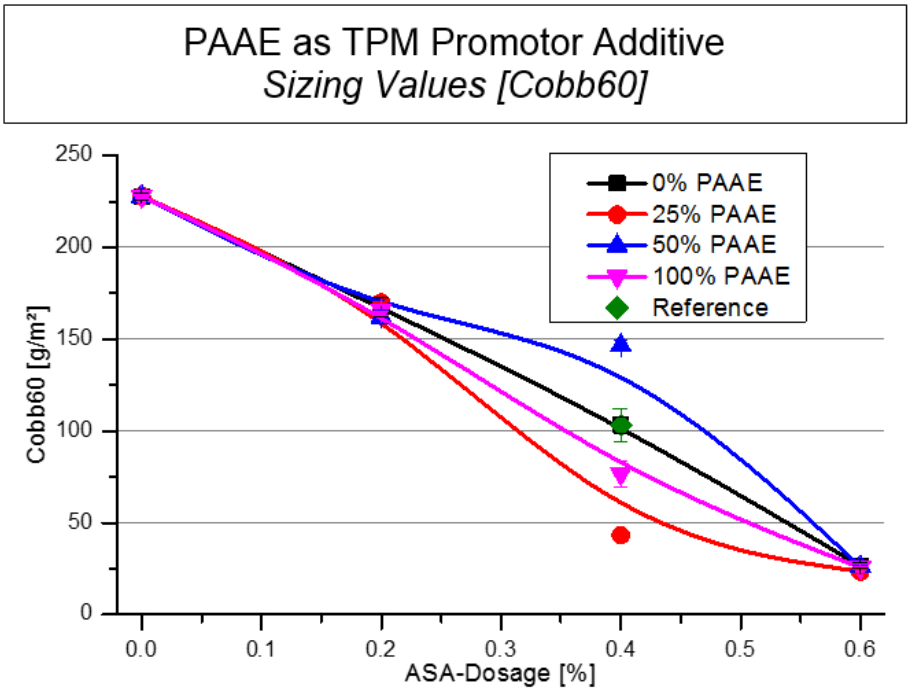

Figure 3.4-5: Impact of PAAE as Promotor Additive on ASA Sizing Performance // TPM / OCC System

The additive dosages, except for ASA, remained static throughout the whole trial. As the TPM trials served as connection from laboratory to industrial application, the reference value which was generated by exactly simulating the industrial production process, is indicated as green diamond. For better comparability, the sizing values are indicated as $Cobb_{60}$ values, as these are of common industrial use. The trial results show that the sizing performance is only affected by PAAE at a dosage of 0.4% ASA, while only the dosages of 100% and especially 25% PAAE are acting in a promoting way. The results further indicate that the PAAE dosage of 25% reduces the Cobb value at 0.4% ASA dosage by ~ 55%, promoting its optimization potential.

3.4.2.3 Industrial-Scale Trials

The last step toward the successful implementation of the developed optimization approach was the transfer to industrial-scale application. This transfer was conducted on a 3-layer fourdrinier board machine for the production of technical liner grades. The machine and product specifications are displayed in Chapter 4.2.2.10. As it was not possible to mix the promoter additive (PAAE) into the emulsification starch via a batch mixing process, the emulsification process had to be adjusted physically, in order to fulfill the given requirements. These process adjustments are explained and displayed in Chapter 4.3.3.5.

During the first trial set, only the sole impact of differing PAAE dosages on the board parameters, with focus on the sizing performance were analyzed. The PAAE dosages of choice were 0%, representing the standard system, 10% and 20%. The results of this trial, contributing to the sizing performance, are displayed in Figure 3.4-6, while on both charts the PAAE dosage is indicated on the x-axis and the sizing performance on the y-axis.

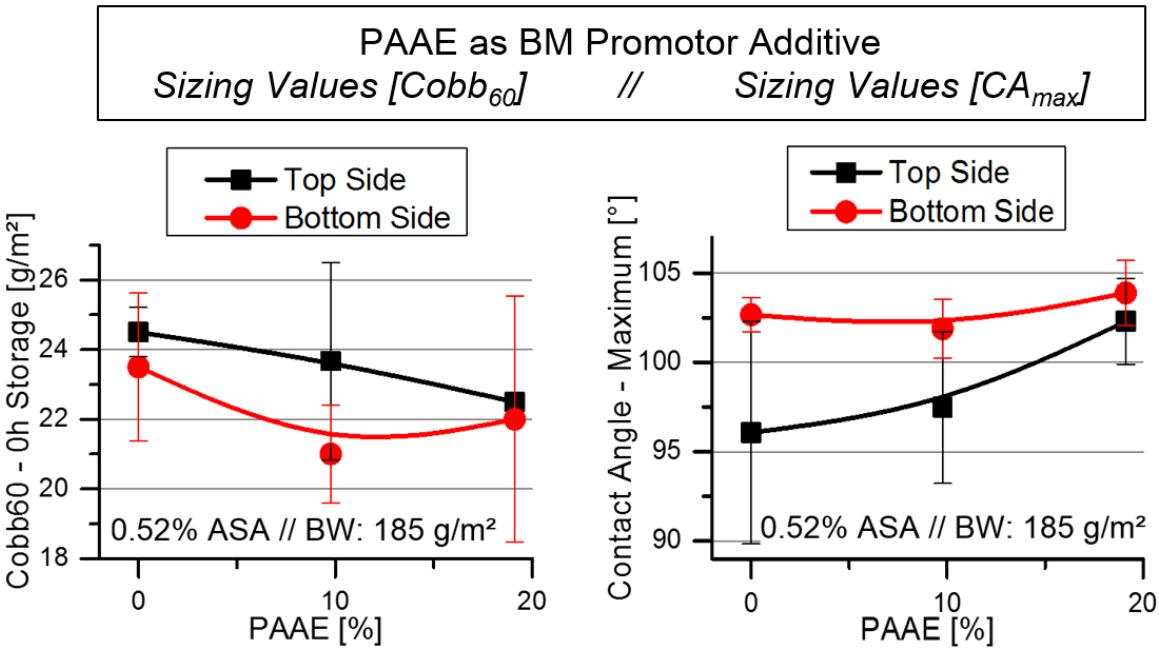

Figure 3.4-6: Impact of PAAE as Promotor Additive on ASA Sizing Performance // ($Cobb_{60}$ / left, CA_{MAX} / right) BM / OCC System

The sizing performance is indicated on the left as the measured $Cobb_{60}$ values and on the right as the maximum contact angle values. The measurement values for the top and bottom side are indicated by different colors (black/red). These values show that PAAE, dosed within the protection colloid is capable of significantly

improving the sizing performance during industrial application of the developed optimization approach. The Cobb values increase over a PAAE dosage from 0% to 20% by ~ 10%, while the maximum performance increase on the bottom side is reached at 10% PAAE dosage. The contact angle's values of both sides increase by PAAE dosage, indicating that not only the structure hydrophobicity is increased, but also the surface hydrophobicity.

Figure 3.4-7 displays PAAEs impact on physical board parameters which significantly define the processability of the produced grade. Both graphs display the PAAE dosage from 0%, over 10% to 20% on the x-axis, while the left graph's y-axis indicates the sheet porosity and the right graphs y-axis the MD-breaking length.

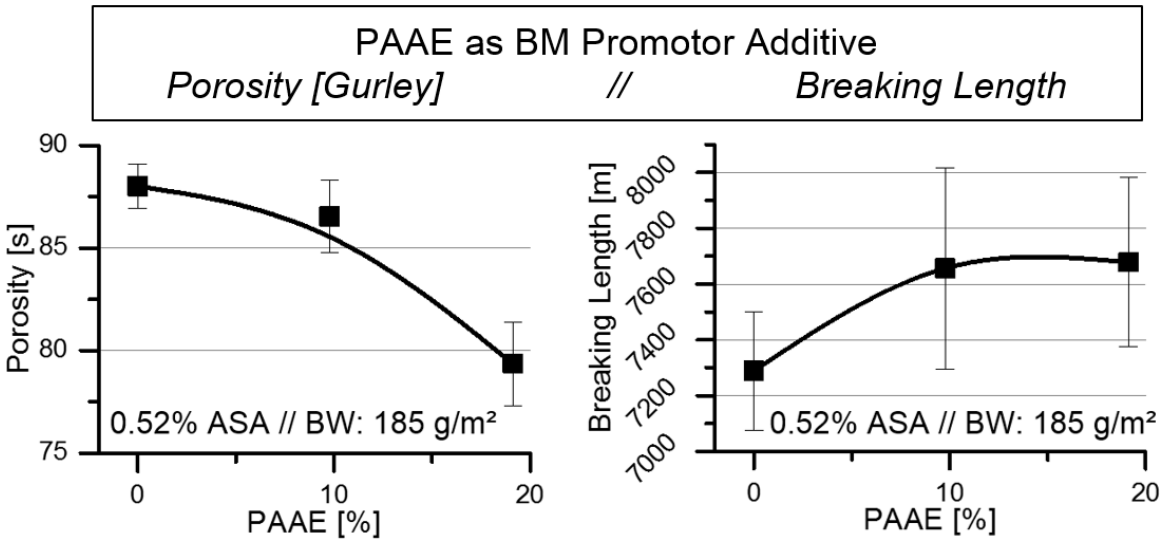

Figure 3.4-7: Impact of PAAE as Promotor Additive on Board Properties // (Porosity [Gurley] / left, Breaking Length / right) BM / OCC System

The results show that the increase in PAAE dosage from 0% to 20% reduces the Gurley value from 86 s to 78 s, indicating a porosity increase of 9.5%. The strength properties, measured via MD-breaking length increase from ~ 7300 m to ~ 7650 m, indicating a strength gain of ~ 5%.

Subsequent to the above-mentioned trial which served the evaluation of the boundary conditions, as well as the determination of the basic potential that is generated by emulsion optimization in industrial-scale, an additional trial was conducted to evaluate further optimization potential. During this trial, which is displayed in Figure 3.4-8, the optimization potential in terms of applicable ASA

reductions was evaluated, while the aging resistance of the respective samples was analyzed as well.

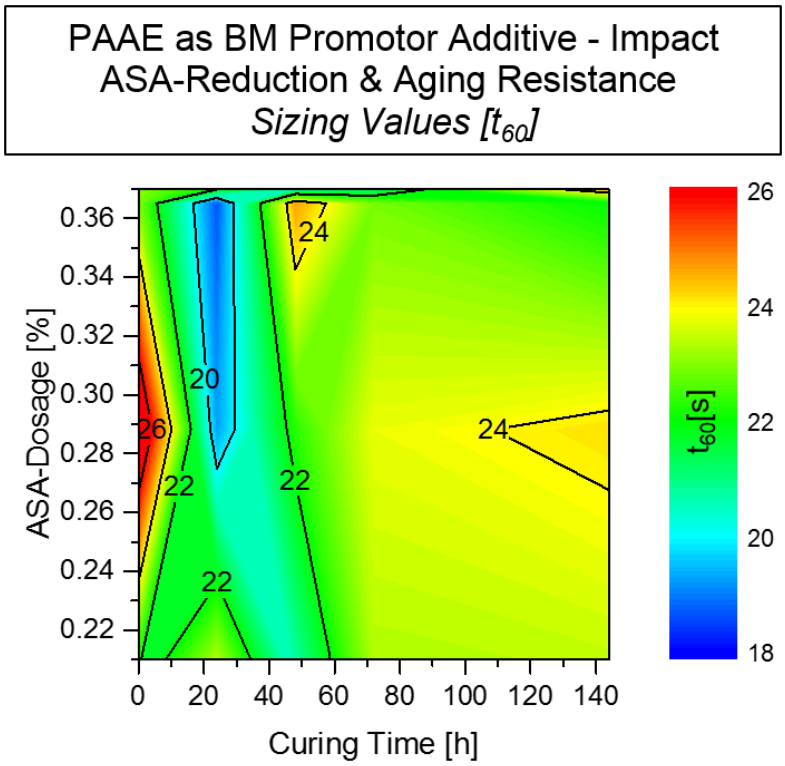

Figure 3.4-8: Impact of PAAE as Promotor Additive on ASA Sizing Performance and Aging Resistance // BM / OCC System

This was an important measure to evaluate the industrial applicability of the optimization approaches, as not only the post-production sizing values are of interest, but also the post-storage sizing values, which are of highest importance to the customers. The trial results are displayed as contour plot, while the x-axis indicates the days of accelerated aging and the y-axis the ASA dosage. This axis is inverted, in order to better visualize the trial progress. The color shading of the contour plot indicates the sizing performance (t_{60}). Within the following chart, the trial starting point is on the bottom left corner, while the progress toward lower sizing agent dosages indicates the trial progress. The trial values were gathered during normal production, while the PAAE dosage was set to 20%.

The trial results show, that it is possible to cut the ASA dosage by ~ 50%, still being able to guarantee constant sizing values. Following the progress of ASA reduction at t_0, it becomes visible that the sizing performance even increases at about 25% reduction. This indicates that the optimized system was already ranging in the section of overdosage. By the sizing agent reduction the saturation section was

passed, by ending up at the top of the linear section (Figure 3.4-1). The aging analysis showed that the sizing agent reduction does not have a negative impact on the aging performance. On the contrary, it smoothens the aging behavior, by equalizing the negative and positive peaks, localized at 24 h and 48 h aging time.

The overall results of the developed and implemented optimization approach show that it is possible to significantly promote the sizing performance of ASA by the method of emulsion optimization with PAAE as promotor additive. The results have further shown that along with the sizing performance improvement, also physical sheet properties, such as porosity or strength values are promoted, which significantly adds value to the produced grades. The final evaluation has shown, that sizing agent reductions of up to 50% are applicable on an industrial-scale, while no drawbacks in sizing performance, or aging resistance have to be experienced.

3.4.2.4 Correlation between Sizing Performance Optimization and Agglomeration Behavior on the Example of PAAE

A question which arises from the above-mentioned results of emulsion optimization, is, if the optimized sizing performance does stand in any correlation to the agglomeration behavior. As mentioned during the introduction to sizing performance optimization (Chapter 3.4.2), this approach was designed with the initial goal to ensure a more homogeneous ASA distribution and anchoring on the surface of the sheets' fiber structure. If this theory is applicable for the observed performance increase by PAAE dosage, the total agglomeration area has to go down correspondingly.

In order to verify the impact of PAAE on the agglomeration behavior, the following trial for correlation determination was conducted. Within this trial, the total agglomeration area and the sizing performance were analyzed within a sample set, which was produced by varying four significant agglomeration- and sizing-performance impacting factors. These were the ASA dosage (0.3% and 0.6%), the PCC dosage (0% and 25%), the PAM dosage (0% and 0.03%) and as final factor the PAAE dosage within the protection colloid (0% and 30%). The results are presented in a combined, Grouped-Box-Whisker plot (Figure 3.4-9), where the

agglomeration behavior (Aggl_A) is displayed in the top section and the sizing behavior (t_{60}) in the bottom section.

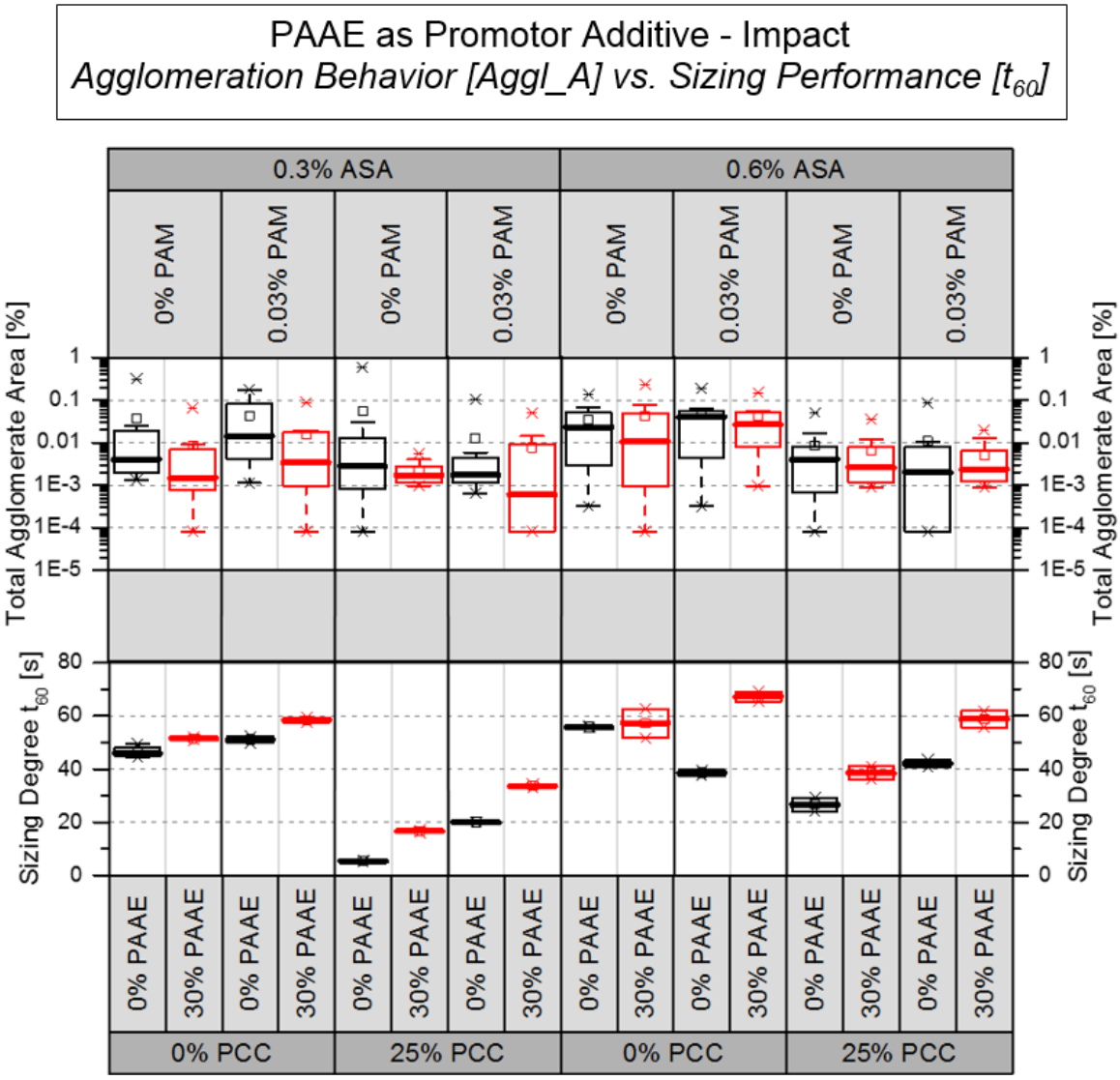

Figure 3.4-9: Impact of PAAE as Promotor Additive on ASA Sizing Performance and Agglomeration Behavior / Comparative Study

The Box-Whiskers are grouped by the hierarchy ASA dosage, PCC dosage, PAM dosage and PAAE dosage, resulting in corresponding values without and with PAAE next to each other. The Box-Whiskers without PAAE are marked in black, while the ones with are marked in red.

The results of this trial show that throughout all settings, a dosage of PAAE leads to a reduction of the total agglomeration area, while the sizing performance increases. This fact enforces the theory, that the dosage of PAAE as promotor additive within the protection colloid is capable of improving the spreading and distribution behavior of ASA on the fiber and filler surfaces. From a theoretical point

of view, this PAAE-induced increased surface coverage leads to a higher degree of ASA distribution, an optimized molecular orientation, and thus to a more homogeneous surface energy reduction, resulting in increasing sizing values.

3.5 Holistic Approach to Sizing Performance Explanation

Based on the results of all conducted work packages within this thesis, it is concluded that the mechanism behind ASA's sizing performance development is based on a homogeneous ASA distribution on the substrate surface in combination with a mordant-induced orientation and not on the esterification reaction with cellulose. The novel physico-chemical model for ASA's sizing mechanism is described in Figure 3.5-1. This model consists of four major steps.

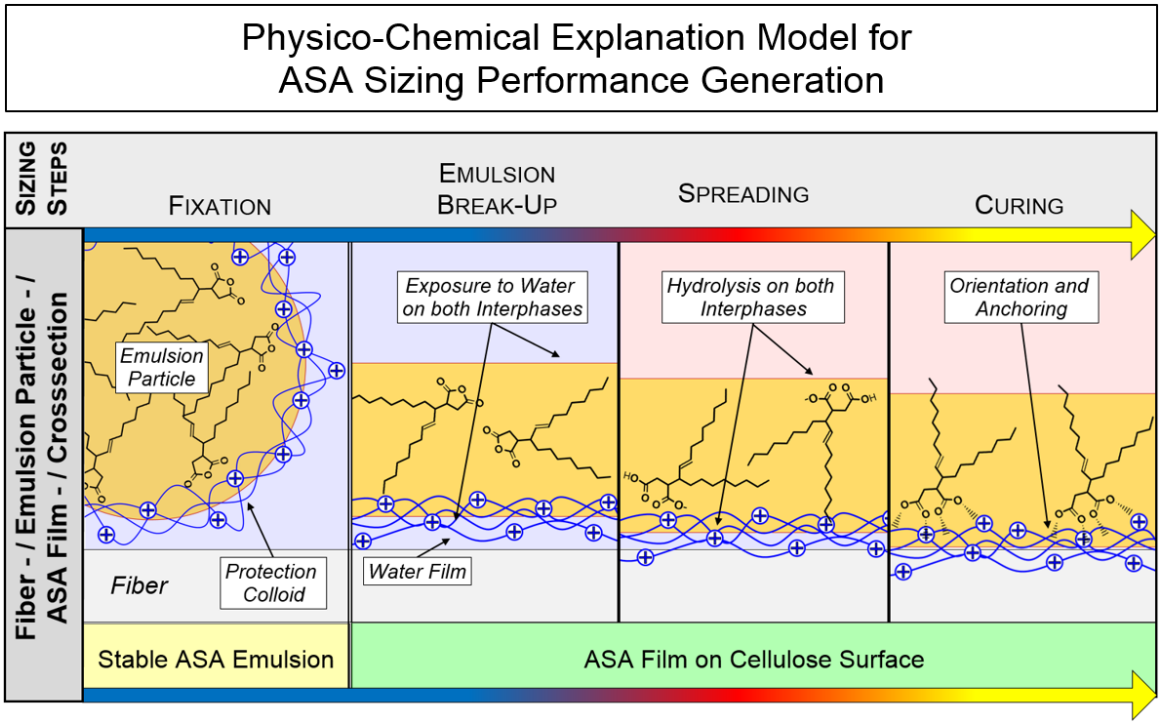

Figure 3.5-1: Physico-Chemical Explanation Model for ASA Sizing Performance Generation

The first step is a successful fixation of the ASA-emulsion droplets on the fiber or filler surfaces, either by self-retention mechanisms or by the support of retention aids or fixatives (Chapter 2.3.1.4). It is of highest importance within this step that the degree of hydrolysis is as low as possible. To fulfill this requirement, the emulsion needs to be properly stabilized by a protection colloid suiting the needs of the system's boundary conditions (Chapter 2.3.1.3.1), and by an optimal dosing procedure (Chapter 2.3.1.3.2). This is required, in order to enable an optimized subsequent spreading behavior.

The emulsion breaks open during the second step, exposing un-hydrolyzed ASA to the interphases on the cellulose side and on the suspension side, causing immediate hydrolysis on the interphases.

During the third step, ASA spreads over the fiber or filler surfaces, while the unreacted ASA share is the driving force for spreading, as its viscosity is significantly lower than the one of hydrolyzed ASA. The hydrolysis on both interphases is proceeding during the spreading step, because the ASA film is still separated from the cellulose by a water layer and the surrounding air is of high relative humidity (drying section). The final surface coverage and thus the possible degree of hydrophobization depends on the energy induced during the drying step, while higher energy inputs lead to enhanced spreading performance. As the spreading process is based on physical migration processes, it needs to be mentioned that the sizing agent requires time to travel and that a minimum of time is required in any case, which cannot be compensated by high temperatures.

Already during spreading, but mostly during curing, the fourth step, at the last dryer cans or on reel, where the moisture content is considerably low, the ASA molecules begin to anchor. This process is promoted either by the cationic charge of the protection colloid, by retention aids, by fixatives or by promotor additives in the protection colloid. Anchoring of ASA molecules can only happen at very high dryness levels. This is based on the three-phase system at low dryness levels, during which the solid phase of cellulose is separated from the liquid ASA phase by a stable water layer. Only if this layer’s thickness decreases to a required minimum in the range of few molecular layers, the ASA molecules are able to approach the mordants’ charge centers (protection colloid, retention aid, fixatives, promotor additives) and anchor via them as bridging molecules on the cellulose. This anchoring process induces the required molecular orientation which leads to the surface energy reduction and thus to the hydrophobizing performance. This is also supposed to be the mechanism of action on whose basis the protection colloid promotor additives work.

Even though the evidence gathered for the foundation of the described approach does not respect the formation of ester bonds between cellulose and ASA, the reactive structure of ASA is considered as key to successful sizing performance generation. Only a high share of pure, unreacted ASA in the emulsion particles

before the break up can provide the required spreading abilities during the drying procedure. A high degree of hydrolysis does not only cause emulsion instability and agglomeration in the aqueous phase prior to fixation, but also an increasing viscosity of the ASA within the emulsion particles. This leads to a reduced spreading performance, based, on the one hand, on the viscosity of the ASA/hydrolysate mixture and, on the other hand, on enhanced chances for coagulations with cationic charges prior to spreading, as the ASA hydrolysates carry a strong anionic charge.

4 Experimental Approach

The following Chapter will describe and characterize all implemented methods, materials, measurement approaches and chemicals, which were utilized during the conduction of the presented work.

4.1 Characterization of Methods, Measurements and Chemicals used for the Optical Localization-Analysis of ASA

4.1.1 Characterization of used Chemicals

4.1.1.1 Preparation of Dyed-ASA Solutions

Dyed-ASA solutions were prepared by mixing pure ASA with the specific dye at 70 °C. After mixing, the solutions were stirred at 70 °C for 10 minutes under exclusion of air (petri film cover). This procedure was done with a heatable, temperature controlled magnetic stirrer. The ready-made solutions were finally stored in light- and airtight containers upon use.

4.1.1.2 Thin Layer Chromatography

Thin Layer Chromatography (TLC) was conducted on silica-gel covered glass plates as stationary phase (adsorbent) and a 1/1 mixture of toluene and ethyl acetate as mobile phase (eluent). Before application on the stationary phase, the samples (solutes) were diluted with acetone in a share of 1/10. After dilution, the solutes were applied by 5 µl capillaries (~ 0.5 µl sample) onto the stationary phase. The starting position was set to 30 mm and the individual clearance of the samples to 20 mm. The separation process was aborted after the mobile phase reached 90% of the maximum possible travelling distance. Result interpretation was done under day and UV light by evaluating and marking the individual travelling distances of each sample's component and by calculating the respective R_f values.

4.1.1.3 Fourier Transformed Infrared Spectroscopy

Fourier Transformed Infrared Spectroscopy (FTIR) was conducted with a "Nicolet 5700" spectrometer by the company Thermo Electron Cooperation. The samples were measured via single reflectance ATR (Type: Quest Single

Reflectance ATR, high throughput diamond pug by Specac Ltd.). The measurement details are displayed in Table 4.1-1:

Table 4.1-1: FT-IR Settings

Laser	633 nm / IR
Beam Splitter	Mid-IR / KBr
Wave Numbers	4000 cm^{-1} to 400 cm^{-1}
Number of Background Scans	32
Number of Sample Scans	32
Resolution	2 cm^{-1}
Amplification	8.0
Mirror Speed	0.6329
Aperture	100.00

4.1.1.4 Emulsification of ASA

ASA emulsions were prepared by the following procedure (Table 4.1-2), if not explicitly mentioned differently in the discussion of results section.

Table 4.1-2: Standard ASA Emulsion - Emulsification Steps

Step 1:	Dilution of 3 g (solid matter) emulsification starch with deionized water to 97 g.
Step 2:	Addition of 3 g ASA to the homogeneous starch solution and gentle agitation until ASA is submerged in starch.
Step 3:	Emulsification by blending at 22,000 rpm for 75 second

The gear used for the standard emulsification process is displayed in Table 4.1-3 and Figure 4.1-1. By the use of the displayed gear and the above-mentioned parameters, the process is standardized to an overall emulsion volume of 100 ml, a constant shear force induction (22,000 rpm / 75 s) and an ASA to starch ratio of 1/1. Prior to use, the emulsion was diluted with deionized water to a suspension of 1% ASA content. The emulsification procedure was repeated every five sheets, or after a maximum emulsion age of 20 minutes, in order to avoid undesired phenomena like hydrolysis or agglomeration.

Table 4.1-3: Standard Emulsification Gear

Laboratory Blender	Type “8010” by the company Waring Laboratory Sciences Low gear: 18,000 rpm (no load) High gear: 22,000 rpm (no load)
Blender Jar	Type “Mini Jar” by the company Oster. Volume: 8 oz / 237 ml
Rotor	Type “Ice Crusher Blade” by the company Oster

Figure 4.1-1: Standard Emulsification Gear, f.l.t.r. Laboratory Blender [252], Blender Jar [253], Rotor [254]

4.1.1.5 Paper Chromatography

Paper chromatography (PC) for emulsion component separation was conducted on 400 g/m² virgin fiber board stripes. These stripes were produced with the ideal stock system, described in Chapter 4.3.1.1, by the sheet forming procedure described in Chapter 4.2.2.3, except that the drying time had to be adjusted to 30 minutes. For the separation process, the board stripes with a size of 3 cm x 12 cm, were put 20 mm deep into a 0.2% dyed-ASA emulsion. The separation process was aborted after the liquid had reached ~ 90% of the board stripe height. Result interpretation was done based on the travelling distances of water (liquid boundary), starch (iodine test), dye (visual / red shade) and ASA (contact angle measurement) after contact drying (Chapter 4.2.2.5) for two revolutions at 120°.

4.1.1.6 Particle Size Measurement

Emulsion particle size measurement was carried out with a unit type „Mastersizer 2000“ by the company Malvern Instruments GmbH. The system had to be calibrated with deaerated (ultra sonic treatment for 10 s) distilled water prior to every measurement. For the measurement a few emulsion drops were added to 800 ml distilled water until a laser shading/extinction of 10% to 20% was reached. The following parameters (Table 4.1-4) were used for analysis:

Table 4.1-4: Particle Size Analysis Parameters

Refractive Index for ASA	1.52
Imaginary Share / Absorption	0.001
Refractive Index for Water	1.33
Analysis Method	Mie-Theory according to ISO 13320-1 [255]

4.1.2 Optical Analysis of ASA Agglomerates

4.1.2.1 Microscopy

Figure 4.1-2: Alicona Infinite Focus G3 [256]

Optical sample analysis was done with a confocal light microscope type “Infinite Focus G3” (Figure 4.1-2 [256]), by Alicona Imaging GmbH. The microscope specifications are displayed in Table 4.1-5. The image acquiring procedure followed the basic principle of a standard automated measurement script provided by Alicona, however, it was necessary to adjust the script settings to the requirements given *(The script is not listed in this thesis, however, it can be requested from MUAS)*.

Table 4.1-5: Infinite Focus G3 - Specifications [256]

General Specifications	
Measuring Principle:	non-contact, 3 dimensional, color focus sensor system
Measuring Result:	dense, true color surface model
Illumination:	co-Axial and dark field
Light Source:	IF-LightSourceLED
Nosepiece:	6 objectives nosepiece
XYZ-Stage:	motorized XYZ on suspension plate
PC-System	
Processor:	Intel®Core™2 /6700 @ 2.66 GHz
Memory:	3 GB
Graphics Board:	ATI Radeon X1950 Pro
Operating System:	Windows XP Professional, SP3
Interfaces:	Firewire with on board power supply, RS232

Optics							
Objectives		2.5x	5x	10x	20x	50x	100x
Lateral Resolution	µm	3.3	1.6	0.8	0.4	0.4	0.4
Vertical Resolution	µm	5-50	0.8-8.0	0.2-2.0	0.1-1.0	0.05-0.5	0.02-0.2
Max. Scan Height	mm	7-70	1.3-13	0.31-3.1	0.15-1.5	0.07-0.7	0.03-0.3
Working Distance	mm	8.8	23.5	17.3	13.0	10.1	3.5
Field of View X	µm	4100	2100	1000	500	200	100
Field of View Y	µm	3300	1600	800	400	150	100
Ext. field of View X	mm	8-80	4-41	2-20	1-10	0.4-4.0	0.2-2.0
Ext. field of View Y	mm	6.5-50.2	3.3-33.5	1.6-16.1	0.8-8.2	0.3-3.0	0.16-1.61
Sensor							
Resolution:		1.3 MPixel with 1280x1024 Pixel					
Pixel Size:		5.2 x 5.2 µm					
A/D Converter:		10 Bit					
Frame Rate:		18 fps / (Full-Frame):					
Interface:		Firewire					
Optical Interface:		C-Mount					
Specimen							
Max. Height of Object:		70 mm					
Max. Lateral Extension:		120 mm x 53 mm					
Max. Weight of Object:		0.5 kg, 5 kg if xyz-stage is not moved					
Sample Positioning:		manual or programmable stage					
Maximum Slope:		up to 90°					
Preparation:		none					
Material:		any solid material					
Software							
Type		Alicona Imaging GmbH / IFM 2.2					
Capturing:		image, sharp image, 3D model, best illumination					
Analysis:		profile (height, roughness,..), area analysis (fractal dimension,...), volume analysis					
Visualization:		single and stereo image, high resolution 3D visualization					

In order to get statistically appropriate data, the script settings were adjusted to capture 12 single images per sample. Defined by the metal sample mask, with six 35 mm x 35 mm windows, a maximum of six samples could be analyzed within one measurement set. Each sample, except stated differently, was placed in the mask with the wire side facing towards the objective. Each picture was taken with 100x optical magnification in random spots amongst the sample surface, resulting in images of ~ 104 µm x 83 µm. The 3D picture depth (scan height) was set to 250 µm, about 250% of the samples' caliper. The scan height was defined as the addition of 125 µm negative height and 125 µm positive height from the zero z-plane. By this feature, it was made sure that all the samples' z-planes were focused during image capturing. The scan height zero plane was defined by an automatic autofocus execution. This feature set the highest and lowest focusable z-planes after initial manual coarse focusing and defined the zero plane as halfway in-between both. The distance between every plane (vertical resolution) was adjusted to 300 nm, in order to achieve very dense data over the z-axis. The IF-LightSourceLED intensity was adjusted to 45° indicator bar angle at the manual light switch (~ 60% intensity), which is the value that shows the best results while using the 100x objective. Exposure was adjusted to 35 ms, the starting gamma value to 2.5 and the saturation to 1.0. These values gave best color and shape results during analyzing samples made of reference stock. In addition, the software was enabled to execute automatic exposure and automatic white balance, two commands needed for proper real color imaging and optimal contrasts. The acquired images were automatically saved as 3D-IFM-formats and as their resulting 2D-projections (*.tiff* files). The 3D formats did serve as validation, in order to make sure that all planes were in focus. The 2D.*tiff* files were subsequently analyzed by Adobe Photoshop. The settings used during automated imaging are additionally displayed in Table 4.1-6.

Table 4.1-6: Alicona IFM 2.2 - Automated Image Capturing Settings

Automation Script: ReLeiPa_1.1 / Part I	
Objective	100x (Table 4.1-5)
Number of Masks	1
Number of Samples per Mask	max. 6
Number of Images per Sample	default: 12 / optional

Automation Script: ReLeiPa_1.1 / Part II	
Image Field	default: single picture / optional: 2x2, 3x3
Vertical Resolution	300 nm
Scan Height	250 µm
Starting Exposure	35 ms
Starting Gamma	2.5
Autofocus	enable
Automatic Exposure	enable
Saturation Value	default: 1.0 / optional: 0.5 – 1.0
Automatic White Balance	enable
Measurement Time	~ 2.7 min/image // ~ 3.25 h/mask

The settings mentioned above are defined for the analysis of sheets made of reference stock (w or w/o filler). Notably, deviations in the stock system might require setting changes.

4.1.2.2 Automated Analysis

The automated agglomerate analysis procedure was based on two major steps. The first step was the processing of the generated *.tiff* images with Adobe Photoshop over several filter sequences in order to define the agglomerates. The second step was a further processing in Adobe Illustrator, where the photoshopped pictures were vectorized for proper agglomerate counting and individual size determination. The process in both software tools followed individual scripts which were elaborated at MUAS (*The scripts are not listed in this thesis; however, they can be requested from MUAS)*.

4.1.2.2.1 *Adobe Photoshop*

Adobe Photoshop (used versions: CS3 & CS6) was utilized in order to separate the captured agglomerates from the fiber and filler background by their respective color information (magenta). By conducting six script-embedded actions, consisting of 136 individual steps, the agglomerates were traced, separated and displayed isolated from the initial background. The action list is displayed in Table 4.1-7.

Table 4.1-7: Adobe Photoshop - Action List

No.	Action	Content
01	Filter Shadows	*Lighting up dark grey areas to avoid confounding with red RGB channel.*
02	Replace Color 1	*Change color information of grey areas to white*
	Convert RGB to CMYK	*Conversion from RGB to CMYK to add black channel "K".*
	Adjust Magenta Curves	*Enhancing magenta color information for better contrast generation.*
03	Replace Color 2	*Change color information of grey and light colored areas to white.*
04	Mix Channels to Black	*Converting all residual color information to black "K".*
05	Increase Contrast of Black	*Removing light grey areas and enhancing the information of dark black ones (agglomerates). Noise reduction.*
06	Crop Image	*Cropping additional picture canvas attached by Alicona Software IFM 2.2. (Information on date, metric size and pixels, as well as black frame)*
	Counting of Black Pixels	*Optional: Giving information on the number of black pixels, respectively the agglomerate pixels.*

4.1.2.2.2 *Adobe Illustrator*

Adobe Illustrator (version CS3 and CS6) was implemented for counting the number of agglomerates and calculating their individual and overall size. This was done by vectorizing the black and white information provided by the photoshopped images via the command "Trace". The elaborated settings for this command are displayed in Table 4.1-8.

Table 4.1-8: Adobe Illustrator - Trace Command Setting

Mode	Black and White
Threshold	30
Trace Settings	Fill, Path
Fitting	2 px
Minimum Area	10 px
Corner Angle	20°
Blur	0 px
View	Raster, No Image, Vector Tracing Result

The results of this action were the total number of agglomerates per image, the total agglomeration area in pixel and µm² per image and, if required, the individual agglomerate size in µm². The required values for analyses “Total Agglomeration Area [%]”, “Number of Agglomerates [n/mm²]” and “Average Agglomerate Size [µm²]” were calculated according to the following formulas (Equation 4.1-1, Equation 4.1-2 and Equation 4.1-3):

− Total Agglomeration Area

$$\mathrm{Aggl\_A} = \frac{P_{Agglomerates}}{P_{Image}^{x} * P_{Image}^{y}} * 100\%$$

Equation 4.1-1: Total Agglomeration Area - Calculation

$$Aggl\_A = Total\ Agglomeration\ Area\ [\%]$$

$$P_{Agglomerates} = Number\ of\ Agglomerate\ Pixels$$

$$P_{Image}^{x} = Number\ of\ Image\ x\text{-}Axis\ Pixels$$

$$P_{Image}^{y} = Number\ of\ Image\ y\text{-}Axis\ Pixels$$

− Number of Agglomerates

$$\mathrm{Aggl\_N} = \frac{n_{Agglomerates} * 10^{6}}{x_{Image} * y_{Image}}$$

Equation 4.1-2: Number of Agglomerates - Calculation

$$N = Number\ of\ Agglomerates\ \left[\frac{n}{mm^2}\right]$$

$$x_{Image} = Image\ x\text{-}Axis\ Dimension\ [\mu m]$$

$$y_{Image} = Image\ y\text{-}Axis\ Dimension\ [\mu m]$$

− Average Agglomerate Size

$$\mathrm{Aggl\_AV} = \frac{A * Z}{N}$$

Equation 4.1-3: Average Agglomerate Size - Calculation

$$AV = Average\ Agglomerate\ Size\ [\mu m^2]$$

$$A = Total\ Agglomeration\ Area\ [\%]$$

$$N = Number\ of\ Agglomerates\ \left[\frac{n}{mm^2}\right]$$

$$Z = Conversion\ Factor\ \left[10^{6}\ \frac{\mu m^2}{mm^2}\right]$$

4.1.2.3 Confocal Laser Scanning Fluorescent Microscopy

Confocal Laser Scanning Fluorescent Microscopy was done with a prototype unit by Toptica Photonics AG at MUAS. The microscope specifications are displayed in Table 4.1-9. The fluorescent dye used was Nile Red, with a concentration of 0.1% in ASA (F-ASA).

Table 4.1-9: Confocal Laser Scanning Fluorescent Microscopy - Settings

Type	Mode-Locked Ytterbium Fiber Laser
Average Wavelength	λ_c: 1030 nm
Puls Duration	τ: 62 fs
Repetition Rate	80 MHz
Average Output	300 mW
Channel A	607 +/- 35 nm
Channel B	525 +/- 20 nm

4.2 Characterization of Used Standard Methods and Measurements

4.2.1 **Stock and Paper Properties**

Sampling and sample handling was conducted in accordance to:

DIN EN ISO 186	Paper, Board and Pulps - Sampling to determine average Quality [257]

All paper & board properties were measured after the minimal required storage time under constant atmosphere for conditioning, as required by the following regulation:

DIN EN 20187	Paper, Board and Pulps - Standard Atmosphere for Conditioning and Testing and Procedure for Monitoring the Atmosphere and Conditioning of Samples [258]

4.2.1.1 Stock pH, Conductivity and Temperature Measurement

Stock pH, conductivity and temperature were measured by a multimeter type “HQ40D” by the company Hach Lange GmbH. This device enables the simultaneous measurement with two electrodes, giving values for temperature, pH and conductivity. Every measurement was conducted after proper stock stirring, in

order to avoid deviations within the sample taken. Each measurement took about 15 seconds to value stabilization. An average of at least two results was used for interpretation.

4.2.1.2 Dry Content / Consistency Measurement

Dry content and consistency were measured according to two regulations. Materials such as sheets, moist or dry stock, and additives in solid form where measured by the following regulation:

DIN EN ISO 638	Paper, Board and Pulps - Determination of Dry Matter Content – Oven-Drying Method [259]

Dry content calculation was done by Equation 4.2-1:

$$w_{dm} = \frac{m_1}{m_0} * 100\%$$

Equation 4.2-1: Dry Content - Calculation [259]

w_{dm}= *Dry Content* [%]

m_0 = *Mass of Dry Sample* [g]

m_1 = *Mass of Wet Sample* [g]

Fibers suspensions of any kind were analyzed by:

DIN EN ISO 4119	Pulps - Determination of Stock Concentration [260]

Concentration calculation was done by Equation 4.2-2:

$$\mathrm{X} = \frac{m_5 - m_4}{m_1} * 100\%$$

Equation 4.2-2: Stock Concentration - Calculation [260]

X= *Stock Concentration* [%]

m_1 = *Mass of Wet Sample* [g]

m_4 = *Dry Mass of Filter Paper* [g]

m_5 = *Dry Mass of Stock plus Filter Paper* [g]

4.2.1.3 Drainability (Schopper-Riegler) Measurement

Stock dewatering resistance was measured according to the following regulation:

DIN EN ISO 5267-1	Pulps - Determination of Drainability – Part 1: Schopper-Riegler Method [261]

4.2.1.4 Base Weight Measurement

Base weight of paper & board samples was measured according to:

DIN 6739-500	Paper & Board - Part 500: Determination of Grammage [262]

The calculation of the base weight was carried out in accordance to Equation 4.2-3:

$$g = \frac{m}{A} * 10^6$$

Equation 4.2-3: Base Weight - Calculation [262]

$$g = Base\ Weight \left[\frac{g}{m^2}\right]$$

$$m = Sample\ Mass\ [g]$$

$$A = Sample\ Area\ [mm^2]$$

4.2.1.5 Ultrasonic Penetration Measurement

The sizing performance of paper & board samples was mainly examined with the ultrasonic penetration device “Dynamic Penetration Analyzer PDA-C 02 MST Module-Standard” (Figure 4.2-1 [263]) by the company emtec Electronic GmbH.

Figure 4.2-1: emtec Electronic GmbH, PDA.C 02 MST Module-Standard [263]

Every sample was measured twice from one side. Each specimen with a size of 5 cm x 7 cm was analyzed with a sound frequency of 2 MHz on a measurement area of 35 mm in diameter. For the measurement, the paper samples needed to be taped onto a Teflon® covered plate. This plate was then fixed in the plate holder. The plate holder shoots the sample into the measurement box, where the ultrasonic sound waves are forced through the sample. The first results are generated with a frequency of one measurement per ms, starting 8 ms after the

first water contact. The measurement duration was adjusted according to the sample's sizing degree and always chosen at least 10 seconds longer than the duration until a 40% intensity loss is reached. The sizing value calculation was done by software and shown either graphically or as crisp numbers. For result interpretation, two significant time values, measured in seconds, were utilized. First, the time after the maximum sound intensity was reached (t_{max}), as a measure for the sample's surface hydrophobicity, and second the time until passing the 40% intensity loss limit (t_{60}), as a measure for the sample's substrate hydrophobicity.

4.2.1.6 Contact Angle Measurement

Contact angle measurements were carried out in accordance to:

Tappi TM 558 om-97	Surface wettability and absorbency of sheet materials using an automated contact angle tester [86]

Figure 4.2-2: Fibro Systems AB, PGX + / Model 68-76 Pocket Goniometer [264]

The used contact angle measurement device was a pocket goniometer type "PGX + / Model 68-76" (Figure 4.2-2 [264]) by the company Fibro Systems AB [264]. This hand held device is working fully automatized based on video analysis. The working fluid was distilled water, droplet size was set to 4 µl and the delay time until the first measurement after drop off was set to 950 ms. The measurement time for dynamic contact angle measurement was 12 seconds, while the maximum value captured (CA_{max}) was used for result interpretation. Every sample was measured on five spots, distributed randomly over the whole specimen area.

4.2.1.1 Cobb Measurement

Paper & board sample Cobb-measurement was conducted according to the following regulation. The water contact time was chosen to be 60 s.

DIN EN ISO 535	Paper & Board – Determination of Water Absorptiveness – Cobb Method [80]

Cobb value calculation was done by Equation 4.2-4:

$$A = (m_2 - m_1) * F$$

Equation 4.2-4: Cobb - Calculation [80]

$$A = Cobb\ Value \left[\frac{\mathrm{g}}{\mathrm{m}^2}\right]$$

$$m_1 = Dry\ Sample\ Mass\ [\mathrm{g}]$$

$$m_2 = Wet\ Sample\ Mass\ [\mathrm{g}]$$

4.2.1.2 Air Permeability Measurements

The samples for air permeability were measured in accordance to the following regulation:

ISO 5636-5	Testing of Paper & Board – Determination of Air Permeability – Part 5: Medium Rate of Air Permeability according to Gurley [265]

$$Gurley = time\ for\ 100\ ml\ air\ permeation\ [s]$$

4.2.1.3 Tensile Strength Measurements

Physical strength properties were measured in accordance to:

DIN ISO 1924-3	Paper & Board – Determination of tensile Properties – Part 3: Constant Rate of Elongation Method (100 mm/min) [266]

The respective braking length was calculated according to Equation 4.2-5:

$$L_B = \frac{\mathrm{F}_T}{\mathrm{BW} * \mathrm{g} * \delta s}$$

Equation 4.2-5: Breaking Length – Calculation

$$L_B = Breaking\ Length [\mathrm{m}]$$

$$F_T = Breaking\ Force\ [\mathrm{N}]$$

$$BW = Base\ Weight \left[\frac{\mathrm{g}}{\mathrm{m}^2}\right]$$

$$g = Average\ Sheet\ Caliper\ [\mathrm{m}]$$

$$\delta_s = Standard\ Gravity \left[\frac{\mathrm{N}}{\mathrm{kg}}\right]$$

4.2.2 **Preparation of Sample Sheets**

4.2.2.1 Stock Preparation

Stock preparation was carried out in accordance to the following regulations for

− disintegration:

DIN EN ISO 5263-1	Pulps – Laboratory wet Disintegration – Part:1 Disintegration of Chemical Pulps [267]

− and dispensing:

Zellcheming Merkblatt V/6/61	Zellcheming Merkblatt V/6/61 – Einheitsmethode für die Festigkeitsprüfung von Zellstoffen – F. Egalisierung des gemahlenen Stoffes und Mengenverteilung [268]

The target consistency in the dispenser was ~ 0.5%, in order to provide proper mixing in combination with an acceptable dispenser yield of 20 sheets. The calculation of the required stock volume was done by Equation 4.2-6:

$$V_{Stock} = \frac{\mathrm{m}_{Sheet}}{\mathrm{X}}$$

Equation 4.2-6: Stock Volume - Calculation

$V_{Stock} = Stock\ Volume$ [ml]

$m_{Sheet} = Sheet\ Mass\ (OD)$ [g]

$X = Stock\ Concentration$ [%]

For RDA sheet forming, the stock was subsequently diluted to 1000 +/- 5 ml.

4.2.2.2 Laboratory Refining (Valley Beater)

The laboratory valley beating procedure, for the sample sets which were produced for the determination of the SR-value impact, was carried out in accordance to:

Tappi ***TM 200 sp-01***	Laboratory Beating of Pulp (Valley Beater Method) [269]

4.2.2.3 RDA Sheet Forming

The laboratory sheet forming procedure was conducted in correlation to:

DIN EN ISO 5269-2	Pulps – Preparation of Laboratory sheets for physical testing – Part 2: Rapid-Köthen Method [270]

Figure 4.2-3: RDA Sheet Former [271]

Deviating from the above-mentioned standard, instead of a RK-sheet forming device, a dynamic sheet forming unit, type “Retention Drainage Analyzer / RDA” (Figure 4.2-3 [271]), distributed by the company Frank PTI GmbH, was used. The RDA sheet former produces hand sheets with a diameter of 19.5 cm on standard RK-wires with only 0.3 – 1.0 l of stock volume under dynamic conditions. These conditions include shear rate, shear duration, sheet forming vacuum and vacuum application time. The RDA layout including auxiliaries is displayed in Figure 4.2-4 [271].The standard settings used, if not explicitly mentioned during the discussion of results, are listed in Table 4.2-1. The residual steps of the sheet forming procedure, including couching and drying, were conducted in accordance to the above-mentioned standard.

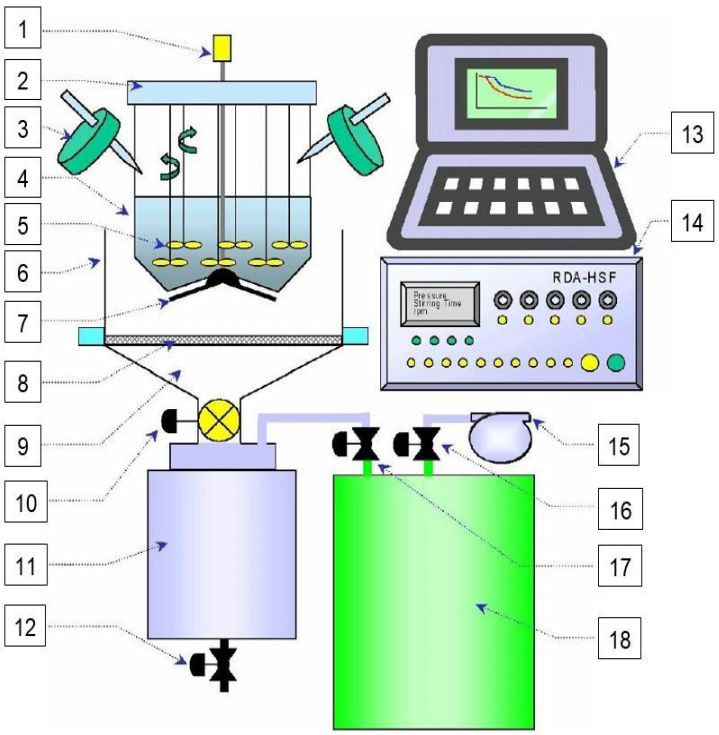

1: Stopper handle
2: Drive part of stirrer
3: Automatic dosing unit
4: Sample vessel (stock tank)
5: Stirrer
6: Forming tank
7: Valve of sample vessel
8: Wire mesh
9: Supplement water tank
10: Dewatering valve
11: White water tank
12: White water valve
13: Computer
14: Control box
15: Vacuum pump
16: 2nd Vacuum valve
17: 1st Vacuum valve
18: Vacuum tank

Figure 4.2-4: RDA Layout including Auxiliaries [271]

Table 4.2-1: RDA-Sheet Forming - Details

Suspension Volume	1000 ml +/- 5 ml
Suspension Consistency	0.295%
Dry Suspension Matter	2.95 g
Target Base Weight	100 g/m² (od)
Pre Stirring Rate / Time	500 rpm / 10 s
Main Stirring Rate (per Additive) / Time	300 rpm / 30 s
Sheet Forming Delay after Stock Release	1 s
Sheet Forming Vacuum (Main & Sub)	250 mmHg
Vacuum Application Time	10 s

4.2.2.4 Additive Dosing

All additives except fillers were dosed in between the RDA stirring steps directly into the vortex of one of the six stirrer units. All fillers were dosed during disintegration in the desired shares. The standard dosing order and dwell times for RDA sheet forming can be seen in Figure 4.2-5. Trial deviations are mentioned specifically in the discussion of results section.

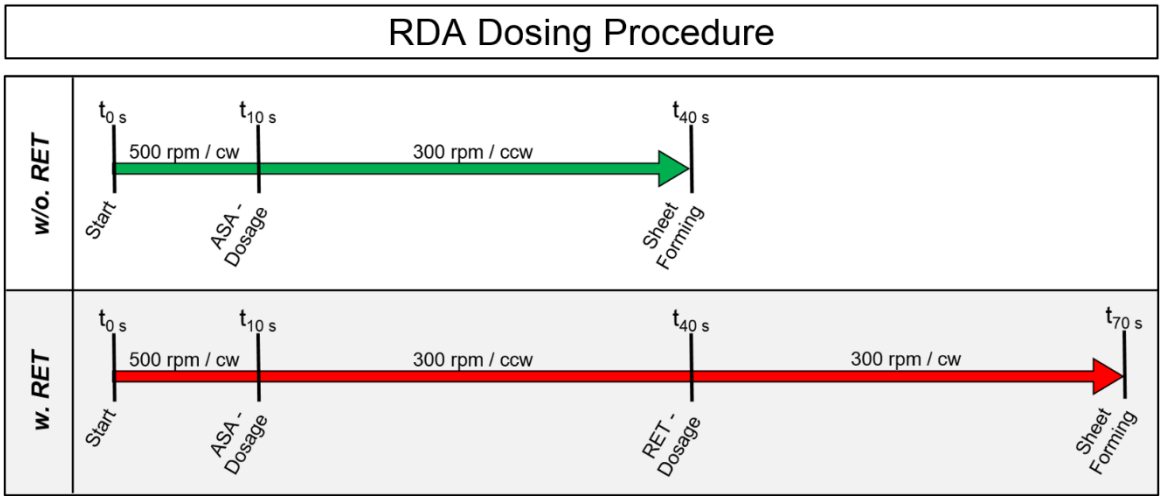

Figure 4.2-5: RDA Dosing Procedure

The standard ASA dosage steps, if not stated differently, for the conduction of this thesis are displayed in Table 4.2-2.

Table 4.2-2: Standard ASA-Dosage Steps

ASA	0%	0.05%	0.1%	0.2%	0.3%	0.4%	0.6%	0.8%

The dosing amount for additives was calculated by Equation 4.2-7:

$$m_{Additive} = \frac{\mathrm{m}_{Sheet} * D_{Additive}}{c_{Additive}}$$

Equation 4.2-7: Additive Dosing Amount - Calculation

$m_{Additive} = Additive\ Dosing\ Amount$ [g]

$m_{Sheet} = Sheet\ Mass\ (OD)$ [g]

$D_{Additive} = Additive\ Dosage$ [%]

$c_{Additive} = Additive\ Concentration$ [%]

4.2.2.5 Contact Curing

Contact curing trials were conducted with a photo contact dryer by the company Gerster. The device was operated in matt-mode with a temperature of 120 °C (if not stated differently) and a speed of 5 min per revolution. The samples were cured for one revolution, facing the cylinder surface with the wire side.

4.2.2.6 Hot Air Curing

Hot air curing was carried out in a standard dryer cabinet, type “UL 40” by the company Memmert GmbH & Co. KG for 15 minutes in accordance to the conditions mentioned in:

DIN ISO 5630	Paper & Board - Accelerated Aging; Part 1: Dry Heat Treatment at 105 °C; Identical with ISO 5630-1: 1991 [272]

4.2.2.7 Sample Aging

Sample aging was done in a climatization cabinet type “VC 0018” by the company Vötsch Industrietechnik GmbH in correlation to the conditions mentioned in the following norm. The aging duration for the conducted trials is mentioned in the discussion of results section.

DIN ISO 5630	Paper & Board - Accelerated Aging; Part 3: Dry Heat Moist Heat Treatment at 80 °C and 65% relative Humidity; Identical with ISO 5630-3 : 1996 [273]

4.2.2.8 Preparation of Hydrolyzed ASA

Hydrolyzed ASA was prepared by boiling 100 g of ASA in 900 ml of highly purified water (HPLC-quality) for an overall time of 7 h. In order to separate the excess of water from the hydrolyzed ASA, the mixture was subsequently treated in a rotation evaporation step until mass constancy was reached. The evaporation was conducted with a unit, type “VV2011”, by the company Heidolph Instruments GmbH & Co. KG, at a pressure of 200 mbar and a water bath temperature of 90 °C. The hydrolyzed ASA was finally transferred into air- and light tight vessels and analyzed by FTIR spectroscopy to verify total hydrolysis.

4.2.2.9 Trial Paper Machine

Continuous lab scale trials were conducted on the trial paper machine (TPM) VPM5 (Kämmerer), operated by the institution IVP. e.V. (Figure 4.2-6.).

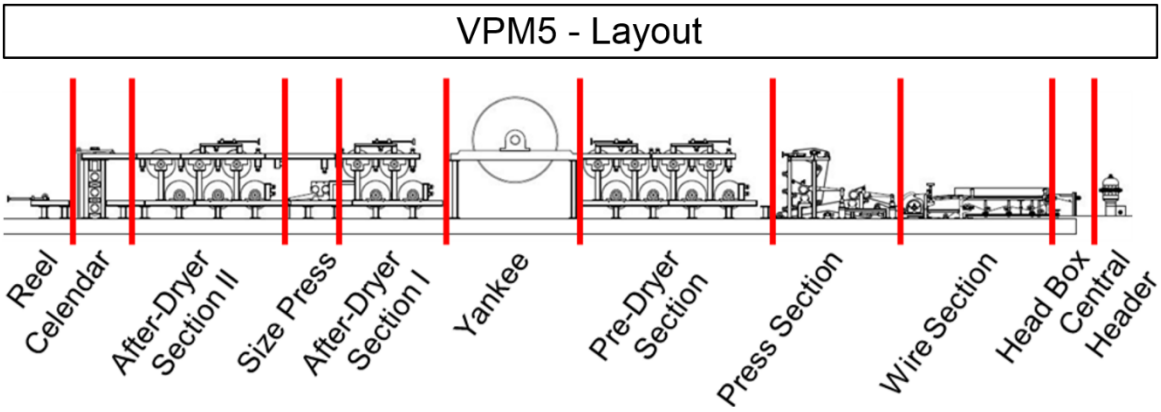

Figure 4.2-6: VPM5©- Layout (© IVP e.V.)

VPM5 is based at MUAS and equipped with all necessary auxiliaries for the simulation of industrial-scale paper/board production, including full automation by a Siemens Simatic PCS7 system.

The approach flow system layout is displayed in Figure 4.2-7. Possible dosing positions are marked with green arrows and the numbers 1-4. For standard trials, the dosing position ② was used for ASA and the position ③ for retention aid. Stock consistency in the storage chest was adjusted to ~ 1.5%. In the white water chest, the stock is diluted to a consistency < 0.1%. An ultraturax is installed prior to the head box to simulate the shear forces of a head box screen. Dilution water is fed into the direct head box flow, in order to adjust formation, CD-profiles and the water

line. Further VPM and production details, as utilized during the trials, are displayed in Table 4.2-3.

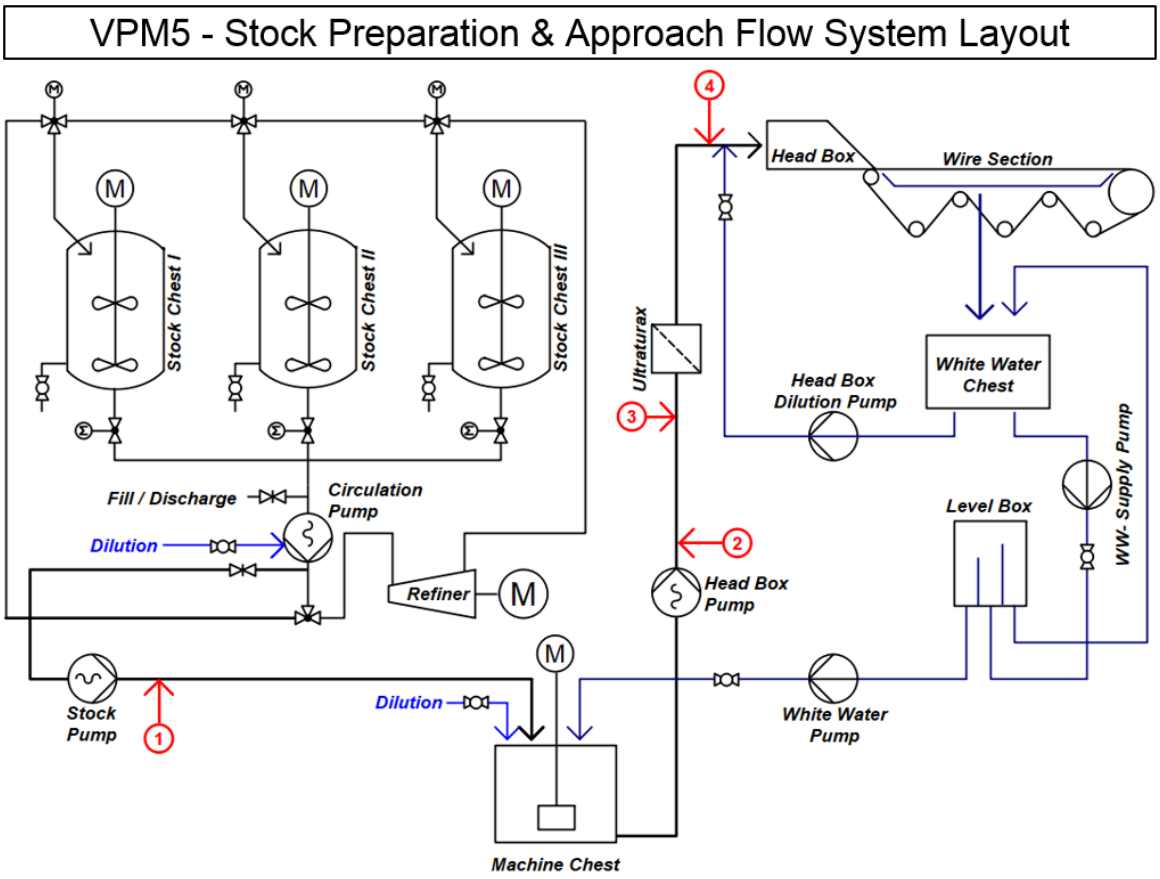

Figure 4.2-7: VPM5 – Stock Preparation & Approach Flow System Layout (created with RI-CAD™)

Table 4.2-3: TPM and Production Details

Producer	Kämmerer / 1961
Production Speed	1.5 m/min
Production Width	24 cm
Base Weight	100 g/m²
Head box	Open / Central Distributer
Wire Section	Fourdrinier / Register Rolls, 3 Suction Bars, Couch Roll
Press Section	2 Press Nips // 1st Bottom-Felted, 4 bar / 2nd Top-Felted, 3 bar
Pre-Dryer Section	8 Cylinders, Electrically Heated Profile [C°]: 60, 60, 80, 80, 90, 90, 100, 100

Yankee	Not in Use / Bypassed
After-Dryer Section I	Not Heated / Pull Group
Size Press	Not in Use / Bypassed
After-Dryer Section II	Not in Use / Bypassed
Calendar	Not Loaded / Pull Group

4.2.2.10 Industrial-Scale Board Machine

For industrial-scale production trials, the board machine BM6 from the company Moritz J. Weig GmbH & Co. KG in Mayen, Germany was used. This three-layer fourdrinier based machine is the world's largest plaster-board-liner production unit. It has a machine width of 530 cm, a grammage operation window of 140 g/m² to 220 (240) g/m², a maximum operation speed of 965 m/min and a capacity of 340,000 t/a. The main grades produced are plaster-board-liner and test liner. The average composition of the produced plasterboard liner grades is displayed in Table 4.2-4.

Table 4.2-4: Composition Plaster Board Liner [274]

Composition of Plaster Board Liner		
15%	Topliner	Sorted light waste paper and cellulose
70%	Centre Ply	Selected waste paper
15%	Backliner	Selected waste paper

The thesis related important board parameters are displayed in Table 4.2-5.

Table 4.2-5: Plaster Board Liner Technical Specifications [275]

Plaster Board Liner Technical Specifications		
Cobb$_{60}$	Top Side	*20 – 30 [g/m²]*
	Gypsum Side	*20 – 50 [g/m²]*
Gurley		*< 100 [s]*

4.3 Characterization of used Materials

4.3.1 **Fibers**

4.3.1.1 Reference Stock System

The reference stock system used for standard sheet forming was composed of 80% Eucalyptus Kraft (EUKA, Aracruz) short fiber pulp and 20% Northern Bleach Softwood Kraft (NBSK, Rosenthal ECF) long fiber pulp. The stock mixture was diluted with deionized water for refining. The refining curve is displayed in Figure 4.3-1. Subsequently, the stock was dewatered with a spin dryer, which was equipped with a sheet forming wire on the walls in order to hold back the fines. To provide a stock mixture of highest purity, the stock was washed in the spin dryer with deionized water until the filtrate conductivity was below 1 µS. The final stock consistency after centrifuging was ~ 33%. The stock was fluffed with pressurized air and stored in airtight barrels. Due to the high degree of washing, no biocides were needed for conservation. The exact refining parameters are displayed in Table 4.3-1.

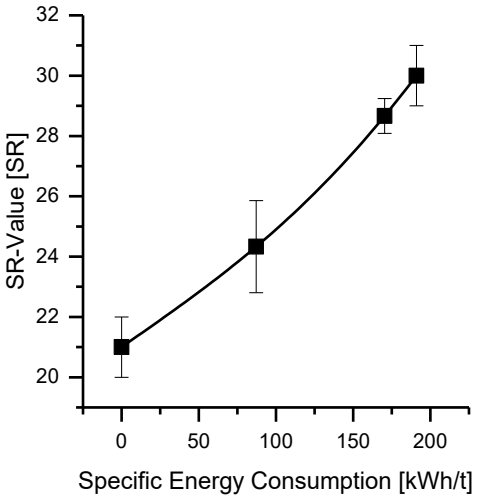

Figure 4.3-1: Reference Stock System / Refining Curve

Table 4.3-1: Reference Stock System / Refining Parameters

Refiner Type	"R1", by Escher Wyss
Fillings	Standard / 30°
Drive	15 kW /1475 rpm
P_{net}	3.73 kW
Cutting Edge Length (CEL)	207.09 km/s
Specific Edge Load (SEL)	0.018 J/m
Specific Energy Consumption (SEC)	191 kWh/t
Stock Consistency	1.5%
Start SR-Value	SR 21
End SR-Value	SR 30

For the calculation of the refining specific measures CEL, SEL and SEC the following formulas (Equation 4.3-1, Equation 4.3-2 and Equation 4.3-3) were used:

$$CEL = z_R * z_s * l * \frac{n}{60}$$

Equation 4.3-1: Cutting Edge Length - Calculation [276]

$$SEL = \frac{P_{net}}{CEL}$$

Equation 4.3-2: Specific Edge Load - Calculation [276]

$CEL = Cutting\ Edge\ Length \left[\frac{\mathrm{m}}{\mathrm{s}}\right]$

$z_R = Number\ of\ Rotor\ Bars$

$z_s = Number\ of\ Stator\ Bars$

$l = Effective\ Bar\ Length\ [\mathrm{m}]$

$n = Rotational\ Speed \left[\frac{\mathrm{r}}{\mathrm{min}}\right]$

$SEL = Specific\ Edge\ Load \left[\frac{\mathrm{J}}{\mathrm{m}}\right]$

$CEL = Cutting\ Edge\ Length \left[\frac{\mathrm{m}}{\mathrm{s}}\right]$

$P_{net} = Effective\ Refining\ Power\ [\mathrm{W}]$

$$SEC = \frac{P_{net}}{q_m * \frac{c_F}{100}} * \rho$$

Equation 4.3-3: Selective Energy Consumption - Calculation [276]

$SEC = Specific\ Energy\ Consumption \left[\frac{\mathrm{kWh}}{\mathrm{t}}\right]$

$P_{net} = Effective\ Refining\ Power\ [\mathrm{W}]$

$q_m = Pulp\ Flow\ through\ Refining\ Zone \left[\frac{\mathrm{m}^3}{\mathrm{h}}\right]$

$c_F = Stock\ Consistency\ [\%]$

$\rho = Stock\ Density \left[\frac{\mathrm{t}}{\mathrm{m}^3}\right]$

4.3.1.2 OCC Fibers

The old-corrugated-container board (OCC) system used was equal to the above-mentioned (Table 4.2-4) center ply system. OCC based laboratory sheets were produced from pre-dried pulp pellets, which were disintegrated in tab water. OCC stock and white water for trial paper machine runs were delivered in IBC containers. Prior to TPM trials, the stock was diluted to ~ 1% with white water.

4.3.1.3 DIP Fibers

The deinked pulp (DIP) system used was equal to a standard news print stock system. DIP based laboratory sheets were produced from pre-dried DIP stock, which was disintegrated in tab water. The DIP stock originated a standard deinking plant for news print stock production.

4.3.2 **Fillers**

For laboratory sheet forming the following (Table 4.3-2) filler types were used. The fillers, either as solids or in suspension, were diluted with deionized water to 10% solids content slurries and subsequently delaminated/dispersed by 120 s of ultraturax treatment.

Table 4.3-2: Used Filler Types

Filler Type	Name	Producer	Solids Content
GCC	Hydrocarb 50	Omya	solid
PCC	Syncarb F0474 MJ	Omya	51%
Clay	Kaolin DSK 50	Gebr. Dorfner GmbH	solid

4.3.3 **Chemical Additives**

4.3.3.1 ASA

The ASA types used are listed in Table 4.3-3, whereas the product “AS 1000” was the chosen standard product. This ASA product is a pure C18 type without emulsification agent. Prior to application, all ASA products had to be emulsified under the listed procedure in Chapter 4.1.1.4. All listed ASA types are Fennosize products by Kemira GesmbH.

Table 4.3-3: Used ASA Types

ASA Type	Composition	Emulsifier
AS 1000	pure C18	none
AS 1100	C16/C18, shares ~ 65/35	none
AS 1300	C16/C18, shares ~ 35/65	none
AS 2000	pure C18	type A
AS 2100	C16/C18, shares ~ 65/35	type A
AS 2300	C16/C18, shares ~ 35/65	type A
AS 3000	pure C18	type B / low shear
AS 3100	C16/C18, shares ~ 65/35	type B / low shear
OS ExPro	C18 + MSOHO + FAA	type C

4.3.3.2 Starches

The starch types used for emulsification were starches from the company Roquette GmbH. Standard emulsification was carried out with a cationic bio polymer based on potato starch, type ”Vector SC 20157”. This is a high cationic starch with a solids content of approx. 18%.

Anionic emulsification was carried out with a bio polymer based on potato starch, type ”Vector IC 2016AS”. This is a high anionic starch with a solids content of approx. 13%.

For emulsification of ASA for TPM OCC systems as well as for the industrial-scale trials, a cationic starch, type “Hi-Cat 5163A”, was used. This powder starch was prepared for TPM trials by cooking in deionized water at 4% consistency for 4 minutes at 800 W in a microwave.

For industrial-scale trials, the starch was prepared in the factory’s standard jet cooking procedure.

4.3.3.3 Retention Aids

Two retention aid types were used for laboratory trials, a standard cationic PAM (Polyacrylamide, type Percol 540 by BASF SE) and a standard cationic PEI (Polyethylenimine, type Polimin SK by BASF SE). Prior to application, both products were diluted with deionized water. PAM was prepared with a consistency of 0.1% and PEI with a consistency of 1%.

4.3.3.4 Poly Aluminum Compounds

The poly aluminum compounds of choice were the products Paper Pac-N and Nicasal by the company Huntsman Pigments. Paper PAC-N is a classical poly aluminum chloride (PAC) and Nicasal a poly aluminum nitrate sulphate (PANS). Both products are considered to have an active matter of 100% and were therefore diluted with deionized water to 1% active matter prior to application.

4.3.3.5 Wet Strength Resin

A polyamidoamin epychlorhydrin wet strength resin type “Giluton 1100/28 N” was used for emulsion optimization. The product was supplied by the company Kurita Europe APW GmbH and had a solids content of ~ 14%. For lab trial emulsion

optimization, the product was diluted with deionized water to 1% consistency before application. During the industrial-scale emulsion optimization trials, the WSR was dosed undiluted from an IBC container to the system, by the scheme displayed in Figure 4.3-2.

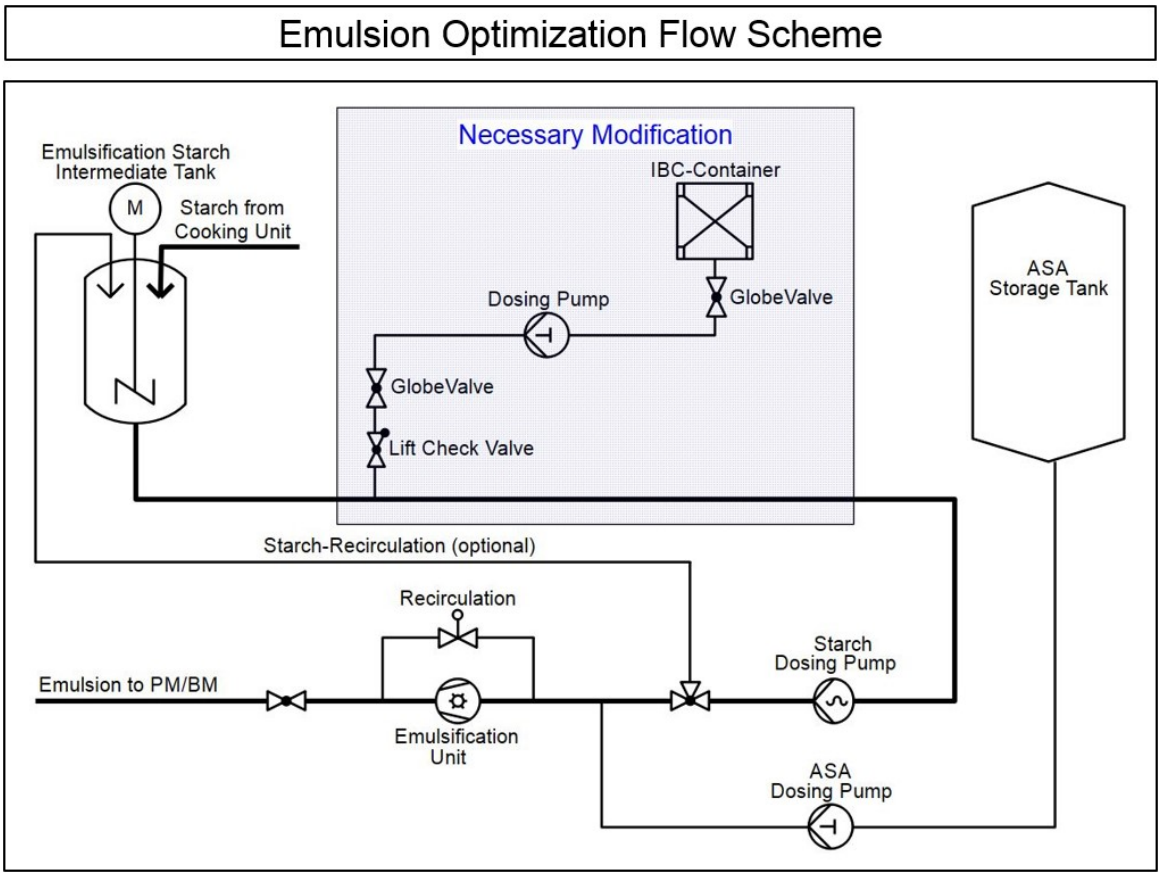

Figure 4.3-2: Emulsion Optimization - Flow Scheme (created with RI-CAD™)

4.3.4 **Characterization of used Additives**

4.3.4.1 Solids Content

The solids content of all additives was analyzed by IR moisture analysis (Scale Type: EM 120, by Precisa Gravimetrics AG). For the measurement, ~ 1 g of the individual sample was put on an aluminum sample pan and then covered with a glass fiber pad for more uniform evaporation. The samples were IR dried at 105 °C until mass constancy was reached. The results were calculated automatically by the scale. The average value of two measurements was used for calculation and interpretation.

4.4 Description of Implemented Advanced Data Analysis- and Visualization Methods

For the statistical interpretation of the presented theoretical background as well as for the generated results, the following advanced approaches were implemented next to standard methods, like pie charts, x-y diagrams, or x-y-y diagrams.

4.4.1 Design of Experiments (DOE)

Some trials which are marked as such, were planned and analyzed by using the statistical trial planning and analysis software Modde 10.1 by Umetrics. This was done in order to statistically analyze the correlation between the factors (ASA dosage; process or stock parameters) and the results (sizing performance or agglomeration behavior) as well as the interactions between these factors. The statistical analysis was done based on full factorial designs, with three center points and two replicates. That means that for a trial set with the following ASA dosages (0%, 0.05%, 0.1%, 0.2%, 0.3% and 0.4%) and six variations of a second factor (e.g., water hardness 0°dh, 5°dh, 10°dh, 25°dh, 50°dh, 100°dh, 500°dh), 58 samples had to be produced and analyzed. The calculation of the total trial runs, which equals the amount of required samples, is done based on Equation 4.4-1:

$$N = ((n_A * n_B) + n_{CP}) * R$$

Equation 4.4-1: Number of Trial Runs - Calculation

$N = Number\ of\ Trial\ Runs$

$n_A = Levels\ of\ Factor\ A$

$n_B = Levels\ of\ Factor\ B$

$n_{CP} = Number\ of\ Center\ Points$

$R = Number\ of\ Replicates$

The results of these trials were subsequently fitted by the software (PLS or MLR) to a model and graphically displayed as contour plots. The descriptive statistics, needed for data interpretation are listed in the appendix for the respective presented trial results.

4.4.2 **Contour Plots**

For most of the graphical trials interpretations within this thesis, contour plots were the tool of choice. This choice is based on two reasons. First, the results of the statistical analysis are best displayed as contour plots. Second, most of the residual trials were conducted following a full factorial trial plan with two factors. For the interpretation of two-dimensional trials, where two factors (x & y) are varied, it is one possibility to induce a third dimension (z) for the results, which is displayed as a differing color within the contour plots.

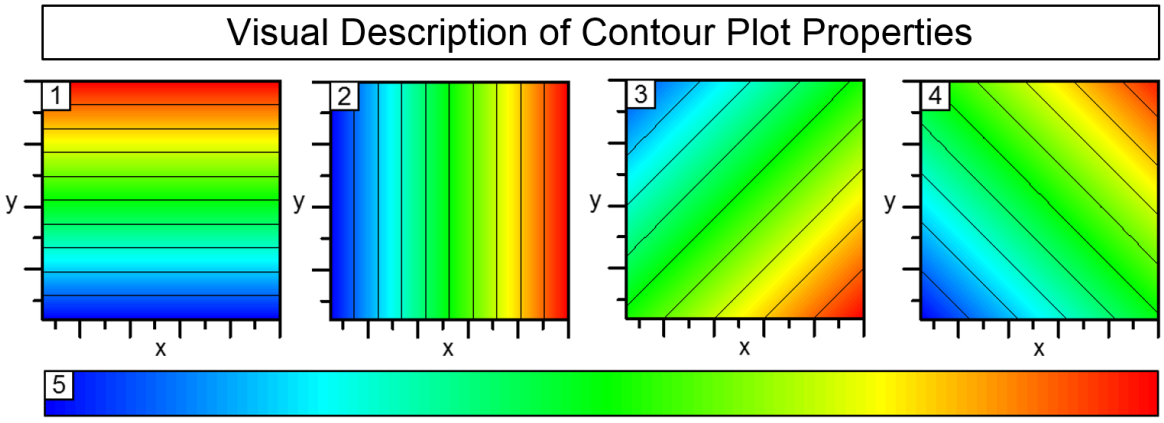

Figure 4.4-1: Visual Description of Contour Plot Properties

Figure 4.4-1describes the general properties of contour plots on the example of four idealized graphs. The specifications of the plots are defined by the impact of the factors x and y:

1. The result is only affected by factor **y**.
2. The result is only affected by factor **x**.
3. The result is affected by factor **x** and **y**, while one is negative and the other positive.
4. The result is affected by factor **x** and **y**, while both are negative or positive.
5. Color indication for result value (**z**)

For the contour plots presented in this thesis, the ASA dosage is always the factor indicated on the y-axis, while the factors on the x-axis are the varied emulsion, process or stock parameters that are varied. The color indication is done for all plots by the same principle. Blue indicates low values, while red indicates high values.

4.4.3 **Box-Whisker Graphs**

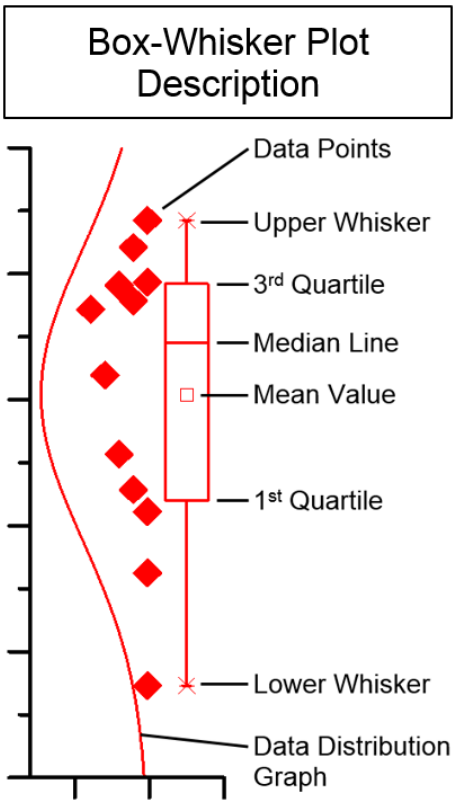

Figure 4.4-2: Box-Whisker Plot Description

For statistical result interpretation and visualization of most optical localization trials, box whisker plots were used. These have the advantage of visualizing the data distribution behavior, as well as the resulting mean and median values. The 1st and 3rd quartile mark the region in-between which 50% of the analyzed data is located. The upper and lower whiskers represent the data that is located within a region of 150% of the interquartiliar distance, a region for moderate outliers. The minimum and maximum values are marked with asterisks, which are for the displayed example, located on the whisker lines, as they are within the region of 150% interquartiliar distance. A feature that is given in Figure 4.4-2, as well as for the first two presented box-whisker graphs, is the display of the data points, including their normal distribution graph. This feature shall serve the better understanding of the presented plots. As a matter of required space, it is skipped during the interpretation of localization behavior influencing factors (Chapter 3.3).

5 Conclusion

The objective of the presented work was to create an approach to holistic understanding of the occurring physico-chemical mechanisms that lead to ASA's hydrophobizing performance. This attempt included an approach to performance explanation via a detailed literature research, a comprehensive analysis of sizing-performance interfering factors and additionally, a development of a novel measurement method, which allows tracing ASA's distribution behavior on a microscopic scale within the structure of ready-made sheets. The combination of the gained results gave the basis for the explanation of the so far not yet clarified pieces to ASA's holistic sizing performance explanation. The final goal was reached by utilizing this knowledge for the development and implementation of a novel sizing-mechanism based approach to industrial scale ASA sizing-performance improvement.

A detailed literature review led to the conclusion that, even though the esterification mechanism is still mentioned within some publications as the sizing-performance-triggering reaction of ASA, no thorough proof could be delivered so far for its scientific verification. Considering the fact that some attempts have shown that only a minor or no share of ASA is unextractably bound within the sheet structure, a description of ASA's sizing-performance-development, based on the same mechanistics as valid for rosin sizing, are considered as the explanation of higher plausibility. By this approach, the actual hydrophobization of the sheet structure is uncoupled from ASA's reactivity, as no covalent bonds, based on the anhydrides reactivity are formed. The hydrophobization is thus rather more supposed to be developed by an equal distribution and orientation of hydrolyzed ASA amongst the sheet structure.

These results were further combined and focused on a theoretical approach to the explanation of the occurring physico-chemical mechanisms, while the phenomena of reaction plausibility and ASA mobility were taken into account. This attempt showed that the reaction of ASA with cellulose under the given circumstances during paper making is very unlikely to happen and that the occurring phenomena

during ASA sizing, such as size revision, size reactivation and ASA migration, are only explainable by intra- and intermolecular mobility, which excludes the factor of a significant extent of esterification.

The comprehensive analysis of the factors that interfere sizing performance has especially displayed the importance of evaluating these at differing ASA dosages. This means that some synergetic effects, as well as negative impacts, did only show at certain ASA dosages, expressing the high sensitivity of the ASA sizing system. The most important factors were clustered within this work in the ASA-type, emulsion parameters, stock parameters and process parameters.

The analysis of the impact on the sizing performance by different ASA types has shown that a high C18 share leads to a better sizing performance in general, while the difference between the most common available ASA types has shown to be of very low extent during the application on the reference furnished used.

The evaluation of the emulsion parameters showed that the content of active ASA (not hydrolyzed) in the emulsion is of highest importance for sizing performance generation, thus enforcing the theory that ASA's active structure is the key to successful application. Further, not only the emulsion stability and an appropriate particle size are crucial for high degrees of hydrophobization, but also the adjustment of the overall emulsion charge by a variation of the shares between emulsification starch and ASA. This variation enables an emulsion charge adjustment to the stock systems requirements. The trials also showed that the manufactured emulsions showed a very high aging resistance and emulsion stability, providing almost no sizing losses over an emulsion storage time of 100 minutes.

The analysis of the stock parameters has brought up the following synergetic, neutral and negative impact factors on ASA's sizing performance. The degree of refining has proven during this analysis to show the highest degree of synergetic effects on the sizing performance, as the morphological changes by refining promote the physics of hydrophobization. Within the analysis of the impact of differing furnish compositions, it has emerged that the share between long and short fiber (both bleached kraft pulps) has no effect at all, while an increasing share

of secondary fibers (DIP, OCC) significantly affects ASA's performance. The pure presence of fillers (GCC, PCC and clay) has proven to significantly affect ASA's performance as well, while PCC showed a comparably moderate impact and thus the highest sizeability.

The determination of possible process parameters impacting sizing performance has brought up the following potentials. The factors of stock temperature and post-dosing dwell time have shown to have no significant impact at all. The trials contributing to the dosing position displayed the importance that ASA has to be dosed to the system, when there are still charge centers available on the fibers, as only then proper self-retention and distribution are guaranteed. The analysis of the sheet-forming shear force impact displayed that the ASA emulsion particles do fixate properly on the fiber surfaces in filler free systems, not causing a significant degree of shear sensitivity. The shear sensitivity increases when filler is present, while the sizing performance correlates to the negatively by shear forces affected filler retention. The most significant negative impacts were triggered by increasing water hardness levels, increasing conductivity levels and by alkaline pH-values. Increasing water hardness and conductivity levels seemed to negatively impact the ASA retention, while the negative impact of alkaline pH-values, especially from pH 7 to pH 9 is not yet clarified. A plausible approach to the occurring phenomena seems to be based on a high extent of in-sheet, pre-spreading hydrolysis, as this would lead to a weakened spreading performance and thus to a decreased degree of hydrophobization. The way of sheet drying has proven to have a significant impact on the sizing performance, while it showed that not the drying temperature alone is affecting the sizing performance, but also the overall induced drying energy, stating that higher energy levels lead to better sizing performance. The analysis of the aging resistance of ASA-sized sheets has shown, that the sizing degree exhibits high sensitivity toward aging, resulting in a linear performance decreasing over aging time.

Within the goal of the development of a localization method suitable for the description of ASA's distribution behavior on a microscopic scale, it was possible to utilize confocal white light microscopy as the method of choice. This method is based on the optical localization of ASA agglomerates. In order to fulfill the

requirements at magnification rates of factor 100 optical zoom, it was necessary to improve the contrast between ASA and cellulose by an ASA dying step with an inert red diazo dye (Sudan Red 7B). During this approach it was verified that the dyeing step has no impact on ASA's processability or its sizing performance. The agglomeration behavior of ASA was analyzed automatically by multiple random imaging of a sample area of approx. 8650 µm² with a minimum resolution for particles of 500 nm in size. The final analysis was done by the implementation of self-developed image processing filtering sequences, by which the agglomeration behavior was put into crisp values in terms of the total agglomeration area (Agg_A [%]), the number of agglomerates (Aggl_N [n/mm²]) and the average agglomerate size (Aggl_AV [µm²]).

During a further step within this approach, the developed method was validated by Raman spectroscopy and by confocal laser scanning microscopy. These attempts turned out negative, as the utilized methods showed either a too low sensitivity and resolution (Raman) or a too high sensitivity toward well distributed ASA, resulting in resonance all over the sheet structure (confocal approaches). A benefit that evolved from confocal laser scanning microscopy was the fact, that the whole sheet structure was covered with ASA. This is considered as proof for ASA's uniform distribution and film-building abilities and that the existence of ASA agglomerates is a result of heterogeneous ASA distribution, even though the majority of the cellulose surface is still covered.

The results of the subsequent combination of the localization behavior with the respective sizing performance, showed that ASA's distribution and agglomeration behavior is significantly influenced by external factors such as conductivity, water hardness, the degree of refining, the dosage of retention aid (PAM), the curing conditions, as well as sample aging. Additionally, it was observed that under static boundary conditions in terms of sizing agent dosage and stock parameters, a relative reduction of the agglomeration area by e.g., the dosage of retention aid or increased drying temperatures, leads to an increase in the overall sizing performance. Hence, these results verify the theory that the sizing performance generating mechanisms of ASA are based on molecular distribution and orientation phenomena and thus of reversible nature, which proves the earlier stated theories

for the explanation of phenomena such as size reversion, migration and reactivation as valid.

The final goal of utilizing the gained knowledge for the development and implementation of a novel sizing-mechanism-based approach to ASA performance improvement, in order to optimize the industrial sizing processes by significant means was further on met by the principle of emulsion modification. This principle is based on the induction of cationic mordants such as PAC, PANS or PAAE, into the emulsification polymer, prior to emulsification. It is supposed by this approach that the mordant remains immobilized within the protection colloid upon spreading, where it is supposed to spread with ASA, acting as an anchor and orientation help over the whole ASA covered area, thus improving ASA's distribution homogeneity. It was possible so far to cut the required sizing agent dosages under production conditions within industrial trials by 50%, providing constant sizing performance, optimized physical properties and aging behavior.

Summarizing the results and findings of the presented work, all evidence leads to the conclusion, that the mechanistic reactions, which lead to ASA's hydrophobizing performance, are solely based on its physical distribution and orientation within the sheet structure, while the distribution homogeneity in microscopic scale accounts most to the sizing performance. However, the reactive structure of ASA is the key to its performance development, as successful application and spreading are only possible if not hydrolyzed. This gained knowledge was transferred into a novel ASA sizing mechanism model, which holistically describes the occurring processes and phenomena.

6 Outlook for Further Work

The research conducted during the presented work, as well as the gained results, have shown that the traditional explanation model for the sizing performance generation by ASA via the principle of esterification reactions cannot be considered as plausible and thus needs to be adjusted or revised.

Further, the necessity evolved to find new explanation approaches to problems or interactions which have commonly been explained by their impact on esterification.

Since the developed localization method is currently the only method capable of analyzing ASA's distribution and mobility behavior by the determination of occurring agglomerates, for validation purposes, it is necessary to find other methods capable of doing the same.

Another approach, implementing quantitative analysis methods in combination with the localization method, could further clarify the mechanisms which cause agglomeration with respect to the actual sizing agent content.

It would further on be of highest interest to combine the invented optical localization method, with a fluorescent microscopy method, in order to combine ASA's agglomeration behavior with its distribution behavior. This could help to understand to which extent surface coverage and agglomeration contribute to the final hydrophobization performance.

As the presented localization method shows a high degree of applicability for ASA, it seems plausible that it is also applicable for AKD, rosin or PSA. This should therefore be evaluated, as this method could also help to better understand the sizing mechanisms of the respective sizing agents.

The industrial optimization potential, which was uncovered within this work should further be implemented in other factories and for other grades, in order to sustainably reduce the required sizing agent amounts. It would further on be of special interest, if this approach is capable of reducing ASA-typical drawbacks, such as scaling tendency, ASA migration or size revision.

7 Bibliography

1. Fourdrinier, H., *Patent for a Machine for Manufacturing Paper*, in *The Repertory of Patent Inventions: And Other Discoveries and Improvements in Arts, Manufactures, and Agriculture ...* 1807, Wilkie, G, Wilkie, T.: London. p. 321-326.
2. Haag, J., *Automation Aspects in Papermaking*, in *MUAS Master of Papertechnology Lecture*. 2009, Voith Paper Automation: Heidenheim.
3. Voith Paper, *Erfolg bei Rhein Papier in Hürth; Weltrekord für Zeitungsdruckpapier.* twogether, 2009(28): p. 74.
4. Tappi over the Wire-Tissue Edition. *Hayat Kimya Tissue Machine sets World Speed Record*. 2012 [cited 2015 19.10.]; [Press Release]. Available from: http://www.naylornetwork.com/PPI-Tissue/articles/print.asp?aid=183108.
5. Rampmaier, S., *Expertise von Voith: Guangxi BM 1 produziert 1.200.000 t hochwertigen Faltschachtelkarton*. 2014, Voith Paper: Heidenheim.
6. Windhagen, K., *Paper 2015 - Annual Report*. 2015, Verband Deutscher Papierfabriken e.V.: Bonn.
7. Rentrop, G.H. and G.A. Geiger, *Paper 2010 - Annual Report*. 2010, Verband Deutscher Papierfabriken e.V.: Bonn.
8. Bocken, S., *Nachhaltigkeit aus Sicht des Prozesslieferanten*, in *Symposium der Papieringenieure*, Voith GmbH, Editor. 2010, Vereingter Papierfachverband München e.V.: Aschaffenburg.
9. Kreibe, S. and R. Peche, *Ökoeffiziente Stoff- und Energieströme in der Papierindustrie*, in *Symposium der Papieringenieure*, bifa Umweltistitut, Editor. 2010, Vereinigter Papierfachverband München e.V.: Aschaffenburg.
10. Kleemann, S., J. Belle, T. Gliese, W.J. Auhorn, A.N. Geller, K. Goebel, B. Götz, A. Gürtler, W. Kamutzki, M. Köcher, U. Künzel, P.-C. Le, K. Niemelä, F. Österberg, R.A. Pelzer, M. Prinz, T. Roick, W. Scholz, J. Schrijver, W.-S. Schultz, R. Thummer, and B. Wirth, *Chemical Additives for the Production of Pulp & Paper; Functionally Essential – Ecologically Beneficial*. 1 ed, ed. ZELLCHEMING Technical Committee “Chemical Additives (CHAD)”. 2008, Frankfurt a. M.: Deutscher Fachverlag.
11. Gess, J.M. and J.M. Rodriguez, *The Sizing of Paper*. 2005, Atlanta: TAPPI PRESS.
12. Ainsworth, J.H., *Paper, the Fifth Wonder*. 1959, Kaukauna, Wis.: Thomas Printing & Pub. Co. 370 p.
13. Pons.de. *The Meaning of the Verb "assidere"*. 2015 [cited 2015 21.10]; [Translation]. Available from: http://de.pons.com/%C3%BCbersetzung?q=assidere&l=dela&in=&lf=la.
14. Lehtinen, E., *Pigment coating and surface sizing of paper*. 810 S. : zahlr. Ill., graph. Darst.
15. Lipponen, J. and T. Olkkonen. *Starch Penetration in Surface Sizing: Finding Optimum Surface Sizing Parameters*. in *Metso Paper Technology Days 2006. Technology for Lifecycle Results*. 2006. Jyväskylä, Finland: Metso Paper.
16. Remmer, J.K. and D.E. Eklund, *Absorption of Starch During Surface Sizing with Different Methods.* Tappi Journal, 1992. **75**(1): p. 179-184.
17. Holik, H., *Handbook of Paper and Board*. 2, Revised and Enlaged ed. Vol. 1. 2013, Weinheim: John Wiley & Sons.
18. Laine, J. and P. Stenius, *Internal Sizing of Paper*, in *Papermaking Chemistry*, R. Alén, Editor. 2007, Finnish Paper Engineers' Association/Paperi ja Puu Oy: Helsinki. p. 124-162.
19. Jinhua, Y. and D. Yulin. *Fatty-Acid Starch Complex in the Application of Linerboard Surface Sizing*. in *PaperCon'09*. 2009. St. Louis, Missouri: TAPPI.

20. Teixeira Moutinho, I.M., A.M. Kleen, M.M. Lopes Figueiredo, and P.J. Tavares Ferreira, *Effect of Surface Sizing on the Surface Chemistry of Paper Containing Eucalyptus Pulp.* Holzforschung, 2009. **63**(3): p. 282-289.

21. Hagiopol, C. and J.W. Johnston, *Chemistry of Modern Papermaking*. 1 ed. 2012, Boca Raton: CRC Press.

22. Krolle, A., *Benetzbarkeit der Papieroberfläche*. Vol. 1. 2014, Munich: Verlag Dr. Hut.

23. Hubbe, M.A., *Paper's Resistance to Wetting - A Review of Internal Sizing Chemicals and Their Effects* BioResources, 2007. **2 (1)**: p. 106-145.

24. Porkert, S., S. Fischer, and S. Kleemann. *Cellulose Structure Hydrophobization by Alkenyl Succinic Anhydride (ASA) – A Novel Approach to Performance Explanation*. in *PTS Symposium GC 1446; PTS International Symposium on Applied Interface Chemistry 2014*. 2014. Munich, Germany: Papiertechnische Stiftung PTS.

25. Luner, P. and M. Sandell, *The Wetting of Cellulose and Wood Hemicelluloses.* Journal of Polymer Science Part C: Polymer Symposia, 1969. **28**(1): p. 115-142.

26. Belle, J., S. Kleemann, J. Odermatt, and A. Olbrich, *Making Fiber-Fiber Bonds Visible*, in *249th ACS National Meeting "Cellulose and Renewable Materials" Divsion of the ACS Session: Cellulose in Solid State and Solution - Structure, Chemistry and Reaction Mechanisms: Anselme Payen Award; Symposium in Honor of Thomas Rosenau*, F.W. Liebner, A. Potthast, L.A. Lucia, and T. Röder, Editors. 2015, ACS: Denver, Colorado, USA.

27. Young, T., *An Essay on the Cohesion of Fluids.* Philosophical Transactions of the Royal Society of London, 1805. **95**: p. 65-87.

28. Ott, G., *Physikalische und chemische Grundlagen der Leimung / Hydrophobierung von Papier, Karton und Pappe*, in *PTS-Seminar GL-SE 957 - Leimen, Füllen und Färben von Papier und Karton*. 1999: München.

29. Shen, W., Y. Filonanko, Y. Truong, I.H. Parker, N. Brack, P. Pigram, and J. Liesegang, *Contact Angle Measurement and Surface Energetics of Sized and Unsized Paper.* Colloids and Surfaces A: Physicochemical and Engineering Aspects, 2000. **173**(1–3): p. 117-126.

30. Heuser, E., *Die Anwendung von Tierleim zum Leimen von Papierstoff.* Papier-Zeitung, 1916. **41**: p. 1365-1368.

31. Martorana, E., S. Fischer, and S. Kleemann, *Untersuchungen zur Papierleimung mit Alkenylbernsteinsäureanhydrid (ASA)*, in *Fakultät Forst-, Geo- und Hydrowissenschaften der Technischen Universität Dresden*. 2010, Technische Universität Dresden: Tharandt.

32. Behnke, J.M., *Paraffin-Emulsionen in der Papierindustrie.* Wochenblatt für Papierfabrikation, 1954. **82**(2): p. 39-40.

33. Gess, J.M., *The Measurement of Sizing in Paper.* Tappi Journal, 1981. **64**(1): p. 35-39.

34. Iselau, F., P. Restorp, M. Andersson, and R. Bordes, *Role of the Aggregation Behavior of Hydrophobic Particles in Paper Surface Hydrophobation.* Colloids and Surfaces A: Physicochemical and Engineering Aspects, 2015. **483**: p. 264-270.

35. Hoffmann, J., *Wechselwirkung von Leimungssystemen mit anderen Papieradditiven*, in *Wet-End-Prozesse (Modul 3): Optimierung der Leimung. PTS-Manuskript PTS-MS 443*. 2004.

36. Hoffmann, J., *Oberflächenleimung – Grundlagen und praktische Anwendungen*, in *PTS-Seminar GL-SE 957 - Leimen, Füllen und Färben von Papier und Karton*. 1999: München.

37. Ott, G., *Oberflächenleimung - Grundlagen und Abgrenzung gegenüber Massenleimung*, in *Wet-End-Prozesse (Modul 3): Optimierung der Leimung. PTS-Manuskript PTS-MS 443*. 2004: München.

38. Tompkins, T.W. and J.A. Shepler, *Combination Sizing. The Use of Synthetic Surface Sizie with an Alkaline Internal Size.*, in *TAPPI Papermakers Conference* 1991, TAPPI Press: Nashville, USA. p. 191-201.

39. Illig, M.F., *Anleitung, auf eine sichere, einfache und wohlfeile Art Papier in der Masse zu leimen: als Beitrag zur Papiermacherkunst*. 1807.

40. Wurster, C., *Paper-Sizing.* Journal of the Franklin Institute, 1878. **106**(6): p. 425.

41. Lacher, R., *Hydrophobierung durch Harzleim, Paraffine und synthetische reaktive Leimungsmittel*, in *PTS-PE333*. 2003: München.

42. Ettl, R., *Hydrophobierung durch Harzleim und synthetische Leimungsmittel*, in *PTS-Manuskript 30 233*. 2002: München.

43. Wenxia, L., C. Zicheng, and D. Hongdong, *Sizing Behavior of Cationic Dispersed Rosin-Ester on Cellulose Fibers.* Nordic Pulp and Paper Research Journal, 2006. **21**(5): p. 586-590.

44. Latta, J.L., *Rosin Based Sizing*, in *Tappi Sizing Short Course*. 1997, TAPPI Press: Nashville.

45. Ostwald, W. and R. Lorenz, *Beiträge zur Kolloidchemie der Papierleimung, II.* Colloid & Polymer Science, 1923. **32**(3): p. 195-209.

46. Zhuang, J., M. Chen, and C.J. Biermann, *Rosin Soap sizing without Mordants by Immersion in Size Solution.* Tappi Journal, 1997. **80**(1): p. 271-276.

47. Zhuang, J. and C.J. Biermann, *Neutral to Alkaline Rosin Soap Sizing with Metal Ions and Polyethylenimine as Mordants.* Tappi Journal, 1995. **78**.

48. Zhuang, J. and C.J. Biermann, *Rosin Soap Sizing with Ferric and Ferrous Ions as Moderants.* Tappi Journal, 1993. **76**(12): p. 141-147.

49. Biermann, C.J., *Rosin Sizing with Polyamine Mordants from pH 3 to 10.* Tappi Journal, 1992. **75**(5): p. 223-228.

50. Xu, Y., B. Hartong, and Y. Deng, *Neutral to Alkaline Rosin Sizing Using Pelyethyleneimine-Epichlorhydrin (PEI-epi) as a Mordant.* Journal of Pulp and Paper Science, 2002. **28**(2): p. 39-44.

51. Downey, W.F., *Higher Alkyl Ketene Dimer Emulsion*, H.P. Company, Editor. 1953, Google Patents: USA. p. 3.

52. Thompson, W.D. and G.I. Keim, *Process of Sizing Paper with an Aqueous Emulsion of Ketene Dimer*, H.P.C. Ltd, Editor. 1956: USA. p. 3.

53. Schumacher, R., *Leimung von Papier und Karton mit AKD*, in *eimen, Füllen und Färben von Papier und Karton*. 1999, PTS München: München.

54. Hoffmann, J., *Reaktivleimungssysteme Teil 1 – Alkylketendimer*, in *Münchner Papierseminar Leimung*. 2005, Prof. Dr. Stephan Kleemann: München.

55. Lindström, T. and P.T. Larsson, *Alkyl Ketene Dimer (AKD) Sizing-A review.* Nordic Pulp and Paper Research Journal, 2008. **23**(2): p. 202-209.

56. Boone, S.R., *Internal Sizing II: Alkaline Keten Dimere Sizes (AKD)*, in *Tappi Sizing Short Course*. 1997, TAPPI Press: Nashville.

57. Bottorff, K., *AKD Sizing Mechanism: A More Definitive Description.* Tappi Journal, 1994. **77**(4): p. 105-116.

58. Song, X., F. Chen, and F. Liu, *Study on the Reaction of Alkyl Ketene Dimer (AKD) and Cellulose Fiber.* BioResources, 2012. **7**(1): p. 652-662.

59. Kumar, S., V.S. Chauhan, and S.K. Chakrabarti, *Separation and Analysis Techniques for Bound and Unbound Alkyl Ketene Dimer (AKD) in Paper: A Review.* Arabian Journal of Chemistry, 2012: p. 7.

60. Seppänen, R., *On the Internal Sizing Mechanisms of Paper with AKD and ASA Related to Surface Chemistry, Wettability and Friction*. 2007, KTH: Stockholm.

61. Odberg, L., T. Lindström, B. Liedberg, and J. Gustavsson, *Evidence for Beta-Ketoester Formation during the Sizing of Paper with Alkyleketene Dimers.* Tappi Journal, 1987. **70**(4): p. 135-139.

62. Lindström, T. and G. Soderberg, *On the Mechanism of Sizing with Alkylketene Dimers, Part 1. Studies on the Amount of Alkylketene Dimer Required for Sizing Different Pulps* Nordic Pulp and Paper Research Journal, 1986. **1**(1): p. 26-33.

63. Nahm, S.H., *Direct Evidence for Covalent Bonding Between Ketene Dimer Sizing Agents and Cellulose.* Journal of Wood Chemistry and Technology, 1986. **6**(1): p. 89-112.

64. Isogai, A., *Mechanism of Paper Sizing by Alkylketene Dimers.* Journal of Pulp and Paper Science, 1999. **25** (7): p. 251-256.

65. Porkert, S., E. Martorana, and S. Kleemann, *Untersuchungen zu Wechselwirkungen bei der AKD-Leimung*, in *Papiertechnik*. 2009, Hochschule für angewandte Wissenschaften München: München.

66. Esser, A. and R. Ettl, *On the Mechanism of Sizing with Alkyl Ketene Dimer (AKD): PhysicoChemical Aspects of AKD Retention and Sizing Efficiency*, in *The Fundamentals of Papermaking Materials*, Pira, Editor. 1997, Pira: Cambridge. p. 997-1020.

67. Roberts, J.C. and D.N. Garner, *The reaction of Ketene Dimer Sizes with Cellulose Model Substrates.* Cellulose Chemistry and Technology, 1984. **18**(3): p. 275-282.

68. Lindström, T. and H. O'Brian, *On the Mechanism of Sizing with Alkylketene Dimers, Part 2. The Kinetics of Reaction Between Alkylketene Dimers and Cellulose.* Nordic Pulp and Paper Research Journal, 1986. **1**(1): p. 34-42.

69. Marton, J. *Practical Aspects of Alkaline Sizing on Kinetics of AKD Reactions Hydrolysis of AKD*. in *Tappi Papermakerts Conference*. 1990. Atlanta: Tappi.

70. Patton, P.A. *On the Chemistry of AKD Sizing and Size Revision*. in *TAPPI Papermakers Conference*. 1991. Seattle, USA: TAPPiu Press.

71. Isogai, A., R. Taniguchi, F. Onabe, and M. Usuda, *Sizing Mechanism of Alkyl Ketene Dimers Part 1. Possibility for AKD to form Ketoesters in Papersheets.* Nordic Pulp and Paper Research Journal, 1992. **7**: p. 193-193.

72. Champ, S. and R. Ettl, *The Dynamics of Alkyl Ketene Dimer (AKD) Retention*, in *5th International Paper and Coating Chemistry Symposium*, P.a.P.T.A.o. Canada, Editor. 2003, Pulp and Paper Technical Association of Canada: Montreal. p. 285-291.

73. Yu, L. and G. Garnier, *The Role of Vapour Deposition during Internal Sizing: A Comparative Study between ASA and AKD.* Journal of Pulp and Paper Science, 2002. **28 (10)**: p. 327-330.

74. Shen, W., H. Zhang, and R. Ettl, *Chemical Composition of "AKD Vapour" and its Implication to AKD Vapour Sizing.* Cellulose, 2005. **12**(6): p. 641-652.

75. Colasurdo, A.R., *The Interactions of Alkyl Ketene Dimer with other Wet-End Chemicals.* Tappi Journal, 1992. **75**(9): p. 143-149.

76. Batten, G.L.J. *A Papermaker's Guide to Synthetic Surface Sizing Agents*. in *Papermakers Conference*. 1992. Nashville: Tappi.

77. Batten Jr, G.L., *The Effects of SMA Surface Sizes on Paper End-Use Properties.* Tappi Journal, 1995. **78**: p. 142-146.

78. Ono, H. and Y. Deng. *Cationic Polystyrene-Based Paper Sizing Agents*. in *Engineering & Paper-Makers Conference*. 1997. Nashville, USA: TAPPI Press.

79. Wang, T., J. Simonsen, and C.J. Biermann, *A New Sizing Agent: Styrene-Maleic Anhydride Copolymer with Alum or Iron Mordants.* Tappi Journal, 1997. **80**(1): p. 277-282.

80. DIN Deutsches Institut für Normung e.V., *DIN EN ISO 535*, in *Papier und Pappe - Bestimmung des Wasserabsorptionsvermögens - Cobb-Verfahren (ISO 535:2014); Deutsche Fassung EN ISO 535:2014*. 2014, Beuth Verlag GmbH.

81. TAPPI, *TAPPI Test Method T 441 om-98*, in *Water Absoptiveness of Sized (Non-Bibulous) Paper, Paperboard, and Corrugated Fiberboard (Cobb Test)*. 1998, TAPPI Press.

82. Hoffmann, J., *Reaktivleimungssysteme Teil 2 – Alkenylbernsteinsäureanhydrid*, in *Münchner Papierseminar / Leimung*. 2005, Prof. Dr. Stephan Kleemann: München.

83. Skinner, F.K., Y. Rotenberg, and A.W. Neumann, *Contact Angle Measurements from the Contact Diameter of Sessile Drops by Means of a Modified Axisymmetric Drop Shape Analysis.* Journal of Colloid and Interface Science, 1989. **130**(1): p. 25-34.

84. Río, O.I.d. and A.W. Neumann, *Axisymmetric Drop Shape Analysis: Computational Methods for the Measurement of Interfacial Properties from the Shape and Dimensions of Pendant and Sessile Drops.* Journal of Colloid and Interface Science, 1997. **196**(2): p. 136-147.

85. TAPPI, *TAPPI Test Method T 458 om-04*, in *Surface Wettability of Paper (Angle of Contact Method)*. 2004, TAPPI Press.

86. TAPPI, *TAPPI Test Method T 558 om-97*, in *Surface Wettability and Absorbency of sheeted Materials using an Automated Contact Angle Tester*. 1997, TAPPI Press.

87. Saarinen, J.F., *Planar Fluidic Channels on TiO2 Nanoparticle Coated Paperboard*, in *International Paper and Coating Chemistry Symposium*, A. Isoai, Editor. 2015, Akira Isogai: Tokyo, Japan.

88. Yang, H. and Y. Deng, *Preparation and Physical Properties of Superhydrophobic Papers.* Journal of Colloid and Interface Science, 2008. **325**(2): p. 588-593.

89. Song, J. and O.J. Rojas, *Approaching Super-Hydrophobicity from Cellulosic Materials: A Review.* Nordic Pulp and Paper Research Journal, 2013. **28**(2): p. 216-238.

90. Grüner, G. *Die Erfassung der Penetrationsdynamik mittels Ultraschall-Dämpfungsmessung – eine Methode zur Untersuchung der Wechselwirkung zwischen Flüssigkeiten und flachen Materialproben wie Papier, Textilien, Glasfasern usw.* 1996 02.06 [cited 2015 26.11]; Available from: https://www.emtec-papertest.de/de/broschuere-zur-erfassung-der-penetrationsdynamik.html.

91. emtech Paper Testing Technology, *Modular Measuring System PDA.C 02 / EST 12, Kurzbeschreibung Ergebnisauswertung*. 2009, emtech-Paper Testing Technology.

92. Grüner, G. *Material- und Kosteneinsparung durch Messung der verarbeitungsprozessrelevanten Oerflächenparameter von Papier und Karton mit einem innovativen Messsystem zur Vorhersage von Verklebbarkeit, Bedruckbarkeit und Streichbarkeit*. PDA.C 02 Penetration Dynamics Analyzer 2012 26.09 [cited 2015 25.11]; Available from: https://www.yumpu.com/en/document/view/7048985/pda-presentation-glueability-printability-coating-base-paper.

93. DIN Deutsches Institut für Normung e.V., *DIN 53126*, in *Prüfung von Papier und Pappe - Bestimmung der Beschreibbarkeit mit Tinte*. 2011, Beuth Verlag GmbH.

94. TAPPI, *TAPPI Test Method T 491 om-95*, in *Water Immersion Test of Paperboard*. 1995, TAPPI Press.

95. TAPPI, *TAPPI Test Method T 530 om-96*, in *Size Test for Paper by Ink Resistance (Hercules-Type Method)*. 1996, TAPPI Press.

96. Kamutzki, W. and T. Krause, *Untersuchungen zur Neutralleimung mit Alkyldiketenen.* Das Papier, 1982. **36**(7): p. 311-317.

97. Wang, F., Z. Wu, and H. Tanaka, *Preparation and Sizing Mechanisms of neutral Rosin Size II: Functions of Rosin Derivatives on Sizing Efficiency.* J Wood Sci, 1999. **45**: p. 475-480.

98. Laitinen, R. *Development of LC-MS and Extraction Methods for the Analyses of AKD, ASA, and Rosin Sizes in Paper Products*. 2007.

99. Laitinen, R., *Quantitative Analysis of AKD and ASA Distribution in Paper*, in *PIRA International Conference. Scientific and Technical Advances in the Internal and Surface Sizing of Paper and Board.*, PIRA, Editor. 1999, PIRA: Florence.

100. Gruber, E., E.S. Saglam, and R. Pätzold, *Massebilanz des Reaktivleimungsmittels ASA (Untersuchungen zur analytischen Erfassung von ASA und dessen Reaktionsprodukte) Abschlussbericht INFOR-Projekt Nr.55.* 2004, Technische Universität Darmstadt, Ernst-Berl-Institut für Technische und Makromolekulare Chemie, Fachgebiet Nachwachsende Rohstoffe.

101. Nishiyama, M., A. Isogai, and F. Onabe, *Structures of Alkenyl Succinic Anhydride (ASA) Components in ASA-Sized Papersheets.* Sen i Gakkaishi 1996. **52**(4): p. 180-188.

102. Lackinger, E., M. Bacher, J. Sartori, T. Zweckmair, A. Potthast, and T. Rosenau, *Synthesis and Characterization of 13C-labeled Alkenyl Succinic Anhydride (ASA) with Defined Double Bond Location.* Current Organic Chemistry, 2014. **18**(9): p. 1208-1217.

103. Ohno, K., A. Isogai, and F. Onabe, *Solid-State 13C-NMR Analysis of Size Components in Handsheets prepared by Fatty Acid Soap Size-Alum Systems.* Journal of Wood Science, 2002. **48**(3): p. 197-203.

104. Sundberg, K., B. Holmbom, R. Ekman, J. Nyman, and J. Axberg, *Determination of ASA in Pulp and Paper Samples by Gas Chromatography*, in *PIRA International Conference. Scientific and Technical Advances in the Internal and Surface Sizing of Paper and Board*, PIRA, Editor. 1999, PIRA: Florence.

105. Nishiyama, M., A. Isogai, and F. Onabe, *Roles of Reactive Alkenyl Succinic Anhydride (ASA) in Paper Sizing.* Sen i Gakkaishi, 1996. **52**(4): p. 189-194.

106. Pyda, M., M. Sidqui, S.D. Keller, and P. Luner, *An Inverse Gas Chromatographic Study of Calcium Carbonate treated with Alkylketene Dimer.* Tappi Journal, 1993. **76**(4): p. 79-85.

107. Körkkö, M., O. Laitinen, A. Žmm„l„, J. Niinimäki, and J. Saari, *Recyclability of Release Paper.* IPW, 2008(9): p. 54-58.

108. Ström, G., G. Carlsson, and M. Kiar, *Bestimmung der Alkylketendimer-Verteilung in Probeblättern mittels Elektronenspektroskopie (ESCA).* Wochenblatt für Papierfabrikation, 1992. **120**(15): p. 606-611.

109. Yamamoto, H., T. Kitaoka, and H. Tanaka, *Sizing Response Factors Characterized by XPS/PyGC Comparative Analysis.* Sen i Gakkaishi, 2003. **59**(7): p. 266-271.

110. Grenz, R., *Reduzierung der Additivkosten bei der Herstellung von Masse-Geleimten Papieren durch Identifizieren, Quantifizieren und Minimieren der negativen Wechselwirkungen von Leimungsmitteln mit Retentionsmitteln und optischen Aufhellern*, in *Abschlussbericht IGF 15172-N*. 2009, PTS München.

111. Nyarku, S. and B.B. Sitholé, *Analysis of Alkyl Ketene Dimer (AKD) by Potentiometric Titration.* Canadian Journal of Chemistry, 1994. **72**(2): p. 274-278.

112. Isogai, A., M. Nishiyama, and F. Onabe, *Mechanism of Retention of Alkenyl Succinic Anhydride (ASA) on Pulp Fibers at Wet-End of Papermaking.* Sen i Gakkaishi, 1996. **52**(4): p. 195-201.

113. Sithole, B. and B. Ambayec, *Identification and Determination of Surface Sizing Agents on Sized Papers.* Pulp and Paper Canada, 2000. **101 (9)**: p. 53-57.

114. Sato, T. and A. Isogai, *Pyrolysis-GC-MS analysis of ASA-Sized Papers by On-Line Butylation with Tetrabutylammonium Hydroxide.* Appita Journal, 2003. **56** (3): p. 206-212.

115. Vrbanac, M. and D. Dixon, *Quantitative Analysis of AKD and ASA in Paper using Pyrolysis Gas Chromatography*, in *Pira International Conference. Scientific and Technical Advances in the Internal and Surface Sizing of Paper and Board*, PIRA, Editor. 1997, PIRA: London.

116. Zimmermann, P.A., D.M. Hercules, H. Rulle, J. Zehnpfenning, and A. Benninghoven, *Direct Analysis of Coated and Contaminated Paper using Time-of-Flight Secondary Ion Mass Spectrometry.* Tappi Journal, 1995. **78 (2)**: p. 180-186.

117. Brinen, J.S. and R.J. Kulick. *Detection of ASA and Desizing Agents in Hard to Size Paper Surfaces by SIMS*. in *8th International Paper and Coating Chemistry Symposium*. 1996. Stockholm, Sweden.

118. Kulick, R.J. and J.S. Brinen, *Probing Paper Surfaces with ToF SIMS: A New Problem Solving Tool.* Tappi Journal, 1998. **81**(2): p. 152-156.

119. Samyn, P., R. Farnood, and R. Sodhi. *Advanced Chemical Surface Characterization of Coated Papers using ToF-SIMS Spectral Analysis and Imaging*. in *PTS Symposium GC 1446; PTS International Symposium on Applied Interface Chemistry 2014*. 2014. Munich, Germany: Papiertechnische Stiftung PTS.

120. Adams, J., *Analysis of Printing and Writing Papers by Using Direct Analysis in Real Time Mass Spectrometry.* International Journal of Mass Spectrometry, 2011. **301**(1–3): p. 109-126.

121. Schweiß, R. and R. Grenz, *Erhöhung der Leimungseffizienz durch Ermittlung des individuellen Einflusses verschiedenen, in Summenparametern eingehender Grössen auf das Massenleimungsergebnis*, in *Abschlussbericht IGF 14698*. 2008, PTS München.

122. Hatanaka, S., Y. Takahashi, and J. Roberts, *Sizing with Saponified Alkenyl Succinic Acid.* Tappi Journal, 1991. **74**(2): p. 177-181.

123. Brüning, F., *Verbesserung der Effizienz von Leimungsmitteln durch die Hochkonsistenz-(HC)-Masseleimung*, PTS, Editor. 2007, PTS München: München. p. 34.

124. Qian, K., W. Liu, J. Zhang, H. Li, H. Wang, and Z. Wang, *Using Urea to Improve Stability, Sizing Performance and Hydrolysis Resistance of ASA Emulsion Stabilized by Laponite.* Colloids and Surfaces A: Physicochemical and Engineering Aspects, 2013. **421**: p. 125-134.

125. Wang, H., W. Liu, X. Zhou, H. Li, and K. Qian, *Stabilization of ASA-in-Water Emulsions by Laponite Modified with Alanine.* Colloids and Surfaces A: Physicochemical and Engineering Aspects, 2013. **436**: p. 294-301.

126. Pigorsch, E. and M. Finger, *Detektion, Identifizierung und Verteilungsanalyse von Additiven im Papier mittels Raman-Mikroskopie*, in *PTS Faserstoffsymposium* T. Arndt and F. Miletzky, Editors. 2015, PTS Paper: Dresden. p. 117-131.

127. Berls, R.J., *Treatment of Fabric with Alkenylsuccinic Acids and Anhydrides to Impart Water Repellency*, A.a. Company, Editor. 1959, Google Patents: USA. p. 3.

128. Wurzburg, O.B. and E.D. Mazzarella, *Novel Paper Sizing Process*, N.S.a.C. Cooperation, Editor. 1963: USA.

129. Hubbe, M.A., *Acidic and Alkaline Sizings for Printing, Writing, and Drawing Papers.* The Book and Paper Group Annual, 2005. **23**: p. 139-151.

130. Wasser, R.B., *The Reactivity of Alkenyl Succinic Anhydride: Its Pertinence with Respect to Alkaline Sizing.* Journal of Pulp and Paper Science, 1987. **13**(1): p. J29-J32.

131. Gess, J.M. and D.S. Rende, *Alkenyl Succinic Anhydride (ASA).* Tappi Journal, 2005. **4**(9): p. 25-30.

132. Porkert, S. and J. Belle, *Leimungswissen Harzleim-AKD-ASA - aus der Forschung für die Praxis*, in *PTS-Fachseminar WE 1542; Wet-End-Prozesse: Effizienter Einsatz chemischer Additive*, R. Grenz, Editor. 2015, Papiertechnische Stiftung PTS: Munich, Germany. p. 131-150.

133. Murray, J., *Eka SA 210, Safety Material Data Sheet*. 2009, Eka Chemicals AB: Düren, Germany.

134. N.A., *Fennosize AS 1000, Technikal Data Sheet*. 2014, Kemira Oyj: Helsinki, Finland.

135. Roberts, J.C. *Chemical Control of Water Penetration in Paper*. in *First International Conference on Interactive Paper*. 1997. International Society for Optics and Photonics.

136. Candy, L., C. Vaca-Garcia, and E. Borredon, *Synthesis and Characterization of Oleic Succinic Anhydrides: Structure-Property Relations.* Journal of the American Oil Chemists' Society, 2005. **82**(4): p. 271-277.

137. Lackinger, E., L. Schmid, J. Sartori, A. Isogai, A. Potthast, and T. Rosenau. *Modified Fatty Oils in Paper Sizing as Green Alternative to Conventional Sizing Agents based on Crude Oil*. in *16th International Symposium on Wood, Fiber and Pulping Chemistry, ISWFPC*. 2011. Tianjin.

138. Lackinger, E., *Novel ASA-Substitutes in Paper Sizing Based on Renewable Raw Materials*, in *Department für Chemie*. 2011, Universität für Bodenkultur: Wien.

139. Quesada, J., M. Morard, C. Vaca-García, and E. Borredon, *Preparation of Alkenyl Succinic Anhydrides from Vegetable Oil FAME.* Journal of the American Oil Chemists' Society, 2003. **80**(3): p. 281-286.

140. Lackinger, E., J. Sartori, A. Potthast, and T. Rosenau, *Novel Paper Sizing Agents Based on Renewables. Part 5: Characterization of Maleated Oleates by Ozonolysis.* Holzforschung, 2012. **66**(1): p. 1-8.

141. Lackinger, E., J. Fallmann, J. Sartori, A. Potthast, and T. Rosenau, *Novel Paper Sizing Agents based on Renewables. Part 6: Sizing Properties of Maleated High Oleic Sunflower Oil.* Journal of Wood Chemistry and Technology, 2012. **32**(1): p. 42-53.

142. Lackinger, E., L. Schmid, J. Sartori, A. Potthast, and T. Rosenau, *Novel Paper Sizing Agents Based on Renewables. Part 4: Application Properties in Comparison to Conventional ASA Sizes.* Holzforschung, 2011. **65**(2): p. 171-176.

143. Lackinger, E., L. Schmid, J. Sartori, A. Isogai, A. Potthast, and T. Rosenau, *Novel Paper Sizing Agents Based on Renewables. Part 2: Characterization of Maleated high Oleic Sunflower Oil (MSOHO).* Holzforschung, 2011. **65**(1): p. 13-19.

144. Lackinger, E., L. Schmid, J. Sartori, A. Isogai, A. Potthast, and T. Rosenau, *Novel Paper Sizing Agents Based on Renewables. Part 1: Preparation of a Paper Sizing Agent Derived from Natural Plant Oils.* Holzforschung, 2011. **65**(1): p. 3-11.

145. Lackinger, E., A. Isogai, L. Schmid, J. Sartori, A. Potthast, and T. Rosenau, *Novel Paper Sizing Agents Based on Renewables. Part 3: Emulsion Stability and Hydrolysis Behavior Compared to Conventional Sizes.* Holzforschung, 2011. **65**(1): p. 21-27.

146. Isogai, A., S. Morimoto, and Y. Adachi, *Emulsion Stability and Sizing Performance of Alkyl Oleate-Succinic Anhydrides.* Paper Technology, 2004. **45**(7): p. 19-24.

147. Isogai, A. and S. Morimoto, *Sizing Performance and Hydrolysis Resistance of Alkyl Oleate Succinic Anhydrides.* Tappi Journal, 2004. **3**(7): p. 8-12.

148. Savolainen, R., *The Effects of Temperature, pH and Alkalinity on ASA Sizing in Alkaline Papermaking*, in *Tappi Papermakers Conference*. 1996, TAPPI Press: Philadelphia, USA.

149. Daud, W. *Fundamental Aspects of Alkenyl Succinic Anhydride Sizing*. in *Proc. APPITA Annual General Conf*. 1993.

150. West, J., A. Brennan, A. Clark, M. Zamora, and L. Hench, *Cyclic Anhydride Ring Opening Reactions: Theory and Application.* Journal of Biomedical Materials Research, 1998. **41**(1): p. 8-17.

151. Sabitha, G., R. Srividya, and J. Yadav, *Ring Opening of Cyclic Anhydrides: Synthesis of Achiral Half-Esters Using Lewis Acids.* Tetrahedron, 1999. **55**(13): p. 4015-4018.

152. Duda, A. and A. Kowalski, *Thermodynamics and Kinetics of Ring-Opening Polymerization*, in *Handbook of Ring-Opening Polymerization*. 2009, Wiley Online Library.

153. McCarthy, W.R. and R.A. Stratton, *Effects of Drying on ASA Esterification and Sizing.* Tappi Journal, 1987. **70**(12): p. 117-121.

154. Isogai, A. *Sizing Behavior of Paper by ASA and Extractability of ASA Components from Sheets*. in *Proceedings of the 1998 65th Pulp and Paper Research Conference*. 1998. Tokyo, Japan: Jpn Tech Assoc Pulp Paper Ind.

155. Hubbe, M.A., *Puzzling Aspects of the Hydrophobic Sizing of Paper and its Inter-Fiber Bonding Ability.* BioResources, 2014. **9**(4): p. 5782-5783.

156. Christen, H.R., *Grundlagen der Organischen Chemie*. Vol. 2. 1972: Verlag Sauerländer. 928.

157. Bart, H., J. Reidetschläger, K. Schatka, and A. Lehmann, *Kinetics of Esterification of Succinic Anhydride with Methanol by homogeneous Catalysis.* International Journal of Chemical Kinetics, 1994. **26**(10): p. 1013-1021.

158. Gliese, T., *Alkenylbernsteinsäureanhydrid (ASA) als Leimungsmittel.* Internationale Papierwirtschaft, 2003. **9**: p. 42-46.

159. Vonach, R., *Review of Key Parameters for Trouble-Free ASA Operation and Recent Trends.* Japan Tappi Journal, 2008. **62**(10): p. 14-18.

160. Martorana, E., J. Belle, and S. Kleemann, *ASA Optimisation–Control of Particle Size, Stability, and Hydrolysis.* Professional Papermaking, 2008. **5**(2): p. 34-42.

161. Wang, D.-Q. and K.-T. Hu, *Hydrolysis Stability of ASA and its Effect on Sizing.* China Pulp and Paper, 2005. **24**(12): p. 14-17.

162. Gess, C.M., *Carboxylic Acids (Including Hydrolyzed ASA) in Neutral/Alkaline Papermaking and the Potential for Deposits*, in *Tappi Papermakers Conference*. 1994, TAPPI Press: San Francisco. p. 609-620.

163. Matsushima, K., M. Takaoka, H. Zako, Y. Sakamoto, and Y. Adati, *Mechanism of Sizing Behavior of ASA* Japan Tappi Journal, 2003. **57**(9): p. 36-43.

164. Chen, M. and C.J. Biermann, *Investigation of the Mechanism of Paper Sizing through a Desizing Approach.* Tappi Journal, 1995. **78**(8): p. 120-120.

165. Isogai, A., *Sizing Behavior of Paper by ASA and Extractability of ASA Components from Sheets*, in *Pulp and Paper Research Conference*. 1998, Japan Tappi: Tokio. p. 178-181

166. Wang, D.-Q., K.-T. Hu, and S.-Y. Song, *Chemical Change of ASA in Sizing Process.* China Pulp and Paper, 2006. **25**(1): p. 12-16.

167. Isogai, A., *The Reason why the Reactive Chemical Structure of Alkenyl Succinic Anhydride is Necessary for Efficient Paper Sizing.* Sen i Gakkaishi, 2000. **56** (7): p. 334-339.

168. Zhmud, B., R. Seppänen, and F. Tiberg, *Hydrolysis and Sizing Action of Cellulose-Reactive Sizes*, in *Advances in Internal and Surface Sizing of Paper and Board. Pira Conference*. 2001: Prague.

169. Isogai, A., *Retention Behavior of Alkenyl Succinic Anhydride Size on Handsheets.* Sen i Gakkaishi, 2000. **56**(7): p. 328-333.

170. Wasser, R.B. and J.S. Brinen, *Effect of Hydrolyzed ASA on Sizing in Calcium Carbonate-Filled Paper.* Tappi Journal, 1998. **81**(7): p. 139-144.

171. Patton, P.A., *Starches for ASA Sizing*, in *TAPPI Papermakers Conference*. 1992, TAPPI Press: San Francisco, USA.

172. Haller, K., R. Proverb, and K. Komarowska, *Emulgierung von ASA mit Flüssigstärken*, in *Einsatz von Staerke bei der Papiererzeugung.* 2000, Blechschmidt J.; Bergh N.O.(Hrsg.): München.

173. Lee, H.L., J.S. Kim, and H.J. Youn, *Improvement of ASA Sizing Efficiency Using Hydrophobically Modified and Acid-Hydrolyzed Starches.* Tappi Journal, 2004. **3**(12): p. 3-6.

174. Isogai, A., *Mechanism of Paper Sizing.* Kami Pa Gikyoshi/Japan Tappi Journal, 1998. **52**(12): p. 1678-1686.

175. Jaycock, M.J., C.J. Meredew, and J.C. Roberts, *Paper Sizing Composition Containing Alkenyl Succinic Anhydride with Long Storage Life and Good Workability*, in *Patent WO 2000020686*. 2000, Raisio Chemicals: UK.

176. Glover, D.E., *Alkenylsuccinic Anhydride Sizing Emulsions Containing Low and High Molecular Weight Cationic Polymers*, in *Patent WO 9749865*. 1997, Buckman Laboratories International, Inc.: USA.

177. Haufe, I., K. Möller, and A. Kurucz, *Aqueous Emulsion of a Sizing Agent*, B. SE, Editor. 2014: Germany.

178. Dostie, D.R. and R.J. Nowicki, *Alkenyl Succinic Anhydride Size Emulsion Containing a Natural Gum for Paper Products*, in *Patent WO 9951816*. 1998, ECC International Inc.: USA.

179. Koskela, J.P., O.E.O. Hormi, J.C. Roberts, and G. Peng, *The Use of Nonionic Galactomannan Polysaccharides for Stabilisation of ASA Emulsions.* Appita Journal, 2003. **56**(3): p. 213-217.

180. Ding, P., W. Liu, and Z. Zhao, *Roles of Short Amine in Preparation and Sizing Performance of Partly hydrolyzed ASA Emulsion Stabilized by Laponite Particles.* Colloids and Surfaces A: Physicochemical and Engineering Aspects, 2011. **384**: p. 150-156.

181. Li, W., L. Yu, G. Liu, J. Tan, S. Liu, and D. Sun, *Oil-in-Water Emulsions Stabilized by Laponite Particles Modified with Short-Chain Aliphatic Amines.* Colloids and Surfaces A: Physicochemical and Engineering Aspects, 2012. **400**: p. 44-51.

182. Lu, P., W. Liu, H. Wang, and Z. Wang, *Using Chitosan as Sizing Promoter of ASA Emulsion Stabilized by Montmorillonite*. 2013. Vol. 8. 2013.

183. Yu, D., Z. Lin, and Y. Li, *Octadecenylsuccinic Anhydride Pickering Emulsion Stabilized by γ-Methacryloxy Propyl Trimethoxysilane Grafted Montmorillonite.* Colloids and Surfaces A: Physicochemical and Engineering Aspects, 2013. **422**: p. 100-109.

184. Tan, H., W. Liu, D. Yu, H. Li, M.A. Hubbe, B. Gong, W. Zhang, H. Wang, and G. Li, *ASA-in-Water Emulsions stabilized by Laponite Nanoparticles modified with Tetramethylammonium Chloride.* Chemical Engineering Science, 2014. **116**: p. 682-693.

185. Yu, D., W. Liu, Y. Li, H. Wang, and G. Li, *Dodecenylsuccinic Anhydride Pickering Emulsion Stabilized by Montmorillonite Nanoparticles Modified with Sodium Fluoride.* BioResources, 2015. **10**(2): p. 2755-2772.

186. Hoffmann, J. *A New User-Friendly ASA Sizing System*. in *Progess in Papermaking and Paper Converting in Central and Eastern Europe*. 2002. Gdansk, Poland.

187. Hoffmann, J. and H. Scholtens, *Erste Produktionserfahrungen mit leicht dispergierbaren ASA-Masseleimen*, in *Internationales Münchner Papier Symposium*. 2006, Prof. Dr. Stephan Kleemann: München.

188. Proverb, R., *Ein leicht dispergierbares ASA Leimungssystem unter Verwendung der low-shear Prozesstechnologie*, in *Internationales Münchner Papier Symposium*. 2006, Prof. Dr. Stephan Kleemann: München.

189. Merisalo, J.-P., *Optimization of ASA Emulsification in Internal Sizing of Paperboard*, in *Faculty of Chemistry and Material Sciences*. 2009, Helsinki University of Technology: Espoo.

190. Chen, G.C.I. and T.W. Woodward, *Optimizing the Emulsification and Sizing of Alkenyl Succinic Anhydride.* Tappi Journal, 1986. **69**(8): p. 95-97.

191. Porkert, S. and S. Kleemann, *Optimierung der ASA Leimung*, in *Schlussbericht INFOR-Projekt 159*, V.D.P. e.V., Editor. 2013, Munich University of Applied Sciences: Munich.

192. Martorana, E., S. Fischer, and S. Kleemann, *Einflüsse auf die Partikelgröße, Stabilität und Hydrolyse von ASA-Emulsionen.* Wochenblatt für Papierfabrikation, 2008. **136 (8)**: p. 392-401.

193. Matula, J. and J. Matula. *Flash Mixing of Wet End Additives Opens New Avenues for Business and for Development of Process Chemistry*. in *PTS Symposium GC 1446; PTS International Symposium on Applied Interface Chemistry 2014*. 2014. Munich, Germany: Papiertechnische Stiftung PTS.

194. Waubert de Puiseau, D. and K. Sundin, *„Last Second – All In One", Injection of Filler, Micro Particles and Retention Aid*, in *24th International Munich Paper Symposium*, S. Kleemann, Editor. 2015, IMPS Management Ltd.: Munich, Germany.

195. Petersen, D., *Neutralleimungsmittel ASA und AKD*. 2000: Hochschule München.

196. Prinz, M. and W.S. Schultz, *Leimungsmittel für Masse-und Oberflächenapplikation.* Wochenblatt für Papierfabrikation, 2006. **134**(22): p. 1329-1335.

197. Porkert, S., S. Fischer, and S. Kleemann, *Physico-Chemical Aspects during Alkenyl Succinic Anhydride Sizing*, in *9th International Paper and Coating Chemistry Symposium* A. Isogai, Editor. 2015: Tokio, Japan.

198. Roberts, J.C., M.J. Jaycock, and C.J. Meredew, *Factors Affecting the Hydrolytic Stability of Alkenyl Succinic Anhydride (ASA) Sizes*, in *EUCEPA Symposium, Chemistry in Papermaking*. 1998: Florence. p. 81-91.

199. Echt, E. and C.L. Bungardt, *Effect of Retention Polymeres and Chemical Environment on Fine Particle Retention and Sizing in Recycled Paper*, in *TAPPI Papermakers Conference* 1991, TAPPi Press: Nashville, USA. p. 449-467.

200. Lacher, R., *Leimung mit AKD und ASA - Trends und Anwendung*, in *Forschungsforum Wet End*. 2006, PTS München: Munich.

201. Martorana, E., S. Fischer, and S. Kleemann, *Neue Erkenntnisse zu Wechselwirkungen und Mechanismen bei der ASA-Leimung.* Wochenblatt für Papierfabrikation, 2010.

202. Geiger, A., I. Brovchenko, and D. Paschek, *Molekulare Eigenschaften und Funktion des Wassers*, in *Unireport*. 2004, Universität Dortmund: Dortmund.

203. Ono, H. and T. Miyanishi, *Comparative Study on the Sizing Efficiency and Kinetics Between ASA und AKD sizing.* Japan Tappi Journal, 2000. **54**(6): p. 812-819.

204. Lindfors, J., J. Salmi, J. Laine, and P. Stenius, *AKD and ASA Model Surfaces: Preparation and Characterization.* BioResources, 2007. **2**(4): p. 652-670.

205. Ye, D. and X. Farriol, *Improving accessibility and reactivity of celluloses of annual plants for the synthesis of methylcellulose.* Cellulose, 2005. **12**(5): p. 507-515.

206. Sunkyu, P., B. John, H. Michael, P. Philip, and J. David, *Cellulose crystallinity index: measurement techniques and their impact on interpreting cellulase performance.* Biotechnology for Biofuels, 2010. **3**.

207. Pérez, S. and D. Samain, *Structure and Engineering of Celluloses*, in *Advances in Carbohydrate Chemistry and Biochemistry*, H. Derek, Editor. 2010, Academic Press. p. 25-116.

208. Chen, Q., Y. Ni, and Z. He, *Using Cationic Polymers to improve Alkenyl Succinic Anhydride (ASA) Sizing Efficiency in High-Yield Pulp Containing Furnish.* BioResources, 2012. **7**(3): p. 3948-3959.

209. Roberts, J., Y. Takahashi, S. Hatanaka, and Y. Takeda. *The Effect of Substituted Alkaline Structure on ASA Sizing*. in *The Chemistry of Papermaking*. 1993. Surrey, UK: Pira International.

210. Smith, D. *ASA Components: Their Synthesis and Relative Sizing Performance*. in *Scientific and Technical Advances in the Internal and Surface Sizing of Paper and Board*. 1999. Surrey, UK: Pira International.

211. Porkert, S., S. Fischer, and S. Kleemann, *Physiko-Chemische Prozesse während der Reaktivleimung mit Alkenyl-Bernsteinsäureanhydrid (ASA)*, in *PTS Faserstoffsymposium* T. Arndt and F. Miletzky, Editors. 2015, PTS Paper: Dresden. p. 132-151.

212. Shah, D.O., *Micelles: Microemulsions, and Monolayers: Science and Technology*, ed. I. Marcel Dekker. 1998, New York: Marcel Dekker, Inc.

213. Bartz, W.J., M.E. Darroch, and F.L. Kurrle, *Alkyl Ketene Dimer Sizing Efficiency and Reversion in Calcium Carbonate Filled Papers.* Tappi Journal, 1994. **77**(12): p. 139-148.

214. Sato, T., A. Isogai, and F. Onabe, *Autoxidation: Predominant Mechanism of Size Reversion for ASA-sized Paper.* Nordic Pulp and Paper Research Journal, 2000. **15**(3): p. 172-176.

215. Novak, R.W. and D.S. Rende, *Size Reversion in alkaline Papermaking.* Tappi Journal, 1993. **76**(8): p. 117-120.

216. Hutton, B.H. and W. Shen, *Sizing Effects via AKD Vaporisation*, in *58th Appita Annual Conference and Exhibition*, Appita, Editor. 2004, Appita: Carlton. p. 401-406.

217. Shen, W., F. Xu, and I.H. Parker, *An Experimental Investigation of the Redistribution Behaviour of Alkyl Ketene Dimers and their Corresponding Ketones.* Colloids and Surfaces A: Physicochemical and Engineering Aspects, 2003. **212**(2–3): p. 197-209.

218. Back, E. and S. Danielsson, *Hot extended Press Nips as Gas-Phase Reactors: Hydrophobation with ASA.* Tappi Journal, 1991. **74**(9): p. 167-174.

219. Mattsson, R., D. Lindström, J. Sterte, and L. ÖDberg, *Influence of Abietic Acid, Betulinol, Sodium Oleate and Tripalmitine on the Migration of AKD in Paper.* Journal of Pulp and Paper Science, 2003. **29**(8): p. 281-285.

220. Gess, J. and R. Lund, *The strong bond/weak bond theory of sizing.* Tappi Journal, 1991. **74**(1): p. 111-113.

221. Bundesinstitut für Risikobewertung, *Empfehlung XXXVI*, in *Papiere, Kartons und Pappen für den Lebensmittelkontakt*. 2015, Bundesinstituf für Risikobewertung: Berlin.

222. U.S. Food and Drug Administration, *Code of Federal Regulations, Title 21 - Food and Drugs, Chapter 1- Food and Drug Administration, Subchapter B - Food for Human Consumption, Part 176 - Indirect Food Additives: Paper and Paper Board Components*, in *Subpart B - Substances for Use only as Components of Paper and Paperboard*. 2015, U.S. Department of Health and Human Services: Silver Spring, Maryland.

223. Farley, C.E. *Use of Alum to Improve ASA Sizing Efficiency in Alkaline Paper*. in *Papermakers Conference* 1991. Seattle: Tappi.

224. Belle, J., S. Kleemann, and J. Odermatt, *Weighing of Different Impact Factors on Wet Web Strength by Full-Factorial Design of Experiments.* BioResources, 2014. **9**(2): p. 1830-1844.

225. Fernandes, S. and A.P. Duarte, *Influence of Wet-End Variables on the Sizing Efficiency of ASA on Fine Papers Produced with Eucalyptus Globulus Kraft Pulps.* Tappi Journal, 2006. **5**(12): p. 17-23.

226. Chen, Q., Y. Ni, and Z. He, *Substitution of High-Yield-Pulp for Hardwood Bleached Kraft Pulp in Paper Production and its Effect on Alkenyl Succinic Anhydride Sizing.* BioResources, 2012. **7**(2): p. 1462-1473.

227. Hu, K., Y. Ni, and X. Zou, *Substitution of Aspen High-Yield Pulp for Hardwood Kraft Pulp in fine Papers and its Effect on AKD Sizing.* Tappi Journal, 2004. **3**(8): p. 13-16.

228. Gliese, T. and V. Kukkamo, *Surface Functionalized Fillers for Highest Filler Levels*, in *18th International Munich Paper Symposium*, S. Kleemann, Editor. 2009, IMPS Management Ltd.: Munich, Germany.

229. Kleemann, S., *Chemische Additive - funktionell unentbehrlich und ökologisch nützlich. Teil III. Einleitung und systematischer Ansatz.* Wochenblatt für Papierfabrikation, 2006. **134**(22): p. 1297-1299.

230. Isermann, R., *Qualitätsverbesserung und Kostenreduktion durch effizienten Einsatz moderner Entschäumer.* BASF Customer Seminar, 2005.

231. Zeno, E., B. Carré, and E. Mauret, *Influence of Surface active Substances on AKD Sizing.* Nordic Pulp and Paper Research Journal, 2005. **20**(2): p. 253-258.

232. Porkert, S., S. Fischer, and S. Kleemann, *Visible Sizing – Causes for Sizing Loss and undesired Interactions*, in *23rd Internatinal Munich Paper Symposium*, S. Kleemann, Editor. 2014, IMPS Management Ltd. & Co. KG: Munich, Germany.

233. Silvestri, L., A. Bria, L. Sacconi, G. Iannello, and F.S. Pavone, *Confocal Light Sheet Microscopy: Micron-Scale Neuroanatomy of the Entire Mouse Brain.* Optics Express, 2012. **20**(18): p. 20582-20598.

234. Gane, P.A.C., M. Salo, J.P. Kettle, and C.J. Ridgway, *Comparison of Young-Laplace Pore Size and Microscopic Void Area Distributions in Topologically Similar Structures: A New*

Method for Characterising Connectivity in Pigmented Coatings. Journal of Materials Science, 2009. **44**: p. 422-432.

235. Vernhes, P., J.-F. Bloch, C. Mercier, A. Blayo, and B. Pineaux, *Statistical Analysis of Paper Surface Microstructure: A Multi-Scale Approach.* Applied Surface Science, 2008. **254**(22): p. 7431-7437.

236. Ozaki, Y., *Application of Confocal Laser Scanning Microscopy (CLSM) for Observing Adhesives in Paper.* Journal of Adhesion Science and Technology, 2011. **25**(6-7): p. 723-741.

237. Pawley, J., *Handbook of Biological Confocal Microscopy*. 2 ed. 1995, New York: Plenum Press.

238. Frank, J., A. Elder, J. Swartling, A. Venkitaraman, A. Jeyasekharan, and C. Kaminski, *A White Light Confocal Microscope for Spectrally Resolved Multidimensional Imaging.* Journal of Microscopy, 2007. **227**(3): p. 203-215.

239. Jordan, H., R. Brodmann, J. Valentin, and M. Grigat, *Confocal White Light Microscopy*. NanoFocus Messtechnik Gmbh: Duisburg.

240. Kubitscheck, U., *Principles of Light Microscopy*, in *Fluorescence Microscopy*. 2013, Wiley-VCH Verlag GmbH & Co. KGaA. p. 33-95.

241. Naredi-Rainer, N., J. Prescher, A. Hartschuh, and D.C. Lamb, *Confocal Microscopy*, in *Fluorescence Microscopy*. 2013, Wiley-VCH Verlag GmbH & Co. KGaA. p. 175-213.

242. Suzuki, T., K. Fujikura, T. Higashiyama, and K. Takata, *DNA Staining for Fluorescence and Laser Confocal Microscopy.* Journal of Histochemistry & Cytochemistry, 1997. **45**(1): p. 49-53.

243. Brundrett, M.C., D.E. Enstone, and C.A. Peterson, *A Berberine-Aniline Blue Fluorescent Staining Procedure for Suberin, Lignin, and Callose in Plant Tissue.* Protoplasma, 1988. **146**(2-3): p. 133-142.

244. Sigma-Aldrich, *Sudan Red 7B*, in *Material Savety Data Sheet*. 2014, Sigma-Aldrich Co. LLC.: sigma-aldrich.com.

245. Sigma-Aldrich, *Sudan Blue II*, in *Material Savety Data Sheet*. 2014, Sigma-Aldrich Co. LLC.: sigma-aldrich.com.

246. Sigma-Aldrich, *Sudan Red III*, in *Material Savety Data Sheet*. 2013, Sigma-Aldrich Co. LLC.: sigma-aldrich.com.

247. Sigma-Aldrich, *Sudan Black B*, in *Material Savety Data Sheet*. 2013, Sigma-Aldrich Co. LLC.: sigma-aldrich.com.

248. Sigma-Aldrich, *Nile Red*, in *Material Savety Data Sheet*. 2013, Sigma-Aldrich Co. LLC.: sigma-aldrich.com.

249. Hubbe, M.A., R.A. Venditti, R.L. Barbour, and M. Zhang, *Changes to Unbleached Kraft Fibers Due to Drying and Recycling.* Progress in Paper Recycling, 2003. **12**(3): p. 11-20.

250. Diniz, F.J.M.B., M.H. Gil, and J.A.A.M. Castro, *Hornification—Its Origin and Interpretation in Wood Pulps.* Wood Science and Technology, 2004. **37**(6): p. 489-494.

251. Li, H., Y. Ni, and M. Sain, *Characterization of BCTMP Fines and Their Effect on Sizing.* Tappi Journal, 2002. **1**(7): p. 3-7.

252. Waring Laboratory Science. *Waring Laboratory Blender 8010*. 2015 [cited 2015 12.10]; [Picture]. Available from: http://sigma.octopart.com/17749491/image/Waring-8010BU.jpg.

253. Oster Manufacturing. *Oster Blender Mini-Jar*. 2015 [cited 2015 12.10]; [Picture]. Available from: http://demandware.edgesuite.net/sits pod22/dw/image/v2/AAMB PRD/on/demandware.static/-/Sites-master-catalog/default/dw2de35de7/images/highres/004937-000-NP0-1.jpg?sw=400&sh=400&sm=fit.

254. Oster Manufacturing. *Oster Ice Crusher Blade*. 2015 [cited 2015 12.10]; [Picture]. Available from: http://demandware.edgesuite.net/sits pod22/dw/image/v2/AAMB PRD/on/demandware.static/-/Sites-master-catalog/default/dw40fb1981/images/highres/004961-011-NP0-1.jpg?sw=400&sh=400&sm=fit.

255. ISO International Organization for Standardization, *ISO 13320-1 - Partikelgrößenanalyse - Laserbeugungsverfahren - Teil 1: Allgemeine Grundlagen*. 1999.

256. Alicona Imaging GmbH, *IFM 2.2 Help*. 2008, Alicona Imaging GmbH: Graz.

257. DIN Deutsches Institut für Normung e.V., *DIN EN ISO 186*, in *Papier und Pappe - Probenahme zur Bestimmung der Durchschnittsqualität (ISO 186:2002) Deutsche Fassung EN ISO 186:2002*. 2002, Beuth Verlag GmbH.

258. DIN Deutsches Institut für Normung e.V., *DIN EN ISO 20187*, in *Papier, Pappe und Zellstoff - Normalklima für die Vorbehandlung und Prüfung und Verfahren zur Überwachung des Klimas und der Probenvorbehandlung (ISO 187:1990); Deutsche Fassung EN 20187:1993*. 1993, Beuth Verlag GmbH.

259. DIN Deutsches Institut für Normung e.V., *DIN EN ISO 638*, in *Papier, Papper und Faserstoff - Bestimmung des Trockengehalts - Wärmeschrankverfahren (ISO 638:2008); Deutsche Fassung EN ISO 638:2008*. 2009, Beuth Verlag GmbH.

260. DIN Deutsches Institut für Normung e.V., *DIN EN ISO 4119*, in *Halbstoffe - Bestimmung der Stoffdichte (ISO 4119:1995); Deutsche Fassung EN ISO 4119:1996*. 1996, Beuth Verlag GmbH.

261. DIN Deutsches Institut für Normung e.V., *DIN EN ISO 5267-1* in *Faserstoffe - Prüfung des Entwässerungsverhaltens - Teil 1: Schopper-Riegler-Verfahren (ISO 5267-1:1999) Deutsche Fassung EN ISO 5267-1:2000*. 2000, Beuth Verlag GmbH.

262. DIN Deutsches Institut für Normung e.V., *DIN 6739-500*, in *Papier und Pappe - Teil 500: Bestimmung der flächenbezogenen Masse*. 2011, Beuth Verlag GmbH.

263. emtech-Paper Testing Technology. *PDA.C 02 Module Standard*. 2004 [cited 2015 25.11]; Available from: http://www.emtec-papertest.de/attachments/article/53/ModuleSTANDARD leaflet deu.pdf.

264. Testing-Machines Inc., *PocketGoniometer PGX+*, F.S. AB, Editor. 2015, Testing-Machines Inc.: Delaware; USA.

265. ISO International Organization for Standardization, *ISO 5636-5*, in *Papier und Pappe - Bestimmung der Luftdurchlässigkeit (mittlerer Bereich) - Teil 5 : Verfahren nach Gurley*. 2013.

266. DIN Deutsches Institut für Normung e.V., *DIN ISO 1924-3*, in *Papier und Pappe - Bestimmung der Eigenschaften bei Zugförmiger Belastung - Teil 3: Verfahren mt konstanter Dehngeschwindigkeit (100 mm/min) (ISO 1924-3:2005)*. 2008, Beuth Verlag GmbH.

267. DIN Deutsches Institut für Normung e.V., *DIN EN ISO 5263-1*, in *Faserstoffe - Nassaufschlagen im Labor - Teil 1: Aufschlagen von Chemiezellstoff (ISO 5263-1:2004); Deutsche Fassung EN ISO 5263-1:2004*. 2004, Beuth Verlag GmbH.

268. Zellcheming e.V., *Zellcheming Merkblatt V/6/61 - Einheitsmethode für die Festigkeitsprüfung von Zellstoffen – F. Egalisierung des gemahlenen Stoffes und Mengenverteilung* 1961, Zellcheming e.V.: Darmstadt.

269. TAPPI, *TAPPI Test Method T 200 sp-01*, in *Laboratory Beating of Pulp (Valley Beater Method)*. 2001, TAPPI Press.

270. DIN Deutsches Institut für Normung e.V., *DIN EN ISO 5269-2* in *Faserstoffe - Laborblattbildung für physikalische Prüfungen - Teil 2: Rapid-Köthen-Verfahren (ISO 5269-2:2004) Deutsche Fassung EN ISO 5269-2:2004*. 2005, Beuth Verlag GmbH.

271. Ryu, J.Y. and B.-K. Song, *Standardization of RDA Conditions for the Simultaneous Analysis of Retention, Drainage and Uniformity of Papers.* Journal of Standards and Standardization, 2011. **2**: p. 95-104.

272. DIN Deutsches Institut für Normung e.V., *DIN ISO 5630*, in *Papier und Pappe - Beschleunigte Alterung - Teil 1: Trockenwärmebehandlung bei 105°C; Identisch mit ISO 5630-1 : 1991*. 1991, Beuth Verlag GmbH.

273. DIN Deutsches Institut für Normung e.V., *DIN ISO 5630-3* in *Papier und Pappe - Beschleunigte Alterung - Teil 3: Feuchtwärmebehandlung bei 80°C und 65% relativer Luftfeuchte*. 1996, Beuth Verlag GmbH.

274. Moritz J. Weig GmbH & Co. KG. *Composition of Plaster Board Liner*. 2015 [cited 2015 07.10]; Available from: http://www.weig-karton.de/de/gipskarton.php.

275. Moritz J. Weig GmbH & Co. KG. *Technical Specification of Plasterboard Liner*. 2011 24.08; Available from: http://www.weig-karton.de/download/gipskarton.pdf.

276. Olejnik, K., *Impact of Pulp Consistency on Refining Process conducted under constant Intensity determined by SEL and SEC factors.* BioResources, 2013. **8**(3): p. 3212-3230.

Appendix

7.1 Localization Method Reproducibility

Table 7.1-1: Statistical Results of Reproducibility Analysis

Total Agglomeration Area / Aggl_A / [%]			
	Mean	**Median**	**SD within one Set**
Sample A	0.0900	0.0803	0.05375
Sample B	0.0922	0.0936	0.0562
Sample C	0.0815	0.0856	0.0391
Average	0.0879	0.0865	0.0497
SD between Sets [%]	+/- 6.4%	+/- 7.67 %	
Number of Agglomerates / Aggl_N / [n/mm²]			
	Mean	***Median***	***SD within one Set***
Sample A	3293	3062	1726
Sample B	3266	3141	1813
Sample C	3328	2950	1331
Average	3296	3051	1623
SD between Sets [%]	+/- 0.93%	+/- 3.14%	
Average Agglomerate Size / Aggl_AV / [µm²]			
	Mean	***Median***	***SD within one Set***
Sample A	0.2874	0.2881	0.1170
Sample B	0.3322	0.2962	0.2199
Sample C	0.2678	0.2651	0.1185
Average	0.2958	0.2848	0.1518
SD between Sets [%]	+/- 11.16 %	+/- 5.7%	

7.2 DOE - Coefficient Lists

7.2.1 Trial 3.3.4 – Impact of Retention Aid (PAM) on Agglomeration Behavior and Sizing Performance

Table 7.2-1: Coefficient Lists - Trial 3.3.4 – Impact of Retention Aid (PAM) on Agglomeration Behavior and Sizing Performance

Aggl_A [%]	Coeff. SC	Std. Err.	P	Conf. int(±)
Constant	0.169552	0.0217325	1.47E-09	0.0439233
ASA	0.198688	0.0220182	3.43E-11	0.0445007
PAM	-0.0158502	0.0220111	0.475652	0.0444864
ASA*PAM	-0.0083905	0.022262	0.70824	0.0449935
N = 45	Q^2 =	0.568	Cond. no. =	**1.095**
DF = 40	R^2 =	0.675	RSD =	**0.1458**
Comp. = 2	R^2 adj. =	0.643	Conf. lev. =	**0.95**
t60 [s]	**Coeff. SC**	**Std. Err.**	**P**	**Conf. int(±)**
Constant	42.2057	1.73664	3.63E-25	3.51265
ASA	35.6585	1.75753	2.50E-22	3.55491
PAM	1.30242	1.75772	0.463148	3.5553
ASA*PAM	2.76237	1.76864	0.1264	3.57739
N = 44	Q^2 =	0.883	Cond. no. =	**1.045**
DF = 39	R^2 =	0.915	RSD =	**11.52**
Comp. = 2	R^2 adj. =	0.906	Conf. lev. =	**0.95**

7.2.2 Trial 3.3.5 – Impact of Contact Curing on Agglomeration Behavior and Sizing Performance

Table 7.2-2: Coefficient Lists - Trial 3.3.5 – Impact of Contact Curing on Agglomeration Behavior and Sizing Performance

Aggl_A [%]	Coeff. SC	Std. Err.	P	Conf. int(±)
Constant	0.169552	0.0217325	1.47E-09	0.0439233
ASA	0.198688	0.0220182	3.43E-11	0.0445007
Curing Temp	-0.0071881	0.0220463	0.746089	0.0445575
ASA*PAM	-0.0083905	0.022262	0.70824	0.0449935
N = 45	Q^2 =	**0.568**	Cond. no. =	**1.095**
DF = 40	R^2 =	**0.675**	RSD =	**0.1458**
Comp. = 2	R^2 adj. =	**0.643**	Conf. lev. =	**0.95**
t60 [s]	**Coeff. SC**	**Std. Err.**	**P**	**Conf. int(±)**
Constant	42.2057	1.73664	3.63E-25	3.51265
ASA	35.6585	1.75753	2.50E-22	3.55491
Curing Temp	3.29467	1.75737	0.0683269	3.55458
ASA*Cure	2.76237	1.76864	0.1264	3.57739
N = 44	Q^2 =	**0.883**	Cond. no. =	**1.045**
DF = 39	R^2 =	**0.915**	RSD =	**11.52**
Comp. = 2	R^2 adj. =	**0.906**	Conf. lev. =	**0.95**

7.2.3 Trial 3.3.6 – Impact of Accelerated Aging on Agglomeration Behavior and Sizing Performance

Table 7.2-3: Coefficient Lists - Trial 3.3.6 – Impact of Accelerated Aging on Agglomeration Behavior and Sizing Performance

t60 [s]	Coeff. SC	Std. Err.	P	Conf. int(±)
Constant	0.954133	0.0561061	9.18E-10	0.122244
ASA	0.464622	0.0582175	3.85E-06	0.126845
Accelerated Aging Time	-0.0783649	0.0582175	0.203159	0.126845
N = 15	Q^2 =	**0.79**	Cond. no. =	**1.073**
DF = 12	R^2 =	**0.849**	RSD =	**0.2173**
Comp. = 2	R^2 adj. =	**0.824**	Conf. lev. =	**0.95**
Aggl_A [%]	**Coeff. SC**	**Std. Err.**	**P**	**Conf. int(±)**
Constant	0.021855	0.00202923	7.56E-08	0.00438388
ASA	0.0125551	0.00210529	4.72E-05	0.0045482
Accelerated Aging Time	-0.0048807	0.00212145	0.0386116	0.00458311
ASA*AA	-0.0028106	0.00197754	0.178785	0.00427222
N = 17	Q^2 =	**0.62**	Cond. no. =	**1.269**
DF = 13	R^2 =	**0.771**	RSD =	**0.008326**
Comp. = 2	R^2 adj. =	**0.718**	Conf. lev. =	**0.95**
Aggl_AV [µm²]	**Coeff. SC**	**Std. Err.**	**P**	**Conf. int(±)**
Constant	0.22514	0.0263902	1.94E-06	0.0574991
ASA	0.135476	0.0276394	3.65E-04	0.0602209
Accelerated Aging Time	0.0250991	0.0291322	0.405818	0.0634733
ASA*AA	0.0133442	0.0247518	0.599663	0.0539293
N = 16	Q^2 =	**0.561**	Cond. no. =	**1.634**
DF = 12	R^2 =	**0.681**	RSD =	**0.1038**
Comp. = 2	R^2 adj. =	**0.601**	Conf. lev. =	**0.95**